Vol. 107 N°2 ISSN 2545-8655

ANALES DE LA ASOCIACIÓN QUÍMICA ARGENTINA

Julio-Diciembre 2020

Anales de la Asociación Química Argentina

Editada desde 1913

Registro de Propiedad Intelectual Nº 164.756

Asociación Química Argentina
Sánchez de Bustamante 1749
1425 Buenos Aires, Argentina
TE/FAX: 54-11-4822-4886
http://www.aqa.org.ar

División de Jóvenes Profesionales
FB @djpq.aqa – TW @jovenes_AQA

Contenido

Vol. 107 Nº2, Julio-Diciembre de 2020 - Fotoquímica

Mini-Reviews

EDITORIAL

Estimados Lectores de Anales de la Asociación Química Argentina:

En este nuevo número de nuestra revista les presentamos el tercer número temático editado por la División de Jóvenes Profesionales en Química, de la Asociación Química Argentina (DJPQ-AQA).

El objetivo central de la División DJPQ-AQA es conectar a los jóvenes profesionales de la química que se encuentran ejerciendo su profesión en distintas regiones de nuestro país, catalizando el intercambio de ideas y la cooperación entre ellos.

De ese intenso intercambio y cooperación surge el contenido de este tercer volumen dedicado a Fotoquímica (Photochemistry) cuyos Editores Invitados son la Dra. Natalia Lorena Pacioni, Investigadora Independiente del CONICET y especialista en Fisicoquímica Orgánica, Nanomateriales y Química Analítica Supramolecular, y el Dr. Juan Elias Argüello, Investigador Independiente del CONICET y especialista en Fisicoquímica Orgánica, Química de Radicales y Fotoquímica. Ambos Editores pertenecen al Instituto de Investigaciones en Físico- Química de Córdoba (INFIQC).

Esperamos que este nuevo número de Mini-Reviews entusiasme a otros jóvenes profesionales de la química a conectarse con la DJPQ-AQA a través del email djpq.aqa@gmail.com.

Dra. Susana A. Larrondo

Editora en Jefe

NOTE FROM THE EDITOR

Dear Readers of Anales de la Asociación Química Argentina:

In this new issue of our journal, we present the third thematic issue edited by the Division of Young Professionals in Chemistry of the Argentine Chemical Association (DJPQ-AQA).

The main objective of the DJP-AQA Division is to connect young Chemists from different regions of our country, encouraging the exchange of ideas and cooperation among them.

From this intense exchange and cooperation emerges the content of this third issue dedicated to Photochemistry whose Guest Editors are Dr. Natalia Lorena Pacioni, Independent Researcher of CONICET and specialist in Organic Physicochemistry, Nanomaterials and Supramolecular Analytical Chemistry, and Dr. Juan Elias Argüello, Independent Researcher at CONICET and specialist in Organic Physical Chemistry, Radical Chemistry and Photochemistry. Both Editors belong to the Instituto de Investigaciones en Físico-Química de Córdoba (INFIQC).

We hope that this new issue of Mini-Reviews will encourage other young chemists to connect with the DJPQ-AQA via email djpq.aqa@gmail.com.

Dra. Susana A. Larrondo

Chief Editor

NOTA DE LOS EDITORES INVITADOS

La luz como parte integral de las investigaciones en Química, en sus diversas áreas, ha mostrado un crecimiento intermitente a lo largo de la historia. Si bien sus inicios datan de fines del siglo XIX con los trabajos pioneros del italiano Giacomo Ciamician, el auge de la Fotoquímica se produjo recién a partir de los años sesenta y particularmente, en Argentina se incrementó alrededor de los años noventa. Así, se podría decir que la Fotoquímica en Argentina es un área de investigación joven, diversa y en continuo crecimiento.

En este número especial, con representación de centros de investigación en diferentes regiones del país, contamos con contribuciones que detallan la luz como parte de las transformaciones químicas y físicas, con importancia en distintos campos como los estudios fotofísicos, como herramienta de remediación ambiental, la síntesis orgánica y la fotobiología.

Primero, Lagorio et al. desde CABA examinan la fluorescencia de clorofila a para obtener información sobre la actividad fotosintética y su aplicación para estudiar los efectos sobre contaminación o estrés ambiental. Luego, Milanesio et a.l desde Río Cuarto evalúan diferentes clases de fotosensibilizadores incluyendo la síntesis y caracterización, como agentes antimicrobianos y Borsarelli et al. desde Santiago del Estero revisan las aplicaciones de fotosensibilizadores supramoleculares. A su vez, Caregnato et al en La Plata, abordan la fotoluminiscencia de nanopartículas de Silicio de 1 a 4 nm de diámetro como potenciales marcadores y fotosensibilizantes. Posteriormente, Massad et al. también desde Río Cuarto, se enfocan en la fotodegradación, directa o mediada por Riboflavina, de pesticidas y antiparasitarios. En Córdoba, Bardagi et al., nos presentan los enfoques modernos del empleo de la fotoquímica como una herramienta en síntesis orgánica, cuyo empleo se ha visto incrementado en los últimos años por la comunidad de Química Orgánica a nivel internacional. Por último, mientras Thomas et al. desde La Plata, resumen la degradación fotosensibilizada de biomoléculas como ADN, proteínas y lípidos por derivados de pterinas, Cabrerizo et al. desde Chascomús, estudian las propiedades fotofísicas y fotoquímicas de alcaloides de la familia de las β-carbolinas con miras a comprender su potencial rol biológico.

En resumen, este volumen de Anales de la Asociación Química Argentina es solo una fracción del desarrollo que ha tenido la fotoquímica a lo largo y a lo ancho de la República Argentina en una amplia diversidad de áreas. Sin bien este número especial no abarca a todos los centros se investigación, consideramos que es un puntapié inicial para poder abarcar en su totalidad a aquellos grupos de investigación que hacen de la fotoquímica su objeto de estudio y herramienta de trabajo.

Dra. Natalia L. Pacioni y Dr. Juan E. Argüello

Editores Invitados

NOTE FROM GUEST EDITORS

Light as an integral part of chemistry research, in its various areas, has shown intermittent growth throughout history. Although its beginnings date back to the late 19th century with the pioneering works of Italian Giacomo Ciamician, the rise of Photochemistry occurred only from the 1960s, and particularly in Argentina, it increased around the 1990s. Thus, it could be said that Photochemistry in Argentina is still in its infancy as a growing and diverse area of research.

In this special issue, with the representation of research centers in different regions of the country, we have contributions that detail light as part of chemical and physical transformations, with importance in different fields such as photophysical studies, as a tool in environmental remediation, organic synthesis, and photobiology.

First, Lagorio et al. from CABA examine chlorophyll-a fluorescence to obtain information about the photosynthetic activity and its application to study the effects on pollution or environmental stress. Then, Milanesio et al. from Río Cuarto evaluate different kinds of photosensitizers, including synthesis and characterization, as antimicrobial agents and Borsarelli et al. from Santiago del Estero review the applications of supramolecular photosensitizers. In turn, Caregnato et al. from La Plata address the photoluminescence of silicon nanoparticles of 1 to 4 nm in diameter as potential markers and photosensitizers. Subsequently, Massad et al. also from Río Cuarto, focus on photodegradation, direct or mediated by Riboflavin, of pesticides and antiparasitic pollutants. In Córdoba, Bardagi et al., present modern approaches to the use of photochemistry as a tool in organic synthesis, whose use has been increased in recent years by the community of Organic Chemistry at an international level. Finally, while Thomas et al. from La Plata, summarize the photosensitized degradation of biomolecules such as DNA, proteins, and lipids by pterin derivatives, Cabrerizo et al. from Chascomús, study the photophysical and photochemical properties of alkaloids of the family of β-carbolines to understand their potential biological role.

In short, this volume of "Anales de la Asociación Química Argentina" shows only a fraction of the development that photochemistry has throughout the República Argentina in a wide variety of areas. Although this special issue does not cover all the research centers, we consider it an initial kick-off to be able to fully encompass those research groups that make photochemistry their object of study and work tool.

Dra. Natalia L. Pacioni y Dr. Juan E. Argüello

Guest Editors

Anales de la Asociación Química Argentina

División Jóvenes Profesionales

Mini-Review

PHOTOCHEMISTRY AND PHOTOPHYSICS OF BIOLOGICAL SYSTEMS. CHLOROPHYLL FLUORESCENCE AND PHOTOSYNTHESIS

Juan M. Romero[1,2], Rocío Torres[1,2], Brian Ospina Calvo[1], Virginia E. Diz[2], Analía Iriel[3], Gabriela B. Cordon[4,5] and M. Gabriela Lagorio[1,2,*]

[1]CONICET, Universidad de Buenos Aires, INQUIMAE, Facultad de Ciencias Exactas y Naturales, Buenos Aires, Argentina.

[2]Universidad de Buenos Aires, Facultad de Ciencias Exactas y Naturales, Dpto. de Química Inorgánica, Analítica y Química Física, Ciudad Universitaria. Pabellón II, 1er piso, C1428EHA, Buenos Aires, Argentina

[3]CONICET, Universidad de Buenos Aires, Instituto de Investigaciones en Producción Animal (INPA), Facultad de Ciencias Veterinarias, Buenos Aires, Argentina.

[4]Universidad de Buenos Aires, Facultad de Agronomía, Área de Educación Agropecuaria, Buenos Aires, Argentina.

[5]CONICET, Universidad de Buenos Aires, Instituto de Investigaciones Fisiológicas y Ecológicas Vinculadas a la Agricultura (IFEVA), Buenos Aires, Argentina.

**Autor Corresponsal: mgl@qi.fcen.uba.ar*

Graphical abstract

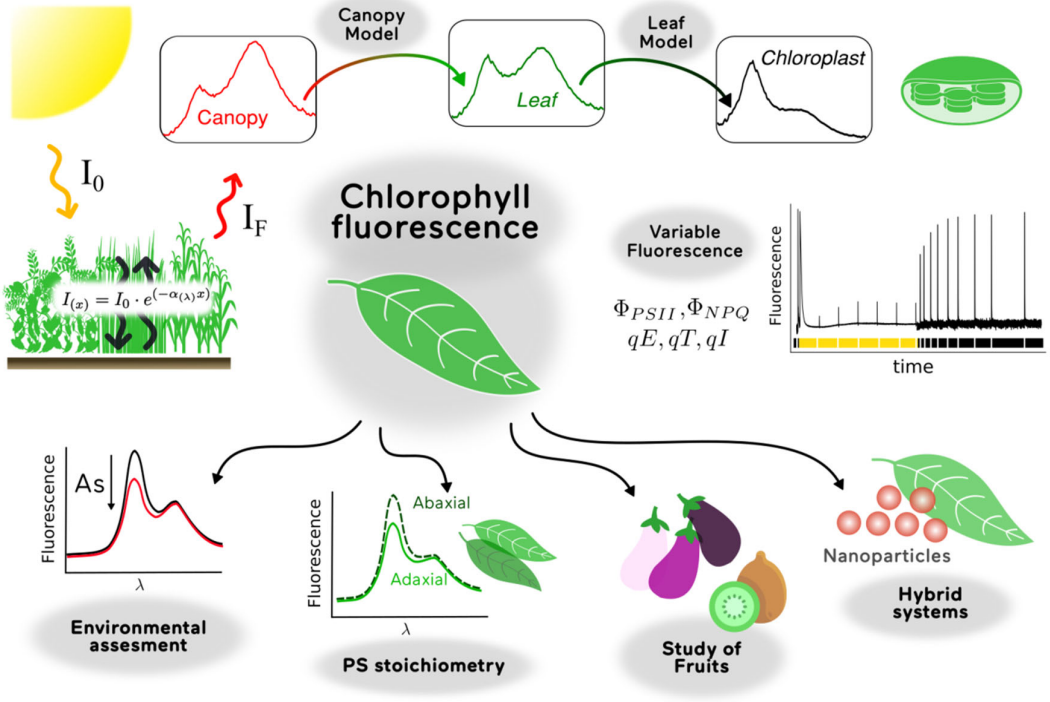

Resumen

El análisis de la fluorescencia de la clorofila−a en plantas permite obtener información relevante sobre la actividad fotosintética. La clave que conecta la fotosíntesis con la fluorescencia se encuentra en la competitividad de los procesos que conducen a la desactivación de la clorofila, una vez que ésta es excitada por absorción de luz o transferencia de energía. Efectivamente, son tres los procesos que compiten entre sí: i) cesión de electrones desde el estado excitado, que inicia el transporte electrónico de la cadena fotosintética, ii) disipación de calor y iii) emisión de la fluorescencia. En este trabajo se presenta una revisión de las metodologías usadas en el análisis de la fluorescencia de la clorofila−a en distintos materiales fotosintéticos, tanto a nivel de laboratorio como de campo y se explican modelos físicos para corregir distorsiones por procesos de reabsorción de luz. Se introduce cómo puede obtenerse información sobre el efecto de la contaminación o estrés ambiental sobre la salud de cultivos a partir del análisis de la emisión fluorescente. Se resumen los principales logros de nuestro grupo de investigación tanto para medios naturales como para sistemas híbridos constituidos por material fotosintético con nanopartículas incorporadas.

Abstract

The analysis of chlorophyll−a fluorescence in plants allows obtaining relevant information about the photosynthetic activity. The key that connects photosynthesis with fluorescence is provided by the competitiveness of the processes that lead to the deactivation of chlorophyll, once it is excited by light absorption or energy transfer. In fact, there are three competing processes: i) transfer of electrons from the excited state, which initiates the electronic transport of the photosynthetic chain, ii) heat dissipation and iii) emission of fluorescence. This paper presents a review of the methodologies used in the analysis of chlorophyll−a fluorescence for diverse photosynthetic materials; both at laboratory and field level, and physical models to correct distortions by light re-absorption processes are explained. It introduces how information on the effect of pollution and/or environmental stress on the health of crops can be obtained from the analysis of the fluorescent emission. The main achievements of our research group are summarized, both for natural media and for hybrid systems constituted by photosynthetic material with incorporated nanoparticles.

Palabras clave: *fluorescencia de clorofila, monitoreo remoto, fotosíntesis, fotosistemas, reabsorción de luz.*

Keywords: *chlorophyll fluorescence, remote sensing, photosynthesis, photosystems, light re-absorption.*

1. Introduction

Red fluorescence from chlorophyll solutions was first observed by Brewster in 1834 and spectroscopically studied by Stokes in 1952 [1,2]. Twenty years later, Müller reported emission from chlorophyll in plants [3]. Later on, in 1931, Hans Kautsky and A. Hirsch found that the quantum yield of chlorophyll fluorescence emitted by leaves varied according to the degree of illumination [4]. Moreover, Kautsky *et al.* could correlate experimentally chlorophyll fluorescence in leaves with the CO_2 assimilation as a function of time [5]. This correlation meant a significant finding since it showed that chlorophyll fluorescence was closely connected with plant photosynthesis. As the analysis of chlorophyll fluorescence may be performed in a non-destructive way, obtaining information on photosynthesis from spectroscopic data has become an attractive and useful tool in the study of plant ecophysiology [6-8], to detect environmental stress [9,10] and in the remote sensing of environment [11-13]. It has also been used to get information about carbon fluxes between plants and the atmosphere which in turn is related to the greenhouse effect and to global warming [14].

The present work presents a review of the methodologies used in the analysis of chlorophyll–a fluorescence covering diverse photosynthetic materials such as chloroplasts, plant leaves, fruits and hybrid systems composed of nanoparticles and plant tissue. The methodologies for measurements at both laboratory and field level are discussed. Corrections of distortions due to light re-absorption processes, which are rare in the literature, are explained in detail and applied to different situations [15].

2. Linking chlorophyll fluorescence with photosynthesis

The light reactions of oxygenic photosynthesis take place in the thylakoid membranes of chloroplasts, where photosystems I and II are located. Both photosystems are protein complexes containing pigments that absorb light and a special pair of chlorophyll-a molecules at the reaction

center. The reaction center of photosystem I (PSI) is called P700 and that of photosystem II (PSII), P680. Surrounding the reaction center is the light-harvesting complex (LHC) or antenna which contains several protein molecules associated with pigments, predominantly chlorophylls, xanthophylls and carotenes. When P680 in PSII is excited by the absorbed light or by the energy transferred from the light harvesting complex, it can transfer one electron to pheophytin (Pheo) (Figure 1) to initiate photosynthesis, it can dissipate the excess energy as heat or it can emit fluorescence. When the plant is adapted to actinic light, an extra mechanism of heat dissipation named non-photochemical quenching (NPQ) takes place. Fluorescence emission from chlorophyll-a in plants can be originated either in PSII or PSI.

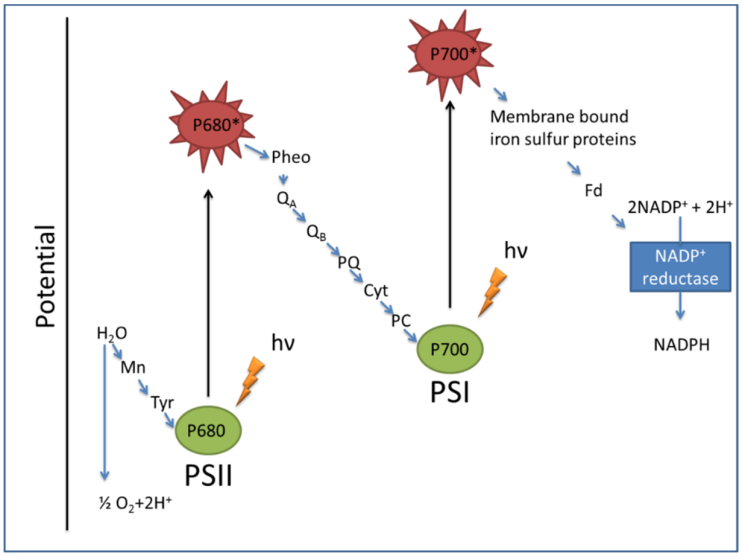

Figure 1. Schematic description of the Photosynthetic process. The abbreviations state for: Mn: Manganese complex bound to PSII, Tyr: a tyrosine in PSII, Pheo: Pheophytin, Q: Quinone, PQ: Plastoquinone, CyT: Cytochrome bf complex, PC: Plastocyanin, Fd: Ferredoxin, P680 and P700 are the reaction centers for PSII and PSI, respectively.

The whole set of physical and chemical processes and the associated kinetics constants affecting the excited P_{680} ($^1P_{680}$*) is schematized in the kinetics reactions given below:

$$P_{680} + h\nu \longrightarrow {}^1P_{680}^* \qquad (1)$$

$$^1P_{680}^* \xrightarrow{k_F} {}^1P_{680} + h\nu_F \qquad (2)$$

$^1P_{680}^*$ $\xrightarrow{k_{ISC}}$ $^3P_{680}^*$ (3)

$^1P_{680}^*$ $\xrightarrow{k_{IC}}$ P_{680} (4)

$^1P_{680}^*$ $\xrightarrow{k_{NPQ}}$ P_{680} + heat (absent in dark-adapted leaves) (5)

$^1P_{680}^*$ $\xrightarrow{k_{PC}}$ Photosynthesis (6)

Chlorophyll-a at the reaction center of PSII (P_{680}) is excited by energy absorption to an electronic singlet state $^1P_{680}^*$ (step 1). This excited state can decay by emitting fluorescence (step 2) or by internal conversion (step 4). It can also undergo intersystem crossing to give rise to a triplet state $^3P_{680}^*$ (step 3). When the photosynthetic organism is adapted to actinic light, dissipation of heat by NPQ is another possible deactivation pathway (step 5). More importantly, $^1P_{680}^*$ can initiate the photosynthetic process: step (6) represents the electron transfer process leading to production of chemical energy and organic matter from CO_2 assimilation. The close relationship between chlorophyll fluorescence and photosynthesis arises from the fact that the photosynthetic process (step 6), the heat dissipation by NPQ (step 5) and the photophysical decay processes which include fluorescence (steps 2, 3 and 4) compete for the same excited state. As a consequence, any increase in one of them should lead to a decrease in at least one of the other two. Furthermore, the presence of photosynthesis is responsible for the variable nature of chlorophyll-a fluorescence in plants.

Steps 2, 3 and 4 represent the basic photophysical decay of $^1P_{680}^*$ and the sum of their respective rate constants ($k_F + k_{ISC} + k_{IC}$) is usually called k_C.

3. Variable Chlorophyll-a fluorescence. Kautsky kinetics

Variable chlorophyll fluorescence is usually recorded by application of a pulse amplitude modulated beam which induces a pulsed fluorescence signal from the sample. In this way, ambient light and non-pulsed fluorescence signal are discarded [16].

The initial fluorescence (F_o) from a dark-adapted leaf recorded with a pulse modulated fluorometer (PAM), under low level of light irradiation, is constant (Figure 2). If a saturating light pulse is then applied, the primary acceptors of electrons in the photosynthetic chain (Figure 1) are reduced and they are not able to accept another electron until they have transferred the received electron to the next acceptor. During this period, the reaction centers are "closed" and the fluorescence emission increases up to a maximum F_m (Figure 2). Then, an actinic light is turned on and fluorescence reaches a peak and then falls to a stationary state, in a process called "fluorescence quenching". Two quenching processes act during the fluorescence decay: i) the photochemical quenching (q_p), which is due to the light-induced activation of enzymes involved in the carbon metabolism and the aperture of stomata and a non-photochemical quenching (q_{Np}), attributed to an increase in heat dissipation [17]. Application of saturating pulses leads to F_m' values, lower than F_m.

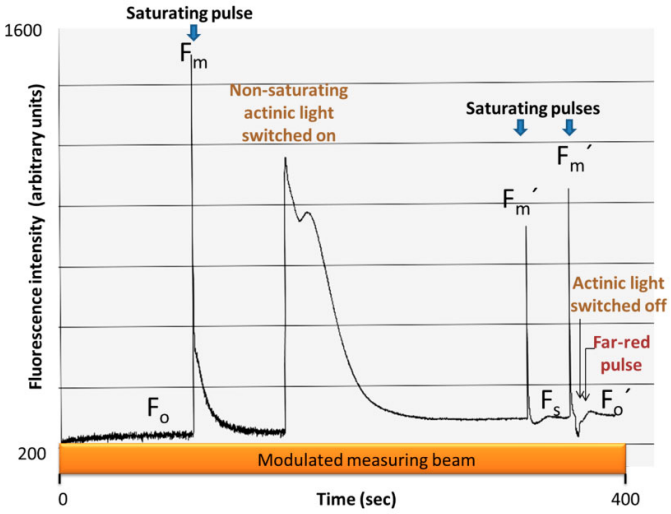

Figure 2. Analysis of variable chlorophyll-a fluorescence. Kautsky kinetics as recorded with a PAM fluorometer.

In a typical experiment, the modulating beam usually consists of pulses of about 1 to 2 μs with long off periods between pulses. The integrated amount of photons that reaches the leaves from

the modulating beam is kept under 0.05 µmol m^{-2} s^{-1}. The saturation pulse, with duration of about 0.5 seconds applies 4000 µmol (photon) m^{-2} s^{-1} on the sample by means of a halogen light. To measure F_o', the actinic light is turned off while simultaneously applying a low intensity pulse of far-red (> 740 nm) light which is preferentially absorbed by PSI and which facilitates the reopening of PSII reaction centers [18].

In order to describe the efficiencies of fluorescence at each point of the curve in terms of mathematical equations, it is useful to define a parameter Q_A which states for the fraction of the oxidized, primary electron acceptor in PSII (equation (7)) [19].

$$Q_A = \frac{[Q_A]}{[Q_A]+[Q_A^-]} \qquad (7)$$

where $[Q_A^-]$ represents the molar concentration of the reduced form of the primary electron acceptor. In dark-adapted leaves, the proportion of Q_A is assumed to be 1 and the reaction centers are said to be open.

The initial fluorescence efficiency may then be written as:

$$F_o = C.\frac{k_F}{[k_F+k_{ISC}+k_{IC}+(k_{PC}*Q_A)]} \quad , \quad \text{with } Q_A = 1 \qquad (8)$$

where *C* is an instrumental factor.

In the maximum, the proportion of Q_A is assumed to approach zero during the saturating pulse (closed reaction centers) and the fluorescence efficiency is given by equation (9).

$$F_m = C.\frac{k_F}{[k_F+k_{ISC}+k_{IC}]} \qquad (9)$$

Application of a saturating pulse to a leaf under actinic light illumination (light-adapted leaf) leads to a maximum value for the fluorescence yield of light-adapted leaves, F_m' (equation (10)).

$$F_m' = C.\frac{k_F}{[k_F+k_{ISC}+k_{IC}+k_{NPQ}]} \qquad (10)$$

It is worth noting that the difference between equation (9) and (10) is the term k_{NPQ} in the denominator which is present only for light-adapted leaves [20].

The steady-state fluorescence (F_s), corresponds to a situation where all the processes are in competition (equation (11)).

$$F_s = C.\frac{k_F}{[k_F+k_{ISC}+k_{IC}+(k_{PC}*Q_A)+k_{NPQ}]},\ 0 < Q_A < 1 \qquad (11)$$

At the end of Kautsky kinetics, F_o' is generally measured by interrupting illumination of the leaf while simultaneously applying a low intensity pulse of far-red (> 740 nm) light which is preferentially absorbed by PSI. The mathematical expression for F_o' is given by equation (12)

$$F_o' = C.\frac{k_F}{[k_F+k_{ISC}+k_{IC}+(k_{PC}*Q_A)+k_{NPQ}]}, \text{ with } Q_A \cong 1. \qquad (12)$$

3. 1. Photosynthetic parameters and energy partition

From the given equations that relate chlorophyll fluorescence with the rate constants of steps 1 to 6, several parameters connected with the photosynthetic activity may be deduced [21].

-*Maximum quantum yield of photosynthesis for dark-adapted leaves* F_v/F_m (equation (13)).

-*Efficiency of PSII,* Φ_{PSII} (equation (14)).

-*Coefficient for the photochemical quenching,* q_P (equation (15)).

-*Coefficient for the non-photochemical quenching,* q_{NP} (equation (16)) and its alternative expression NPQ (equation (17)).

- *Quantum yield of NPQ*, Φ_{NPQ} (equation (18)).

- *Quantum yield of photophysical decay*, Φ_C (equation (19)).

$$\frac{F_v}{F_m} = \frac{F_m-F_0}{F_m} = \frac{k_{PC}}{[k_F+k_{ISC}+k_{IC}+k_{PC}]} \qquad (13)$$

$$\Phi_{PSII} = \frac{F_m\prime - F_s}{F_m\prime} = \frac{k_{PC} * Q_A}{[k_F + k_{ISC} + k_{IC} + (k_{PC} * Q_A) + k_{NPQ}]} \quad (14)$$

$$q_P = \frac{F_m\prime - F_s}{F_m\prime - F_0} \quad (15)$$

$$q_{NP} = \frac{F_m - F_m\acute{}}{F_m - F_0} \quad (16)$$

$$NPQ = \frac{F_m - F_m\prime}{F_m\prime} \quad (17)$$

$$\Phi_{NPQ} = NPQ.\frac{F_s}{F_m} \quad (18)$$

$$\Phi_C = \frac{F_s}{F_m} \quad (19)$$

In particular, equations (14), (18) and (19) express the partition of the energy absorbed by PSII among the different processes: photosynthesis, heat dissipation (NPQ) and photophysical decay (including fluorescence). As it arises from the kinetics mechanism (steps 1 to 6), the sum of the quantum yields of these processes is equal to unity (equation 20).

$$\Phi_{PSII} + \Phi_{NPQ} + \Phi_C = 1 \quad (20)$$

A detailed approach of energy partition in plants was presented by Hendrickson *et al.* (2004) [22] and by Guadagno *et al*. (2010) [23]. The quantum yield of non-photochemical quenching, which was also described in literature as the quantum yield of non-functional reaction centers [22,24] constitutes a plant mechanism of defense against excess energy excitation. It has different contributions: a fast component, qE, which represents the energy dependent quenching, an intermediate quenching, qT, related to a transition state and a slow component, qI, related to the photoinhibition process [25,26].

The activation of qE in higher plants is usually associated to the xanthophyll cycle. Xanthophylls may act as either light-harvesting pigments, or as photoprotectors of photosynthetic organisms from the harmful effects of excessive light. In fact, under high light conditions, there is a decrease in the pH value of thylakoid lumen and in the protonation of proteins at the light harvesting

complex, which leads to the conversion of Violaxanthin into Zeaxanthin. Violaxanthin has a higher S_1 state than Zeaxanthin and while the former can transfer energy to chlorophyll-a in the reaction centers, the latter cannot, thus protecting the reaction centers from excessive light [27-29].

The qT component (state transition related quenching) is connected to the mechanism which redistributes the excitation energy between both photosystems I and II for adequate performance of the linear electron transfer [30]. When PSI is preferentially excited, the light harvesting complex II is associated with PSII and this condition is defined as state 1. However, when light conditions favors PSII excitation (state 2), a pool of the light harvesting complex (LHC) moves from PSII to PSI to balance the differences in light absorption between photosystems. It was suggested that the moving LHCIIs are located near the grana-margins in the state 1, such that migration into the stroma lamellae (in state 2) requires a short travelling distance [31].

Finally, the qI component is usually associated with the damage of the D1 protein [32].

After the induction of variable fluorescence, once the emission reaches the steady state F_o' (Figure 2), the recovery of the signal may be analyzed by applying saturating pulses each minute from the beginning of the dark period (Figure 3) in order to obtain NPQ components [25].

According to Ahn *et al.*, 2009 [25], the value for the fast component ΦqE of the NPQ quantum yield may be calculated from eq. (21)

$$\Phi qE = \frac{Fm'' - Fm'}{Fm''} . \frac{Fs}{Fm'} \qquad (21)$$

and the sum of the intermediate (ΦqT) and slow (ΦqI) components can be calculated from eq. (22).

$$\Phi qT + \Phi qI = \frac{Fm - Fm''}{Fm} . \frac{Fs}{Fm''} \qquad (22)$$

The values of F_m' and F_m'' to be used in equations (21) and (22) are labeled in Figure 3. It may be observed that F_m'' is the value measured at around ten minutes after turning off the actinic light.

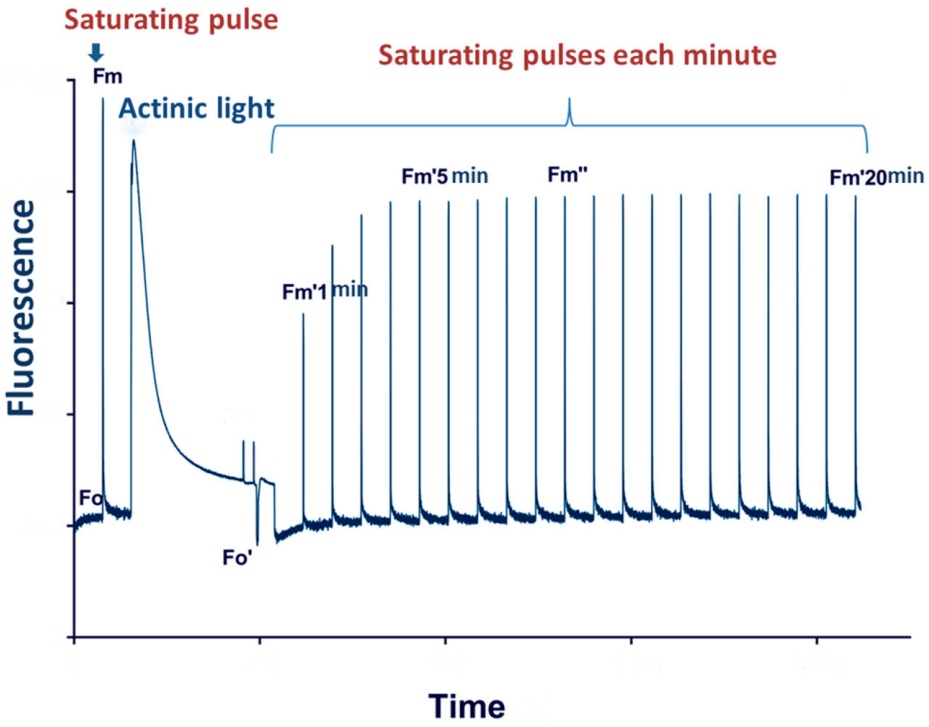

Figure 3. Variable chlorophyll fluorescence recorded by a pulse modulated fluorometer. Complete trace to calculate the photosynthetic parameters presented in equations (13) to (22).

The possibility of inferring information about photosynthesis and on the distribution of energy in plants using a non-destructive methodology makes the analysis of variable chlorophyll fluorescence a tool of great relevance in plant physiology, in evaluation of environmental stress and in agricultural sciences.

3. 2 Corrections of photosynthetic parameters for PSI contributions

Variable fluorescence is reasonably attributed only to PSII since during the evolution from F_o (open reaction centers) to F_m (closed reaction centers), PSII emission appreciably increases while PSI fluorescence is kept constant. It was found that for wavelengths longer than 700 nm, the relative contribution of PSI varied between 30% (for C3 plants) and 50% (for C4 plants) at F_o and 6 to 12% approximately at F_m [33].

Despite this, ignoring the constant contribution of PSI to total fluorescence at room temperature may lead to underestimation of several photosynthetic parameters as F_v/F_m, Φ_{PSII}, NPQ, Φ_{NPQ} and Φ_C, while it has no effect on q_P and q_{NP} [34]. To illustrate this point, the correct equation for F_v/F_m (taking into account PSI contribution) is shown (equation 23)

$$\frac{F_v}{F_m} = \frac{F_m^{PSII} + F_m^{PSI} - (F_0^{PSII} + F_0^{PSI})}{F_m^{PSII} + F_m^{PSI}} = \frac{F_m^{PSII} - F_0^{PSII}}{F_m^{PSII} + F_0^{PSII}} \quad (23)$$

where F_m^{PSI} and F_o^{PSI} were cancelled to account for the fact that there is no variable fluorescence for PSI.

Comparison of equation (23) with equation (13) allows concluding that strictly, F_v/F_m is the maximum quantum yield of PSII, when the contribution of PSI to F_m is negligible.

4. Spectral distribution of chlorophyll fluorescence *in vivo*

At room temperature, fluorescence spectrum of chlorophyll-a in photosynthetic organisms is characterized by two bands: one in the red, F_{red} (around 680 nm) due to PSII emission and one in the far-red, $F_{far\text{-}red}$ (around 730 nm) due to both PSII and PSI emissions (Figure 4) [33,35].

The ratio $F_{red}/F_{far\text{-}red}$ is called the fluorescence ratio and was found to change with environmental stress. As this experimental ratio increases with decreasing chlorophyll concentration, it was proposed in literature as a good inverse indicator of the chlorophyll concentration in leaves [36]. Other authors have shown that this ratio not only depends on chlorophyll concentration but also on photosystems stoichiometry [33,37].

Taking into account the overlap between the emission and absorption spectra, observed fluorescence spectra are usually distorted and the fluorescence ratio is affected by light re-absorption processes within the leaves. Corrections for these processes are possible by using physical models developed in literature (see section Physical models for light re-absorption processes below) [38.39]. Recent works have related the fluorescence ratio corrected by light re-

absorption processes with photosystems stoichiometry [19,40] and with the blockage of electron transfer between PSII and PSI [41].

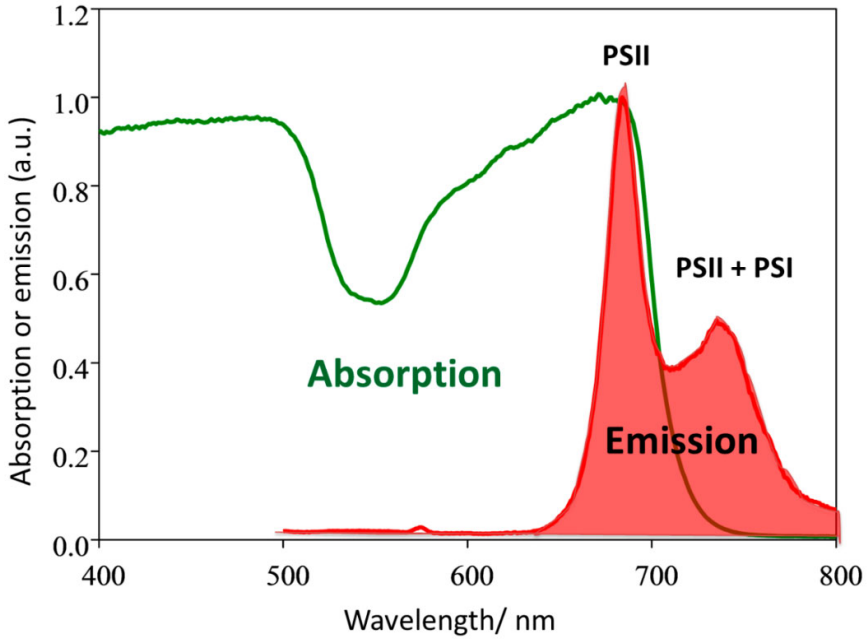

Figure 4. Chlorophyll-a fluorescence spectrum from plant leaves. Overlapping between the absorption and the fluorescence spectra may be observed.

The spectral distribution of fluorescence varies under different light conditions. In fact, the fluorescence ratio $F_{red}/F_{far\text{-}red}$ increases on going from F_o to F_m during the Kautsky kinetics. At F_s the fluorescence ratio is again similar to the value at F_o [42].

The spectral distribution of chlorophyll-a fluorescence at leaf-level is usually recorded with a standard steady-state fluorometer, in front-face geometry, and the signal is expressed in number of photons (counts). As this distribution depends on the photon flux received by the leaves, care should be taken in order to obtain constant spectra in well-defined conditions. Thus, it is recommended to perform experiments either on previously dark-adapted leaves (during at least 15 minutes) under excitation with low photon flux (lower than 20 µmol m^{-2} s^{-1}) as not to induce Kautsky kinetics, or on light-adapted leaves excited with a non-saturating beam of intensity close

to a standard actinic light. In the first case, spectra correspond to the initial fluorescence state F_o (Figure 2) and the second case to the steady-state F_s (Figure 2).

The spectral distribution of fluorescence and the relative contributions of each photosystems are strongly dependent on temperature. Changes in temperature from 25 to 4 °C lead to an increase in both F_{red} and $F_{far\text{-}red}$ and to a decrease of the fluorescence ratio [37].

At extremely low temperature (77 K), emissions from both photosystems are well separated (PSII contributes to the red band and PSI contributes preferentially to the far-red band) [33]. A thorough discussion and revision about emission of both photosystems at 77 K for different photosynthetic organisms was recently performed by Kalaji *et al*. [43].

5. Chlorophyll fluorescence. Field measurements

For the measurement of chlorophyll fluorescence at field level, there are basically two available methodologies: induction of fluorescence directly by sunlight (passive techniques) and induction of fluorescence by artificial light (active techniques) (Figure 5). Within these two large groups, several variants have been developed. Examples are shown below.

5.1 Passive techniques

The signal recorded for the sun-induced chlorophyll fluorescence (SIF) is very weak compared to the light reflected by the plants (only 2-3% of the absorbed radiation). Despite this, it is possible to measure SIF in the absorption lines of the different gases that make up the solar and terrestrial atmosphere. In these bands the irradiance values are lower than in other parts of the spectrum, which makes possible the calculation of fluorescence emission [44].

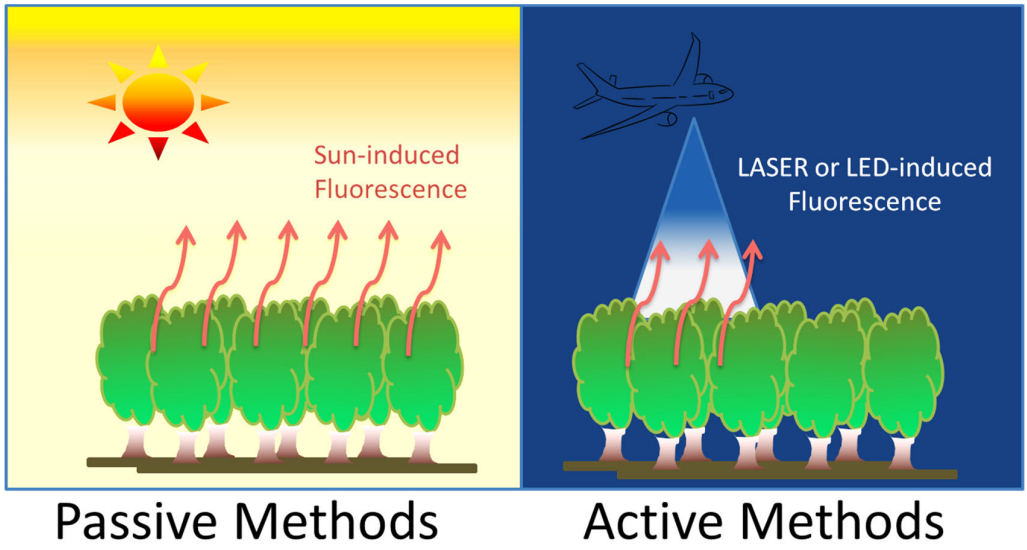

Figure 5. Measurement of chlorophyll fluorescence at field level. In passive methods, the excitation source is the sunlight while in active methods, fluorescence is induced by illumination with an artificial source (LASER, LED, etc.)

Undoubtedly, the most widespread technique for estimating chlorophyll fluorescence at field level is based on measurements of radiance and derives from the principle proposed by Plascyk [45] known as Fraunhofer Line Depth (FLD). This methodology was initially proposed for the dark lines of absorption of the sun and for that reason that denomination was used. Currently, the same designation is kept for the absorption lines of the compounds present in the Earth's atmosphere, although in this case they are not strictly Fraunhofer lines. The FLD and all the methods derived from it: 3FLD, cFLD, iFLD, eFLD, SFM, etc. are based on the comparison of the measured radiance signal within the dark line considered with the signal measured outside it. The usual dark lines are: Hα (solar line) at 656 nm, O_2-B (telluric line) at 687 nm, O_2-A (telluric line) at 760 nm, and K D1 (solar) at 769 nm) [46,47]. In particular, the signal outside the considered line contains background solar irradiance information.

Depending on the method to be applied, the radiance signal outside the considered band is integrated in a close range when the standard method (FLD) is used. In other cases, two (cFLD)

or three (3FLD) wavelength intervals close to the dark line of interest are used. With other methodologies, the full spectral range of the line under study is used as in the iFLD, eFLD and Spectral Fitting Methods (SFM) methods. In practice, measurements of solar irradiance plus radiance of the plant cover are required. Each particular methodology makes different assumptions. However, all of them require measurements with a hyperspectral spectrometer with high spectral and radiometric resolution and elevated signal-to-noise ratio in order to retrieve the fluorescence signal induced by the sun [48].

Fluorescence signals measured with this type of methodologies are usually expressed in physical units of radiance (W m^2 nm^{-1} sr^{-1}). On the other hand, whenever a radiometer is not calibrated, the signal is expressed in arbitrary units. Units are particularly important when comparing measurements at field level by means of a radiometer with measurements performed at leaf level at the lab with a steady-state fluorometer.

A compilation of three papers was recently published with the aim of synthesizing all the knowledge that exists so far to achieve high quality SIF measurements [46,49,50].

According to Cendrero-Mateo *et al.* (2019) [50], field level research is important because it is the basis for the calibration and validation of future satellite missions that will seek to measure SIF from space. The first work to achieve a global and seasonal map of chlorophyll fluorescence from space is the work of Joiner *et al*. [51] that used images from the GOSAT sensor. There are other works that used images of this sensor to evaluate chlorophyll fluorescence globally [52,53] as well as other satellite sensors such as GOME-2 [12] and OCO-2 [54].

5.2 Active techniques

At leaf level, PAM systems have become indispensable instruments in the laboratories of plant physiology. However, there is no active equipment available to evaluate the photosynthetic activity of leaves in forests or even in canopies *in vivo*, at distances greater than a few meters [55]. The first

attempts in this direction were the works of Flexas *et al*. [56,57], and Ounis *et al*. [58], that used modified PAM systems to successfully diagnose water stress in plants. The FIPAM (frequency-induced pulse amplitude modulation fluorimeter) fluorometer was built by Moya *et al.* to measure chlorophyll fluorescence *in vivo* at distances between 0.5 and 6 m, by using a 10 mW laser diode centered at 635 nm as the excitation source [56].

Another equipment of this type is the Multiplex® developed by the Laboratory of Ecology, Systematics and Evolution of the University of Paris-Sud (Orsay, France). It has also been designed to work in field conditions under sunlight. Multiplex® is a multiparameter fluorescence sensor, which uses an optical head with several LEDs (6 UV and 3 RGB) as excitation sources and three synchronized photodiodes to detect the fluorescence signal in the area of yellow, red and far-red of the electromagnetic spectrum [59]. In particular, it has been widely used in research related to precision viticulture [60,61].

Atherton *et al*. (2019) recently developed a new technique to measure the complete spectral distribution (between 650 and 850 nm) of the chlorophyll fluorescence of canopies of red cranberries and wild pines *in vivo* [62]. They used a multicolored 4-in-1 LED arrangement (Red-Green-Blue-White) of 12 W of power as excitation source and all measurements were made overnight which prevented the superposition of the light reflected by the canopies with the chlorophyll fluorescence signal. As a detector, a handheld ASD spectrometer was used.

An alternative to obtain the complete spectral distribution of chlorophyll fluorescence was recently presented by our research group. A closed black box was used to avoid the interaction of plants with sunlight, thus avoiding measurements during the night. In this work, a 3W blue LED light centered on 460 nm was used. Measurements achieved inside the box allowed us to validate a physical model to quantify the effects of the fluorescence re-absorption process within a canopy (See section 6.2) [63].

Our group has also contributed with the estimation of the primary productivity of crops from chlorophyll fluorescence analysis [64,65].

The work of Cordon *et al*. (2006) [64] provides relevant results to the possible alternatives to estimate in a quantitative and non-destructive way the photosynthetic efficiency in the use of radiation (EUR) of plant coverings, a fundamental parameter in the model proposed by Monteith to estimate the primary productivity or C gain of a plant cover [66]. The results suggest that both the photosystem II (Φ_{PSII}) and the apparent quantum yield of sun-induced fluorescence at 760 nm are directly related to the Photochemical Reflectance Index or PRI, which is currently the most promising indicator to estimate the EUR.

The work of Paruelo *et al*. (2019) [65] explores the use of the PRI index under different approaches and at different scales to estimate the EUR from the use of remote sensing in perennial fodder resources of the grassland region of the Río de la Plata. Experiences were carried out to assess the relationship between PRI and SIF at both individual plant and artificial canopy levels [65].

6. Corrections of fluorescence spectra by light re-absorption processes. Physical models

The overlap between the absorption spectrum of plant leaves and the emission spectrum of chlorophyll-a leads to fluorescence re-absorption processes. As a consequence, the red emission band, which is the most affected by this process, suffers a decrease in intensity. Consistently, a reduction in the observed fluorescence ratio takes place. As information about the plant physiological state, the photosystem ratio or obstruction in the electron transfer from PSII to PSI can be derived from the fluorescence ratio, it is essential to correct distortions by light re-absorption processes [67].

6.1 Leaf level

Spectra correction by light re-absorption is not very common in literature and was ignored for many years. Lately, it has been incorporated into studies more frequently. Agati *et al.* developed a theoretical model to correct experimental fluorescence spectra from leaves assuming an infinitesimal layer in the leaf where the excitation beam is attenuated exponentially [38]. According to this model, to get the corrected spectrum, the experimental fluorescence signal from a plant leaf (once corrected by the detector response) is multiplied by a correction factor f (equation 24) which is in turn calculated by equation (25).

$$I_f^c(\lambda) = I_f^e(\lambda).f \tag{24}$$

$$f = \frac{\ln\left(1/(r_{\lambda_0}+t_{\lambda_0})\right)+\ln\left(1/(r_\lambda+t_\lambda)\right)}{\ln\left(1/(r_{\lambda_0}+t_{\lambda_0})\right)} \frac{1-r_{\lambda_0}-t_{\lambda_0}}{1-(r_{\lambda_0}+t_{\lambda_0}).(r_\lambda+t_\lambda)} \tag{25}$$

Where λ and λ_0 denote emission and excitation wavelengths, respectively. The parameters r and t are reflectance and transmittance, respectively.

Later, Ramos and Lagorio applied a correction model based on a two-flux model [71], which was developed previously by Lagorio *et al.* for fluorescent dyes immobilized on inert materials [68-70]. This last method was validated by comparing corrected spectra from leaves with spectra of thin layers of chloroplasts where no appreciable light re-absorption took place [71]. According to this physical approach, to obtain the corrected spectrum, the experimental fluorescence signal from a thick layer of plant leaves which does not transmit light (once corrected by the detector response) is divided by a correction factor γ (see equations 26-27).

$$I_f^c(\lambda) = \frac{I_f^e(\lambda)}{\gamma(\lambda,\lambda_0)} \tag{26}$$

$$\gamma(\lambda,\lambda_0) = \frac{1}{1+\sqrt{\frac{F(R_\lambda)}{F(R_\lambda)+2}}} \cdot \frac{1}{1+\sqrt{\frac{F(R_\lambda)\left(F(R_\lambda)+2\right)}{F(R_{\lambda_0})\left(F(R_{\lambda_0})+2\right)}}} \tag{27}$$

where $F(R_\lambda)$ is the remission function at wavelength λ, calculated by equation (28) from the diffuse reflectance for a thick layer of leaves (R_λ).

$$F(R_\lambda) = \frac{(1-R_\lambda)^2}{2R_\lambda} \quad (28)$$

The correction methods for re-absorption of chlorophyll fluorescence emission in leaves were subject to several controversies in literature. A detailed discussion on the available models to retrieve the spectral distribution of fluorescence at chloroplast level from that at leaf-level has been performed by Cordon and Lagorio (2006) [39].

6.2 Canopy level

A new model to account for light- reabsorption at canopy level was recently published by Romero *et al.* [63] This approach retrieves the spectral distribution of fluorescence at leaf-level ($I_f(\lambda)^c$) from data recorded at canopy level ($I_f(\lambda)^e$). Equation (29) relates both quantities.

$$I_f^c(\lambda) = I_f^e(\lambda).\chi(\lambda, \lambda_0) \quad (29)$$

where $\chi(\lambda, \lambda_0)$ represents the correction factor that takes into account light re-absorption processes within the canopy.

The factor $\chi(\lambda, \lambda_0)$ may be calculated by means of equation (30)

$$\chi(\lambda, \lambda_0) = \left[1 + \frac{\ln \xi(\lambda)}{\ln \xi(\lambda_0)}\right].\left[\frac{1-\xi(\lambda_0)}{1-\xi(\lambda_0)\xi(\lambda)}\right] \quad (30)$$

where $\xi(\lambda)$ may be estimated by equation (31) from experimentally available measures: the reflectance of the whole system (R), the canopy transmittance (T_c) and the soil reflectance (R_b).

$$\xi(\lambda) = R(\lambda) + T_c(\lambda)(1 - R_b(\lambda)) \quad (31)$$

Combination of this model with those developed for plant leaves allows obtaining the spectral distribution at chloroplast level from the fluorescence of the canopy, which represents a valuable tool to get physiological information from remotely acquired data (Figure 6).

6.3. Chlorophyll fluorescence corrected by light re-absorption and its relation with photosystem stoichiometry

As already explained above, at room temperature, the fluorescence band in the red is due to PSII emission and in the far red to the emission of both photosystems. Hence, in the absence of stress processes that interrupt or block electron transport from PSII to PSI, the fluorescence ratio (red/far red) corrected by light reabsorption processes must reflect, in some way, the photosystems stoichiometry. Results in consistency with this hypothesis have been recently presented in bibliography, where chlorophyll fluorescence spectra of photosynthetic organisms grown under different light conditions were analyzed [19,40,72]. In fact, it is already known that excitation of chloroplasts with longer wavelengths which are preferentially absorbed by PSI induces an increase in the amount of PSII and/or its antenna size to balance the energy absorption by both photosystems. This condition is manifested by an increase in the true or corrected fluorescence ratio (red/ far-red) as it was concluded in the cited references.

7. Applications of Chlorophyll fluorescence

7.1 Chlorophyll fluorescence to assess environmental pollution

Chlorophyll fluorescence is related to the photosynthetic activity and plant health, and so it is a valuable tool to reveal the presence of hazardous compounds in the environment. The use of the chlorophyll emission in the evaluation of environmental pollution has numerous advantages: a) it is a non-destructive technique, b) it enables quick, cost-effective and *in situ* determinations for

either organic or inorganic pollutants and c) determinations at lab or field scale are possible. A good review on the application of chlorophyll fluorescence for the assessment of pollutants was presented by Buonasera *et al.* [73]

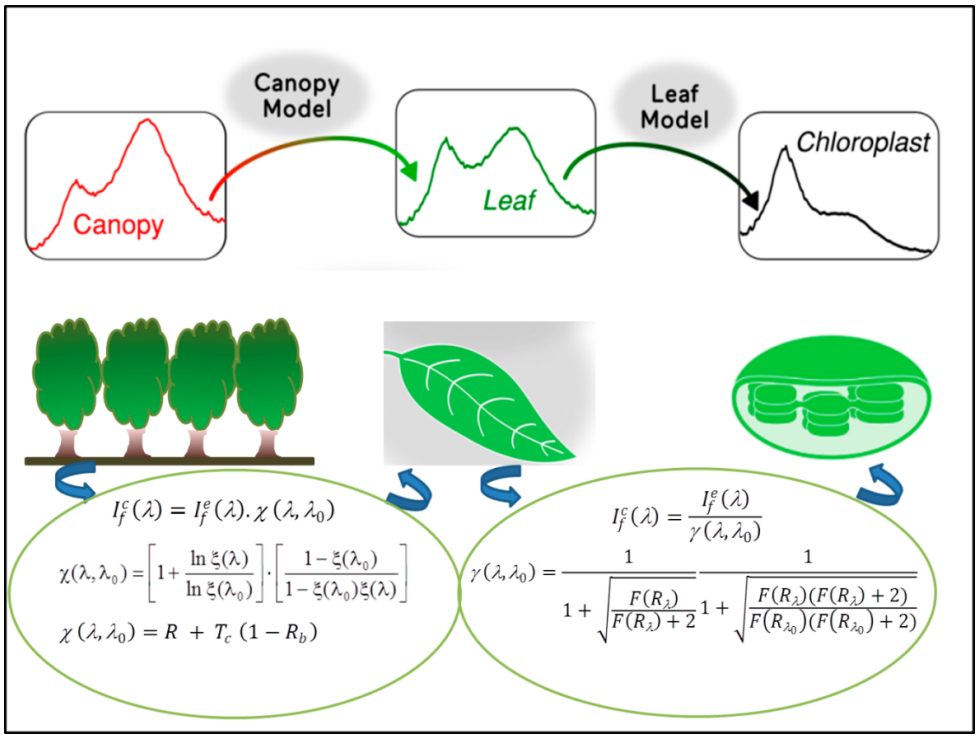

Figure 6. Schematic representation of correction models to account for light re-absorption processes both at canopy and leaf-level.

The presence of micropollutants in environmental matrixes (soil, air and water) may have a natural or anthropogenic origin. In particular, in Argentina, high concentrations of As, V, B and other elements are found due to the Andes volcanic activity and to the application of agrochemicals in the fields. The low environmental concentrations and the complexity of the environmental matrixes turn the evaluation of the pollutant concentrations to be very expensive and time demanding. Additionally, the synergic effects and the ecotoxicological impacts are difficult to be properly evaluated from the standard chemical analyses.

Our group has studied the effect of As in watering of crops growing under different environmental conditions. Arsenic-treated *Cichorium intybus* plants displayed an increase of the fluorescence

ratio when compared with control plants [74]. Taking into account the large land areas cultivated with soybean crop, we have also studied the possibility of use *Glycine max* as a biomonitor to track the presence of natural micropollutants such as As and associated elements [75]. In that study, the simultaneous presence of micropollutants showed a clear synergic effect and the quantum yields of PSII and NPQ turned out to be the most sensitive indicators of chemical stress.

In aquatic plants treated with As, it was observed an opposite behavior regarding steady-state fluorescence spectra: a diminution of the fluorescence ratio was recorded in presence of As for *Vallisneria gigantea* and *Azolla filiculoides* suggesting a preferential damage of PSII [76]. In that study, the quantum efficiency of PSII resulted the more sensitive photosynthetical parameter to monitor the As presence. In another work, a linear relation was found between the arsenic concentration in the media and the fluorescence ratio for *Vallisneria gigantean* plants [77].

The effect of other stressors on the chlorophyll fluorescence of plants has also been studied in our group [41,78,79].

Interestingly, Guo and Tan documented the advances in the application of chlorophyll emission from PSII to the early detection of not only toxic chemicals but also virus and diseases [80].

The variation of the photosynthetic parameters, obtained from the analysis of chlorophyll fluorescence, has been additionally used to state risk assessment for organisms belonging to terrestrial and aquatic environments [81,82].

7.2. Chlorophyll fluorescence and post-harvesting evaluation of fruits

Fruits usually contain chlorophyll during their growth. Some of them still keep important quantities of this pigment in the harvesting and post-harvesting stages and display variable chlorophyll fluorescence like plant leaves.[83] This feature may be conveniently used to assess their quality during storage.[84-86] In general, these non-destructive methods are based on the observation

of changes in the photosynthetic parameters (F_v/F_m, Φ_{PSII}, etc.), acquired on the intact fruits, as a function of time or storage conditions. PAM fluorometers are currently used for this purpose.

Analysis of chlorophyll fluorescence has been carried out in kiwis,[87] cucumbers,[88] tomatoes,[89] pears,[90] tangerines,[91] bananas,[90] lemons,[92] avocados,[93] strawberries and cantaloupes,[94] among others. In particular, this kind of quality assessment was thoroughly applied in apples.[95-97] A physical model to correct the spectral distribution of fluorescence in Granny Smith apples was published by Ramos and Lagorio [98].

Recently, a thorough analysis and modeling of chlorophyll fluorescence in eggplant fruits was performed in our research group [40].

7.3. Chlorophyll fluorescence in hybrid systems composed of nanoparticles and photosynthetic tissue

The increasing use of nanoparticles in the industry has led to a great release of them into the environment in the last years, and this tendency is expected to be even greater in the next future [99].

The effect of nanoparticles on the biology of plants depends heavily on the size, shape, surface charge and chemical nature of the nanoparticulate system; as well as the type of interaction with the plant which can be either physical or chemical. Due to their nanometric sizes, the potential penetration of biological membranes is very high, the interaction with biota may be really harmful and hence, their environmental impact should be evaluated. In particular, the interaction between nanoparticles and plants or algae has been largely studied and reviewed recently [100-103].

However, the study of hybrid systems not only has an environmental interest. In fact, systems composed by nanoparticles and plant material have been investigated for the potential sensor design [104].

The interaction of nanoparticles with photosysnthetic organisms from a photophysical and photochemical point of view is particularly interesting and appealing.

A comprehensive spectroscopic study for gold nanoparticles (AuNps, average diameter: 10–14 nm) embedded in plants, at both leaf and chloroplast-levels were performed by our group.[105] AuNps quenched significantly chlorophyll fluorescence and also produced a decrease in the fluorescence ratio (reduction in the fluorescence emission of the PSII relative to that of the PSI). Surprisingly, the analysis of Kautsky's kinetics, the rate of oxygen evolution and the rate of photo-reduction of 2,6-dichlorophenolindophenol, led to an apparent increase in the photosynthetic capacity. A detailed analysis showed that there was not such a photosynthesis enhancement. Instead, to fully interpret the results, a new reaction involving electrons transfer from the excited P_{680}^* to AuNPs (in the chemical mechanism described by steps 1 to 6), should be added (Figure 7).

It was additionally verified in that work that chemicals which are able to accept electrons from P_{680}^* can falsify measurements of photosynthetic activity based on oxygen evolution, Hill reaction or chlorophyll fluorescence.

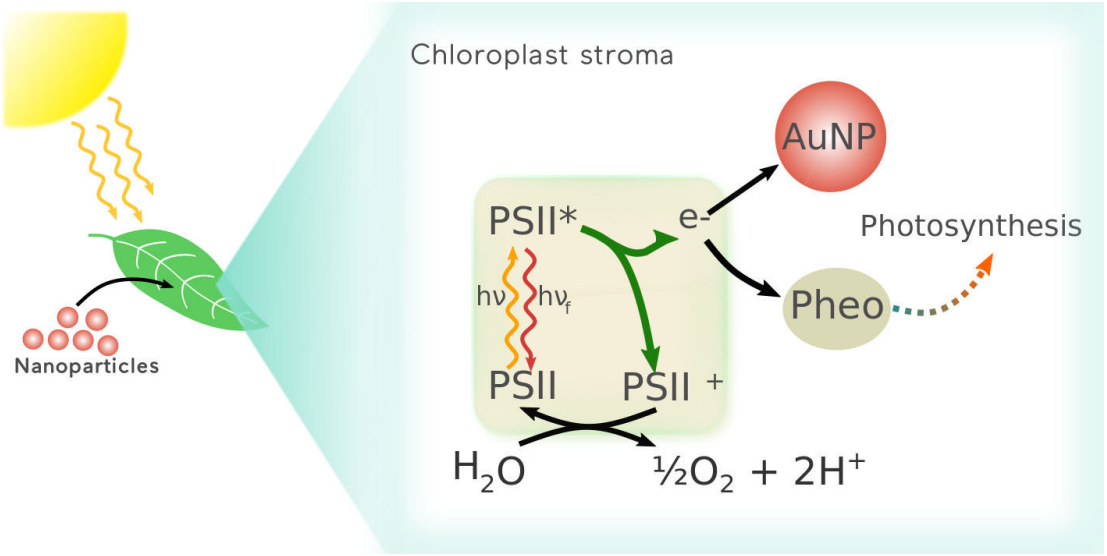

Figure 7. Electron transfer to gold nanoparticles competes with the initiation of the photosynthetic process.

8. Conclusions

In this review we have discussed the analysis of chlorophyll fluorescence in photosynthetic organisms. Very important parameters such as the maximum photosynthetic efficiency (in the dark) and the photochemical, non-photochemical and photophysical yields during actinic irradiation may be evaluated from the variable fluorescence. Energy partition during actinic irradiation –the normal situation for vegetation– is strongly dependent on actinic intensity and this dependence is key to characterizing plant physiology in different environments. Lastly, analysis of the recovery phase after actinic irradiation allows the estimation of different NPQ components, related to the dissipation of heat which plants use as protective mechanism.

Apart from variable fluorescence, the spectral distribution of steady state fluorescence offers additional information. The fluorescence ratio from these spectra is a very popular indicator of environmental stress and has also been related to photosystems stoichiometry. Steady state fluorescence can be measured at leaf scale using a fluorimeter but also, and much more challenging, at field scale by active or passive techniques. Due to the overlap between chlorophyll absorption and emission spectra in the red region, spectral distributions of fluorescence recorded at leaf and field scale are distorted by fluorescence re-absorption processes, which leads to inaccurate interpretations. Our group has made very important achievements to get correction factors for this particular topic.

Finally, by measuring chlorophyll fluorescence and adequately correcting the re-absorption processes it is possible to apply these techniques to a wide variety of situations. We have made contributions to asses environmental pollution (As, V, B), for post-harvesting evaluation of fruits, and for the developing of hybrid systems. Particularly, we have shown how the incorporation of gold nanoparticles affected photosynthesis and fluorescence.

Chlorophyll fluorescence is by far the most promising indicator of plant physiology available nowadays. Due to its direct connection with photosynthesis and regulatory processes, it offers

immediate and detailed information about them. Nevertheless, the chemical and photochemical reactions underlying these processes are so complex that a careful and deep understanding is required to do precise measures and draw accurate conclusions.

Acknowledgments:

The authors are grateful to the University of Buenos Aires (UBACyT20020130100166BA UBACyT20020170100037BA) and to the Agencia Nacional de Promoción Científica y Tecnologica (PICT 2012-2357) for the financial support. JR and RT developed their works with a fellowship from CONICET and BOC from ANPCyT and CONICET. MGL, AI and GBC are Research Members of CONICET (Argentina).

References

(1) Brewster, D. Trans. R. Soc. Edinburgh. **1834**, 12 (2), 538-545.
(2) Stokes, G. G. Philos. Trans. R. Soc. London. **1852**, 142, 463-562.
(3) Müller, N. J. C. Jahrb. Wiss. Bot. **1874**, 9, 42-49.
(4) Kautsky, H.; Hirsch, A. Naturwissenschaften. **1931**, 19 (48), 964-964.
(5) Kautsky, H.; Appel, W.; Amann, H. Biochem. Z. **1960**, 332, 277-292.
(6) Govindjee. Aust. J. Plant Physiol.. **1995**, 22 (2), 131 -160.
(7) Govindjee. Chlorophyll a Fluorescence: A Bit of Basics and History. In: Chlorophyll a Fluorescence. Springer, Dordrecht, **2004**.
(8) Krause, G. H.; Weis E. Annu. Rev. Plant. Biol. **1991**, 42 (1), 313-349.
(9) Murchie, E. H.; Lawson, T. J. Exp. Bot. **2013**, 64 (13), 3983-3998.
(10) Guidi, L.; Landi, M.; Lo Piccolo, E. Front. Plant. Sci. **2019**, 10, 174.
(11) Moya, I.; Cerovic, Z. G. Remote Sensing of Chlorophyll Fluorescence: Instrumentation and Analysis. In: Chlorophyll a Fluorescence. Springer, Dordrecht, **2004**.
(12) Guanter, L.; Zhang, Y.; Jung, M.; *et al*. Proc. Natl. Acad. Sci. **2014**, 111 (14), E1327-E1333.
(13) Disney, M. Remote Sensing of Vegetation: Potentials, Limitations, Developments and Applications. In: Canopy Photosynthesis: From Basics to Applications. Springer, Dordrecht, **2016**.
(14) Grace, J.; Nichol, C.; Disney, M.; Lewis, P. Glob. Chang. Biol. **2007**, 13 (7), 1484-1497.
(15) Lagorio, M. G.; Cordon, G. B.; Iriel, A. Photochem. Photobiol. Sci. 2015, 14 (9), 1538-1559.
(16) Lichtenthaler, H. K.; Buschmann, C.; Knapp, M.; Photosynthetica. **2005**, 43 (3), 379-393.
(17) Maxwell, K.; Johnson, G. N. J. Exp. Bot. **2000**, 51 (345), 659-668.
(18) Zhen, S.; van Iersel, M.W. J. Plant. Physiol. **2017**, 209, 115-122.
(19) Ospina Calvo, B.; Lagorio M. G. Photochem. Photobiol. **2019**, 95 (6), 1360-1368.
(20) Kornyeyev, D.; Hendrickson, L. Functional Plant Biology, **2007**, 34, 214-220.
(21) Genty, B.; Briantais, J-M.; Baker, N. R. Biochim. Biophys. Acta (BBA) - General Subj. **1989**, 990 (1), 87-92.
(22) Hendrickson, L.; Furbank, R.T.; Chow, W. S. Photosynth. Res. **2004**, 82 (1), 73-81.
(23) Guadagno, C. R.; Virzo De Santo, A.; D'Ambrosio, N. Biochim Biophys Acta - Bioenerg. **2010**, 1797 (5), 525-530.
(24) Hendrickson, L.; Förster, B.; Pogson, B. J.; Wah, S. C. Photosynth. Res. **2005**, 84 (1-3), 43-49.
(25) Ahn, T. K.; Avenson, T. J.; Peers, G.; Li, Z.; Dall'Osto, L.; Bassi, R.; Niyogi, K. K.; Fleming, G. R. Chem. Phys. **2009**, 357 (1-3), 151-158.
(26) Derks, A.; Schaven, K.; Bruce, D. Biochim Biophys Acta (BBA)-Bioenergetics. **2015**, 1847 (4-5), 468-485.
(27) Frank, H. A.; Cua, A.; Chynwat, V.; Young, A.; Gosztola, D.; Wasielewski, M. R. Photosynt. Res. **1994**, 41 (3), 389-395.
(28) Niyogi, K. K.; Shih, C.; Chow, W. S.; Pogson, B. J.; Della Penna D.; Björkman, O. Photosynth. Res. **2001**, 67 (1-2), 139-145.
(29) Li, X. P., Müller-Moulé, P.; Gilmore, A. M.; Niyogi, K. K. Proc. Natl. Acad. Sci. USA. **2002**, 99 (23), 15222-15227.
(30) Haldrup, A.; Jensen, P. E.; Lunde, C.; Scheller, H. V. Trends. Plant. Sci. **2001**, 6 (7), 301-305.

(31) Wientjes, E.; Drop, B.; Kouřil, R.; Boekema, E. J.; Croce, R. J. Biol. Chem. **2013**, 288 (46), 32821-32826.
(32) Aro, E. M.; Suorsa, M.; Rokka, A.; *et al*. J. Exp. Bot. **2004**, 56 (411), 347-356.
(33) Pfündel, E. Photosynth. Res. **1998**, 56 (2), 185-195.
(34) Lagorio, M. G. Chlorophyll fluorescence emission spectra in photosynthetic organisms. In: Chlorophyll: Structure, Production and Medicinal Uses. Nova Science Publishers, New York, **2011**.
(35) Franck, F.; Juneau P.; Popovic R. Biochim. Biophys. Acta - Bioenerg. **2002**, 1556 (2-3), 239-246.
(36) Buschmann, C. Photosynth. Res. **2007**, 92 (2), 261-271.
(37) Agati, G. Pure Appl .Opt. **1998**, 7 (4), 797-807.
(38) Agati, G.; Fusi F.; Mazzinghi P.; di Paola M. L. J. Photochem. Photobiol. B Biol. **1993**, 17 (2), 163-171.
(39) Cordon, G. B.; Lagorio M. G. Photochem. Photobiol. Sci. **2006**, 5 (8), 735-740.
(40) Ospina Calvo, B.; Parapugna, T. L.; Lagorio, M. G. Photochem. Photobiol. Sci. **2017**, 16 (5), 711-720.
(41) Iriel, A.; Mendes Novo, J.; Cordon, G. B.; Lagorio, M. G. Photochem. Photobiol. **2014**, 90 (1), 107-112.
(42) Franck, F.; Dewez, D.; Popovic, R. Photochem. Photobiol. **2005**, 81 (2), 431-436.
(43) Kalaji, H. M.; Schansker, G.; Brestic, M.; *et al*. Photosynth. Res. **2017**, 132 (1), 13-66
(44) Porcar-Castell, A.; Tyystjärvi, E.; Atherton, J.; van der Tol, C.; Flexas, J.; Pfündel, E. E.; Moreno, J.; Frankenberg, C.; Berry, J. A. J. Exp. Bot. **2014**, 65 (15), 4065-4095.
(45) Plascyk, J. A. Opt. Eng. **1975**, 14 (4), 144339.
(46) Pacheco-Labrador, J.; Hueni, A.; Mihai, L.; *et al*. Remote Sens. **2019**, 11 (8), 960.
(47) Meroni, M.; Rossini, M.; Guanter, L.; *et al*. Remote Sens. Environ. **2009**, 113 (10), 2037-2051.
(48) Grossmann, K.; Frankenberg, C.; Magney, T. S.; Hurlock,S. C.; Seibt, U.; Stutz J. Remote Sens. Environ. **2018**, 216, 311-327.
(49) Aasen, H.; Van Wittenberghe, S.; Medina, N. S.; Damm, A.; Goulas, Y.; *et al*. Remote Sens. **2019**, 11 (8), 927.
(50) Cendrero-Mateo, M. P.; Wieneke, S.; Damm, A.; Alonso, L.; Pinto, F.; Remote Sens. **2019**, 11 (8), 962.
(51) Joiner, J.; Yoshida, Y.; Vasilkov, A. P.; Middleton, E. M. Biogeosciences. **2011**, 8 (3), 637-651.
(52) Frankenberg C.; Fisher J. B.; Worden J.; Badgley G.; Saatchi S. S.;. *et al*. Geophys. Res. Lett. **2011**, 38 (17), 351-365.
(53) Guanter, L.; Frankenberg, C.; Dudhia, A.; Lewis, P. E.; Gomez-Dans, J.; Kuze, A.; Suto, H.; Remote Sens. Environ. **2012**, 121, 236-251.
(54) Sun, Y.; Frankenberg, C.; Jung, M.; Joiner, J.; Guanter, L.; *et al*. Remote Sens. Environ. **2018**, 209, 808-823.
(55) Osmond, B. Tree Physiol. **2014**, 34 (7), 671-673.
(56) Flexas, J.; Briantais, J-M.; Cerovic, Z.; Medrano, H.; Moya, I. Remote Sens. Environ. **2000**, 73 (3), 283-297.
(57) Flexas, J.; Escalona, J. M.; Evain, S.; Gulías, J.; Moya, I.; *et al*. Physiol. Plant. **2002**, 114 (2), 231-240.
(58) Ounis, A.; Evain, S.; Flexas, J.; Tosti, S.; Moya, I. Photosynth. Res. **2001**, 68 (2), 113-120.
(59) Ghozlen, N. B.; Cerovic, Z. G.; Germain, C.; Toutain, S.; Latouche, G. Sensors. **2010**, 10 (11), 10040-10068.
(60) Bellow, S.; Latouche, G.; Brown, S. C.; , A. Cerovic, Z. G.; J. Exp. Bot. **2013**, 64 (1), 333-341.
(61) Bramley, R. G. V.; Le Moigne, M.; Evain, S.; Ouzman, J.; Florin, L.; *et al*. Aust. J. Grape Wine Res. **2011**, 17 (3), 316-326.
(62) Atherton, J.; Liu, W.; Porcar-Castell, A. Remote Sens. Environ. **2019**, 231 (15), 111137
(63) Romero, J. M.; Cordon, G. B.; Lagorio, M. G. Remote Sens. Environ. **2018**, 204,138-146.
(64) Cordon, G. B.; Lagorio, M. G.; Paruelo, J. M. J. Plant. Physiol. **2016**, 199, 100-110.
(65) Paruelo, J.; Oyarzabal, M.; Cordon, G. B.; Lagorio, M. G.; Pereira Machín, M. Estimación de la eficiencia de la radiación en recursos forrajeros perennes del Uruguay. En: Bases ecológicas y tecnológicas para el manejo de pastizales II, Serie FPTA-INIA, Montevideo, **2019**.
(66) Monteith, J. L. J. Appl. Ecol. **1972**, 9 (3), 747-766.
(67) Rodríguez, H. B.; Mirenda, M.; Lagorio, M. G.; San Román, E.; Acc. Chem. Res. **2019**, 52 (1), 110-118.
(68) Lagorio, M. G.; Dicelio, L. E.; Litter, M. I.; San Román, E. J. Chem. Soc. Faraday Trans. **1998**, 94 (3), 419-425.
(69) Lagorio, M. G.; San Román, E.; Zeug, A.; Zimmermann, J.; Röder, B. Phys. Chem. Chem. Phys. **2001**, 3 (8), 1524-1529.
(70) Rodríguez, H. B.; Lagorio, M. G.; San Román, E.; Photochem. Photobiol. Sci. **2004**, 3 (7), 674-680.
(71) Ramos, M. E.; Lagorio, M. G. Photochem. Photobiol. Sci. **2004**, 3 (11-12), 1063-1066.
(72) Cordon, G. B.; Lagorio, M. G. Photochem. Photobiol. Sci. 2007, 6 (8), 873-882.
(73) Buonasera, K.; Lambreva, M.; Rea, G.; Touloupakis, E.; Giardi, M. T. Anal. Bioanal. Chem. **2011**, 401 (4), 1139 -1151.
(74) Cordon, G. B.; Iriel, A.; Cirelli, A. F.; Lagorio M. G. Chemosphere. **2018**, 204, 398-404.
(75) Iriel, A.; Cordon, G. B.; Cirelli, A. F.; Lagorio, M. G. Ecotoxicol. Environ. Saf. **2019**, 182, 109368.
(76) Iriel, A.; Dundas, G.; Fernández Cirelli, A.; Lagorio, M. G. Chemosphere. **2015**, 119, 697-703.
(77) Iriel, A.; Lagorio, M. G.; Cirelli, A. F. Chemosphere. **2015**, 138, 383-389.
(78) Ferreyroa, G. V.; Lagorio, M. G.; Trinelli, M. A.; Lavado, R. S.; Molina, F. V. Ecotoxicol. Environ. Saf. **2017**, 140, 123-130.
(79) Yaryura, P.; Cordon, G. B.; León, M.; Kerber, N.; Pucheu, N.; Rubio, G.; García, A.; Lagorio, M. G. J. Agron. Crop. Sci. **2009**, 195 (3), 186-196.
(80) Guo, Y.; Tan, J. Photochem. Photobiol. **2015**, 91 (1), 1-14.

(81) González-Naranjo, V.; Boltes, K.; de Bustamante, I.; Palacios-Diaz, P. Environ. Sci. Pollut. Res. **2015**, 22 (9), 6920-6931.
(82) Wilkinson, A. D.; Collier, C. J.; Flores, F.; Negri, A. P. Sci. Rep. **2015**, 5, 17443.
(83) Blanke, M. M.; Lenz, F. Plant Cell. Environ. **1989**, 12 (1), 31-46.
(84) Noh, H. K.; Lu, R. Postharvest Biol. Technol. **2007**, 43 (2), 193-201.
(85) Beaudry, R. M.; Song, J.; Deng, W.; Mir N.; Armstrong P.; Timm E.; Chlorophyll fluorescence: a nondestructive tool for quality measurements of stored apple fruit. In: Proc. International Conference on Sensors for Nondestructive Testing: Measuring the Quality of Fresh Fruits and Vegetables. Vol 56,**1997**.
(86) DeEll, J. R.; Toivonen, P. M. A. Use of chlorophyll fluorescence in postharvest quality assessments of fruits and vegetables. In: Practical Applications of Chlorophyll Fluorescence in Plant Biology. Springer; Boston, **2003**.
(87) Mendes Novo, J.; Iriel, A.; Lagorio, M. G. Photochem. Photobiol. Sci. **2012**, 11 (4), 724-730.
(88) Donnini, S.; Guidi, L.; Degl'Innocenti, E.; Zocchi, G. J. Plant. Nutr. Soil Sci. **2013**, 176 (5), 734-742.
(89) Murkowski, A. Biol. Plant. **2001**, 44 (1), 53-57.
(90) Prange, R. K.; DeLong, J. M.; Leyte, J. C.; Harrison, P. A. Postharvest Biol. Technol. **2002**, 24 (2), 201-205.
(91) Gross, J.; Ohad, I. Photochem. Photobiol. **1983**, 37 (2), 195-200.
(92) Nedbal, L.; Soukupová, J.; Whitmarsh, J.; Trtílek, M. Photosynthetica. **2000**, 38 (4), 571-579.
(93) Woolf, A. B.; Laing, W. A. J. Am. Soc. Hortic. Sci. **1996**, 121 (1), 147-151.
(94) Vargas, A. M.; Kim, M. S.; Tao, Y.; Lefcourt, A.; Chen, Y-R. Safety inspection of cantaloupes and strawberries using multispectral fluorescence imaging techniques. In: 2004 ASAE Annual Meeting. American Society of Agricultural and Biological Engineers; **2004**.
(95) Song J.; Deng W.; Beaudry R. M.; Armstrong P. R. HortScience. **1997**, 32 (5), 891-896.
(96) DeEll, J. R.; Prange, R. K.; Murr, D. P. HortScience. **1995**, 30 (5), 1084-1085.
(97) DeEll, J. R.; Prange, R. K.; Murr, D. P. Postharvest Biol. Technol. **1996**, 9 (1), 1-6.
(98) Ramos, M. E.; Lagorio, M. G. Photochem. Photobiol. Sci. **2006**, 5 (5), 508-512.
(99) de Aberasturi, D. J.; Serrano-Montes, A. B.; Liz-Marzán, L. M.; Adv. Opt. Mater. **2015**, 3 (5), 602-617.
(100) Rastogi, A.; Zivcak, M.; Sytar, O.; Kalaji, H. M.; He, X.; Mbarki, S.; Brestic, M. Front. Chem. **2017**, 5, 78.
(101) Yan, A.; Chen Z. Int. J. Mol. Sci. **2019**, 20 (5), 1003.
(102) Lv, J.; Christie P.; Zhang S. Environ. Sci. Nano. **2019**, 6 (1), 41-59.
(103) Chen, F.; Xiao, Z.; Yue, L. Wang, J.; Feng, Y.; Zhu, X; Wang, Z.; Xing, B.; Environ. Sci. Nano. **2019**, 6 (4), 1026-1042.
(104) Giraldo, J. P.; Landry, M. P.; Faltermeier, S. M.; McNicholas, T. P.; Iverson, N. M.; Boghossian ,A. A.; Reuel, N. F.; Hilmer, A. J.; Sen, F.; Brew, J. A.; Strano, M. S. Nat. Mater. **2014**, 13 (4), 400-408.
(105) Torres, R.; Diz, V. E.; Lagorio, M. G. Photochem. Photobiol. Sci. **2018**, 17 (4), 505-516.

Juan Manuel Romero was born in Buenos Aires, Argentina. He obtained his degree in biology from the Buenos Aires University (UBA) in 2015. In his bachelor thesis, he studied the ligand binding and dimerization rate of lectin Galectin-1, using both experimental and computational techniques. Juan is now working on his Ph. D in Chemistry in UBA through a CONICET scholarship and under the guidance of Dr. María Gabriela Lagorio and Dr. Gabriela Cordon. His doctoral thesis is focused on modeling light interaction with photosynthetic material –mainly plants but also algae- with the aim of using fluorescence as an indicator of physiological state. He is 1st assistant teacher in the Inorganic Chemistry department at UBA and also works with farmers from Santiago del Estero (Argentina) in the development of algae-based sensors for water analysis.

Rocio Torres obtained her Degree in Chemistry in 2016 at the Universidad de Buenos Aires. She is currently a PhD student with a CONICET scholarship at INQUIMAE. She is working on the effect of nanoparticles in photosynthetic systems with a study at the photophysical level under the guidance of Dr. María Gabriela Lagorio and Dr Virginia Diz. In addition, she carries out chemistry teaching and dissemination activities at the Facultad de Ciencias Exactas y Naturales of the Universidad de Buenos Aires.

Brian Ospina Calvo was born in Armenia, Quindío, Colombia. He graduated in 2012 with a degree in Chemistry in the Quindío University (Colombia). In 2019 obtained his Ph.D. degree from Buenos Aires University (Argentina) under the supervision of Professor Maria Gabriela Lagorio. His work was the study of non-photochemical quenching of chlorophyll fluorescence and related photosynthetic parameters in plants and algae. Currently his research interests include: the photochemical processes in biosystems and the chlorophyll fluorescence biomonitoring.

Virginia Emilse Diz was born in Buenos Aires, Argentina. She obtained her degree of Professor in Chemistry and Applied Chemistry in 1984 from INSPT (UTN). She worked in the private activity and as chemistry teacher in public school (Otto Krause) and in public University (UTN) (UBA) between 1984 and 2004. She obtained her chemistry degree in 2004 from UBA. Subsequently, she started her research activities Ad Honorem during 3 years in UBA. Then, she continued her research activities under supervision of Lelia Dicelio, obtaining her PhD in Chemical Sciences (UBA) in 2012. She is presently a Lecturer at UBA. She is interested in the design, characterization and functionalization of nanoparticulate systems, focusing on the photophysical study of photosensitive molecules associated with these nanoparticles, as well as in environmental remediation processes.

Analia Iriel was born in Santa Fe, Argentina in 1975. She received her chemistry degree in 1999 from the University of the Litoral. In 2006 she obtained her PhD at the University of Buenos Aires under the supervision of Enrique San Román. She is currently Associate Professor at the Science and Technology School of the San Martin University. She is an Associate Scientist researcher of CONICET (National Research Council of Argentina). Her current research interests include micropolutants (natural and antropogenic) in environmental matrixes, phytoremediation technologies to remove arsenic from groundwater and non-destructive methodologies to assess environmental risk associated to the presence of plaguicides from agricultural activities.

Gabriela Cordon was born in Mar del Plata, Buenos Aires, Argentina. She received a degree in environmental analysis from National University of San Martín (UNSAM) and obtained her Ph.D degree from University of Buenos Aires (UBA) under the supervision of Prof. M. G. Lagorio. Currently, she is Associate Investigator of CONICET (National Research Council of Argentina), Assistant Professor at Faculty of Agronomy of UBA, member of the Regional analysis and remote sensing laboratory (LART) and of the Agricultural plant physiology and ecology research institute (IFEVA). Her current research interests include the use of chlorophyll fluorescence and reflectance spectroscopy as non-destructive tools for agricultural and environmental monitoring at the leaf, plant and canopy level. Her investigation also focuses on achieving quantitative estimates of the efficiency in the use of radiation in the process of photosynthesis based on non destructive measurements.

María Gabriela Lagorio was born in Buenos Aires, Argentina. She obtained her B.S. (Chemical Sciences) in 1982 at UBA. She worked in the private industry from 1983 to 1987. Subsequently, she started her research activities, obtaining her PhD in Chemical Sciences (UBA) in 1991 under the supervision of Dr. Silvia Braslavsky and Dr. Enrique San Roman. She is presently Professor at UBA and scientist researcher of CONICET. She is the head of the Research Group in Photochemistry and Photobiology in the Department of Inorganic, Analytical and Physical Chemistry/ INQUIMAE (FCEN, UBA). Her research field involves the photophysical and

photochemical study of plant material and hybrid systems and her work is focused on the modeling and analysis of the interaction of light with biological entities.

Anales de la Asociación Química Argentina

División Jóvenes Profesionales

Mini-Review

IN THE WAR AGAINST PATHOGENS: PHOTOSENSITIZERS OPTIMIZATION FOR PHOTODYNAMIC INACTIVATION

Andrés M. Durantini, Natalia S. Gsponer, Daniel A. Heredia, Mariana B. Spesia, M. Gabriela Alvarez, M. Elisa Milanesio*, Edgardo N. Durantini*

IDAS-CONICET, Departamento de Química, Facultad de Ciencias Exactas, Físico-Químicas y Naturales, Universidad Nacional de Río Cuarto, Ruta Nacional 36 Km 601, X5804BYA Río Cuarto, Córdoba, Argentina.

**Autores Corresponsales: mmilanesio@exa.unrc.edu.ar; edurantini@exa.unrc.edu.ar*

Graphical abstract

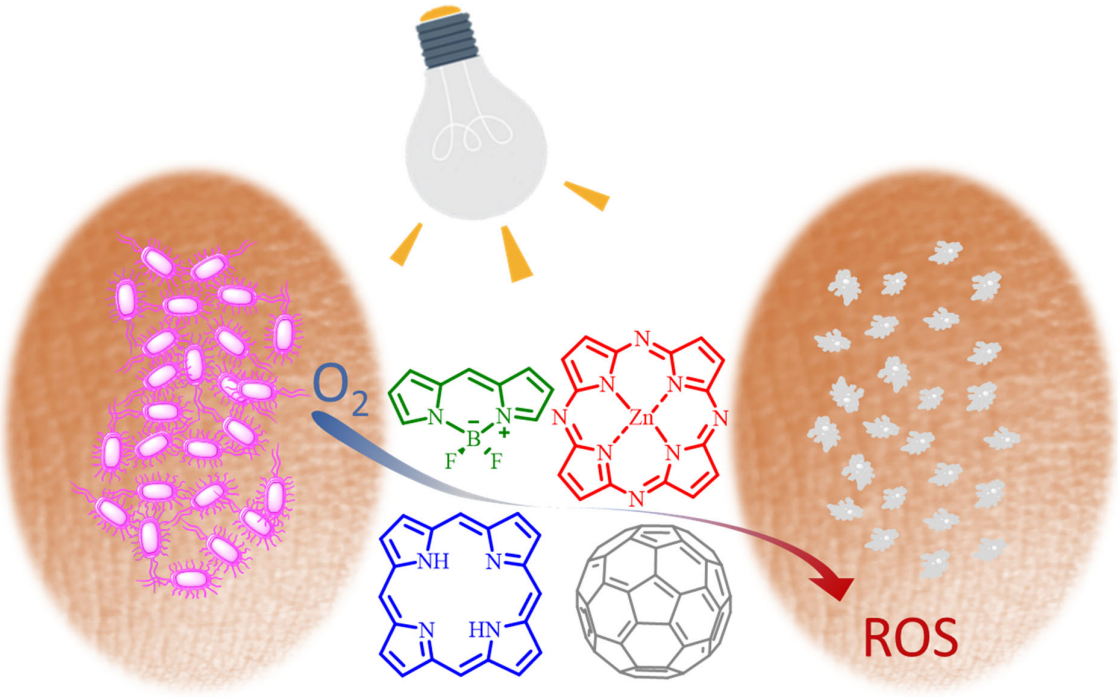

Resumen

Hoy en día, las infecciones causadas por microorganismos son cada vez más difíciles de erradicar debido a la aparición continua de cepas resistentes a múltiples fármacos. En consecuencia, es necesaria la búsqueda de nuevas terapias efectivas. La inactivación fotodinámica (PDI) de los microorganismos ha sido propuesta como una alternativa para controlar las infecciones microbianas. Esta metodología se basa

en la administración de un fotosensibilizador que se une rápidamente a las células microbianas. En aerobiosis, la excitación del fotosensibilizador con luz de una longitud de onda apropiada produce especies reactivas de oxígeno (ROS), las cuales reaccionan con las biomoléculas de las células, conduciendo a la muerte de los microbios. Por lo tanto, el objetivo de esta revisión es examinar las diferentes clases de fotosensibilizadores que se han diseñado, sintetizado, caracterizado y evaluado racionalmente como agentes antimicrobianos en nuestro grupo de investigación. Estos compuestos son principalmente estructuras derivadas de porfirina, clorina y ftalocianina. Además, se han investigado nuevos compuestos de anillo basados en BODIPY y fullereno C_{60} para fotoinactivar microorganismos. Los resultados indican que las moléculas anfifílicas, que llevan cargas positivas intrínsecas o grupos catiónicos precursores, son efectivas como posibles fotosensibilizadores antimicrobianos de amplio espectro. Por otro lado, las principales ventajas que presenta la PDI son que los microorganismos se pueden erradicar en tiempos cortos, el desarrollo de la resistencia en las células objetivo es improbable y se puede evitar el daño a los tejidos del huésped adyacente y a la microflora normal.

Abstract

Nowadays, infections caused by microorganisms are becoming difficult to eradicate due to the continuous emergence of multidrug-resistant strains. Consequently, the search for new effective therapies is awfully necessary. In this way, photodynamic inactivation (PDI) of microorganisms has been proposed as an alternative to controlling microbial infections. This approach is based on the administration of a photosensitizer that rapidly binds to microbial cells. Under aerobiosis, excitation of the photosensitizer with light of an appropriate wavelength produces reactive oxygen species (ROS). These ROS react with the biomolecules into de cells, leading to the microbes death. Therefore, the goal of this review is to survey the different classes of photosensitizers that have been rationally designed, synthesized, characterized, and tested as antimicrobial agents in our research group. These compounds mainly involve porphyrin, chlorin, and phthalocyanine derivatives. In addition, new ring structures based on BODIPY and fullerene C_{60} have been investigated to photoinactivate microorganisms. The results indicate that amphiphilic structures, bearing intrinsic or precursor of cationic charges, are effective as potential broad-spectrum antimicrobial photosensitizers. The main advantages of PDI are that microorganisms can be eradicated in a very short time, resistance development in the target cells is improbable and damage to adjacent host tissues and disruption of normal microflora can be avoided.

Palabras Clave: *fotosensibilizadores, especies reactivas de oxígeno, inactivación fotodinámica, antimicrobianos, microorganismos.*

Keywords: *photosensitizers, reactive oxygen species, photodynamic inactivation, antimicrobial, microorganism.*

1. Introduction

The use of antibiotics to eliminate microorganisms selectively has meant one of the most revolutionary advances made in scientific medicine. However, the advent of resistance to multiple drugs in microbes has posed new challenges for researchers [1]. The main causes of this lack of response are attributed to the inadequate prescription of antibiotics, the failure of some patients to complete the treatments, and the widespread use of antibiotics in livestock feed [2]. This process is aggravated by the administration of antimicrobials in hospitals as a measure of prophylaxis in surgical operations, the tendency to use broad-spectrum antibiotics and self-medication. In addition, the systemic use of antimicrobials negatively affects the normal flora. In this sense, the epidemiologically recognized resistance with high clinical influence involves the Gram-positive pathogen *Staphylococcus aureus* [3]. Furthermore, *Escherichia coli* strains, which in an initial phase were susceptible to conventional antibiotics, started to acquire resistance to antimicrobial treatments [4]. Although fungal infections are not as common as diseases caused by bacteria, they can produce higher mortality [5]. Not only bacteria have developed resistance, but also systemic fungal infections are a very difficult task. The antifungal drug resistance is an important factor causal of therapeutic failure [6]. Thus, *Candida albicans* can produce diseases that involve from superficial mucosal infections to systemic disorders [7,8]. Therefore, the search for new strategies that promote the elimination of resistant microbial cells is of vital importance. These promising anti-microbial include phages, bacteriocins, killing factors, antibacterial activities of non-antibiotic drugs, quorum quenching, and photosensitization [9,10].

This review summarizes the main contribution of our research group, obtained in recent years, to the development of new phototherapeutic agents for application in the PDI of microorganisms.

2. Photodynamic inactivation of microorganisms

Photodynamic inactivation (PDI) of microorganisms has been proposed as an interesting alternative to kill microbes (Figure 1) [11,12]. PDI is based on the addition of a photosensitizer (PS) that quickly binds to microbial cells. After that, the aerobic irradiation of the microorganisms with visible light induces the formation of reactive oxygen species (ROS), which react with the biomolecules in the cells. These reactions produce a decrease in biological functions that lead to cell death.

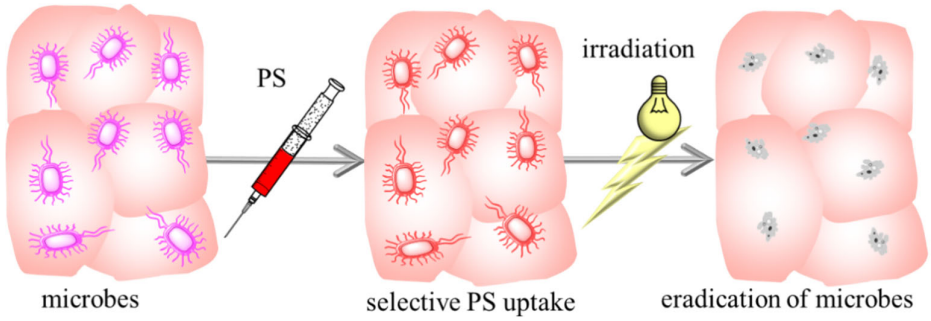

Figure 1. Schematic representations of the PDI of microorganisms.

The studies have shown that Gram-positive bacteria are efficiently photoinactivated by a variety of PSs, whereas Gram-negative bacteria are unaffected by the action of negatively charged or neutral agents [11]. The resistance of Gram-negative bacteria to the action of PSs has been ascribed to the presence of a highly organized outer membrane (OM), which hinders the interaction of the PS with the cytoplasmic membrane and intercepts the ROS [13]. The bacterial envelope is a highly complex multilayered structure that consists of a planar peptidoglycan sheet to which the OM is anchored [14]. The additional membrane layer in the cell wall architecture, which is located outside the peptidoglycan layer, shows an asymmetric lipid structure composed of negatively charged lipopolysaccharides (LPS), lipoproteins and proteins with porin function. Therefore, LPS molecules provides a polyanionic external surface that is partly neutralized by divalent cations Mg^{2+} and Ca^{2+} [15]. Thus, cationic groups on the PS structures produce a tight electrostatic

interaction with negatively charged sites at the outer surface of the Gram-negative bacteria. This effect can increase the photoinactivation induced by the PSs [16]. On the other hand, the fungal wall is composed of β-glucans, chitin and mannoproteins, which confer rigidity and morphology to the cells [12,17]. The layer of β-glucan and chitin provide a permeability barrier, which results in some resistance to the photoinactivation process. The cell envelope of fungi produces a permeability intermediate between Gram-positive and Gram-negative bacteria. Therefore, the photosensitized processes are more significant when agents can penetrate into the inner cell area. Experimental studies have indicated that yeasts can be effectively photokilling *in vitro* by different PSs [18,19]. Consequently, the development of appropriate PSs is very important to improve the efficacy of PDI [20-22].

3. Photosensitizing structures for applications in PDI

The purpose of this section is to review exclusively our original contributions to the design and development of organic PSs derived from pyrrolic macrocycles and fullerenes. To facilitate and fully understand the context of the discussions, we grouped the PSs in five families of compounds: BODIPYs, porphyrins, chlorins, phthalocyanines, and fullerenes.

The wide synthetic flexibility of these PSs allows the perfect "fine-tuning" between the molecular structures and the desired spectroscopic, photodynamic and physical-chemistry properties. Our research has been focused on improving the PSs properties through the appropriate combination of substituent groups on its periphery. Despite the extensive range of PSs, to date there is not a perfect PS that meets all the characteristics to act as an ideal agent. That is the main reason why we continue with the development of different organic compounds that can serve as adequate and efficient PSs.

3.1. BODIPYs

In the recent years, BODIPYs have been proposed as phototherapeutic agents in PDI [23]. The versatility of the synthetic pathways to obtain and modify the BODIPY core allowed the development of suitable PS with adequate properties. The main BODIPY structures are resumed in Figure 2. They were prepared by condensation of the corresponding pyrrole and benzaldehyde derivatives, followed by oxidation with DDQ and complexation with boron [24,25]. Cationic BODIPYs were obtained by exhaustive methylation of the corresponding non-charged BODIPYs. The main structural differences between **1** and **2** are present in the pyrrolic units and the linker between of the cationic center and the *meso*-phenyl group. The 1,7-substituents in **1** prevent the free rotation of the *meso*-aromatic group, while the no β-substitution in **2** gives rise to the free rotation of the *meso*-substituents. In addition, the propoxy bridge in the phenyl substituent of **2** not only provides greater mobility that can facilitate interaction with the cell envelope, but also the charge has a negligible effect on the electronic density of the BODIPY. The positive charge on **1**, **2** and **7** promotes a strong electrostatic interaction with the negative charges of the cell envelope of microorganisms, increasing the efficiency in cell inactivation. An attractive way to promote the ROS generation is by the introduction of bromine and iodine atoms directly attached to the *s*-indacene ring, as is in the case of BODIPYs **5-7** [23]. The replacement of hydrogen at positions 2 and 6 with bromine atoms, through an aromatic electrophilic substitution, promotes a type II mechanism via a heavy-atom effect [25,26]. These bromination reactions were carried out in mild conditions using *N*-bromosuccinimide in trifluorotoluene. Parallel to **5**, the structurally correlated non-halogenated analogue **4** can be used for inspection of the cellular uptake and fluorescence imaging. The presence of the pentafluorophenyl (PFP) group in **4** and **5** can increase the cytotoxicity by binding to amine substituents of membrane-embedded proteins. Furthermore, this group is a versatile platform to introduce a wide variety of nucleophiles via regioselective nucleophilic aromatic substitution

(S_NAr) of the *para*-fluorine atom [27,28]. The PFP group can also be used to bind the fluorophore to polymers or nanoparticles using S_NAr reactions [29].

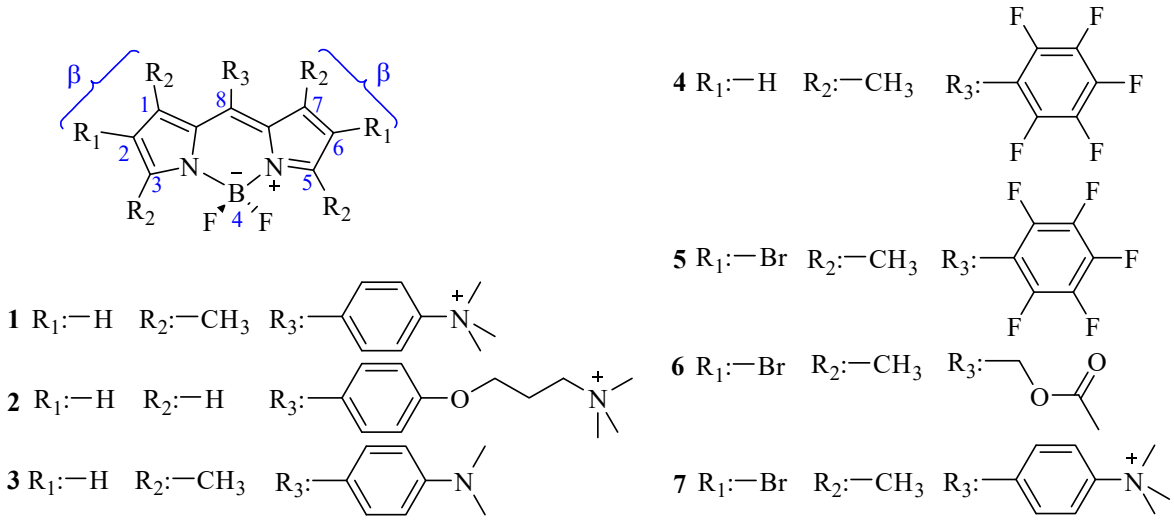

Figure 2. Structures of BODIPYs **1-7**.

3.2. Porphyrins

The synthetic accessibility of porphyrins has allowed the construction of an unlimited number of derivatives with quite elaborate structures and without disproportionate synthetic efforts. The preparation of the symmetric and asymmetric *meso*-substituted porphyrins (5,10, 15, and 20 positions) showed in Figure 3 was carried out using Lindsey's method [30], by condensation of the corresponding dipyrromethane and aromatic aldehyde [31,32]. Cationic porphyrin **8** was obtained by treating porphyrin **9** with methyl iodide. The quaternary ammonium salt in porphyrin **8** could impart water solubility. Porphyrins **10** and **11** present a combination of dimethylaminopropoxy and PFP groups with different patterns of peripheral distribution. The dimethylaminopropoxy substituents act as precursors of cationic centers, since the nitrogen atom in the basic amine group can be protonated at physiological pH [32]. Furthermore, these precursors of the cationic charge are separated from the porphyrin core by a propyl aliphatic chain, which confers a minimal effect on the photophysical properties of the PS. For porphyrins

10 and **11**, the combination of highly lipophilic PFP group and polar amino groups generates an increase in the amphiphilic character of the structure, favoring the interaction and binding to microbial cells. Also, the presence of PFP units can be used as ^{19}F magnetic resonance imaging agents in combination with fluorescence spectroscopy for *in vivo* assays. Similar to BODIPYs **4** and **5**, the PFP group can be used to attach the porphyrin to other system by S_NAr reactions.

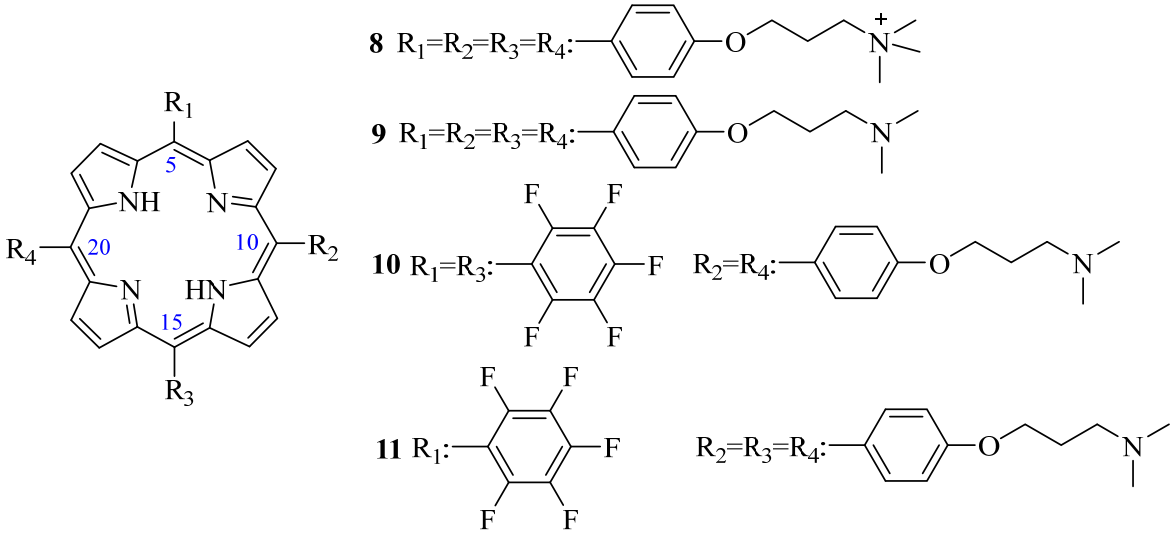

Figure 3. Structures of porphyrins **8-11**.

3.3. Chlorins

An approach to improve the PDI efficacy of porphyrinoids is to enhance the absorption in the red and near-infrared regions (600-900 nm) in order to achieve a deeper light penetration into the soft tissues and blood. Chlorins are promising candidates on account of their strong red absorption and negligible dark toxicity. Structurally, chlorins are derivatives of porphyrins, without two β-pyrrolic protons, i.e. a double bond on the pyrrole of the macrocycle is reduced. In this way, we developed a synthetic design that involved the peripherical substitution of the chlorins with intrinsic positive charges **12** and precursors of the cationic charges **13** (Figure 4) [33,34]. Both PSs were obtained from their analogous A_4-porphyrins by a two-step procedure. First, the symmetrically substituted porphyrins were reduced with *p*-toluenesulfonhydrazide,

producing a mixture of the corresponding chlorin and bacteriochlorin. Then, the bacteriochlorin derivatives were selectively oxidized into the chlorins using *o*-chloranil. The tetracationic PS **12** was obtained by an *N*-alkylation with dimethyl sulfate [33]. Thus, this PS substituted by four cationic groups on the periphery of the macrocycle could facilitate the interaction with the biological membrane. On the other hand, **13** has four basic amino moieties linked through an alkyl chain to the macrocycle, which not only give them higher mobility, but also can acquire positive charges, depending on the medium in which the PS is located.

Chlorin derivative **15** was synthesized by a 1,3-dipolar cycloaddition reaction between *meso-tetra*-(pentafluorophenyl)porphyrin and an azomethine ylide, generated from 4-(*N,N*-dimethylamino)benzaldehyde and *N*-methylglycine. Chlorin **14** was formed like a side product as a consequence of the Strecker degradation of *N*-methylglycine. Chlorin **15** contains a chlorin core incorporating a *syn* adduct of a pyrrolidine-fused ring bearing a C linked *N,N*-dimethylaminophenyl residue. This compound is based on a two-segment molecule, an electron-accepting macrocycle constituted by the *tetra*-substitution of PFP electron-withdrawing groups at *meso* position and an electron-donating *N,N*-dimethylamino group. Taking into account this donor-acceptor structure, a photoinduced electron transfer (PeT) results from the amine moiety to the tetrapyrrolic core. This PeT process has a remarkable effect on the photophysical and photodynamic properties that is going to be discus below. These properties change noteworthy under protonation of the amino segment. Therefore, **15** represents a fascinating PS since protonation of the amino group can be used as an off/on molecular switch [35].

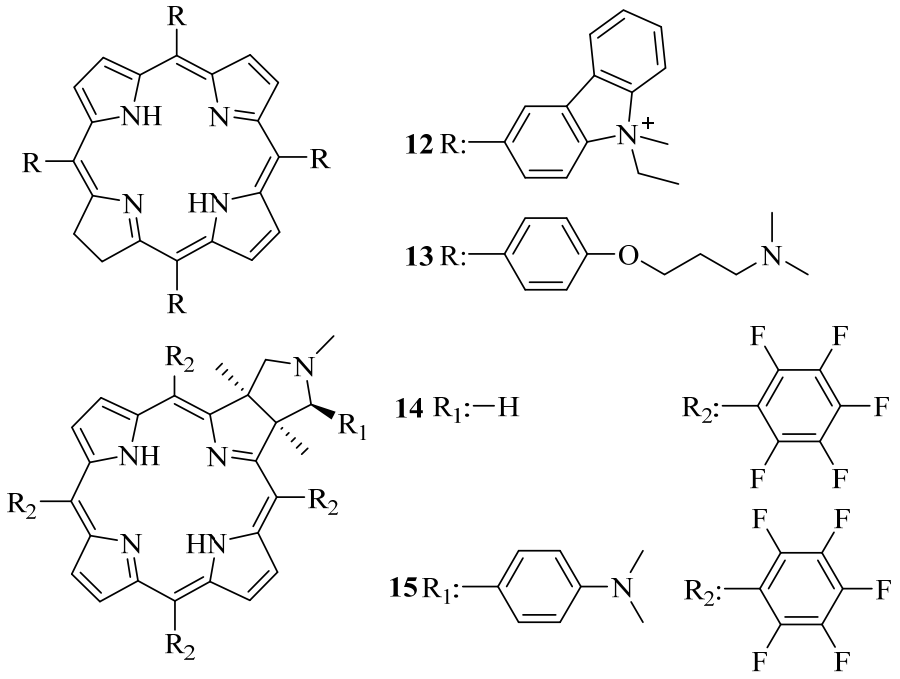

Figure 4. Structures of chlorins **12-15.**

3.4. Phthalocyanines

Other types of aromatic macrocycles with high absorption in the red region are phthalocyanines, which consist of four isoindole units linked by nitrogen atoms. Figure 5 shows some tetracationic metallophthalocyanines synthesized in our research group [36-38]. The presence of cationic moieties can modulate the amphiphilic character of these complexes. This effect also enhances the binding and penetration into the microbial cells. The positively charged phthalocyanines **16-18** were prepared by a three-step procedure. First, a nucleophilic *ipso*-nitro substitution reaction of 4-nitrophthalonitrile by treatment with the corresponding nucleophiles and K_2CO_3 lead to the dinitrile derivative. Then, the cyclotetramerization of those dinitrile with $Zn(OAc)_2$ in the presence of 1,8-diazabicyclo[5.4.0]-undec-7-ene afforded the no charged macrocycle. The last step to obtain the positively charged phthalocyanines was an alkylation reaction using an excess

of methyl iodine. For **16** the last two steps were carried out. Metal complexes **16-18** have a central Zn atom, which favors high triplet quantum yields. In contrast to **16**, phthalocyanines **17** and **18** have four intrinsic positive charges on the outer of the macrocycle, separated by a spacer that allows a minimal influence on the electronic properties of the phthalocyanine. This helps to conserve the photophysical properties of the macrocycle.

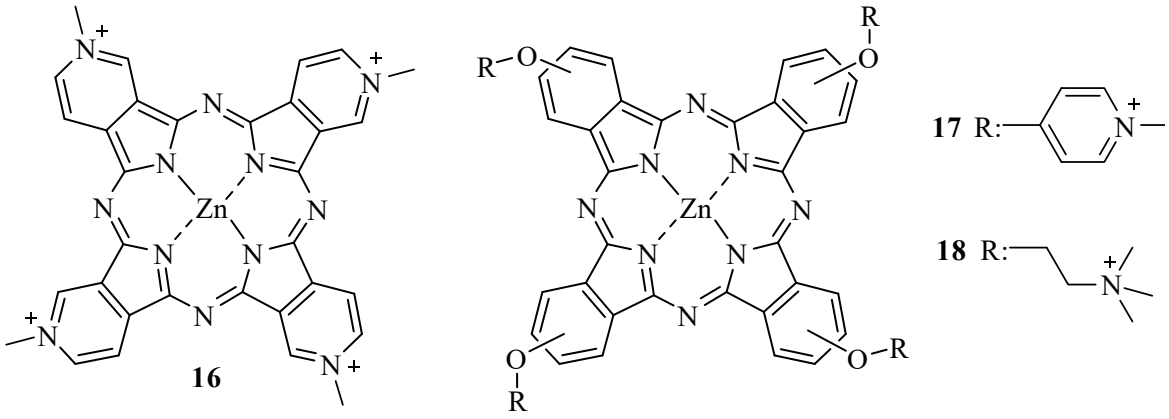

Figure 5. Structures of phthalocyanines **16**-**18**.

3.5 Fullerenes

Fullerenes are nanomaterials constituted solely by carbon atoms. Our research has been focused on developing new fullerene structures derivatized with suitable functional groups to apply in PDI [39]. The structures of several fullerene C_{60} obtained in our group are exhibited in Figure 6. We functionalized the lipophilic sphere by the attachment of functional hydrophilic cationic substituents. Thus, amphiphilic fullerenes C_{60} enhanced the biological activity and therefore are attractive PSs to inactivate a variety of microbial cells. Fulleropyrrolidine derivatives were synthesized by the reaction of fullerene C_{60} with *N*-methylglycine and the corresponding benzaldehyde derivative in refluxing toluene [40,41]. This 1,3-dipolar cycloaddition reaction between azomethine ylides and fullerene C_{60} was developed by Prato and co-workers, and it is one of the most used methods to obtain fulleropyrrolidines [42]. After the Prato reaction, the cationic group was introduced by an exhaustive methylation reaction. The formation of cationic

amphiphilic cycloadduct **24** has similar structural features that PSs described above, where one of the cationic centers is isolated by a propoxy bridge. Thus, this charge has minimal influence on the electronic density of the fullerene [41]. Monoadducts **20** and **22**, non-charged and monocationic compound, respectively, were prepared to compare the spectroscopic and photodynamic properties of the remaining fullerene derivatives. Fulleropyrrolidine **21** has two basic tertiary amine groups that can be protonated and hence it can acquire positive charges, depending on pH where the PS is located. On the other hand, structures **23** and **24** are formed by the hydrophobic carbon sphere containing two intrinsic positive charges that provide an amphiphilic character [40,41].

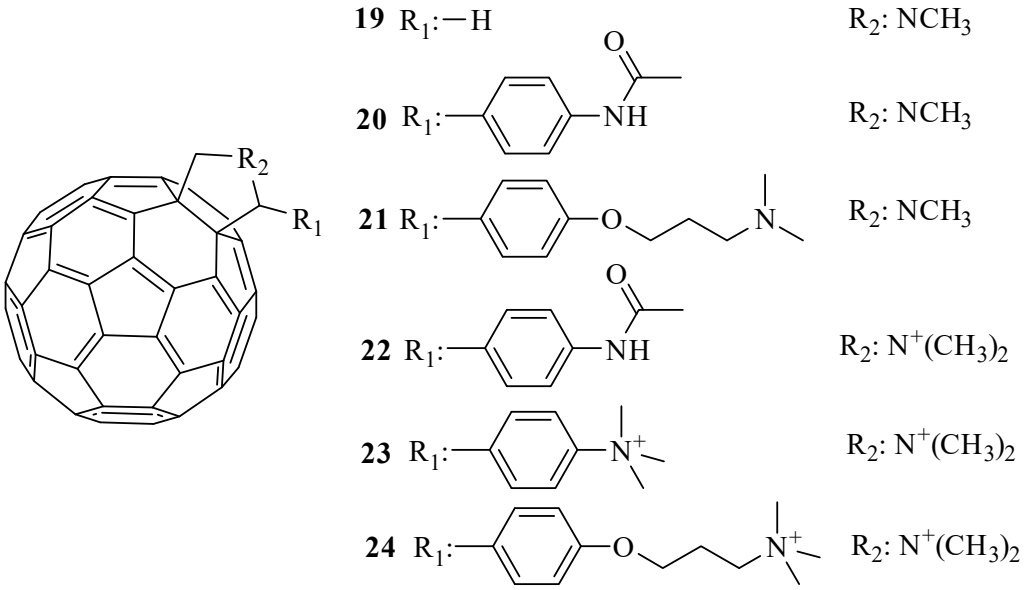

Figure 6. Structures of fullerenes **19**-**24**.

Finally, one drawback of fullerene C_{60} is the low absorption in the visible region [39]. This is a spectroscopic limitation to use them as PSs, especially when deeper light penetration is required. A convenient approach to solve this complication is the development of dyads structures (Figure 7) by covalent bonding between fullerene and light-harvesting antennas, thus improving the absorption in the phototherapeutic windows. In this frame, we made use of porphyrins and BODIPYs as antenna structures to enhance light absorption [43,44]. In addition, they present a vast

flexibility for *post* and *pre*-synthetic functionalization. Both kind of light-harvesting antenna structures have high absorption coefficients and fluorescence emission in the desired wavelengths. Porphyrin-linked fullerene C_{60} dyad **25** was synthesized starting from the AB_3-porphyrin, which was efficiently prepared from a binary combination of aromatic aldehydes and a suitable dipyrromethene [43]. Then, porphyrin bound to fullerene C_{60} was obtained by a 1,3-dipolar cycloaddition between AB_3-porphyrin and fullerene in presence of sarcosine (Prato's reaction conditions). Moreover, porphyrin core **25** is linked to peripherals carbazole moieties that are useful light-harvesting antenna at lower wavelengths. The dyad structure **25** was the precursor to prepare the tetracationic dyad **26** by methylation of the nitrogen atoms in the carbazole units and pyrrolidinic ring [43]. In the structure of dyad **27,** the BODIPY was covalent attachment to fullerene C_{60} through an *N*-methylpyrrolidinic ring (Figure 7) [44]. The first synthetic step to obtain **27** was a Vilsmeier-Haack formylation at the 2 position of BODPY **3**. Subsequently, the submission of the mono-β-formylated BODIPY to a 1,3-dipolar cycloaddition reaction with fullerene C_{60} in presence of sarcosine afforded dyad **27**.

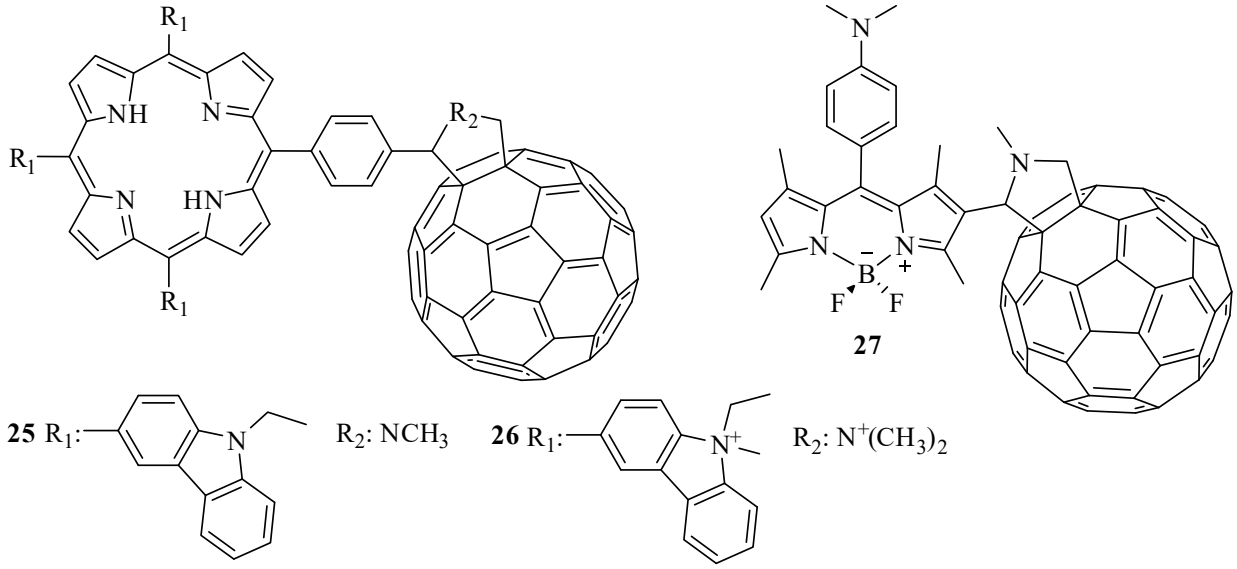

Figure 7. Structures of dyads **25**-**27**.

4. Spectroscopic properties of PSs

The spectroscopic properties of the different families of PSs are compiled in Table 1 and Table 2. The main absorption band of BODIPYs was attributed to the 0-0 vibrational band of a strong $S_0 \rightarrow S_1$ transitions with high molar extinction coefficients ($\varepsilon \sim 8x10^4$ M^{-1} cm^{-1}) [45,46]. The absorption spectra of **1**-**3** are typical of *meso*-substituted BODIPYs, with the band centered at ~500 nm in *N*,*N*-dimethylformamide (DMF) or acetonitrile (ACN) [24,25]. In the absence of structural modifications, theoretical calculations of these BODIPYs predict that the lowest-lying $S_0 \rightarrow S_1$ excitation is almost exclusively associated with the HOMO→LUMO transition of the π-system [47,48]. The effect of bromine atoms at the 2,6-positions in compounds **5**-**7** produced a bathochromic shift of ~20-40 nm [25,49]. The absorption and fluorescence emission spectra of BODIPYs are almost mirror images of each other, which disclose that the emitting and absorbing species are similar [24,25]. This emission band was assigned to the 0-0 vibrational band of the $S_1 \rightarrow S_0$ electronic transition. These compounds produce green fluorescence emission (Table 1) and the fluorescence quantum yield (Φ_F) decreases in brominated compounds **5**-**7** when compared with the unsubstituted molecules. This decrease in the Φ_F was attributed to the heavy atom effect that facilitates intersystem crossing (ISC) processes. Low fluorescence was found with **3** because the amine group acts as an electron donor producing reductive photoinduced electron transfer (a-PeT) [23]. Thus, methylation of the amine group in BODIPY **1** avoids a-PeT and the fluorescence considerably increases in this fluorophore. The low fluorescence observed in BODIPY **2** can be due to a-PeT and the free rotation of the *meso*-substituents [50,51].

The absorption spectra of porphyrins **8**-**11** are characterized by the typical Soret band at ~420 nm ($\varepsilon > 1x10^5$ M^{-1} cm^{-1}) and the four Q-bands between 515-650 nm (Table 1) [54,32]. The Q-bands of porphyrin involves the transitions $Q_x(0,0)$, $Q_x(1,0)$, $Q_y(0,0)$ and $Q_y(1,0)$ that are associated with D_{2h} symmetry [52,53]. These porphyrins showed the characteristic spectra of the *etio* type [$\varepsilon_I > \varepsilon_{II} >$

$\varepsilon_{III} > \varepsilon_{VI}$]. Fluorescence emission spectra of porphyrins **8-11** present two bands characteristic of porphyrin derivatives, which are centered around 650 and 715 nm. These emission bands correspond to Q_x(0-0) and Q_x(0-1) transitions [32,54]. The values of Φ_F determined for these porphyrins are ~0.1.

Table 1. Photophysical properties of BODIPYs, porphyrins and chlorins.

PS	Solvent	λ_{max}^{abs} (nm)	λ_{max}^{em} (nm)	Φ_F	Φ_Δ	Ref.
1	DMF	502	513	0.29	0.07	24
2	DMF	498	512	0.03	0.03	24
3	DMF	498	512	0.03	0.03	44
4	ACN	512	523	0.98	0.02	25
5	ACN	543	561	0.15	0.75	25
6	ACN	543	562	0.14	0.79	25
7	ACN	524	543	0.15	0.11	25
8	DMF	412	660	0.13	0.49	54
9	DMF	422	660	0.15	0.53	54
10	DMF	418	651	0.09	0.33	32
11	DMF	420	655	0.11	0.36	32
12	DMF	431	656	0.23	0.49	33
13	DMF	421	653	0.15	0.54	34
14	DMF	404	653	0.16	0.42	35
15	DMF	405	653	0.0019	- [h]	35

Absorption spectra of chlorins **12-15** show a higher intensity band around ~420 nm (Soret band, ε>1x10^5 M^{-1} cm^{-1}, Table 1) [33-35]. The Q-bands intensities of chlorins following the sequence $\varepsilon_I > \varepsilon_{VI} \sim \varepsilon_{III} > \varepsilon_{II}$, with an intense Q_x(0-0) band (ε~1x10^4 M^{-1} cm^{-1}). The fluorescence emission spectra of chlorins present two bands around 650 and 725 nm, which were assigned to Q_x(0-0) and Q_x(0-1) transitions. Chlorins **12-14** emits fluorescence with Φ_F~0.2, while the fluorescence emission of **15** was effectively quenched by the attached amine unit. The addition of an acid medium was used to protonate the amino group in **15**, leading to a considerable increase in the fluorescence emission (Φ_F = 0.15) [35].

The absorption spectrum of these phthalocyanines **16**-**18** shows a typical Soret band at ~350 nm and intense Q-bands in the region of ~670 nm (ε>1x10^5 M^{-1} cm^{-1}, Table **2** 2) [36,37]. The fluorescence emission spectra showed two bands in the red spectral region, which are characteristic for similar Zn(II) phthalocyanines. The values of Φ_F of these cationic phthalocyanines (Table **2** 2) are appropriate for the quantification of PSs bound to the microbial cells by fluorescence emission techniques.

Fullerenes **19**-**24** show moderately strong π-π* absorption bands in the UV region [40,41]. In the visible region, a broader range of absorption up to almost 710 nm was observed with a sharp peak at 430 nm (ε~4x10^3 M^{-1} cm^{-1}, Table 2). Also, a very weak broader band characteristic of C_{60} derivatives was detected at 710 nm [55]. Monofunctionalization of the fullerene core influences the electronic structure and leads to a change of the I_h-symmetry of pristine C_{60}, which adapts an effective C_{2v} symmetry. Fluorescence emission spectra of fullerenes showed a band centered at ~715 nm, which are characteristic for similar fulleropyrrolidines [56]. The fluorescence spectrum of *N*-methylfulleropyrrolidine is in agreement with the mirror imaged absorption features [56]. This reflects the fact that the force constants of vibrational levels in the first singlet excited state resemble those in the singlet ground state. The good match of the longest-wavelength absorption and the shortest wavelength emission and the fact that they exhibit the highest oscillator strengths are convincing evidence for an assignment to 0*→0 transition bands. In general, fullerene C_{60} derivatives present a low fluorescence emission due to ISC [57].

The spectra of the dyads **25**-**27** are essentially a linear combination of the spectra of the corresponding moieties, with only minor differences in wavelength maxima and band shapes [43,44]. Thus, the absorption spectra are consistent with only a weak interaction between the moieties in the ground state and both chromophores retain their individual identities. Dyads **25** and **26** show only very weak emission from the porphyrin moiety, indicating strong quenching of the porphyrin excited singlet state by the attached fullerene moiety [43]. In these cases, the energy transfer (EnT) from the locally excited porphyrin singlet state to the C_{60} moiety is an exothermic

process. Also, dyad **27** showed only very weak emission from the BODIPY moiety, indicating strong quenching of the BODIPY excited singlet state by the attached C_{60} moiety [44].

Table 2. Photophysical properties of phthalocyanines, fullerenes and dyads.

PS	Solvent	λ_{max}^{abs} (nm)	λ_{max}^{em} (nm)	Φ_F	Φ_Δ	Ref.
16	pyridine	665	677	0.30	0.50	36
17	DMF	680	686	0.22	0.59	38
18	DMF	678	686	0.24	0.47	38
19	DMF	430	711	$4x10^{-4}$	0.65	44
20	DMF	430	712	$3x10^{-4}$	0.72 [a]	40
21	DMF	430	717	$5x10^{-4}$	0.76	41
22	DMF	429	711	$2x10^{-4}$	0.69 [a]	40
23	DMF	429	710	$5x10^{-4}$	0.07 [a]	40
24	DMF	430	716	$3x10^{-4}$	0.44	41
25	DMF	431	667	$4x10^{-3}$	0.01	43
26	DMF	432	667	$5x10^{-3}$	0.02	43
27	DMF	512	544	$3x10^{-3}$	0.56	44

[a] DMF/water (10%)

5. Photodynamic activity of PSs

PDI requires the interaction of a PS, light of an appropriated wavelength, and molecular oxygen $O_2(^3\Sigma_g^-)$ [12]. The excitation of PS ground state (^{0}PS) with visible light leads to the population of the singlet excited state ($^1PS^*$) (Figure). The lifetime of this intermediate state is relatively short. In addition to losing energy by fluorescence emission or internal conversion, the $^1PS^*$ can undergo rapidly ISC to the long-lived (tens to hundreds of microseconds) excited triplet state ($^3PS^*$). In presence of $O_2(^3\Sigma_g^-)$, the $^3PS^*$ can produce ROS. Two mechanisms are mainly involved after activation of the PS [58]. In the type I pathway, the PS excited triplet state can react with different substrates by electron or proton transfer to form free radicals. These radicals can also interact with $O_2(^3\Sigma_g^-)$ producing ROS, such as superoxide radical anion ($O_2^{\bullet-}$), hydroxyl radical ($HO^\bullet$) and hydrogen peroxide (H_2O_2). In the type II partway, the PS generates singlet molecular oxygen, $O_2(^1\Delta_g)$, by energy transfer (EnT) [59]. Thus, the generation of ROS can simultaneously

occur through type I and type II mechanisms. The ROS generated can rapidly react with a variety of substrates in the cells inducing damage to biomolecules, leading to the death of microbes.

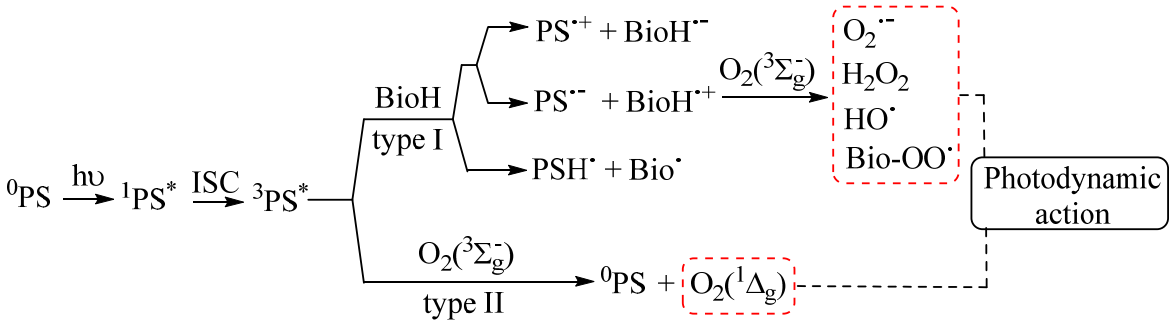

Figure 8. Representation of type I and type II mechanisms.

Table **1** 1 and 2 summarize the $O_2(^1\Delta_g)$ quantum yield (Φ_Δ) for the different PSs. Cationic BODIPYs **1** and **2** photosynthesized $O_2(^1\Delta_g)$ with low Φ_Δ values, in DMF [24]. Nevertheless, the photodynamic activity increases in a microheterogenic medium formed by AOT reverse micelles. Localization of BODIPYs in the micellar interface decreases the vibrational decay, favoring the photosensitization of $O_2(^1\Delta_g)$. Moreover, both BODIPYs were able to produce a rapid photooxidation of L-tryptophan (Trp). A significant contribution of type I mechanism was found for the photodecomposition of Trp by BODIPYs **1** and **2**. In these cases, the addition of KI increases the photoinduced oxidation of Trp. Also, an improvement in the formation of the BODIPY triplet states was observed with the addition of the KI [60]. Iodide anions can increase the formation of triplet excited state by external heavy-atom effect [61]. Besides, the formation of reactive iodine species can be formed in this system [24]. In addition, low values of Φ_Δ were obtained for BODIPYs **3** and in DMF and ACN, respectively [25,44]. The heavy-atom effect in the structure of PSs favors enhancing spin-orbit coupling. Thereby, the presence of bromine in the BODIPYs **5** and **6** improved remarkably the Φ_Δ in ACN. However, the bromination of BODIPY **1** to obtain **7** did not generate an increase of $O_2(^1\Delta_g)$ production, which could be attributed to aggregation of this dye in ACN [25].

Photodynamic activity of porphyrin **9** and its tetracationic derivative **8** were studied in homogeneous media and in microheterogeneous systems [54]. Comparable values of Φ_Δ were obtained for both PSs in DMF, which are quite reasonable values for free-base porphyrins dissolved as monomers. However, the ability to produce $O_2(^1\Delta_g)$ in THF and toluene decreased in presence of cationic porphyrin **8**, which was not dissolved as monomer in these solvents. Moreover, similar values of $O_2(^1\Delta_g)$ formation rates were found for **8** and **9** in water. In addition, both porphyrins photodecompose Trp in water and DMF. In particular, Trp was fast photooxidized by **8** in a biomimetic media formed by AOT reverse micelles. Slightly lower values of Φ_Δ were found for **10** and **11** in DMF [32]. Also, the Φ_Δ values of these PSs agree with those previously reported for free-base porphyrins [62].

Chlorins **12** and **13** were able to photosensitize $O_2(^1\Delta_g)$ with Φ_Δ similar to those found for their porphyrin analogues [33,34]. Therefore, whereas $O_2(^1\Delta_g)$ can be generated effectively by photoexcited chlorins, it was also found that $O_2^{\bullet-}$ was produced especially in the presence of a reductant, such as NADH. Moreover, similar Φ_Δ was found for chlorin **14** in DMF. In contrast, chlorin **15** was unable to attain a triplet excited state in DMF [35]. This amino chlorin derivative was designed as a proton-dependent switchable PS for acidic media. The protonation of the amino group in acid medium leads to a considerable increase in the formation of triplet excited state and $O_2(^1\Delta_g)$ because the PeT from the amine segment to the chlorin macrocycle is inhibited. These results indicate that **15** is an interesting molecular structure, in which protonation of the amino group can be used as an off/on molecular switch capable to produce ROS.

Tetracationic phthalocyanines **16-18** produce efficiently $O_2(^1\Delta_g)$ and these are quite reasonable values for Zn(II) phthalocyanines in solution [37,38]. Faster decomposition of Trp, which was used as a biological substrate model, was obtained using **17** as the PS. Also, Trp can quench $^1PS^*$ by an electron transfer process. Since cationic PSs can bind to this substrate, probably by

electrostatic interaction, an electron transfer pathway may also be contributing together with Type II photoprocess to Trp decomposition in DMF [63].

Non-charged fullerenes **19**-**21** and the monocationic derivative **22** are efficient generators of $O_2(^1\Delta_g)$ [40,41]. Introduction of substituents on the fullerene core produces a decrease in the photodynamic activity respect to C_{60} and it appears that this effect is not significantly dependent on the kind of addend. On the other hand, the production of $O_2(^1\Delta_g)$ sensitized by dicationic fullerene **23** was one order of magnitude lower than those of non-charged fullerene derivatives. This low $O_2(^1\Delta_g)$ production of **23** is probably due to an incomplete monomerization of the cationic fullerene in the DMF/water medium. In contrast, quite reasonable Φ_Δ value was found for fullerene **24**, indicating that this monosubstituted dicationic fullerene is mainly dissolved as a monomer in DMF [41]. Moreover, dicationic fullerenes **23** and **24** were able to generate effectively $O_2^{\bullet-}$ in the presence of NADH. Also, photosensitized decomposition of Trp was investigated in presence of **21** or **24** in DMF. A high photooxidation of Trp were obtained using these fullerenes as PSs. Probably, interactions between these fullerenes and Trp can be favoring an electron transfer process. This behavior is possibly due to an electron transfer pathway may also be contributing, together with type II photoprocess, to Trp decomposition in DMF [41].

In these dyads **25** and **26**, the values of Φ_Δ were strongly dependent on the solvent polarity. These dyads present a higher capacity to form PeT and the electron transfer process competes with the $O_2(^1\Delta_g)$ production depending of the media. In more polar solvent, such as DMF, the $O_2(^1\Delta_g)$ generated by dyads was significantly diminished due to stabilization of charge-transfer state (Table 2) [43]. Thus, depending on the microenvironment where the PS is localized, this compound could produce a biological photodamage through either an $O_2(^1\Delta_g)$-mediated photoreaction process or a free radical mechanism. As opposed to those observed in DMF, dyad **26** photosensitized the formation of $O_2(^1\Delta_g)$ in the AOT micellar system (Φ_Δ~0.5). Two effects can be involved in this different behavior. First, the cationic dyad was partially aggregated in

toluene. Nevertheless, the AOT reverse micelles helped disaggregate the dyad **26**, which results in an increase in the photodynamic activity. Second, even though this dyad interacts strongly with the AOT micelles, due to the high lipophilic character of the fullerene sphere, it is expected that dyad **25** will be located at the micellar interface with the moiety of the C_{60} placed at the nonpolar solvent. Localization of C_{60} in the toluene pseudophase decreases the formation of the charge-separation state, favoring the photosensitization of $O_2(^1\Delta_g)$ from the fullerene triplet state. Therefore, dyads **25** and **26** acted as efficient PS to generate $O_2(^1\Delta_g)$ in this microheterogeneous medium. Studies in the presence of an electron acceptor and an electron donor confirm that dyads **25** and **26** are capable to form a PeT in a polar medium [64]. Furthermore, both dyads produced $O_2^{\bullet-}$ in the presence of NADH, as a biological reducing agent. Although both dyads have a very low production of $O_2(^1\Delta_g)$, they sensitized the photooxidation of Trp. Therefore, both dyads oxidize Trp mainly by type I mechanism of action in DMF containing water. In the dyad **27**, dimethylaminophenyl-BODIPY unit acts as a visible light-harvesting antenna and singlet energy or electron donor, while fullerene C_{60} moiety is the singlet energy or electron acceptor and the spin converter to produce $^3C_{60}{}^*$ [44]. Spectroscopic and redox properties indicate that intramolecular PeT can take place from the dimethylaminophenyl-BODIPY to the fullerene structure. The $O_2(^1\Delta_g)$ production of the dyad was dependent on the solvent polarity. In toluene, BDP-C_{60} produced $O_2(^1\Delta_g)$ with high efficiency, when the BODIPY antenna was selectively irradiated. In a more polar solvent, such as DMF, the formation of $O_2(^1\Delta_g)$ was diminished due to stabilization of charge-separated state according to computational calculations and electrochemical studies. In the presence of TFA, the production of $O_2(^1\Delta_g)$ was similar to that obtained in toluene because protonation of the dimethylaminophenyl group inhibits PeT and increases EnT. In addition, dyad **27** produced $O_2^{\bullet-}$ by type I mechanism and efficiently photooxidized Trp in DMF. Moreover, BDP-C_{60} becomes an effective PS after proton-activated photodynamic effect. These results indicate that the presence of BODIPY as a visible light-

harvesting antenna enhances ROS production by both mechanisms and optimizes the photodynamic action of fullerene C_{60}.

Therefore, ROS production is dependent on the medium and substantially diminishes when the PS is aggregated. Also, the results of the photodynamic properties obtained in solution may not be directly extrapolated to those produced in a biological microenvironment. In consequence, there are limitations to predict the photodynamic activity of PSs in biological media on the based of photophysical investigations in solution.

6. PSs for antimicrobial photoinactivation

Researches on PDI have shown promising results for the eradication of microorganisms. Consequently, the discovery of appropriate PSs is decisive to improve the effectiveness of PDI. In this regard, a large number of potential PSs have been proposed for different pathogens [11,12,23].

BODIPYs derivatives have demonstrated to be efficient PSs against a wide range of microorganisms [22,23]. The photodynamic inactivation mediated by **1** and **2** was investigated on *S. aureus*, *E. coli* and *C. albicans* [24,60]. The photoinactivation induced by these BODIPYs was effective for all of these bacterial strains. After 5 min irradiation, both BODIPYs (1 μM) produced a reduction >5 log in the cell survival of *S. aureus* and after 15 min irradiation complete eradication was obtained. In *E. coli*, these BODIPYs (5 μM) induced a ~2.5 log and ~4.5 log decrease in cell survival after 15 min and 30 min irradiation, respectively. Therefore, the Gram-positive bacterium was inactivated sooner and with a lower concentration of PS than the Gram-negative bacterium. In *C. albicans*, the photodynamic activity of BODIPY **1** yielded a 3.7 log decrease in the cell viability after 30 min irradiation using 5 μM PS. In contrast, BODIPY **2** induced a 0.9 log reduction in the survival of the yeast. However, the addition of KI (50 mM) produced an enhanced photoinactivation of 1.1 log and 3.5 log for BODIPY **1** and **2**, respectively [60]. The greater ISC together with the formation of reactive iodine species induced by

BODIPYs may be contributing to improve the inactivation of microorganisms. Therefore, these BODIPYs represent interesting PSs to inactivate microorganisms. In particular, BODIPY **1** in combination with KI was highly effective as a broad-spectrum antimicrobial PS. Moreover, BODIPYs **2**, **5, 6** and **7** were selected to analyze the phenotypic heterogeneity allowing bacteria to persist during PDI treatment using mainly methicillin resistant *S. aureus* (MRSA) and *E. coli* [25]. PSs efficacy showed that cationic compounds **2** and **7** were outstandingly effective at inactivating Gram-positive and Gram-negative bacteria, including ESKAPE members.

Agents derived from the porphyrin family are one of the most used PSs for PDI. Porphyrin **8** bearing four cationic intrinsic charges was effective to inactivate *E. coli* [65]. Also, photoinactivation mediated by porphyrin **8** and its analogue **9** without intrinsic charges were compared in *C. albicans* [66]. Porphyrin **9** was similarly effective to eradicate *C. albicans* than **8**, indicating that the basic amino groups can be protonated in cellular microenvironments. Porphyrin derivatives **9-11** were investigated to photoinactivate two bacteria strains and a yeast [32]. Specifically, PS **11** achieved a 7 log reduction of *S. aureus* treated with 1 μM PS after 15 min of irradiation. On the other hand, a similar photoinactivation was obtained in *E. coli*, but using 7.5 μM **11** and 30 min of irradiation. When *C. albicans* (~10^6 CFU/mL) cells were incubated with 2.5 μM **11** for 15 min at 37 ºC in the dark and irradiated with visible light for 30 min induced a photoinactivation of 1.5 log decrease. However, when 5 μM **11** was used, the photocytotoxic activity remained elevated with a decrease of 5 log (> 99.999%). Moreover, this porphyrin induced the photodynamic activity mainly through the intermediacy of $O_2(^1\Delta_g)$. In particular, **11** was a highly effective PS with application as a broad-spectrum antimicrobial. This porphyrin contains three basic aliphatic amino groups and it is substituted by a lipophilic PFP group, which confers an amphiphilic character to the tetrapyrrolic macrocycle. This effect can increase the interaction with the cell envelopment, improving the cytotoxic activity against the microorganisms.

The photoinactivation capacity of agents derived from chlorins was dependent on the substituents. Chlorin **12** was poorly effective to induce an efficient photoinactivation of microorganisms [33]. However, chlorin **13** was highly effective PS to be applied as a broad-spectrum antimicrobial [34]. The PDI of chlorin **13** was investigated on *S. aureus*, *E. coli* and *C. albicans* cells. After 15 min irradiation, a 7 log reduction of *S. aureus* was found for cells treated with 1 μM PS. A similar result was obtained with *E. coli* after using a higher concentration (5 μM) and longer irradiation time (30 min). In addition, the photodynamic effect induced by **13** in *C. albicans* using 1 μM PS yielded a ~5 log decrease in the cell viability after 30 min irradiation. For cells treated with 5 μM **13**, a fast decrease of *C. albicans* survival (~5.5 log) was detected after 2 min irradiation with visible light. (> 99.999%). On the other hand, PDI of *E. coli* sensitized by **15** was negligible at neutral pH [35]. However, this chlorin becomes highly effective in inactivating *E. coli* cells under acidic conditions. Although acid pH values are very harsh conditions, some microorganisms can still overcome them even in human gastric juice. Strains of *E. coli* resistant to acid media and antibiotics can be dangerous to human health, inducing diseases in the highly acidic mammalian stomach. Therefore, these results indicate that **15** is an interesting molecular structure in which protonation of amino group can be used as an off/on molecular switch activating red fluorescence emission and photodynamic activity capable of eradicating bacteria.

Phthalocyanines represent an important group of PSs as antimicrobial agents. Previous studies have shown that cationic phthalocyanines are effective PSs against bacteria [36,37]. PDI of *E. coli* and *Streptococcus mitis* sensitized by cationic phthalocyanines **16**-**18** was studied in different media containing blood derivatives [38]. After visible light irradiation, a higher photoinactivation of *E. coli* cells was found for **17**, while **18** was the more effective PS to eradicate *S. mitis* cells. In both bacteria, photoinactivation is possible in presence of human red blood (HRB) cells. Mainly, **18** is effective to photoinactivate *S. mitis* with a low hemolysis of erythrocytes. However, inactivation of *E. coli* by **17** decreases in medium with HRB cells. The presence of

plasma considerably reduces the photocytotoxic effect, which mainly affects the eradication of *E. coli*. However, the PDI of *S. mitis* by **18** is even possible in presence of blood derivatives. Moreover, photoinactivation of *C. albicans* induced by **17** was analyzed using different phthalocyanine concentrations and irradiation periods [67]. Cells treated with 1 μM **17** produced a photoinactivation of 99.99% (~4 log decrease) after 30 min irradiation. Using higher phthalocyanine concentration (>5 μM) no colony formation was detected. These results represent a value greater than 99.999% of cellular inactivation. The accumulation behavior of **17** suggests that mainly an affinity-mediated binding mechanism can be involved. The photodynamic mechanism that occurs in the PDI of *C. albicans* cells mediated by **17** involves the intermediacy of $O_2(^1\Delta_g)$ [68]. Therefore, **17** is an interesting phthalocyanine for PDI of yeasts in liquid suspensions. On the other hand, the photodynamic activity of chlorin **13** and phthalocyanine **17** were investigated as PSs to inactivate *S. aureus* biofilms and prevent their formations in different culture media [69]. It is well-known that most of the bacteria species form biofilm structures, especially in clinical infections [70]. However, PSs **13** and **17** proved to be efficient to prevent and eliminate *S. aureus* biofilms under different environmental conditions. *S. aureus* biofilm was equally PDI susceptible, producing > 99.9% of biofilm inactivation, when was treated with 5 μM PS and 30 min irradiation.

Several fullerene C_{60} derivatives have been designed as potential PSs to inactivate microorganisms [39]. Photosensitized inactivation of *E. coli* cell suspensions by dicationic fullerene **23** exhibits a ~3.5 log decrease of cell survival (99.97% of cellular inactivation), when the cultures are treated with 1 μM PS and irradiated for 30 min. In *C. albicans* suspensions, 10 μM **23** was an effective PS, which produced a ~5 log decrease of cell survival when the cultures were irradiated for 30 min with visible light [71]. Photocytotoxicity activity induced by this dicationic fullerene derivative involves the intermediacy of both $O_2^{\bullet-}$ and $O_2(^1\Delta_g)$. Photosensitized inactivation of *S. aureus* mediated by fullerenes **21** and **24** was investigated using different conditions [41]. Cell suspensions of 10^8 cells/mL incubated with 0.5 μM fullerene

and irradiated for 30 min exhibited 4.4 and 5.0 log decrease of cell survival by **21** and **24**, respectively. Under aerobic condition, the photocytotoxicity activity induced by **24** was mainly mediated by a contribution of type II process [72]. Moreover, photoinactivation of *S. aureus* was possible with **24** in the presence of azide anions under anoxic condition. However, these conditions were not effective to photoinactivate *E. coli*. On the other hand, the addition of potassium iodide produced an increase in the photokilling of bacteria, depending on the KI concentration and irradiation times. The formation of reactive iodine species may be contributing to inactivate *S. aureus* cells photoinduced by **24**.

The photoinactivation ability of dyads **25** and **26** was investigated in *S. aureus* cell suspensions [43]. Photosensitized inactivation of *S. aureus* by dyad **26** exhibits a 4.5 log decrease of cell survival (99.997% cell inactivation), when the cultures are treated with 5 μM PS and irradiated with visible light for 30 min. Under these conditions, a lower photocytotoxic effect was found for **25** (3.2 log decrease). Furthermore, photoinactivation induced by **26** was higher than those obtained with the separate moieties of the dyad. Dyad **25** appears to act in microbial cells mainly through the mediation of $O_2(^1\Delta_g)$, while a contribution of type I mechanism was found for cells death induced by **26** [64]. Therefore, these dyads with high capacity to produce photoinduced charge-separated state represent interesting PSs to inactivate microorganisms by type I or type II mechanisms. In particular, **25** may be located in a non-polar microenvironment into the cells favoring a type II pathway, while a contribution of type I mechanism was produced using the cationic **26**. Moreover, a covalently linked BODIPY-fullerene C_{60} dyad **27** was evaluated to inactivate bacteria [44]. At physiological pH, photosensitized inactivation of *S. aureus* mediated by 1 μM dyad **27** exhibited a 4.5 log decrease of cell survival (> 99.997%) after 15 min irradiation. Similar result was obtained with *E. coli* using 30 min irradiation. Furthermore, proton-activated photodynamic action of **27** turned this dyad into a highly effective PS to eradicate *E. coli*. Therefore, **27** is an interesting photosensitizing structure in which the light-

harvesting antenna effect of the BODIPY unit combined with the protonation of the dimethylaminophenyl group can be used to improve the photoinactivation of bacteria.

7. Conclusions and future directions

The "post-antibiotic" era is near due to the decrease in the effectiveness of conventional antibiotics and other antimicrobial agents. Excessive use of antibiotics in hospitals and agriculture to promote the growth of livestock quickly leads to the proliferation of drug-resistant microorganisms, which are then spread through human travel and poor public health practices. Therefore, it is indispensable the search for alternative therapies to cure antibiotic-resistant infections. In this sense, PDI represents a promising therapy in development with numerous applications in health.

The investigations cited above indicate that several PSs are potential phototherapeutic agents with applications in the treatment of microbial infections. In general, effective PSs for PDI exhibit a high absorption coefficient in the visible region of the spectrum and a long lifetime of $^3PS^*$ to produce efficiently ROS. According to the structure, it can be an advantage the presence of cationic groups or precursors of positive charges in combination with lipophilic substituents to form amphiphilic PSs, which are highly effective as a broad-spectrum antimicrobial. Thus, BODIPY derivatives are very useful and effective PSs to eradicate microorganisms. Moreover, these compounds can be used as fluorophores or therapeutic agents, controlling the balance between the fluorescence emission and the photodynamic activity. In addition, several porphyrins meet these requirements and they have been successfully tested as photokilling agents against microbes. Unlike porphyrins, chlorins and phthalocyanines derivatives show an intense absorption in the red region of the spectrum. This is an important feature in biomedical applications when a deeper penetration of light into tissue is required. In contrast, a possible disadvantage of fullerenes is their optical absorption properties, which is higher in the blue regions of the spectrum. However, this can be solved using a light-harvesting antenna attached to C_{60}, increasing the absorption in the

visible region. The most important favorable property of fullerenes is their rather unusual photochemical mechanism. Fullerenes can act by both kinds of pathways, type I and type II, while tetrapyrrolic macrocycles prove mainly type II photochemistry.

The main advantages of the PDI approach are a fast eradication of microorganisms, a double selectivity, specific accumulation of PS in microbial cells and light delivery to affected area, similar effectiveness to kill microbes regardless of antibiotic resistance and lack of induction of resistance to photodynamic treatments. Moreover, PDI presents several potential applications that involve the inactivation of pathogens in a localized focus of infection, disinfection of microbes in different biological fluids, the formation of permanent antimicrobial surfaces and decontamination of waste effluents and disinfection of polluted water.

Acknowledgments:

Authors are grateful to CONICET, ANPCYT, MINCYT Córdoba and SECYT-UNRC. Authors are Scientific Members of CONICET.

References

(1) Ragheb, M. N.; Thomason, M. K.; Hsu, C.; Nugent, P.; Gage, J.; Samadpour, A. N.; Kariisa, A.; Merrikh, C. N.; Miller, S. I.; Sherman, D. R.; Merrikh, H. Mol. Cell. **2019**, 73, 157-165.
(2) Frieri, M.; Kumar, K.; Boutin, A. J. Infect. Public Health. **2017**, 10, 369-378.
(3) Shrestha, N. K.; Fraser, T. G.; Gordon S. M. Clin. Microbiol. Infect. **2019**, 25, 71-75.
(4) Furusawa, C.; Horinouchi, T.; Maeda, T. Curr. Opin. Biotech. **2018**, 54, 45-49.
(5) Whibley, N.; Gaffen, S. L. Cytokine. **2015**, 76, 42-52.
(6) Criseo, G.; Scordino, F.; Romeo, O. J. Microbiol. Methods. **2015**, 111, 50-56.
(7) Morace, G.; Perdoni, F.; Borghi, E. J. Glob. Antimicrob. Resist. **2014**, 2, 254-259.
(8) Tong, Y.; Tang, J. Microbiol. Res. **2017**, 198, 27-35.
(9) Ghosh, C.; Sarkar, P.; Issa, R.; Haldar, J. Trends Microbiol. **2019**, 27, 323-338.
(10) Durantini, E. N. Virulence. **2016**, 7, 493-494.
(11) Alves, E.; Faustino, M. A.; Neves, M. G.; Cunha, A.; Tome, J.; Almeida, A. Fut. Med. Chem. **2014**, 6, 141-164.
(12) Hamblin, M. R. Curr. Opin. Microbiol. **2016**, 33, 67-73.
(13) Gsponer, N. S.; Spesia, M. B.; Durantini, E. N. Photodiagn. Photodyn. Ther. **2015**, 12, 67-75.
(14) Hernandez Alvarez, B. Bassler, J.; Lupas, A. N. Intern. J. Med. Microbiol. **2019**, 309, 351-358.
(15) Cama, J.; Henney A. M.; Winterhalter, M. J. Mol. Biol. **2019**, 431, 3531-3546.
(16) Durantini, E. N. Curr. Bioact. Compd. **2006**, 2, 127-142.
(17) Gow N. A. R.; Hube, B. Curr. Opinion Microbiol. **2012**, 15, 406-412.
(18) Calzavara-Pinton, P. G.; Venturini, M.; Sala, R. J. Photochem. Photobiol. B: Biol. **2005**, 78, 1-6.
(19) Pereira Gonzales, F.; Maisch, T. Fungal Biol. **2012**, 116, 1-10.
(20) Alves, E.; Faustino, M. A. F.; Neves, M. G. P. M. S.; Cunha, Â.; Nadais, H.; Almeida, A. J. Photochem. Photobiol. C: Photochem. Rev. **2015**, 22, 34-57.
(21) Martinez de Pinillos Bayona, A.; Mroz, P.; Thunshelle, C.; Hamblin, M. R. Chem. Biol. Drug. Des. **2017**, 89, 192-206.
(22) Agazzi, M. L.; Ballatore, M. B.; Durantini, A M.; Durantini, E. N.; Augusto, T. C. J. Photochem. Photobiol. C: Photochem. Rev. **2019**, 40, 21-48.

(23) Durantini, A. M.; Heredia, D. A.; Durantini, J. E.; Durantini, E. N. Eur. J. Med. Chem. **2018**, 144, 651-661.
(24) Agazzi, M. L.; Ballatore, M. B.; Reynoso, E.; Quiroga, E. D.; Durantini, E. N. Eur. J. Med. Chem. **2017**, 126, 116-121.
(25) Martínez, S. R.; Palacios, Y. B.; Heredia, D. A.; Agazzi, M. L.; Durantini, A. M. ACS Infect. Dis. **2019**, 5, 1624-1633.
(26) Kamkaew, A.; Lim, S. H.; Lee, H. B.; Kiew, L. V.; Chung, L. Y.; Burgess, K. Chem. Soc. Rev. **2013**, 42, 77-88.
(27) Gutsche, C. S.; Ortwerth, M.; Gräfe, S.; Flanagan, K. J.; Senge, M. O.; Reissig, H.-U.; Kulak, N.; Wiehe, A. Chem. Eur. J. **2016**, 22, 13953-13964.
(28) Golf, H. R. A.; Reissig, H.-U. Wiehe, A. Org. Lett. **2015**, 17, 982-985.
(29) Carvalho, C. M. B.; Alves, E.; Costa, L.; Tomé, J. P. C.; Faustino, M. A. F.; Neves, M. G. P. M. S.; Tomé, A. C.; Cavaleiro, J. A. S.; Almeida, A.; Cunha, Â.; Lin, Z.; Rocha J. ACS Nano **2010**, 4, 7133-7140.
(30) Lindsey, J. S. Acc. Chem. Res. **2010**, 43, 300-311.
(31) Caminos, D. A. Durantini, E. N. J. Porphyrins Phthalocyanines 2005, 9, 334-342.
(32) Scanone, A. C.; Gsponer, N. S.; Alvarez, M. G.; Durantini E. N. Photodiagn. Photodyn. Ther. **2018**, 24, 220-227.
(33) Ferreyra, D. D.; Spesia, M. S.; Milanesio, M. E.; Durantini, E. N. J. Photochem. Photobiol. A: Chem. **2014**, 282, 16-24.
(34) Ferreyra, D. D.; Reynoso, E.; Cordero, P.; Spesia, M. B.; Alvarez, M. G.; Milanesio, M. E.; Durantini, E. N. J. Photochem. Photobiol. B: Biol. **2016**, 158, 243-251.
(35) Heredia, D. A.; Durantini, A. M.; Sarotti, A. M.; Gsponer, N. S.; Ferreyra, D. D.; Bertolotti, S. G.; Milanesio, M. E.; Durantini, E. N. Chem. Eur. J. **2018**, 24, 5950-5961.
(36) Dupouy, E. A.; Lazzeri. D.; Durantini E. N. Photochem. Photobiol. Sci. **2004**, 3, 992-998.
(37) Scalise I.; Durantini, E. N. Bioorg. Med. Chem. **2005**, 13, 3037-3045.
(38) Spesia, M. B.; Rovera, M.; Durantini, E. N. Eur. J. Med. Chem. **2010**, 45, 2198-2205.
(39) Spesia, M. B.; Milanesio, M. E.; Durantini, E. N. Fullerene Derivatives in Photodynamic Inactivation of Microorganisms, Chapter 18, in Nanostructures for Antimicrobial Therapy. Elsevier, Amsterdam, Netherlands. **2017**, pp. 413-433.
(40) Spesia, M. B.; Milanesio, M. E.; Durantini, E. N. Eur. J. Med. Chem. **2008**, 43, 853-861.
(41) Agazzi, M. L.; Spesia, M. B.; Gsponer, N. S.; Milanesio, M. E.; Durantini, E. N. J. Photochem. Photobiol. A: Chem. **2015**, 310, 171-179.
(42) Maggini, M.; Scorrano, G.; Prato, M. J. Am. Chem. Soc. **1993**, 115, 9798-9799.
(43) Ballatore, M. B.; Spesia, M. B.; Milanesio, M. E.; Durantini, E. N. Eur. J. Med. Chem. **2014**, 83, 685-694.
(44) Agazzi, M. L.; Durantini, J. E.; Gsponer, N. S.; Durantini, A. M.; Bertolotti, S. G.; Durantini, E. N. ChemPhysChem. **2019**, 20, 1110-1125.
(45) Baruah, M.; Qin, W.; Flors, C.; Hofkens, J.; Vallée, R.A.L.; Beljonne, D.; Van der Auweraer, M.; De Borggraeve, W. M.; Boens, N. J. Phys. Chem. A. **2006**, 110, 5998-6009.
(46) Shivran, N.; Tyagi, M.; Mula, S.; Gupta, P.; Saha, B.; Patro, B. S. Eur. J. Med. Chem. **2016**, 122, 352-365.
(47) Lu, H.; Mack, J.; Nyokong, T.; Kobayashi, N.; Shen, Z. Coord. Chem. Rev. **2016**, 318, 1-15.
(48) Wu, W.; Guo, H.; Wu, W.; Ji, S.; Zhao, J. J. Org. Chem. **2011**, 76, 7056-7064.
(49) Durantini, A. M.; Greene, L. E.; Lincoln, R.; Martínez, S. R.; Cosa, G. J. Am. Chem. Soc. **2016**, 138, 1215-1225.
(50) Hedley, G. J.; Ruseckas, A.; Harriman, A.; Samuel, D.W. Angew. Chem. Int. Ed. **2011**, 50, 6634-6637.
(51) Zhang, M.; Hao, E.; Zhou, J.; Yu, C.; Bai, G.; Wang, F.; Jiao, L. Org. Biomol. Chem. **2012**, 10, 2139-2145.
(52) Maximiano, R. V.; Piovesan, E.; Zílio, S. C.; Machado, A. E. H.; de Paula, R.; Cavaleiro, J. A. S.; Borissevitch, I. E.; Ito, A. S.; Gonçalves, P. J.; Barbosa Neto, N. M. J. Photochem. Photobiol. A: Chem. **2010**, 214, 115-120.
(53) Baskin, J. S.; Yu, H-Z.; Zewail, A. H. J. Phys. Chem. A. **2002**, 106, 9837-9844.
(54) Mora, S. J.; Milanesio, M. E.; Durantini, E. N. J. Photochem. Photobiol. A: Chem. **2013**, 270, 75-84.
(55) Guldi, D. M.; Prato, M. Acc. Chem. Res. **2000**, 33, 695-703.
(56) Eckert, J.-F.; Nicoud, J.-F.; Nierengarten, J.-F.; Liu, S.-G.; Echegoyen, L.; Barigelletti, F.; Armaroli, N.; Ouali, L.; Krasnikov, V. J. Am. Chem. Soc. **2000**, 122, 7467-7479.
(57) Milanesio, M. E.; Durantini, E. N. Fullerene derivatives as antimicrobial photosensitising agents, Chapter 6, in Comprehensive Series in Photodynamic inactivation of microbial pathogens: medical and environmental applications. Royal Society of Chemistry, Cambridge, United Kingdom. **2011**, pp. 161-184.
(58) Szaciłowski, K.; Macyk, W.; Drzewiecka-Matuszek, A.; Brindell M.; Stochel, G. Chem. Rev. **2005**, 105, 2647-2694.
(59) Ogilby, P. R. Photochem. Photobiol. Sci. **2010**, 9, 1543-1560.
(60) Reynoso, E.; Quiroga, E. D.; Agazzi, M. L.; Ballatore, M. B.; Bertolotti, S. G.; Durantini, E. N. Photochem. Photobiol. Sci. **2017**, 16, 1524-1536.
(61) Chmyrov, A.; Sanden, T.; Widengren, J. J. Phys. Chem. B. **2010**, 114, 11282-11291.
(62) Redmond, R. W.; Gamlin, J. N. Photochem. Photobiol. **1999**, 70, 391-475.
(63) Milanesio, M. E.; Alvarez, M. G.; Silber, J. J.; Rivarola, V.; Durantini, E. N. Photochem. Photobiol. Sci. **2003**, 2, 926-933.

(64) Ballatore, M. B.; Spesia, M. B.; Milanesio M. E.; Durantini E. N. RSC Adv. **2018**, 8, 22876-22886.
(65) Caminos, D. A.; Spesia, M. B.; Durantini, E. N. Photochem. Photobiol. Sci. **2006**, 5, 56-65.
(66) Quiroga, E. D.; Mora, S. J.; Alvarez, M. G.; Durantini. E. N. Photodiag. Photodyn. Ther. **2016**, 13, 334-340.
(67) Di Palma, M. A.; Alvarez, M. G.; Ochoa, A. L.; Milanesio, M. E.; Durantini, E. N. Fungal Biol. **2013**, 117, 744-751.
(68) Di Palma, M. A.; Alvarez M. G.; Durantini, E. N. Photochem. Photobiol. **2015**, 91, 1203-1209.
(69) Reynoso, E.; Ferreyra, D. D.; Durantini, E. N.; Spesia, M. B. Photodermatol. Photoimmunol. Photomed. **2019**, 35, 322-331.
(70) Kumar, A.; Alam, A.; Rani, M.; Ehtesham, N. Z.; Hasnain, S. E. Intern. J. Med. Microbiol. **2017**, 307, 481-489.
(71) Milanesio, M. E.; Spesia, M. B.; Cormick, M. P.; Durantini, E. N. Photodiagn. Photodyn. Ther. **2013**, 10, 320-327.
(72) Gsponer, N. S.; Agazzi, M. L.; Spesia, M. B.; Durantini, E. N. Methods. **2016**, 109, 167-174.

Andrés M. Durantini studied at the National University of Río Cuarto (UNRC), Argentina, where he received his BSc degree in Chemistry in 2008. In 2013 he obtained his PhD degree in physical organic chemistry and photochemistry involving the study of soft matter. After graduate school, he started a post-doctoral fellow at McGill University, Montreal, Canada; where he gained expertise in organic chemistry and photobiology. His present position is Adjunct Researcher of CONICET at UNRC. His current area of research includes drug design, organic photochemistry and photodynamic inactivation. https://orcid.org/0000-0002-7898-4033.

Natalia S. Gsponer obtained her Microbiology degree from the National University of Río Cuarto (UNRC) in 2008 and her PhD degree in Biology in 2013. Then, she was awarded the posdoc fellowship from CONICET for two years at UNRC in PDI research group. Her project was focused in porphyrins conjugated magnetic nanoparticles for the treatment of microbial infections by photodynamic inactivation of bacteria. At present, she is Assistant Researcher of the CONICET at the UNRC. Her main research topic is focus on photosensitizers of natural and synthetic origin for the reduction of microbial contamination in fruits and vegetables.
https://orcid.org/0000-0003-3012-7590.

Daniel A. Heredia is an Adjunct Researcher of CONICET at National University of Río Cuarto (UNRC). He graduated in 2009 with a BSc and he received his PhD degree in 2014 from UNRC. He obtained a postdoctoral research fellowship at the Institute of Chemistry of Rosario, where he did research into the total synthesis of structurally relevant natural products. His interests are wide, ranging from organic synthesis to the development of new materials and their photophysical characterization. His current research activities focus on the synthesis of organic materials to apply in photodynamic inactivation and optoelectronic devices. http://orcid.org/0000-0002-0667-3906.

Mariana B. Spesia obtained her degree in Microbiology (2003) and her PhD in Biology Science at National University of Río Cuarto (UNRC, 2009). She worked in the development of new photosensitizing agents derived from phthalocyanines with application in the photodynamic inactivation of bacteria. During her posdoctoral research she specialized in molecular biology techniques to detect biofilms (2010). At present, she is Adjunct Researcher of CONICET and teaching assistant of UNRC. Her main research topic is focus on different strategies to enhance the photoinactivation of bacterial biofilms. https://orcid.org/0000-0002-7471-8950.

M. Gabriela Alvarez received her Microbiologist degree from Río Cuarto Nacional University (UNRC, 1997). In 2004, she obtained her PhD in Biology Sciences focused in photodynamic activity of porphyrins on Hep-2 human carcinoma cell line. Then, she performed a postdoctoral research at University of Buenos Aires and Río Cuarto (2005-2007) investigating the induction of apoptosis by aminolevulic acid and modulation of heme biosynthesis. She currently is a Professor at UNRC and Independent Researcher of CONICET. Her research centers on photoinactivation of microorganisms. https://orcid.org/0000-0002-1051-3390.

M. Elisa Milanesio obtained her BSc in Chemistry at the National University of Río Cuarto (UNRC) in 2001 and her PhD in 2006. She then performed a postdoctoral research at UNRC. At present, she is Adjunct Researcher of CONICET and Teaching Assistant at UNRC. Her main research focus is the synthesis and photodynamic characterization of structures derived from tetrapyrrolic macrocycles and fullerene C60 with application in the photodynamic inactivation of microorganisms. https://orcid.org/0000-0002-1100-3931.

Edgardo N. Durantini is a Full Professor at National University of Río Cuarto (UNRC, Argentina) and Principal Investigator of CONICET. He received his BSc degree in Chemistry in 1990 and PhD degree in 1994 from the UNRC. He was a Postdoctoral Research Associate at Arizona State University, USA in 1996-98. His experience was focused on biomimetic molecules of photosynthetic process and imaging agents for diagnosis of neoplastic diseases. At the present, his main research topics are focused on novel photosensitizers for the photoinactivation of microorganisms and the development of optoelectronic devices.

Group home page https://pdiresearchgroup.wixsite.com/research

ORCID: https://orcid.org/0000-0001-8901-7543

Anales de la Asociación Química Argentina

División Jóvenes Profesionales

Mini-Review

SYNTHESIS, CHARACTERIZATION AND OPTICAL PROPERTIES OF 1–4 nm SIZE SILICON NANOPARTICLES

Manuel J. Llansola-Portoles, Mónica C. Gonzalez and Paula Caregnato*

Instituto de Investigaciones Fisicoquímica Teóricas y Aplicadas (INIFTA) – Departamento de Química, Facultad de Ciencias Exactas, Universidad Nacional de La Plata (UNLP) – CONICET. C.C. 16 Suc.4, 1900, La Plata, Argentina.

**Autor Corresponsal: caregnato@inifta.unlp.edu.ar*

Graphical abstract

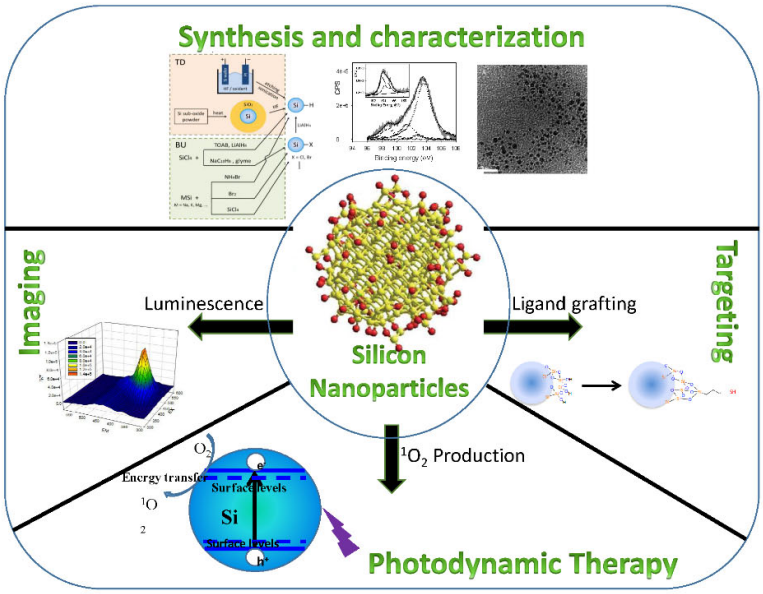

Resumen

Las nanopartículas de silicio (SiNp), en particular aquellas de diámetro comprendido entre 1–4nm, combinan propiedades de alto rendimiento cuántico de fotoluminiscencia, la capacidad de producir especies reactivas del oxígeno, y la facilidad de derivatizar con moléculas orgánicas su superficie.

La modificación química superficial permite aumentar su solubilidad en agua, el tiempo de circulación en sistemas biológicos, y por lo tanto su biocompatibilidad.

Por irradiación, la eficiencia en la producción de especies reactivas del oxígeno y el corrimiento en la banda de emisión, pueden modificarse con el tamaño, los mecanismos de síntesis y la oxidación/modificación

superficial de las SiNp. Es decir, que es posible diseñar nanopartículas con características especiales para su potencial aplicación en diagnóstico por imágenes, fototerapia y alcances a blancos específicos.
En el presente mini-review, se presentan las propiedades superficiales y ópticas de las SiNp, como también diferentes vías de síntesis y derivatización superficial, que permiten comprender sus propiedades luminiscentes, lo que las convierte en potenciales marcadores y fotosensibilizadores para diversos usos biológicos.

Abstract

Silicon nanoparticles (SiNp), particularly nanoparticles of diameter 1–4 nm, combine high quantum yield photoluminescence, the capacity for reactive oxygen species generation, and the richness of silicon surface derivatization.
Chemical surface modifications may lead to an increase in aqueous solubility, biocompatibility, targeting potential, and circulation time in biological systems.
Size, synthetic procedures and surface derivatization/oxidation may strongly affect the particles efficiency for reactive oxygen species yield and the redshift luminescence. On the whole, it is possible to develop multifunctional nanoparticles with potential applications in imaging, targeting and therapy.
In this mini-review, we present and discuss the surface and optical properties that make SiNp potential markers and photosensitizers for biological uses. In addition, some synthesis path and surface functionalization procedures in order to understand the basics of photoluminescence of these particles.

Palabras clave: *silicio, nanomateriales, luminiscencia, fotosensibilizador.*

Keywords: *silicon, nanomaterials, luminescence, photosensitizer.*

1. Introduction

Silicon technology has revolutionized everyday life compared to the past few decades. Silicon semiconductor clusters is currently one of the most active frontiers in physics and chemistry and the last studies have focused on developing their unique structures, stability, and optical, electronic and chemical reactivity [1].

Reducing the size of Si from bulk to nanoscale level brings about new properties and functionalities [2].

Fabricating Si nanoparticles (SiNp) in the range of 1–5 nm could be critical to the understanding of nanostructures and would be of significant interest to the microelectronics, biological industries and optoelectronics, especially light-emitting applications [3,4].

Silicon is inert, nontoxic, abundant and a low-cost material. In addition, SiNp provide a number of remarkable advantages, such as easy surface modification with various organic molecules [5], easily oxidized in water, or in damp ambient, promoting mild surface oxidation with a Si core of different controlled diameters [6], and a vast surface-to-volume ratio [7].

Bulk crystalline silicon does not show efficient light emission at room temperature, because of its band structure with an indirect gap of 1.1 eV. In both amorphous silicon and crystalline Si bulk samples, luminescence is observed in the near-infrared spectral region only at low temperatures when samples are excited in the Vis-IR region [8].

The poor luminescence properties of bulk silicon can be modified by the spatial confinement of excitons and electrons in a small volume.

Quantum-confinement effects can significantly enhance photoluminescence, by increasing radiative recombination via direct bandgap transitions and reducing phonon-assisted indirect band-gap transitions. Such effects become important in Si nanostructures with physical dimensions close to the bulk-Si exciton Bohr radius of about 4 nm [9].

The photoluminescence (PL) peak energies of the spectra observed for crystalline and amorphous Si nanostructures are blue shifted compared from those of bulk silicon and that effect is mainly caused by the quantum confinement of excitons in the nanoparticles [8].

Possessing electronic energy levels in the range of 1–5 eV (1240–245 nm) semiconductor nanoparticles can perform as photosensitizers just like organic fluorophores [10].

Bandgap of semiconductor nanoparticles is also potentially enough to produce reactive oxygen species (ROS). SiNp reduce oxygen to superoxide radical anion ($O_2^{\bullet -}$) or oxidize water or

hydroxide ions to hydroxyl radical ($HO^{\bullet}$) and produce singlet oxygen ($^1O_2$) in photosensitization process [11-13].

The main properties mentioned of silicon nanomaterials such as interaction with radiation and PL, toxicity, and surface activity, suggest that these materials are promising candidates for bio-applications, such as imaging, targeting and photodynamic therapy [14].

SiNp biocompatibility and unique optical properties (strong fluorescence coupled with photostability) make them candidates of fluorescent nanoprobes for imaging analysis.

For every possible application, the surface functionalization of the SiNp determines their interaction with the environment. These interactions not only affect the colloidal stability of the particles, but also could change both luminescence quantum yield and a shift in the maximum peak positions [14, 15].

Silicon nanoparticles meet criteria for good photosensitizers: they are not cytotoxic in the absence of light but have a potential to induce cytotoxicity under irradiation by production of reactive oxygen species.

2. Synthesis and surface derivatization

There are several synthetic routes to obtain nanostructured semiconductor silicon. Chemical routes can be further classified as ‘‘bottom-up’’ (BU) or ‘‘top-down’’ (TD) methods based on whether Si nanoparticles are synthesized by self-assembly processes from molecular silicon precursors (BU) or via breaking down and etching of bulk silicon materials (TD).

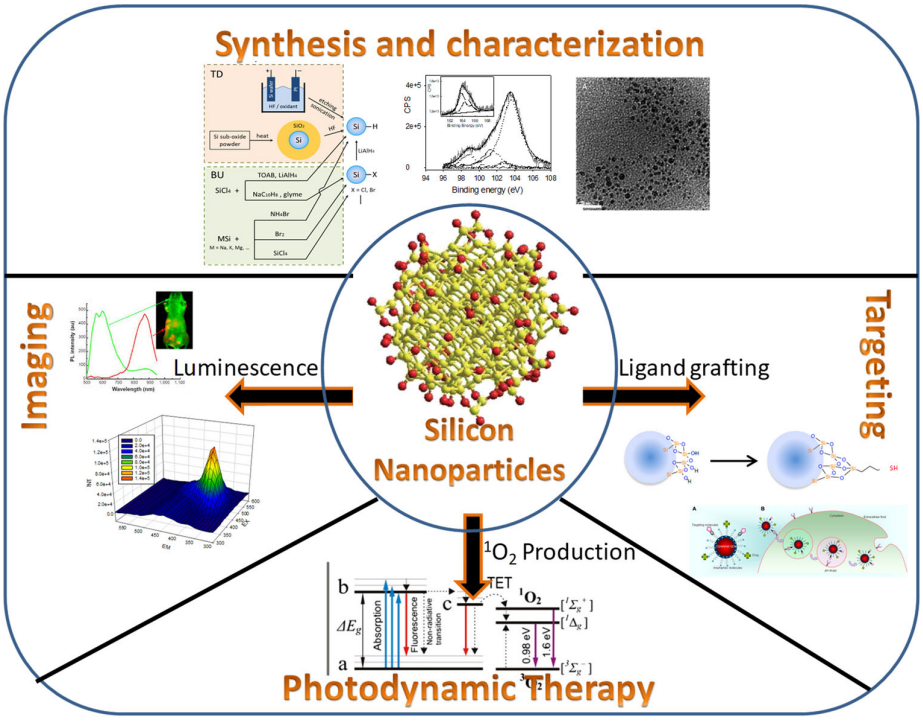

Scheme 1. Silicon nanoparticles promising applications [10, 16, 17, 18, 19, 20].

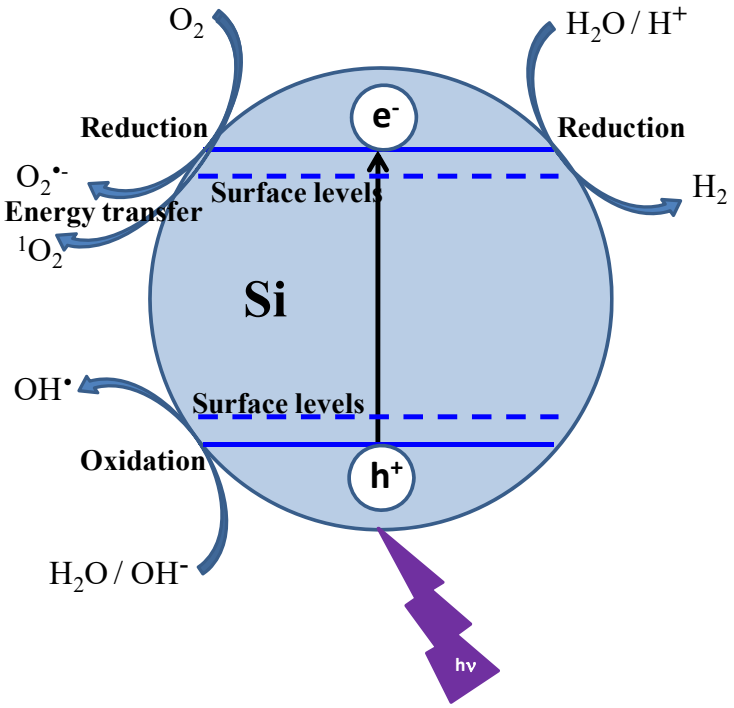

Scheme 2. Schematic representation of the generation of ROS that occurs when a silicon nanoparticle interacts with a photon (ultraviolet, visible light, near infrared radiation): charge transfer and photosensitization processes [16].

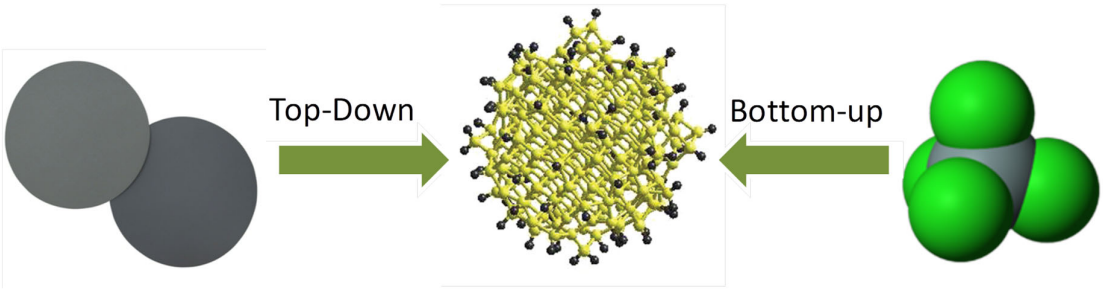

Scheme 3. Main synthetic routes to obtain silicon nanoparticles.

TD methods include electrochemical etching of p-type crystalline silicon wafers (resistivity between 1.0 and 10.0 Ωcm). It is based on the anodic etching of crystalline silicon in HF electrolytic solutions ($HF/CH_3OH/H_2O$) in a current density of 5 - 20 mA/cm, to form a porous silicon structure on the wafer surface followed by ultrasonic fracturing to release H-terminated Si nanocrystals along with larger porous silicon structures, which are separated by filtration [5, 6].

It is possible to obtain silicon nanocrystals keeping the solid residue from filtration and treated with HF/CH_3OH solution until it became completely clear after 24 h. TD SiNp of diameter of 1.7 nm are obtained [19].

The porous silicon nanostructures without further treatment (TD PSi) present a particle diameter of 50-150 nm.

BU routes consist of solution synthesis methods based on self-assembly processes and redox reactions from silicon molecular precursors. Depending on the oxidation state of silicon in the molecular precursor, synthesis can occur via oxidation or reduction pathways. Reduction pathways use reducing agents with silane precursors in solution [21]. The inclusion of surfactants with formation of inverse micelles in the reaction media, known as microemulsion techniques, reduces the problem of size control leading to smaller sizes and narrow particle distributions [22]. Tetraoctylammonium bromide (TOAB) is the most generally used surfactant in these techniques, particularly in toluene solution.

Reduction of $SiCl_4$ by $LiAlH_4$ in ethyl ether in the presence of TOAB was performed and produces small H-terminated Si nanoparticles in the 1–2 nm range. No evidence of crystalline structure was found [6].

On the other hand, oxidation pathways in solution use silicon Zintl salts as precursors. The oxidation of sodium silicide (Na_4Si_4) with ammonium bromide produces H-terminated 2–4 nm size Si nanocrystals [16].

Surface terminated H–Si and Cl–Si particles, which are chemically active surfaces, are unstable towards O_2. Therefore, the as-prepared silicon nanoparticles were oxidized during storage of their suspensions under air-saturation for several days [6], as confirmed by characterization surface techniques as FTIR and XPS spectra.

Surface properties of SiNp have a strong influence on band-gaps, emission spectra and stability in colloidal suspensions. On the whole, surface functionalization is important to provide specific surface properties to SiNp.

Surface modification strategies with the formation of organic monolayers through more stable Si–C or Si–O covalent linkages, takes place with silylation or sylanization reactions.

It is known that organosilane 3-mercaptopropyltrimethoxysilane (MPTS), commonly used as a silanization reagent, quickly reacts with the oxidized surfaces of silicon materials containing –OH groups, generating strong covalent Si–O–Si bonds with terminal thiol groups [19, 23]. The pendant–SH groups are useful in surface modification strategies owing to their diversified reactions. For example, nanoparticles used for drug and gene delivery, where thiol groups are used as linkers for binding biomolecules (with other thiol groups forming disulfide bonds with the target molecule) [24].

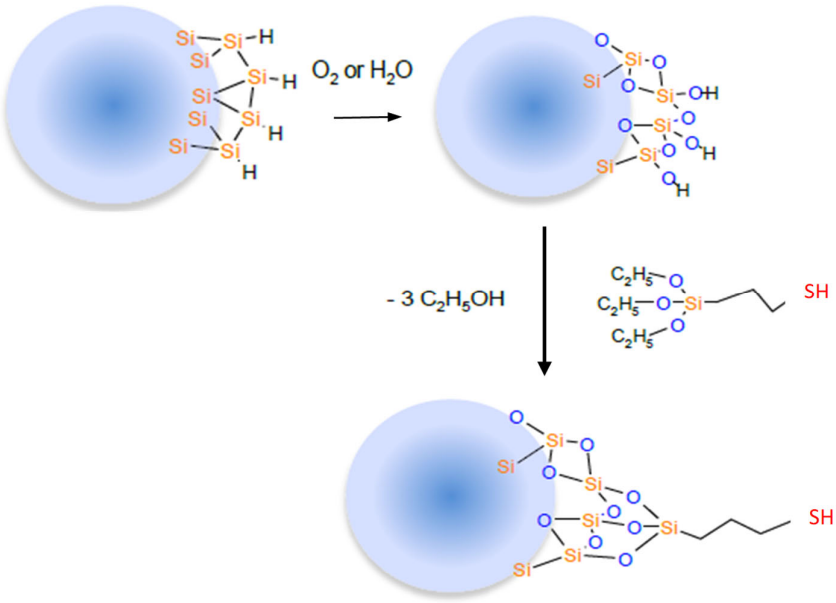

Scheme 4. Reaction scheme of oxidation and sylanization surface modification with MPTS of SiNp.

Morphology and surface chemistry were studied by several surface techniques such as Microscopies (Transmission Electron Microscopy (TEM), Scanning Tunneling Microscopy (STM), Atomic Force Microscopy (AFM)), spectroscopies (Fourier Transformed Infrared Spectroscopy (FTIR), Raman spectroscopy and X-ray Photoelectron Spectroscopy (XPS).

Microscopies of SiNp obtained from BU reverse micelles and TD method, showed particles diameter in the range 1.5–2.5 nm [16] (See Figures 1 and 2).

The diffraction pattern in HR-TEM measurement indicates an essentially crystalline nature for TD NpSi. On the other hand, BU NpSi showed no evidence of particle crystalline structure.

XPS spectra verify the contribution of different environments for the silicon atoms in SiNp, assigned to Si–Si and Si(–O–)$_x$ coordinated compounds with x = 2, 3, and 4.

Raman and FTIR spectroscopies showed the characteristics vibration modes of (C)–S–H and C–H stretching of the attached thiol propyl groups in SiNp derivatized with MPTS [19].

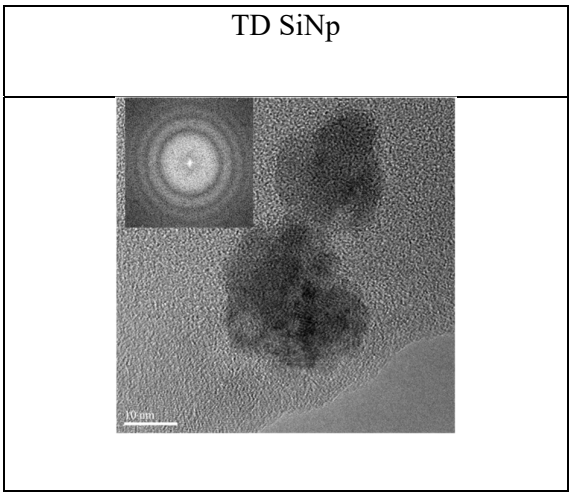

Figure 1. HR-TEM image of SiNp particles [16] .

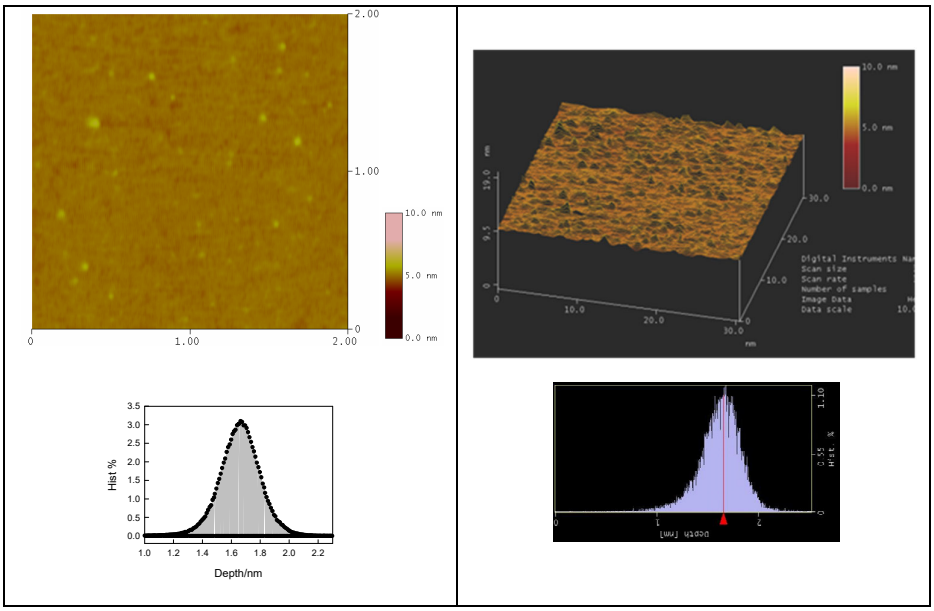

Figure 2. AFM image of SiNp dropcast from toluene dispersion onto mica substrate (left) and STM image of SiNp-SH on a Au(111) substrate (right) with the corresponding histograms of heights [16].

3. Photoluminescence

SiNp show PL in the wavelength range from 250 to 600 nm, with the emission spectrum strongly depending on the excitation wavelength in the specified range. The dependence of the emission spectrum on the excitation wavelength indicates the contribution of different emitters due to the different particle sizes, agglomeration, oxidation grade and molecules adsorbed on the surface [6].

A minimum of three different species contributing to the total emission of the bare surface particles is observed for SiNp synthesized by both TD and BU methods.

The maximum of the species from excitation–emission matrix of toluene suspensions are:

($\lambda_{exc.}$/nm, $\lambda_{em.}$/nm): (295, 360), (330, 380), and (355, 430).

Depending on the synthesis route and therefore, the structure property (if it is crystalline or amorphous), the species has different relative emission intensity.

For BU SiNp, which show an amorphous structure and are partially oxidized, the three species showed the same relative intensity.

On the other hand, the crystalline TD SiNp, emit with higher intensity in the UV region, at 360 nm [19] (Figure 3).

3.1. Effect of the surface groups

Derivatization of the silicon surface with MPTS (SiNp–SH) modifies the spectrum and/or the relative intensity of the emitter peaks.

MPTS grafting to BU SiNp leads to an increase in the emission intensity of the (375, 430) nm band.

Surface-derivatized TD SiNp show that the relative contribution of each specie to the overall emission is inverted, with bigger intensity in bands at (340, 380) and (370, 430).

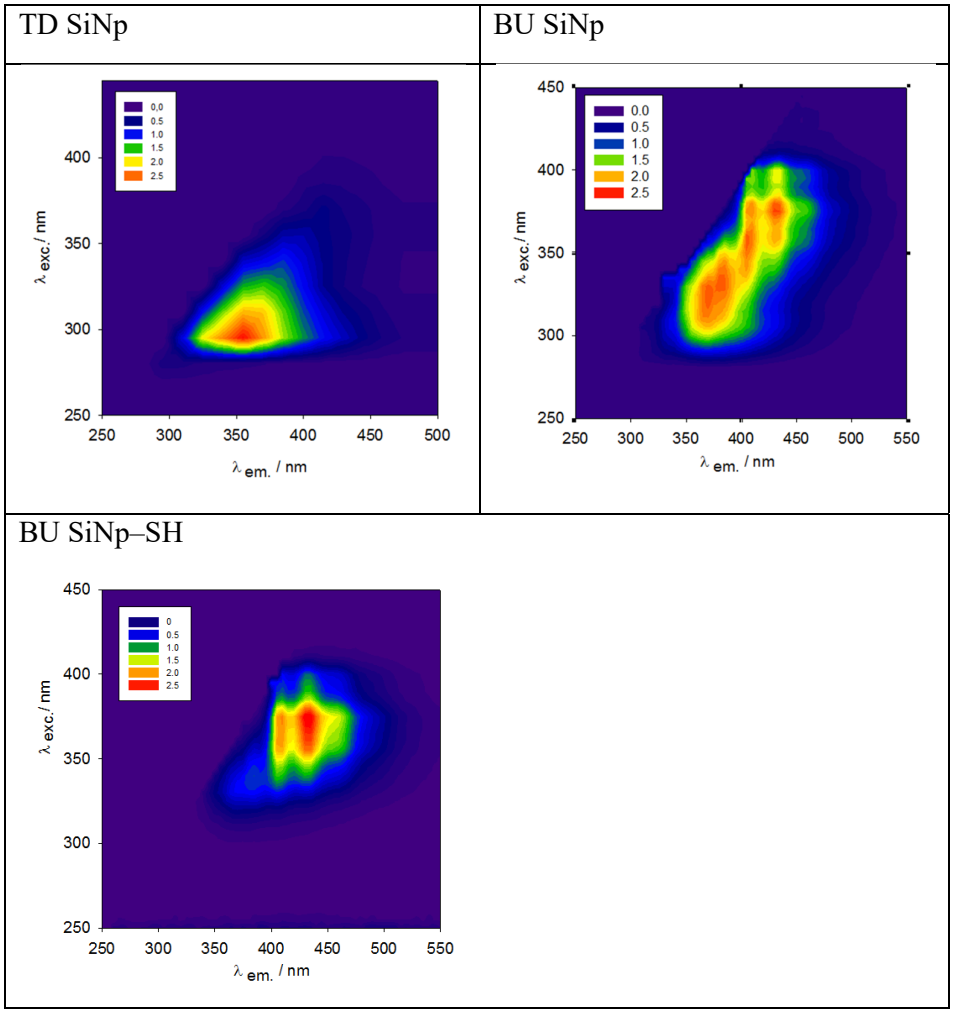

Figure 3. Excitation-emission matrix of SiNp toluene suspensions synthesized by different routes.

Comparing (370, 430) emitters before and after MPTS chemisorptions, although they absorb and emit in the same wavelength range, their different emission spectra intensity and decay times suggest that they are originating from different emitting species. The results clearly show that the emitter of surface modified particles has a PL decay time of (1.8 ± 0.1) ns. However, the emitter of bared particles yields decay signals with (3.3 ± 0.2) ns decay time [19].

During the silanization reaction with MPTS on partially oxidized silicon nanoparticles, Si–O–Si–$(CH_2)_3$–SH structures are formed on the surface. These nanoparticles retain the luminescence, changing the PL intensity of the different contributing emitters to the excitation–emission matrix. Silanized particles synthesized by the two different methods show similar PL

characteristics: an increase in the PL intensity emission at wavelengths from 400 to 430 nm and a PL quenching of peaks at shorter wavelengths. SiO_x may introduce defect states in the gap that permit radiative electron-hole recombination at energies smaller than the cluster band gap. Silanization reaction introduces a SiO_x surface layer leading to a similar transition.

Agglomeration of particles has a PL effect with emitters in the excitation–emission matrix at (450, 500) [6]. It was observed when SiNp are surface modified with Polyethylene glycol (PEG) through an amide link yielding PEG–NHSiNp particles. Surface functionalization of SiNp with PEG did not modify the luminescence properties of the particles, but reduced the surface charge with a consequent increase in the size of particle aggregates [20].

Larger TD PSi particles show PL in the visible range up to 500 nm.The emission band has been tuned across the entire visible range from deep red to blue and has received by far the most attention to date, and has the most technological, since it can be efficiently electrically excited [25].

4. ROS generation

Singlet oxygen ($^1O_2$) formation upon 266 nm irradiation of SiNp in acetonitrile suspensions is evidenced by the time-resolved phosphorescence traces observed at 1270 nm. 1O2 traces were fitted to an exponential decay law according to the equation: $I^1O_2(t) = I^1O_2(t=0) \times \exp(-t/\tau_\Delta)$ with I the phosphorescence intensity (see fitting curves in Figure 4) and τ_Δ the $^1O_2$ lifetime.

$^1O_2$ generation quantum yield $\Phi_\Delta = 0.35 \pm 0.02$ is obtained for SiNp, taking phenalenone as reference in acetonitrile.

Singlet oxygen lifetimes obtained in suspensions of SiNp and SiNp–SH (see traces in inset of Figure 4) are smaller than τ_Δ obtained for the references, indicating a possible reaction between

$^1O_2$ generated and the particles surface. The τ_Δ value of SiNp–SH, is smaller than that of thiol-free surface-oxidized PSi, showing an effect of organic thiol on $^1O_2$ reactivity.

The reactivity of the nanoparticles with $^1O_2$ was evaluated in toluene using the reference TPP (tetraphenylporphyrin).

Fitting an exponential decay function to $^1O_2$ traces yielded information on the lifetime of $^1O_2$ in the presence (τ_Δ) and absence (τ^0_Δ) of SiNp. A Stern-Volmer plot of the inverse of $^1O_2$ lifetimes vs. [SiNp] (Eq. (1)) yielded $^1O_2$ quenching rate constants of the particles due to physical and reactive mechanisms [26]. A value of $\tau^0_\Delta = 31$ μs was obtained, in agreement with values reported in toluene [27]. The slopes of the lines of τ_Δ^{-1} vs [SiNp] shown in Fig. 4 yielded $^1O_2$ quenching constants kq= of $(3.0\pm0.4)\times10^4$ and $(4.7\pm0.4)\times10^4$ $Lg^{-1}s^{-1}$ for SiNp and SiNp–SH in toluene, respectively.

$$\frac{1}{\tau_\Delta} = \frac{1}{\tau^0_\Delta} + k_q \times [\text{SiNp}] \qquad \text{Eq. 1}$$

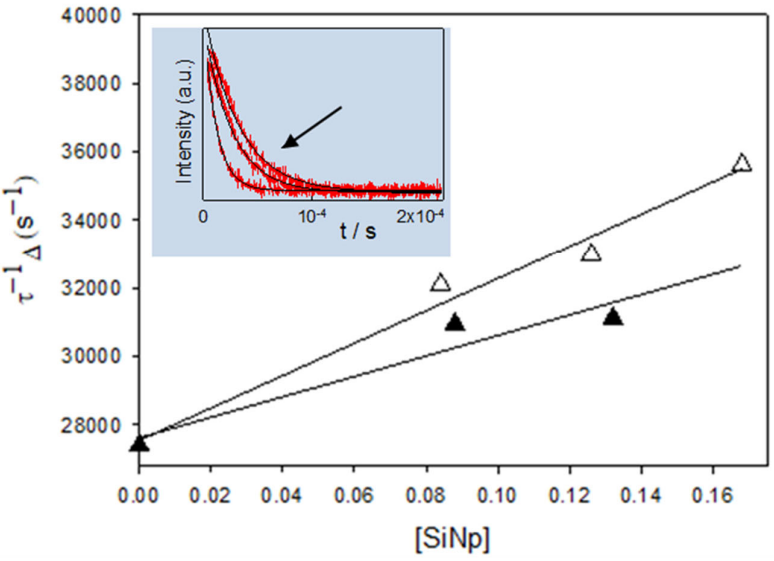

Figure 4. Plots of τ_Δ^{-1} vs. [SiNp] (g L^{-1}) for SiNp and SiNp–SH. Inset: $^1O_2$ near-infrared phosphorescence traces at 1270 nm obtained upon excitation at 355 nm of TPP in air-saturated toluene solution (upper curve) and after addition of SiNp and SiNp–SH (succeeding curves in the direction of the arrow). Black lines indicate the curve fitted to a single exponential decay equation.

5. Conclusions

In this mini-review, we have described main characteristic of semiconductor silicon nanoparticles focusing on their synthesis, functionalization and optical properties. The understanding of photoluminescence and photosensitizing properties is required to optimize the design of the particles as therapeutic agents and sensors.

Acknowledgments:

PC and MCG are research members of CONICET, Argentina. MJLP is actually a CNRS Researcher in the Institut des Sciences du Vivant Frédéric Joliot, CEA Paris-Saclay, France.

This research had financial support from ANPCyT (PICT 2014-2746) and UNLP.

References

(1) Park Y, Yoo J, Kang MH, Kwon W, Joo J. Photoluminescent and biodegradable porous silicon nanoparticles for biomedical imaging. J Mater Chem B. **2019**;7(41):6271-6292. doi:10.1039/c9tb01042d.
(2) Baig MI, Ingole PG, Jeon J deok, et al. Water vapor selective thin film nanocomposite membranes prepared by functionalized Silicon nanoparticles. Desalination. **2019**;(May):59-71. doi:10.1016/j.desal.2017.06.005
(3) Belomoin G, Therrien J, Smith A, et al. Observation of a magic discrete family of ultrabright Si nanoparticles. Appl Phys Lett. **2002**;80(5):841-843. doi:10.1063/1.1435802
(4) Zhu B, Ren G, Tang M, et al. Fluorescent silicon nanoparticles for sensing Hg^{2+} and Ag^{+} as well visualization of latent fingerprints. Dye Pigment. **2018**;149(August 2017):686-695. doi:10.1016/j.dyepig.2017.11.041
(5) Portoles MJ, Nieto FR, Soria DB, et al. Photophysical properties of blue - emitting silicon nanoparticles. J Phys Chem C Nanomater Interfaces. **2009**;113(31):13694-13702. doi:10.1021/jp903727n
(6) Llansola Portoles MJ, Diez RP, Dell 'arciprete ML, et al. Understanding the Parameters Affecting the Photoluminescence of Silicon Nanoparticles. J Phys Chem C. **2012**;116(20):11315−11325. doi:10.1021/jp2117938
(7) Sailor MJ, Lee EJ. Surface chemistry of luminescent silicon nanocrystallites. Adv Mater. **1997**; 9(10):783-793. doi:10.1002/adma.19970091004
(8) Kanemitsu Y. Efficient light emission from crystalline and amorphous silicon nanostructures. J Lumin. **2002**;100(1-4):209-217. doi:10.1016/S0022-2313(02)00425-8
(9) Kang Z, Liu Y, Tsang CHA, et al. Water-soluble silicon quantum dots with wavelength-tunable photoluminescence. Adv Mater. 2009;21(6):661-664. doi:10.1002/adma.200801642
(10) Juzenas P, Chen W, Sun YP, et al. Quantum dots and nanoparticles for photodynamic and radiation therapies of cancer. Adv Drug Deliv Rev. **2008**; 60(15):1600-1614. doi:10.1016/j.addr.2008.08.004
(11) Ipe BI, Lehnig M, Niemeyer CM. On the generation of free radical species from quantum dots. Small. **2005**;1(7):706-709. doi:10.1002/smll.200500105
(12) Romero JJ, Wegmann M, Rodríguez HB, et al. Impact of iron incorporation on 2-4 nm size silicon nanoparticles properties. J Phys Chem C. **2015**; 119(10):5739-5746. doi:10.1021/acs.jpcc.5b00172
(13) Llansola Portolés MJ, David Gara PM, Kotler ML, et al. Silicon nanoparticle photophysics and singlet oxygen generation. Langmuir. **2010**; 26(13):10953-10960. doi:10.1021/la100980x
(14) Sperling R a, Parak WJ. Surface modification, functionalization and bioconjugation of colloidal inorganic nanoparticles. Philos Trans A Math Phys Eng Sci. **2010**; 368(1915):1333-1383. doi:10.1098/rsta.2009.0273
(15) Romero JJ, Llansola-portole MJ, Arciprete D, Rodr B, Moore AL, Gonzalez C. Photoluminescent 1 − 2 nm Sized Silicon Nanoparticles: A Surface- Dependent System. Chem Mater. **2013**.
(16) Caregnato P, Dell'Arciprete ML, Monica C. Gonzalez CRL, Rodrıguez HB, Romero and JJ. Versatile silicon nanoparticles with potential uses as photoluminiscent sensors and photosensitizers. In: Albini A, Fasani E, eds. Photochemistry. Royal Society of Chemistry; **2017**: 324-347. doi:10.1039/9781782626954-00322

(17) Lin G, Wang X, Yin F, Yong KT. Passive tumor targeting and imaging by using mercaptosuccinic acid-coated near-infrared quantum dots. Int J Nanomedicine. **2015**; 10:335-345. doi:10.2147/IJN.S74805
(18) Xu G, Mahajan S, Roy I, Yong KT. Theranostic quantum dots for crossing blood-brain barrier in vitro and providing therapy of HIV-associated encephalopathy. Front Pharmacol. **2013**; 4 NOV(November):1-8. doi:10.3389/fphar.2013.00140
(19) Caregnato P, Dell 'Arciprete ML, Gonzalez MC. Silanization effect on the photoluminescence characteristics of crystalline and amorphous silicon nanoparticles. Photochem Photobiol Sci. **2013**; 12(9):1658-1655. doi:10.1039/c3pp50067e
(20) Lillo CR, Romero JJ, Portolés ML, Pis Diez R, Caregnato P, Gonzalez MC. Organic coating of 1–2-nm-size silicon nanoparticles: Effect on particle properties. Nano Res. **2015**; 8(6):2047-2062. doi:10.1007/s12274-015-0716-z
(21) Douglas-Gallardo OA, Burgos-Paci MA, Mendoza-Cruz R, et al. A novel one-pot room-temperature synthesis route to produce very small photoluminescent silicon nanocrystals. J Nanoparticle Res. **2018**;20(3). doi:10.1007/s11051-018-4174-x
(22) Rosso-Vasic M, Spruijt E, Van Lagen B, De Cola L, Zuilhof H. Alkyl-functionalized oxide-free silicon nanoparticles: Synthesis and optical properties. Small. **2008**; 4(10):1835-1841. doi:10.1002/smll.200800066
(23) Caregnato P, Forbes MDE, Soria DB, Mártire DO, Gonzalez MC. Chemisorbed Thiols on Silica Particles: Characterization of Reactive Sulfur Species. J Phys Chem C. **2010**;114(11):5080–5087. doi:10.1021/jp911253f
(24) Xu L, Liao J, Huang L, Gu N, Zhang H, Liu J. Pendant thiol groups-attached Pd(II) for initiating metal deposition. Appl Surf Sci. **2003**; 211(1-4):184-188. doi:10.1016/S0169-4332(03)00226-5
(25) Cullis AG, Canham LT, Calcott PDJ. The structural and luminescence properties of porous silicon. J Appl Phys. **1997**; 82(3):909-965. doi:10.1063/1.366536
(26) Schweitzer C, Schmidt R. Physical mechanisms of generation and deactivation of singlet oxygen. Chem Rev. **2003**; 103(5):1685-1757. doi:10.1021/cr010371d
(27) Darmanyan AP, Foote CS. Solvent effects on singlet oxygen yield from n,.pi.* and .pi.,.pi.* triplet carbonyl compounds. J Phys Chem. **1993**; 97(19):5032-5035. doi:10.1021/j100121a029

Dr. Manuel J. Llansola-Portoles scientific carrier began with a bachelor's degree in Chemical Engendering at the University Jaume I (Spain) in 2004. He pursued a Ph.D. on silicon quantum dots and their biomedical applications in the group of Prof. M.C. Gonzalez at the National University of La Plata (Argentina). After obtaining a Ph.D. in 2011, he became interested in renewable energy and specifically in solar energy gathering. To increase his knowledge of the basic principles of ultra-fast energy and charge transfer, Dr. Llansola became a Postdoctoral Research Associate in the group of Prof. Ana L. Moore in the Department of Chemistry and Biochemistry of Arizona State University (USA). In 2015, he was fascinated by the possibilities that artificial photosynthesis offers and the need for studying and understanding the quantum effects in natural photosynthesis in order to design highly efficient bio-inspired constructs. He got in contact with Prof. B. Robert CEA Saclay (France), and I worked in his group, studding the pigment configuration of light-harvesting complexes of algae, plants, and cyanobacteria as well as their implication on their exceeding efficiency for energy and charge transfer. At this moment, Dr. Llansola Portolés' interests focus lays on the study of cascade energy and electron events in the photosynthetic apparatus, and the vibrational quantum role on these mechanisms for implementation on bio-inspired compounds. He recently obtained a position as CNRS Researcher being part of the" Institute Of Biology Intégrative De La Cellule, Universite Paris-Saclay."

Mónica C. Gonzalez is a Principal Researcher at CONICET, INIFTA in La Plata.

Her major projects are: "Development of photoluminescent and magnetic nanomaterials based on semiconductors (silicon, carbon, and carbon nitride quantum dots) for environmental and biomedical applications,"

"Development of biomaterials based on calcium phosphates for Tissue Engineering and drug delivery," "Development of nanophotosensitizers for singlet oxygen generation in different environments," and "Effect of environmental conditions (solar irradiation and humic substances) in the cytotoxicity of commercial nanomaterials."

Paula Caregnato received her Ph.D. in Chemistry from the Universidad Nacional de La Plata in 2006, under the joint supervision of Prof. Monica Gonzalez (UNLP) and Prof. Daniel Martire (UNLP).

During October 2006, she joined Prof. Russo at Universitá della Calabria in Italy. In the period 2007-2008, she had a postdoctoral Fellow with Prof. Malcolm Forbes at the University of North Carolina at Chapel Hill, working with the detection of organic radicals in micelles by Electron Spin Resonance (ESR) technique.

Since 2008 she is a Researcher of CONICET at INIFTA (Instituto de Investigaciones Fisicoquimicas Teoricas y Aplicadas) in the group of Photochemistry and Nanomaterials for the Biology and Environment. Her research interests include the reactive species generation and luminescent properties of silicon nanomaterials combined with magnetic nanoparticles and derivatized with organic molecules of biological interests. Besides, the development of ZnO photocatalysts for the degradation of emerging pollutants in water using visible irradiation.

Anales de la Asociación Química Argentina

División Jóvenes Profesionales

Mini-Review

SUPRAMOLECULAR PHOTOSENSITIZERS AS IMPROVED TOOLS FOR ANTICANCER AND ANTIMICROBIAL TREATMENTS

Claudia C. Vera[1], Fiorella Tulli[1] and Claudio D. Borsarelli[1,2] *

[1] Instituto de Bionanotecnología del NOA (INBIONATEC). CONICET - Universidad Nacional de Santiago del Estero (UNSE); RN9, km 1125. G4206XCP, Santiago del Estero, Argentina.
[2] ICQ - Facultad de Agronomía y Agroindustrias. UNSE

**Autor Corresponsal: cdborsarelli@gmail.com*

Graphical abstract

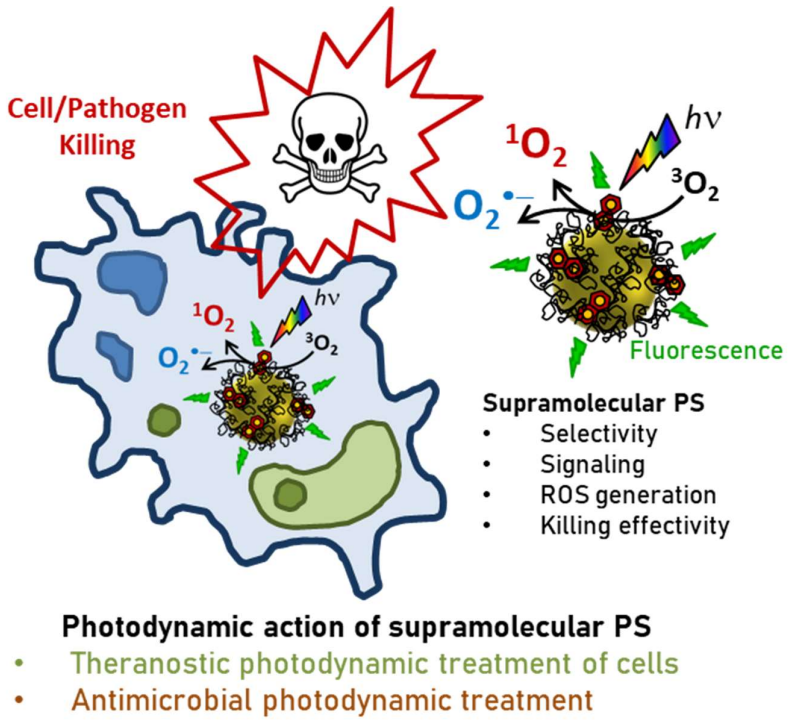

Resumen

La absorción de luz por una molécula llamada fotosensibilizador (PS) en presencia de oxígeno molecular desencadena la generación de especies reactivas de oxígeno (ROS), que en un medio biológico son capaces de degradar las moléculas objetivo. Este efecto se denomina acción fotodinámica (PDA) y es la raíz de la terapia fotodinámica (TFD), que en los últimos años se convirtió en una herramienta muy útil y versátil para inactivar tanto a las células dañinas como a los patógenos. Con el desarrollo de estructuras

supramoleculares funcionalizadas con propiedades fotosensibilizantes, hoy en día los horizontes de la TFD en aplicaciones antitumorales y antimicrobianas han mejorado y ampliado enormemente. En este artículo de revisión, discutimos los conceptos básicos de los procesos de fotosensibilización y TFD, revisando algunos de los avances más recientes en aplicaciones emergentes de fotosensibilizadores supramoleculares contra patógenos resistentes a múltiples fármacos, así como en tratamientos teranósticos del cáncer, donde se realiza con el mismo conjunto supramolecular tanto el diagnóstico como la terapia.

Abstract

Light absorption by a molecule called photosensitizer (PS) in the presence of molecular oxygen triggers the generation of reactive oxygen species (ROS), which can degrade target molecules in a biological milieu. This effect is called photodynamic action (PDA) and is the root of photodynamic therapy (PDT), which in recent years became a very useful and versatile tool for killing both harmful cells and pathogens. With the development of functionalized supramolecular structures with photosensitizing properties, nowadays the horizons of PDT in antitumoral and antimicrobial applications have been greatly improved and expanded. In this review article, we discussed the basics of the photosensitization and PDT processes, reviewing some of the most recent advances on emerging applications of supramolecular photosensitizers against multi-drug resistant pathogens as well as in cancer theranostic treatments, where both diagnostic and therapy is performed with the same supramolecular ensemble.

Palabras Clave: *fotosensibilización, terapia fotodinámica, fotosensibilizadores supramoleculares, antimicrobianos, anticancerígenos.*

Keywords: *photosensitization, photodynamic therapy, supramolecular photosensitizers, antimicrobial, anticancer.*

1. Basics of photosensitization

Solar light is a ubiquitous vector that promotes life on our planet, mainly by bacterial and plant photosynthesis. However, the photon flux incoming from the Sun also induces other photophysical and photochemical processes, such as visual and non-visual photoreception, photomovement, photoionization, photosensitization, photodegradation, environmental photochemistry, and photobiology, among others [1]. From all of them, from a biological point of view, photosensitization is particularly relevant due to their involvement from energy conversion to cell killing processes [2].

According to the "Gold Book" of the International Union of Pure and Applied Chemistry (IUPAC), the term photosensitization refers *to the process by which a photochemical or*

photophysical alteration occurs in one molecular entity as a result of initial absorption of radiation by another molecular entity called a photosensitizer (PS) [3]. Hence, a very vast number of natural and artificial photochemical and photobiological processes are easily initiated through photosensitized mechanisms by the absorption of lower energy photons of the visible or near-infrared region, *i.e.* above 400 nm, improving the utilization of the solar irradiation that impacts the Earth´s surface [1, 4].

Scheme 1 summarizes the photophysical and photochemical pathways involved during the photosensitization process of a PS molecule. The first step is the absorption of light by the ground state of the PS to finally produce the triplet excited state (^{3}PS*) by intersystem crossing from the lowest singlet excited state (^{1}PS*). Due to the spin-forbidden nature of the $S_0 \leftarrow T_1$ transition, the ^{3}PS* is a long-lived species (usually in a time-scale from hundreds of nanoseconds to the millisecond in fluid solutions) allowing a larger reactivity during its lifetime [5].

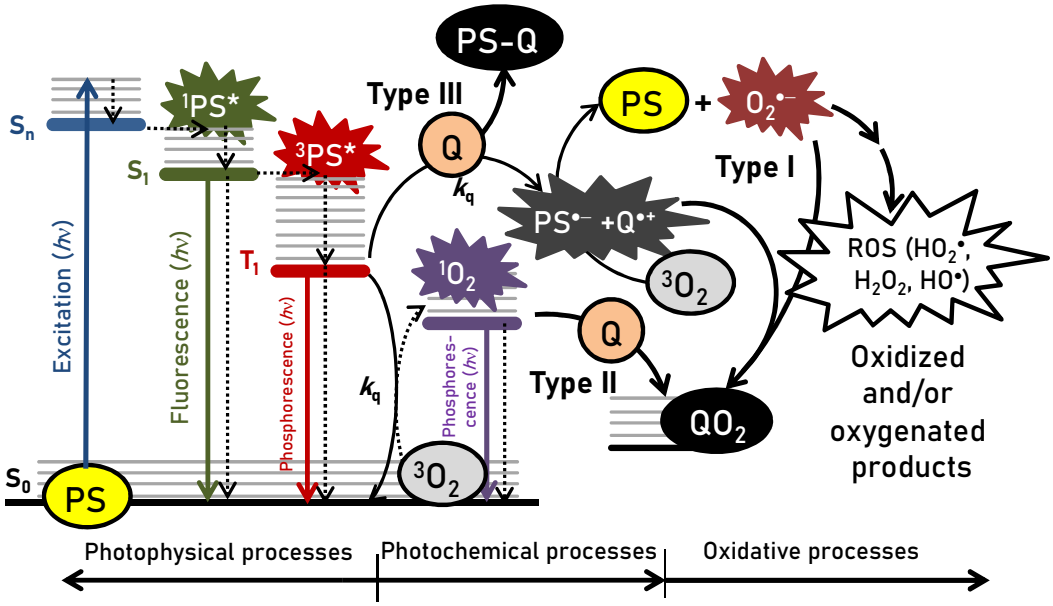

Scheme 1. Photophysical and photochemical pathways involved in photosensitized processes. See text for abbreviation meaning.

The primary photochemical reaction of ^{3}PS* with Q can produce radical/radical ion species by either hydrogen atom abstraction or electron-transfer reactions, respectively [6, 7]. Even if H-atom

transfer or electron-transfer reactions can take place in both directions, the ^{3}PS* acts most commonly as an oxidant. Thus, under aerobic conditions, the neutral or anion radicals PS$^{\bullet}$/PS$^{\bullet-}$ can react with molecular oxygen $^3O_2$ to generate anion superoxide ($O_2^{\bullet-}$) and the PS ground state molecule (*type I mechanism*) [6, 7]. In turn, $O_2^{\bullet-}$ can produce other reactive oxygen species (ROS) in subsequent secondary steps, such as hydroperoxyl radical ($HO_2^{\bullet}$), hydroxyl radical ($HO^{\bullet}$), and hydrogen peroxide (H_2O_2), as well as other oxidants involving a substrate R, *e.g.* peroxyl radicals ($ROO^{\bullet}$) and alkoxyl radicals ($RO^{\bullet}$) [6-8].

Conversely, the diffusion-controlled quenching of ^{3}PS* by $^3O_2$ through an efficient down-hill energy-transfer process ($k_q^{O2} \approx 10^9$ $M^{-1}s^{-1}$) produces singlet molecular oxygen ($^1O_2$) and the ground state of the PS. $^1O_2$ is the lowest excited state of $^3O_2$, with an energy gap of 22.5 kcal mol^{-1}, showing in solution a lifetime ranging between hundreds of ns to several ms depending on the solvent nature, while in gas phase up to several seconds [9]. Since $^1O_2$ is an electrophilic species, it can react with electron-rich biomolecules such as guanine (but not with other nucleic acids), unsaturated lipids, and amino acid residues to form mainly endoperoxides from [4 + 2] cycloadditions, dioxetanes from [2 + 2] cycloadditions, hydroperoxides from *"ene"* reactions or phenol oxidations, and sulfoxides from sulfide derivatives [7,10,11]. The oxidation of target molecules by the photosensitized generation of $^1O_2$ is termed the *type II* mechanism [6,7].

On the other hand, the ^{3}PS* can also react with Q to form a stable product (P) [8,12]. This oxygen-independent process is sometimes denominated as a *type III* reaction, but strictly it cannot be considered as a photosensitized reaction since the PS molecule is depleted [7, 13].

Hence, both *type I* and *type II* photosensitization mechanisms drive to the final formation of highly reactive and harmful ROS species that react with biological molecular targets (*e.g.* DNA, lipids, proteins) inducing damage of subcellular organelles, which in turn can lead to tissue injury, inflammation, and finally cell killing [14-17]. Usually, *type II* mechanism prevails and the main ROS generated is $^1O_2$, albeit the *type I* pathway can eventually result in the generation of

the highly toxic hydroxyl radical (HO•) from the secondary transformation of H_2O_2 by Fenton reaction with iron (II) [18].

Thus, the term "photodynamic action" (PDA) refers exclusively to oxygenation reactions of organic substrates that only occurs under the illumination of the PS added to the reaction mixture, but not in darkness, and that the PS is not consumed during these reactions [18]. Hence, any cell-killing process produced by the combined use of light, photosensitizer, and $^3O_2$ is denominated photodynamic therapy (PDT), while the use of the term "oxygen-independent photodynamic action" to describe the *type III* reaction is inaccurate [7].

2. Molecular and supramolecular PS

Molecular photosensitization is a field of high current interest in several scientific and technological areas. Figure 1A shows the exponential growth of the number of published articles since 1985 reported by the Scopus® database obtained by using "molecular photosensitizer" as the search term. Hundreds of organic and inorganic molecules have been used as PS in organic synthesis, energy conversion, clinical and environmental applications among others [19-21].

Many natural and artificial PS have been tested in PDT, mainly those with high efficiency of $^1O_2$ generation (type II mechanism) [22, 23], albeit *type I* oxidation processes are also relevant in the modification of nucleic acids [7, 24, 25] and proteins [26-30].

Typical organic PS include compound groups like tetrapyrroles (*e.g.* porphyrins, chlorins, phthalocyanines); organic dyes (*e.g.* xanthenic and phenothiazines derivatives such as rose bengal (RB) and methylene blue (MB), respectively, boron-dipyrromethenes BODIPYs, cyanines, and coumarins); quinones (anthraquinones and hypericins), isoalloxazines derivatives or flavins (lumiflavin, riboflavin, flavin mononucleotide), phenalenones, biological molecules (proteins, chlorophylls, verdins, vitamins, etc.) [1, 2, 14, 17, 19, 22, 23, 31, 32] . Chart 1 shows some of these structures, but most of them can be found in the preceding citations.

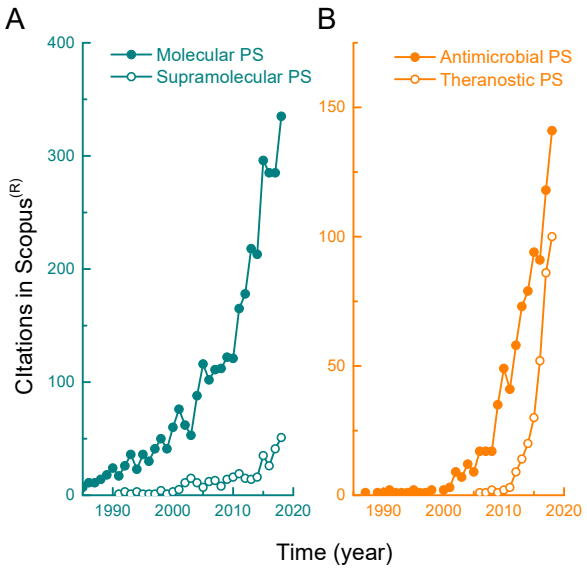

Figure 1. Number of the photosensitizer (PS)-related papers published since 1985 obtained from Scopus® database by searching in the title, abstract, and keyword sections the following terms: (A) "molecular photosensitizer" and ''supramolecular photosensitizer''; and (B) ''antimicrobial photosensitizer'' and "theranostic photosensitizer".

An ideal molecular PS for photodynamic applications is expected to fulfill several photophysical and photochemical features, such as a high molar absorptivity coefficient, mainly in the visible and near-infrared (NIR) light spectrum, efficient intersystem crossing leading to high excited triplet quantum yields ($\Phi_T \geq 0.2$), with larger triplet-state energy than that of $^1O_2$ (*i.e.* > 22.5 kcal mol^{-1}) and long lifetime (~μs) to increase the probability of interaction with triplet molecular oxygen for the subsequent efficient ROS generation [15, 31, 33]. Figure 2 shows the absorptivity spectra of some typical organic molecular PS covering the visible region together with their singlet oxygen quantum yield average values in fluid solutions (Φ_Δ). Furthermore, PS molecules are expected to be photo-stable and no cytotoxic in the absence of light, together with the ability to interact with cell targets [15, 33]. Nevertheless, all these requirements are very difficult to be satisfied by a simple molecule, and hence new strategies are required to obtain PS systems able to satisfy multiple functions [34-42].

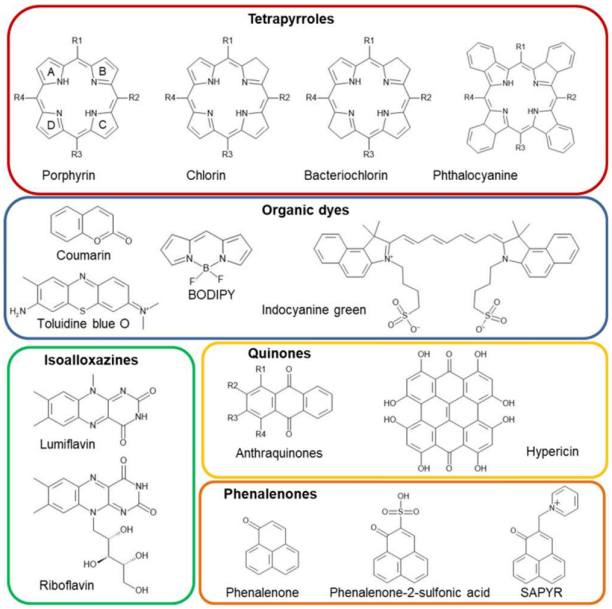

Chart 1. Molecular structures of some selected organic photosensitizers.

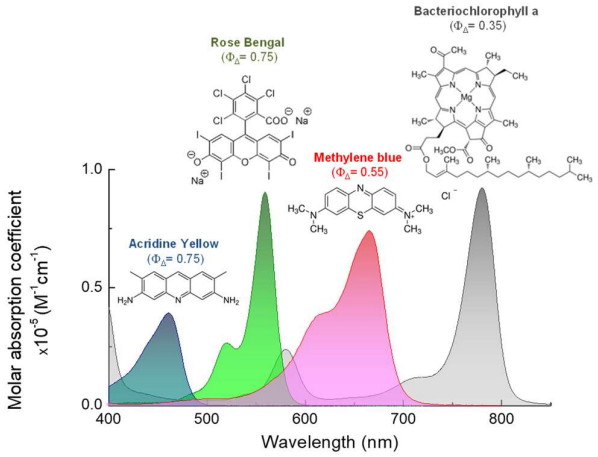

Figure 2: Structure and absorptivity spectra and singlet oxygen quantum yield (Φ_Δ) values of typical molecular PS covering the visible region of the electromagnetic spectrum.

Regarding this, ***supramolecular chemistry*** can afford practical solutions for the development and design of PS systems with multiple desired functionalities. The concept behind supramolecularity is to obtain molecular systems of higher complexity by the association of two or more chemical species held together due to intermolecular forces [43, 44]. The association driving forces include van der Waals, electrostatic, hydrogen bonding, hydrophobic interactions, etc.,

some of which are often cooperatively working in one supramolecular complex [43, 44]. Even more, in many cases, the supramolecular complex owns new advantageous properties missing in the individual components [44]. Nature is an inspiration source of supramolecular examples, for instance, the building of three-dimensional structures of proteins, DNA, and phospholipid membranes, among others [45, 46]. The development of facile approaches to fabricate submicron-structured assemblies allows to obtain supramolecular structures with high specificity, selective targeting and/or signaling, generation or scavenging of ROS (pro- or antioxidant function, respectively), sensitive to external stimuli (pH, ionic strength, light, temperature, etc.) [45-47].

A new article search in Scopus® using the term "supramolecular photosensitizer" leads to a fewer number of articles than the former search for "molecular photosensitizer" in the same period, but with almost twice-faster growth in the last decade (Figure 1A). In particular, photosensitizing processes using supramolecular devices are being intensively explored, especially for medical and energy conversion applications [38, 48, 49].

Usually, the bottom-up strategy is selected for the building up of the supramolecular PS, using a large diversity of nanomaterials (*e.g.* metal nanoparticles, fullerenes, carbon nanotubes, semiconductors, nanocellulose, etc) [35, 37, 40, 50-54], biomolecules as proteins [26, 55-58], and self-assembled nano/micro-systems (micelles, vesicles, multilayers, microcapsules, polymers, peptides, etc.) [24, 53, 59-63]. Chart 2 shows a pictorial representation of some representative supramolecular PS systems.

Figure 1B also shows the evolution of reported articles on photosensitization oriented to antimicrobial [64-67], and cancer theranostic applications [68-70]. The term ***theranostics*** implies the combination of **therapy** + diag**nostic** functions by a single composite and is a new field of medicine allowing specific targeted diagnostic and efficient therapy [71]. Hence, supramolecularity became a very helpful tool for the design of photosensitizing systems with multiple functions and/or properties.

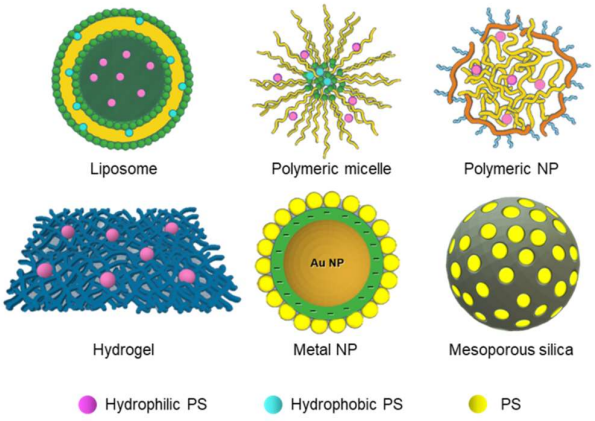

Chart 2. Schematic representation of some supramolecular PS systems

Both applied research areas have blasted within the last two decades, probably associated with two world-wide concerns: i) the increase of microbial resistance to the common antibiotics used to treat infections caused by bacteria, fungi, viruses, and parasites, that has become one of the leading causes of morbidity and mortality [72-74], and ii) the need of painless and less invasive cancer treatments [75]. For the latter, the design of supramolecular PS became a very interesting challenge oriented to obtain theranostic agents with multiple functions such as specific targeting to the neoplastic cells, tracking through the body tissues by exploiting the intrinsic luminescence/photoacoustic/magnetic responses, and with efficient PDT in the treated cells [76-78]. This application field shows a promising horizon for PDT as illustrated by the increase of reported articles since 2010 (Figure 1B).

3. Antitumoral vs. antimicrobial photodynamic treatments

Despite the PDA was discovered more than a hundred years ago by Oscar Raab [79], who found that *Paramecium* spp. protozoans were killed after staining with acridine orange and subsequent exposure to bright light, it was not until a quarter of a century ago that photodynamic therapy (PDT) was clinically approved for the treatment of a small number of selected tumors [15, 33]. Nowadays, its application has been tremendously expanded to include health specialties such as

cardiology, urology, immunology, ophthalmology, dentistry, dermatology, and cosmetics [15, 33, 80, 81]. Hence, the PDT term was initially coined to describe the minimally invasive therapeutic modality used for the selective treatment of a variety of neoplastic and non-neoplastic diseases [15, 33]. In PDT, the photo-generated cytotoxic species induce the killing of the target cells by different death mechanisms, *e.g.* necrosis, apoptosis, and autophagy [82].

Most effective anti-cancer PS molecules are relatively lipophilic compounds, with little or no overall positive or negative charges, so they can rapidly diffuse towards subcellular membrane structures such as mitochondria and endoplasmic reticulum (ER) of tumor cells. Nevertheless, for more polar PS, slower incorporation by endocytosis can be expected [15].

The successful utilization of an anticancer PS depends on several factors: a) good light-absorbing properties in the "phototherapeutic window" located between 650 and 1300 nm, where the absorption and scattering of light by tissues is minimal; b) large capability of $^1O_2$ generation close to the target biomolecules or organelles in the treated cells or tissues, considering the short lifetime (ns to μs) of this species; c) selective up-take of the PS into neoplastic cells to minimize non-desired toxic effects on healthy cells; and d) photobleaching capability (*i.e.* light-mediated destruction of the PS) since some new studies suggest that this phenomenon can avoid undesired over-treatment effects [14, 17, 36, 54, 83].

Most PS used in PDT show absorption bands in the far-red and NIR spectral regions for deeper tissue penetration [17, 31, 33, 81, 83]. Cyclic tetrapyrrolic structures as porphyrins and their analogs, chlorins, bacteriochlorins, phthalocyanines, etc. absorb light in the "phototherapeutic window" where tissue components such as hemoglobin and water are poor light absorbers [31].

The development of high power NIR lasers has overcome the poor or no light absorption by PS in the phototherapeutic window, *i.e.* PS with absorbing properties at the UVA and blue-light edges, through a two-photon excitation process allowing deeper penetration in the tissue, enhancement of the three-dimensional space selectivity, and less PS photobleaching, improving

the application of PDT in precise cancer treatment [84-86]. Furthermore, two-photon imaging was successfully integrated with PDT to diagnose diseases, to guide and monitor the treatment, and to assess the success of therapy (*i.e.* theranostic action) [84-86].

Another application field of PDT was prompted by the increasing challenge of antimicrobial resistance [72-74]. The so-called ‘‘ESKAPE’’-pathogens (*Enterococcus faecium, Staphylococcus aureus, Klebsiella pneumoniae, Acinetobacter baumannii, Pseudomonas aeruginosa and Enterobacter* strains) are one of the main current threats to public health for they have become resistant to almost all kinds of available antibiotic treatments [73]. As for antifungal drugs, the development of resistance against all drug classes has been reported in *Candida* and *Aspergillus* species such as *Candida glabrata*, *Candida auris*, and *Aspergillus fumigatus* [87]. Nowadays, with the recent COVID-19 outbreak, more scientific research efforts on the efficacy of photosensitized and PDT methods to combat the SARS-CoV-2 virus is needed, but until now, few reported articles about PDT methods applied to treat COVID-19 can be found [88].

Moreover, several microorganisms, such as bacteria, fungi, green algae, cyanobacteria, and lichen, possess the ability to grow in biofilm ecosystems rather than as planktonic single-species cultures, where they are usually incorporated in a matrix of extracellular polymeric substances (EPS) auto-produced by the microorganisms. Biofilm communities have developed resistance mechanisms that act synergistically, making them even less susceptible to antibiotic treatments [89, 90]. These mechanisms include, but are not limited to, slow penetration of antimicrobial agents through the biofilm matrix and interaction with its components, reduced growth rates, the formation of a sub-population of “persister cells”, the quorum-sensing systems, and the inter-species propagation of antibiotic resistance through horizontal gene transfer [74, 89, 91]. For the above mentioned, and considering that 80% of human infections are caused by biofilms [92], the search for treatments that allow the eradication of biofilms has become a key issue.

In this context, antibacterial photodynamic therapy (APDT) was outlined as a suitable alternative antimicrobial treatment to deal with the antibiotic-resistance issue [16, 35, 72, 74, 80, 93]. One advantage

of APDT over conventional antibiotic treatments is its unspecific killing mechanism since it involves the generation of ROS that can react with a wide variety of molecular components in the pathogen, with the additional potential that the PS can behave as a broad-spectrum antimicrobial agent. Thus, the possibility that microorganisms generate resistances through random mutations becomes extremely unlikely.

In general terms, PSs for antimicrobial applications do not need to absorb light in the "phototherapeutic window" as in the case of anti-cancer PSs, since the superficial nature of the microbial infections and contaminations does not require a deep light penetration, being also very efficient the PS molecules absorbing blue-light [22, 23, 67, 93]. Besides, antimicrobial PS are expected to be photo-stable, mainly in the case of immobilized PS intended to be reutilized [20, 34, 41, 51], lack dark toxicity and to be active within an appropriate concentration range, among other parameters involved in the photodynamic inactivation of pathogens to avoid harming eukaryotic mammalian cells [80]. Additional structural features of antimicrobial PS should be considered regarding their ability to interact with microbial targets. Molecular photosensitizers generally consist of planar π-conjugated aromatic structures, a prerequisite for light absorption in the visible and NIR regions. However, for this reason, these types of molecules tend to be hydrophobic and prone to aggregation, and hence self-quenching processes of the excited states of the PS constrains their applicability on APDT in aqueous media [20, 34, 41].

Furthermore, for the same PS, APDT efficiency can be different among microbial agents, mainly due to their variable cell surface structures. A good antimicrobial PS must photo-induce the reduction of the colony-forming unit (CFU) by at least 3 log units. Positively charged PSs have a broader action spectrum, being able to inactivate both Gram (+) and Gram (−) bacteria, as well as pathogenic yeasts [16, 64, 80, 94]. Hence, Gram (+) bacteria and yeasts are the most susceptible to APDT, as they are also affected by neutral and negatively charged PS molecules. Moreover, the porosity of Gram (+) outer wall, located outside the cytoplasmic membrane, allows the passage of complex nutrients with molecular weights between 30–60 KDa, so they are as well permeable

to supramolecular PSs within this size range [95]. In contrast, Gram (–) bacteria have an additional asymmetric and highly organized outer membrane to which porins, lipopolysaccharide, and lipoprotein constituents bestow a high negative charge density. This extra barrier constrains cell permeability, letting only small hydrophilic molecules (up to ~700 Da) pass through [96].

For the above mentioned, the impartment of positive charges in a PS proved to be a successful strategy to improve antimicrobial photodynamic activities of all kind of PS families (phenothiazidium dyes, porphyrins, phthalocyanines, flavins, among others) [16, 97]. An illustrative example is represented by a water-soluble phenalen-1-one derivative, *i.e.* (2-((4-pyridinyl)methyl)-1H-phenalen-1-one chloride) termed SAPYR, Chart 1 [98]. This cationic phenalenone derivative showed a similar $^1O_2$ quantum yield close to one, as the anionic derivative PNS [1H-Phenalen-1- one-2-sulfonic acid] [99]. However, PNS did not produce APDT action because of its negative charge, while the positively charged pyridinium-methyl moiety in SAPYR facilitated its incorporation in bacteria, allowing a successful APDT for inactivation of a polybacteria biofilm in a single treatment, with efficacy of ≥ 99.99% [98].

4. Antitumoral supramolecular PS

Most of anti-cancer PDT difficulties that could not be resolved by a single molecular PS have been overcome by combining concepts of supramolecular chemistry, nanotechnology, and photophysics to obtain new supramolecular PS systems with dual or multiple functions, *e.g.* imaging, specific recognition and attaching to cancer cells, drug/PS transport and controlled delivery, ROS generation, etc. [37, 54, 68, 69, 77, 78, 100-105].

The role of supramolecular and nanocomposites structures to build multifunctional theranostic PSs using metal nanoparticles, carbon nanotubes, carbon quantum dots, fullerenes, titanium dioxide, polymeric dendrimers, vesicles, microbubbles, graphene, mice, silica nanoparticles, nanogels, etc., have been extensively described in several recent reviews [17, 34, 37, 38, 68, 83,100,105-107].

Among the diagnostic techniques used are the optical microscopy (OM), photoacoustic image (PAI), computed tomography (CT), positron emission tomography (PET), single-photon computed tomography (SPCT), magnetic resonance imaging (MRI), ultrasound (US), etc. [68, 77, 78, 84, 103, 108-110]. Some of the most recent examples of theranostic supramolecular PS are discussed in the following paragraphs.

Chlorin e6 (Ce6) was loaded onto superparamagnetic iron oxide (SPION) nanoparticles via an oil-in-water emulsion [77]. The Ce6-SCs nanocomposite of 92 nm of size showed high solubility and excellent stability under physiological conditions. The enhanced permeability and retention achieved by this supramolecular formulation led to its selective accumulation within tumors, as observed by magnetic resonance (MR) and fluorescence dual-mode imaging following intravenous injection of the nanocomposite in a murine tumor model. After Ce6-SCs administration, PDT was performed through the excitation of Ce6 by a 665 nm laser. A high singlet oxygen generation was observed leading to a significant delay of tumor growth in mice.

Wu et al. [102] tested a theranostic nanocomposite prepared through the electrostatic interaction between a cationic tetraplatinated porphyrin complex (PtPor) and negatively charged carbon quantum dots (CQDs) for PDT against human cervical carcinoma cells (HeLa). The CQDs@PtPor nanocomposite integrates both optical properties of CQDs and the anticancer PDA of porphyrins. The PDT efficiency of CQDs@PtPor was stronger than that of the organic molecular PtPor, mainly by the enhanced production of $^1O_2$ induced by the presence of CQDs.

Li et al. [60] have recently revised peptide-modulated self-assembly strategies for supramolecular nanotheranostics. Three major assembly schemes were discussed: (1) self-assembly of peptide-photosensitizers, (2) self-assembly of peptide-anticancer drugs, and (3) multicomponent cooperative (PS-anticancer drugs) self-assembly. In the case of supramolecular PS systems, the desired strategy is the precise releases of the PS at tumoral cells as induced by some tumor microenvironment stimulus (*e.g.* pH < 6.0, heightened glutathione (GSH) level, overexpressed

enzymes, and biomarkers) to achieve controlled photosensitizer activation at tumor sites rather than normal tissues.

Non-covalent assembled nanoparticles made with the conjugated polymer poly(9,9-dioctylfluorene-alt-benzothiadiazole) (F8BT) and the amphiphilic copolymer stabilizer (PS-PEG-COOH) doped with hydrophobic platinum octaethylporphyrin (PtOEP) as PS were tested as theranostic PDT agent in glioblastoma (T98G), colorectal adenocarcinoma (SW480) and macrophage (RAW 264.7) cell lines.[62] The non-covalent assembled nanoparticles showed $\Phi_\Delta = 0.24$ in water, as confirmed by monitoring the NIR phosphorescence emission of $^1O_2$, and the PDT treatment was effective in the three types of cells [62].

Self-assembled micelles and liposomes were formerly used as nano-spherical carriers of molecular PS [83, 107, 111, 112]. Micelles can carry hydrophobic PS in their hydrocarbon interior [111], while liposomes can encapsulate either hydrophilic drugs within the aqueous regions or lipophilic molecules within the lipid bilayers [107]. Liposomes were used as delivery systems for 5-aminolevulinic acid (5-ALA), a pro-drug for the biosynthesis of the potent endogenous photosensitizer protoporphyrin IX (PpIX) in neoplastic cells, and the synthetic lipophilic temoporfin (mTHPC), for PDT of superficial skin lesions [107]. Liposomes bearing PS enhance penetration and accumulation of the PS in the skin compared with free molecules, leading to higher PDT efficacy and enable topical applications for deep and hyperkeratotic skin lesions. Moreover, PDT-driven by liposomes reduced the absorption of the PS into systemic circulation compared with the free drug, minimizing the risk of generalized photosensitivity.

Recently, Xu et al. [108] showed a study of various PS such as benzoporphyrin monoacid ring A (BPD), tetraphenylporphinesulfonate (TPPS4), and sodium 4-[2-[(1*E*,3*E*,5*E*,7*Z*)-7-[1,1-dimethyl-3-(4-sulfonatobutyl)benzo[e]indol-2-ylidene]hepta-1,3,5-trienyl]-1,1-dimethylbenzo[e]indol-3-ium-3-yl]butane-1-sulfonate (ICG) targeted with polyethyleneglycol (PEG) attached to 1,2-dipalmitoyl-sn-glycero-3-phosphocholine (DPPC) nanoliposomes (50-100 nm). *In vitro* studies showed that BDP encapsulated in PEGylated liposomes (LBDP) had an

increase in the efficiency of PDT and greater destruction of blood vessels in tumor tissues compared to free BPD. The *in vivo* localization of the supramolecular PS in tumor-bearing mice was performed by both fluorescence imaging (FLI) and photoacoustic imaging (PAI) dual-model. This multifunctional theranostic agent has exhibited its potential for clinical translatability since liposomal encapsulation of PS is the most popular clinically accepted nanosized drug delivery strategy.

The use of semiconductor-based PS like titanium dioxide (TiO_2) for PDT applications is strongly restricted by the low penetration of UV light into the tissues. Despite TiO_2 shows minimal dark cytotoxicity, it needs UVA light for ROS generation (*e.g.* the stronger oxidant $HO^{\bullet}$). However, this limitation can be overcome by using NIR two-photon excitation through upconversion energy processes using lanthanides [113]. Within this framework, Hou et al.[84] presented a novel NIR light-activated photosensitizer for PDT based on TiO_2-coated upconversion nanoparticle (UCNP) core-shell nanocomposites (UCNPs@TiO2 NCs), using a $NaYF4:Yb^{3+},Tm^{3+}@NaGdF4:Yb^{3+}$ core/shell. The UCNPs can efficiently convert NIR light to UV emission, corresponding to the TiO_2 shells absorption region. The nanocomposite is able to generate intracellular ROS under NIR irradiation, decreasing the mitochondrial membrane potential to release cytochrome c into the cytosol and then activating caspase 3 to induce cancer cell apoptosis. Thus, the combination of penetrating NIR radiation with efficient light-triggered ROS generation is a powerful weapon for cancer cell destruction.

Mesoporous silica nanoparticles (MSNs) functionalized with amine groups were used as a support to build up a layer-by-layer (LbL) supramolecular structure for tumor theranostic application. Multilayer coated MSNs (MCMSN) were obtained by alternative sequential adsorption of 1) hyaluronic acid (HA) with β-cyclodextrin (CD) and 2) 5, 10, 15, 20 - tetrakis (4-sulfonatophenyl) - porphyrin (TPPS4) onto the nanoparticles [69]. Then, tirapazamine (TPZ) was introduced due to its cytotoxicity toward tumoral cells, obtaining the nanoplatform (TPZ@MCMSN). Finally, the integrated TPZ@MCMSN-Gd^{3+} theranostic agent was formed by

a chelation reaction with gadolinium-III (Gd3+). TPZ@MCMSN-Gd^{3+} was tested in SCC-7 (Squamous cell carcinoma), MCF-7 (human breast adenocarcinoma), and COS7 (African green monkey kidney fibroblast) cell lines. The developed TPZ@MCMSN-Gd^{3+} supramolecule showed several advantages, such as dual-model imaging (NIR fluorescence and MR) guidance, effective tumor targeting, and efficient tumor growth inhibition by enhanced ROS production.

The correlation between the photobiological and photophysical properties of the organometallic compounds of Ru(II) with the extent of the π conjugation of the cyclometalation ligand was investigated [103]. Three of the organometallics derived from non-π-expansive cyclometalating ligands presented dark cytotoxic to cancer cells, which was not appreciable amplified by light exposure. On the other hand, the Ru(II) organometallic system derived from a π-expansive cyclometalating ligand, such 4,9,16-triazadibenzo[a,c]napthacene (pbpn), was completely non-toxic to cells in the dark, but photo-toxicity to cancer cells increased with a moderate light treatment. In addition to excellent its photocytotoxicity, this compound displayed intense green intracellular fluorescence.

Zhang et al. [104] reported that nanoscale supramolecular network formed by co-assembly of the amphiphilic amino acid 9-fluorenylmethyloxycarbonyl-L-leucine (Fmoc-L-L) and ionic manganese (Mn^{2+}) to encapsulate Ce6. The obtained bio-metal-organic nanoparticles exhibit a high Ce6 loading capability, inherent good biocompatibility, robust stability and smart disassembly in response to glutathione (GSH). The cooperative assembly of the multiple components is synchronously dynamic in nature and enables enhanced PDT to damage tumor cells and tissue by efficiently delivering of Ce6 via the competitive coordination of GSH with Mn^{2+}. Real-time in vivo evaluation of the antitumor effect was done by MRI through the long-term intracellular biochelation of Mn^{2+}.

An interesting combination of covalent and supramolecular chemistry for efficient antitumoral activity was reported by Ren et. al. [101] with the development of a nanosized supramolecular system formed by hyaluronic acid (HA) as carrier polymer with Ce6 as PS

covalently linked by an adipic dihydrazine bridge, and the anticancer drug doxorubicin (DOX) bound by non-covalent interactions. Despite the nanocomposite HA-Ce6 (DOX) could specifically bind to A549 cells through the CD44-HA receptor, it showed no PDA due to Ce6 molecular crowding. The study of cellular uptake and distribution of HA-Ce6 (DOX) by confocal fluorescence microscopy showed that, under acidic conditions and enzymatic stimulation, both Ce6 and DOX drugs were quickly released inside A549 cells, improving the therapeutic effect for individual photodynamic or chemotherapy with free Ce6 or DOX, respectively. Thus, the pH-responsive nanocomposite resulted in a potent anticancer theranostic agent [101].

5. Antimicrobial supramolecular PS

The increasing antibiotic resistance developed by the microorganisms [72-74, 89], together with some significant drawbacks of molecular PS for the application of APDT in clinical treatments, like their lack of selectivity and photobleaching, accelerated the application of supramolecular PS in APDT as a new alternative for the local treatment of infections as well as for disinfection of different surfaces and materials [20, 35, 39, 41, 65, 92, 114-117].

As well as for cancer PDT applications, self-assembled polymeric micelles and liposomes have been successfully used as nanocarriers for the delivery of PSs molecules into microbial cells, as they can prevent PS aggregation and preserves its photophysical properties [111, 112, 114].

Poly (β-amino ester)s with pH buffering capacities were recently employed for the encapsulation of Ce6 in charge-conversion nanoparticles, resulting in an efficient targeting and photodynamic inactivation of pathogenic bacteria in a weakly acidic urinary tract infection environment [118]. Surface charge switching on the nanoparticles conferred them an enhanced recognition towards Gram (+) and Gram (–) bacteria (*S. aureus* and *E. coli*, respectively). Moreover, the nanoparticles yielded efficient ROS photo-production leading to significant in vitro antibacterial effect, with increased minimum inhibitory concentration (MIC) values when compared to free Ce6, but with

low systemic cytotoxicity [118]. Ce6 grafted onto α-cyclodextrin (α-CD) was also used for selective targeting and photodynamic inactivation of *P. aeruginosa* and methicilin-resistant *Staphylococcus aureus* (MRSA) biofilms towards the formulation of bacteria-targeted PS delivery polymeric micelles. Selectivity was achieved by the covalent bounding of antimicrobial peptide Magainin I to PEG, then exploiting α-CD/PEG supramolecular assembly by host-guest complexation [119].

An amphiphilic calix[4]arene was utilized for the formation of micellar-like nanocontainers ca. 40 nm in diameter to encapsulate hydrophilic and hydrophobic phthalocyanine and porphyrin derivatives, respectively [120]. In aqueous solutions, the hydrophilic phthalocyanine showed self-aggregation with consequent changes on its spectral properties precluding its use as PS, while the hydrophobic porphyrin derivative was insoluble and photochemically inactive under these conditions. However, in the presence of the amphiphilic calix[4]arene micellar-like nanocontainers, both PS@calixarene nanoassemblies showed high quantum yields of $^1O_2$ photogeneration and remarkable visible light-induced inactivation of *S. aureus and P. aeruginosa*, representative Gram (+) and Gram (–) bacteria, respectively [120].

Metallic nanoparticles (MNP), *e.g.* Au, Ag, and Pt, have been extensively used for the conjugation, coating or loading of PSs for their application in APDT [114]. As MNP have antimicrobial activities themselves [121], they can act synergistically with the PS through PDA for the inactivation of microbial pathogens. Gold NP (AuNPs) obtained from green-synthesis using *Aloe vera* leaf extracts and conjugated with the phenothiazidium dyes MB and toluidine blue O (TBO) as PSs showed photodynamic inactivation activity when tested against both planktonic and biofilm *C. albicans* populations [122]. Moreover, in vivo experiments in mice demonstrated the ability of AuNP@MB and AuNP@TBO conjugates to suppress superficial skin as well as oral *C. albicans* infection, suggesting their potential application on APDT of cutaneous and nosocomial infections [122]. Other formulations comprising non-covalent conjugates of MB and

AuNPs also showed inhibitory effect over MRSA biofilms and *S. aureus* isolates from impetigo lesions, when irradiated with a red laser (≈660 nm) [123, 124].

A nanocomposite formed by conjugating the phenothiazidium dye TBO with AgNPs (AgNP@TBO) was tested for the photo-sensitized inactivation of *Streptococcus mutans* [125]. The resulting AgNP@TBO composites showed a higher photo-toxicity against *S. mutans* biofilm than the isolated TBO, as it was evidenced by an increased uptake of propidium iodide and by the leakage of cellular constituents. Fluorescence spectroscopic studies were conducted to confirm that photo-toxicity corresponded to a type I mechanism, with the generation of $HO^{\bullet}$ as the main ROS [125].

A large variety of supramolecular formulations involved the association of PSs with synthetic or naturally occurring polymers to yield diverse structured photo-active materials, such as polymeric nanoparticles, hydrogels, antimicrobial coatings, or surfaces [41, 51, 65, 66, 114, 126, 127].

Chen et al. [50] proposed a double-advantageous strategy for biofilm elimination based on degradable polymers. On one hand, high local concentrations of an organic PS are achieved by its binding to a supramolecular photodynamic polymer through host-guest interactions. Besides, after light-induced inactivation of the microorganism, the PS can be detached by competition with cucurbit[7]uril, favoring polymer degradation, and thus hindering the progression of drug resistance [50].

Manjón and co-workers employed porous silicone as a support for the immobilization of two different Ru(II) complexes (RDP^{2+} and RDB^{2+}) by hydrophobic interactions [128]. The resulting PS-doped porous silicon materials (RDP/pSil and RDB/pSil) yielded increased $^1O_2$ lifetimes compared to those of PSs in water, and were effective for waterborne *Enterococcus faecalis* photodynamic inactivation using a lab-scale solar simulator or a solar photoreactor as illumination sources. After sunlight irradiation, reloading of RDP/pSil with free RDP^{2+} resulted in even higher photodynamic efficiencies than the unused material, which was explained in terms

of the aggregation of the silicone-supported photosensitizer on pSil surface, as evidenced by photochemical characterization [128]. On a later work of the same group, RDP/pSil was compared with silicon-supported pristine C60-fullerene or its derivative 1-(4-methyl)-piperazinylfullerene (MPF), for their photodynamic water solar disinfection abilities [129]. C60/pSil showed poor photo-induced antibacterial activity due to fullerene aggregation, which results in a negatively charged surface. However, the positively charged MPF fullerene derivative was not effective either, because the C60 structural modification introduced led to lower $^1O_2$ generation efficiency [129].

Mesoporous silica nanoparticles (MSNP) functionalized with either amino- or mannose- moieties were reported as MB delivery systems for APDT [130]. Loading of MB into the MSNPs was driven by electrostatic interactions, and two populations of the dye were differentiated according to its location on the outer surface of the MSNPs or on the walls of the inner mesopores, as suggested by time-resolved spectroscopic studies. Both MSNPs showed photo-inactivation activities similar to free MB when tested against *E. coli* and *P. aeruginosa* [130].

A sort of polymer-based structure that has been widely explored for the immobilization of PSs is represented by hydrogels, which consist of three-dimensional networks made of cross-linked water-soluble polymers [114]. Some shared characteristics of these platforms are their high porosity, biocompatibility, biodegradability, and flexible shape [114]. For example, an anti-infective intraocular lens were developed by immobilization of a cationic porphyrin on the surface of hydrogels made of acrylate co-polymers. The incorporation of the porphyrin resulted in a great reduction of bacterial adhesion on the material [131].

The development of antimicrobial surfaces involving PSs loaded on polymeric matrices was exploited as a healthcare infection prevention strategy. Cahan et al. reported the physical immobilization of RB, TBO, or MB by scattering a mixed powder of poly(vinylidene fluoride) (PVDF) and PSs onto a polyethylene sheet, and further pressing with a heating press device [41]. This procedure yielded hydrophobic surfaces with antibacterial photodynamic properties as demonstrated by the reduction of *E. coli* and *S. aureus* CFUs by >4 logs when illuminated with

a fluorescent lamp during 6-24 h [41]. More recently, a photodynamic spray coating was formulated by taking advantage of the host-guest interaction between β-cyclodextrin and MB, which prevented MB aggregation and resulted in a material with high $^1O_2$ photogeneration efficiency with low PS density [132].

An antimicrobial coating with combined virucidal and bactericidal activities was obtained by the immobilization of C70 fullerene and AgNPs into polystyrene-block-poly- 4-vinylpyridine (PS-P4VP) templates, yielding photo-active thin films [133]. This nanocomposite presents two distinct nanoscale functional domains as C70 is preferentially integrated into PS block domains (due to speculated π–π interactions), whereas AgNPs are formed in situ in P4VP domains. The significant amounts of $^1O_2$ generated by visible-light activation of C70, together with the Ag^+ release properties, allowed a synergistic inactivation of both *E. coli* and PR772 bacteriophage [133].

Biopolymer-based nanoparticles, mainly chitosan and cellulose, have shown to be a very advantageous PSs delivery agent in APDT due to their biocompatibility, stable formulation, versatility and generally easy preparation [134]. Chitosan can be isolated from the chitin exoskeleton of crustacea and is structurally composed of poly(D-glucosamine) chain. Due to its protonated amino groups, chitosan has an intrinsic antimicrobial activity that can be enhanced by covalent or non-covalent association with different bioactive compounds, among which are PS molecules for APDT applications. Recently, Castro and co-workers reported the ability of porphyrinic-chitosan films to inhibit *Listeria innocua* attachment and prevent subsequent biofilm formation [127].

Several works have reported the application of PS-chitosan hydrogels on topic APDT for wound infections, alone or in association with other components, such as hydroxypropylmethylcellulose, to improve the mechanical properties of the gels. Chitosan hydrogels were combined with PSs like MB or TBO for APDT against both planktonic and biofilm-forming pathogens [134, 135].

Supramolecular structures involving cellulose association with PSs have been explored in multiple configurations for APDT applications. For example, photo-active antimicrobial cellulosic fabrics were obtained by embedding the polymeric material with porphyrins, which resulted to be immobilized both by electrostatic and covalent interactions, as confirmed by diffuse reflectance (UV-Vis) spectroscopy [126]. Immobilization of cationic zinc phthalocyanine (ZnPc) derivatives on the negatively-charged surface of sulfated cellulose nanocrystals (CNC) by electrostatic interactions, yielded hybrid structures with photodynamic inactivation properties that outcome those observed for the free ZnPc [51]. Both PS concentrations and light doses applied for the photodynamic inactivation of *S. aureus* and *E. coli* were one to two orders of magnitude lower than those reported in the literature for similar but covalently linked porphyrin-based systems [136, 137]. Interestingly, the ZnPc@CNC composites in aqueous solution did not photogenerate $^1O_2$, suggesting that the observed efficient APDT relies on the transfer of ZnPc from the CNC surface to the microorganism, standing out the advantage of a non-covalent supramolecular strategy [51].

Carbon-based nanomaterials such as graphene, carbon nanotubes, fullerenes, carbon dots, and mesoporous carbon nanoparticles have been used for APDT applications either as PSs carriers or as nanomaterials with inherent photosensitizing properties. Akbari et al. [138] demonstrated the enhanced PDA of indocyanine green (ICG) conjugated with graphene oxide (GO), if compared with ICG alone [138]. The conjugate ICG@GO, in which ICG was loaded on the surface of GO by strong π–π stacking and hydrophobic interactions, not only showed a 1.3 more effective APDT activity against *E. faecalis* biofilms but also presented some advantages for endodontic applications, such as its cost-effectiveness and the much lower dye concentrations needed, with concomitantly reduced toxicity. A later work from the same group reported that nanocomposites of carnosine-GO decorated with hydroxyapatite had a better ICG loading capacity and longer stability than the conjugates prepared with GO alone [139].

Multi-walled carbon nanotubes (MWCNT) have been also utilized as delivery vehicles of toluidine blue (TB) for the efficient photo-inactivation of *P. aeruginosa* and *S. aureus* both in planktonic cultures and biofilms [140]. The nanocomposite MWCNT@TB allowed the gradual releases of the dye and led to a greater APDT efficiency when compared to free TB [140].

6. Conclusions

In this review, we have presented several supramolecular strategies addressed to overcome some of the limitations of molecular photosensitizers (PS) for photodynamic therapy (PDT) and antimicrobial photodynamic therapy (APDT) applications.

Typically, those supramolecular strategies included nanostructured PS self-assemblies, PS co-assemblies with antibiotics or anticancer drugs, and PS non-covalently and covalently attached with polyelectrolytes, biopolymers, and nanoparticles together with other additional materials. The main goal is to regulate ROS generation for specific and efficient anticancer or antimicrobial therapies, with a focus on the increment of ROS generation at tumor cells or tissue lesions, and also taking advantage of known anomalies in tumoral cells and tissues to triggering ROS generation with the light stimulus.

As mentioned through the review, the use of nano/micro-sized supramolecular systems for emerging photodynamic applications against multi-drug resistant pathogens and in the theranostic application in tumors became a powerful tool, since supramolecular PS systems can be designed with very high selectivity to target either tumor or pathogen cells, and with poor or null toxicity for normal cells. Also, in the field of theranostic treatments, a large variety of optical and non-optical monitoring signals can be obtained, allowing a large variety of tracking non-invasive methods. Nevertheless, most supramolecular PS systems are still in the initial development stages and their safety in animals has not been fully evaluated. Therefore, before clinical applications, the safety issues of supramolecular PS should be fully addressed.

Advanced or interested readers can find extra information in recent comprehensive reviews on both PDT and APDT application fields [16, 17, 20, 31, 32, 37-40, 54, 65, 66, 68, 92, 93, 105, 197, 114].

Acknowledgments:

C.C.V. and F.T. thank Consejo Nacional de Investigaciones Científicas y Técnicas (CONICET) for postdoctoral fellowships at INBIONATEC. C. D. B. is member of the Research Career of CONICET. Authors also thank Universidad Nacional de Santiago del Estero (Grant# CICyT-23A215), CONICET (Grant# PUE-2018-0035), and ANPCyT-FONCyT (Grant# PICT-2015-0828) for financial supports.

References

(1) K. C. Smith, Ed. , The Science of Photobiology, Plenum Press, New York and London, **1989**.
(2) L. O. Björn, Ed. , Photobiology: The Science of Light and Life, Springer, New York, **2015**.
(3) A. D. McNaught, A. Wilkinson, IUPAC. Compendium of Chemical Terminology, Blackwell Scientific Publications, Oxford, **1997**.
(4) Lars Olof Björn, Ed. , Photobiology. The Science of Light and Life, Springer, New York, **2015**.
(5) J. D. Coyle, Introduction to Organic Photochemistry, John Wiley & Sons Ltd, London, UK, **1986**.
(6) C. S. Foote, Photochem. Photobiol. **1991**, 54, 659–659.
(7) M. S. Baptista, J. Cadet, P. Di Mascio, A. A. Ghogare, A. Greer, M. R. Hamblin, C. Lorente, S. C. Nunez, M. S. Ribeiro, A. H. Thomas, et al., Photochem. Photobiol. **2017**, 93, 912–919.
(8) G. Laustriat, Biochimie **1986**, 68, 771–778.
(9) C. Schweitzer, R. Schmidt, Chem. Rev. **2003**, 103, 1685–1757.
(10) A. Greer, Acc. Chem. Res. **2006**, 39, 797–804.
(11) P. Di Mascio, G. R. Martinez, S. Miyamoto, G. E. Ronsein, M. H. G. Medeiros, J. Cadet, Chem. Rev. **2019**, 119, 2043–2086.
(12) R. Mang, H. Stege, J. Krutmann, Contact Dermatitis **2011**, 97–104.
(13) A. D. McNaught, A. Wilkinson, IUPAC. Compendium of Chemical Terminology, Blackwell Scientific Publications, Oxford, **1997**.
(14) E. J. Dennis, G. J. Dolmans, D. Fukumara, K. J. Rakesh, Nat. Rev. Cancer **2003**, 3, 375–380.
(15) L. Benov, Med. Princ. Pract. **2015**, 24, 14–28.
(16) M. Tim, J. Photochem. Photobiol. B Biol. **2015**, 150, 2–10.
(17) H. Abrahamse, M. R. Hamblin, Biochem. J. **2016**, 473, 347–364.
(18) A. A. Krasnovsky Jr., in Photodyn. Ther. Cell. Lev. (Ed.: A.B. Uzdensky), Research Signpost, **2007**, 17–62.
(19) M. C. DeRosa, R. J. Crutchley, Coord. Chem. Rev. **2002**, 233–234, 351–371.
(20) C. Spagnul, L. C. Turner, R. W. Boyle, J. Photochem. Photobiol. B Biol. **2015**, 150, 11–30.
(21) B. Quintero, M. A. Miranda, Ars Pharm. **2000**, 41, 27–46.
(22) R. W. Redmond, J. N. Gamlin, Photochem. Photobiol. **1999**, 70, 391–475.
(23) F. Wilkinson, W. P. Helman, A. B. Ross, J. Phys. Chem. Ref. Data **1993**, 22, 113–262.
(24) M. P. Serrano, C. Lorente, C. D. Borsarelli, A. H. Thomas, ChemPhysChem **2015**, 16, 2244–2252.
(25) M. P. Serrano, C. D. Borsarelli, A. H. Thomas, Photochem. Photobiol. **2013**, 89, 1456–1462.
(26) E. Alarcón, A. M. Edwards, A. Aspée, C. D. Borsarelli, E. A. Lissi, Photochem. Photobiol. Sci. **2009**, 8, 933–943.
(27) C. L. Hawkins, M. J. Davies, Biochim. Biophys. Acta **2001**, 1504, 196–219.
(28) M. J. Davies, Biochem. J. **2016**, 473, 805–825.
(29) M. Mariotti, C. Lopez-Alarcon, M. Rykaer, P. Hägglund, M. J. Davies, F. Leinisch, Free Radic. Biol. Med. **2017**, 112, 240–252.
(30) E. Alarcón, A. M. Edwards, A. M. Garcia, M. Muñoz, A. Aspée, C. D. Borsarelli, E. A. Lissi, Photochem. Photobiol. Sci. **2009**, 8, 255–263.
(31) I. Yoon, J. Z. Li, Y. K. Shim, Clin. Endosc. **2013**, 46, 7–23.
(32) R. Yin, M. Hamblin, Curr. Med. Chem. **2015**, 22, 2159–2185.
(33) P. Agostinis, K. Berg, K. Cengel, CA Cancer J Clin **2011**, 61, 250–281.
(34) J. Mosinger, K. Lang, P. Kubát, Top. Curr. Chem. **2016**, 370, 135–168.
(35) K. Liu, Y. Liu, Y. Yao, H. Yuan, S. Wang, Z. Wang, X. Zhang, Angew. Chemie Int. Ed. **2013**, 52, 8285–8289.

(36) S. Wang, R. Gao, F. Zhou, M. Selke, J. Mater. Chem. **2004**, 487–493.
(37) G. M. F. Calixto, J. Bernegossi, L. M. De Freitas, C. R. Fontana, M. Chorilli, A. M. Grumezescu, Molecules **2016**, 21, 1–18.
(38) E. Paszko, C. Ehrhardt, M. O. Senge, D. P. Kelleher, J. V. Reynolds, Photodiagnosis Photodyn. Ther. **2011**, 8, 14–29.
(39) S. Perni, P. Prokopovich, J. Pratten, I. P. Parkin, M. Wilson, Photochem. Photobiol. Sci. **2011**, 10, 712-720
(40) X. Li, S. Lee, J. Yoon, Chem. Soc. Rev. **2018**, 47, 1174–1188.
(41) R. Cahan, R. Schwartz, Y. Langzam, Y. Nitzan, Photochem. Photobiol. **2011**, 87, 1379–86.
(42) S. Sansaloni-Pastor, J. Bouilloux, N. Lange, Pharmaceuticals **2019**, 12, 148.
(43) P. A. Gale, Philos. Trans. R. Soc. A Math. Phys. Eng. Sci. **2000**, 358, 431–453.
(44) K. Ariga, in Biomater. Nanoarchitectonics (Ed.: M. Ebara), Elsevier Inc., Oxford, **2016**, 25–40.
(45) B. Bhushan, Philos. Trans. R. Soc. A Math. Phys. Eng. Sci. 2009, 367, 1445–1486.
(46) M. Sarikaya, C. Tamerler, A. K. Jen, K. Schulten, F. Baneyx, Nat. Mater. **2003**, 2, 577–585.
(47) E. Dujardin, S. Mann, Adv. Mater. **2002**, 14, 709–716.
(48) H. Ahmad, S. K. Kamarudin, L. J. Minggu, M. Kassim, Renew. Sustain. Energy Rev. **2015**, 43, 599–610.
(49) A. P. Nikalje, Med. Chem. (Los. Angeles). **2015**, 5, 81–89.
(50) L. Chen, Y. Yang, P. Zhang, S. Wang, J. F. Xu, X. Zhang, ACS Appl. Bio Mater. **2019**, 2, 2920–2926.
(51) E. Anaya-Plaza, E. van de Winckel, J. Mikkilä, J. M. Malho, O. Ikkala, O. Gulías, R. Bresolí-Obach, M. Agut, S. Nonell, T. Torres, et al., Chem. Eur. J. **2017**, 23, 4320–4326.
(52) M. R. Hamblin, Photochem. Photobiol. Sci. **2018**, 17, 1515–1533.
(53) X. Li, S. Yu, D. Lee, G. Kim, B. Lee, Y. Cho, B. Y. Zheng, M. R. Ke, J. D. Huang, K. T. Nam, et al., ACS Nano **2018**, 12, 681–688.
(54) C. K. Lim, J. Heo, S. Shin, K. Jeong, Y. H. Seo, W. D. Jang, C. R. Park, S. Y. Park, S. Kim, I. C. Kwon, Cancer Lett. **2013**, 334, 176–187.
(55) E. Alarcón, A. M. A. M. Edwards, A. M. A. M. Garcia, M. Muñoz, A. Aspée, C. D. C. D. Borsarelli, E. A. E. A. Lissi, Photochem. Photobiol. Sci. **2009**, 8, 255–263.
(56) M. R. Hamblin, E. L. Newman, J. Photochem. Photobiol. B Biol. **1994**, 26, 147–157.
(57) S. Monti, I. Manet, Chem. Soc. Rev. **2014**, 43, 4051–4067.
(58) M. B. E. Turbay, V. Rey, N. M. Argañaraz, F. E. Morán Vieyra, A. Aspée, E. A. Lissi, C. D. Borsarelli, J. Photochem. Photobiol. B Biol. **2014**, 141, 275–282.
(59) C. Li, F. Lin, W. Sun, F. G. Wu, H. Yang, R. Lv, Y. X. Zhu, H. R. Jia, C. Wang, G. Gao, et al., ACS Appl. Mater. Interfaces **2018**, 10, 16715–16722.
(60) S. Li, Q. Zou, R. Xing, T. Govindaraju, R. Fakhrullin, X. Yan, Theranostics **2019**, 9, 3249–3261.
(61) W. Q. Lim, G. Yang, S. Z. F. Phua, H. Chen, Y. Zhao, ACS Appl. Mater. Interfaces **2019**, 11, 16391–16401.
(62) L. E. Ibarra, G. V. Porcal, L. P. Macor, R. A. Ponzio, R. M. Spada, C. Lorente, C. A. Chesta, V. A. Rivarola, R. E. Palacios, Nanomedicine **2018**, 13, 605–624.
(63) R. M. Spada, L. P. Macor, L. I. Hernández, R. A. Ponzio, L. E. Ibarra, C. Lorente, C. A. Chesta, R. E. Palacios, Dye. Pigment. **2018**, 149, 212–223.
(64) F. Cieplik, D. Deng, W. Crielaard, W. Buchalla, E. Hellwig, A. Al-Ahmad, T. Maisch, Crit. Rev. Microbiol. **2018**, 44, 571–589.
(65) M. Q. Mesquita, C. J. Dias, M. G. P. M. S. Neves, A. Almeida, M. A. F. Faustino, Molecules **2018**, 23, 2424.
(66) R. A. Craig, C. P. McCoy, S. P. Gorman, D. S. Jones, Expert Opin. Drug Deliv. **2015**, 12, 85–101.
(67) M. Tim, J. Photochem. Photobiol. B Biol. **2015**, 150, 2–10.
(68) P. Rai, S. Mallidi, X. Zheng, R. Rahmanzadeh, Y. Mir, S. Elrington, A. Khurshid, T. Hasan, Adv. Drug Deliv. Rev. **2010**, 62, 1094–1124.
(69) W. H. Chen, G. F. Luo, W. X. Qiu, Q. Lei, L. H. Liu, S. B. Wang, X. Z. Zhang, Biomaterials **2017**, 117, 54–65.
(70) G. Yu, S. Yu, M. L. Saha, J. Zhou, T. R. Cook, B. C. Yung, J. Chen, Z. Mao, F. Zhang, Z. Zhou, et al., Nat. Commun. **2018**, 9, 4335.
(71) S. S. Kelkar, T. M. Reineke, Bioconjug. Chem. **2011**, 22, 1879–1903.
(72) R. K. Fukuda, Antimicrobial Resistance: Global Report on Surveillance, World Health Organization, Geneva, **2014**.
(73) S. Santajit, N. Indrawattana, Biomed Res. Int. **2016**, 2455067.
(74) N. Venkatesan, G. Perumal, M. Doble, Future Microbiol. **2015**, 10, 1743–1750.
(75) K. G. Andersen, H. Kehlet, J. Pain **2011**, 12, 725–746.
(76) Y. Qin, L. J. Chen, F. Dong, S. T. Jiang, G. Q. Yin, X. Li, Y. Tian, H. B. Yang, J. Am. Chem. Soc. **2019**, 141, 8943–8950.
(77) A. Amirshaghaghi, L. Yan, J. Miller, Y. Daniel, J. M. Stein, T. M. Busch, Z. Cheng, A. Tsourkas, Sci. Rep. **2019**, 9, 1–9.

(78) Z. Liu, W. Shi, G. Hong, W. Chen, B. Song, X. Peng, X. Xiong, F. Song, J. Control. Release **2019**, 310, 1–10.
(79) O. Raab, Zeitung Biol . **1900**, 39, 524–526.
(80) G. B. Kharkwal, S. K. Sharma, Y. Y. Huang, T. Dai, M. R. Hamblin, Lasers Surg. Med. **2011**, 43, 755–767.
(81) R. Mang, H. Stege, J. Krutmann, in Contact Dermatitis (Ed.: Springer), **2011**, 97–104.
(82) J. Soriano, I. Mora-Espí, M. E. Alea-Reyes, L. Pérez-García, L. Barrios, E. Ibáñez, C. Nogués, Sci. Rep. **2017**, 7, 1–13.
(83) S. A. Sibani, P. A. McCarron, A. D. Woolfson, R. F. Donnelly, Expert Opin. Drug Deliv. **2008**, 5, 1241–1254.
(84) Z. Hou, Y. Zhang, K. Deng, Y. Chen, X. Li, X. Deng, Z. Cheng, H. Lian, C. Li, J. Lin, ACS Nano **2015**, 9, 2584–2599.
(85) Y. Q. Huang, L. J. Sun, R. Zhang, J. Hu, X. F. Liu, R. C. Jiang, Q. L. Fan, L. H. Wang, W. Huang, ACS Appl. Bio Mater. 2019, 2, 2421–2434.
(86) Z. Zheng, T. Zhang, H. Liu, Y. Chen, R. T. K. Kwok, C. Ma, P. Zhang, H. H. Y. Sung, I. D. Williams, J. W. Y. Lam, et al., ACS Nano **2018**, 12, 8145–8159.
(87) D. S. Perlin, R. Rautemaa-Richardson, A. Alastruey-Izquierdo, Lancet Infect. Dis. **2017**, 17, e383–e392.
(88) M. Eickmann, U. Gravemann, W. Handke, F. Tolksdorf, S. Reichenberg, T. H. Müller, A. Seltsam, Vox Sang. **2020**, 146–151.
(89) C. W. Hall, T. F. Mah, FEMS Microbiol. Rev. **2017**, 41, 276–301.
(90) P. S. Stewart, J. William Costerton, Lancet **2001**, 358, 135–138.
(91) O. Ciofu, E. Rojo-Molinero, M. D. Macià, A. Oliver, APMIS **2017**, 125, 304–319.
(92) X. Hu, Y. Y. Huang, Y. Wang, X. Wang, M. R. Hamblin, Front. Microbiol. **2018**, 9, 1–24.
(93) J. Ghorbani, D. Rahban, S. Aghamiri, A. Teymouri, A. Bahador, Laser Ther. **2018**, 27, 293–302.
(94) T. Dai, B. B. Fuchs, J. J. Coleman, R. A. Prates, C. Astrakas, T. G. St. Denis, M. S. Ribeiro, E. Mylonakis, M. R. Hamblin, G. P. Tegos, Front. Microbiol. **2012**, 3, 1–16.
(95) G. Jori, M. Camerin, M. Soncin, L. Guidolin, O. Coppellotti, Antimicrobial Photodynamic Therapy: Basic Principles, **2011**.
(96) L. Leive, Ann. N. Y. Acad. Sci. **1974**, 235, 109–129.
(97) A. Segalla, C. D. Borsarelli, S. E. Braslavsky, J. D. Spikes, G. Roncucci, D. Dei, G. Chiti, G. Jori, E. Reddi, Photochem. Photobiol. Sci. **2002**, 1, 641–648.
(98) F. Cieplik, A. Späth, J. Regensburger, A. Gollmer, L. Tabenski, K. A. Hiller, W. Bäumler, T. Maisch, G. Schmalz, Free Radic. Biol. Med. **2013**, 65, 477–487.
(99) S. Nonell, M. Gonzalez, F. R. Trull, Afinidad **1993**, 50, 445–450.
(100) J. Xie, S. Lee, X. Chen, Adv. Drug Deliv. Rev. **2010**, 62, 1064–1079.
(101) Q. Ren, Z. Liang, X. Jiang, P. Gong, L. Zhou, Z. Sun, J. Xiang, Z. Xu, X. Peng, S. Li, et al., Int. J. Biol. Macromol. **2019**, 130, 845–852.
(102) F. Wu, L. Yue, H. Su, K. Wang, L. Yang, X. Zhu, Nanoscale Res. Lett. **2018**, 13, 357.
(103) T. Sainuddin, J. McCain, M. Pinto, H. Yin, J. Gibson, M. Hetu, S. A. McFarland, Inorg. Chem. **2016**, 55, 83–95.
(104) H. Zhang, K. Liu, S. Li, X. Xin, S. Yuan, G. Ma, X. Yan, ACS Nano **2018**, 12, 8266–8276.
(105) O. J. Fakayode, N. Tsolekile, S. P. Songca, O. S. Oluwafemi, Biophys. Rev. **2018**, 10, 49–67.
(106) N. Fomina, J. Sankaranarayanan, A. Almutairi, Adv. Drug Deliv. Rev. **2012**, 64, 1005–1020.
(107) N. Dragicevic-Curic, A. Fahr, Expert Opin. Drug Deliv. **2012**, 9, 1015–1032.
(108) H. Xu, Y. Liu, J. Qu, Z. Yuan, J. Innov. Opt. Health Sci. **2019**, 12, 1–9.
(109) S. Jenni, A. Sour, Inorganics **2019**, 7, 1–13.
(110) S. M. Janib, A. S. Moses, J. A. MacKay, Adv. Drug Deliv. Rev. **2010**, 62, 1052–1063.
(111) C. F. Van Nostrum, Adv. Drug Deliv. Rev. **2004**, 56, 9–16.
(112) H. Cabral, K. Miyata, K. Osada, K. Kataoka, Chem. Rev. **2018**, 118, 6844–6892.
(113) M. Nyk, R. Kumar, T. Y. Ohulchanskyy, E. J. Bergey, P. N. Prasad, Nano Lett. **2008**, 8, 3834–3838.
(114) Y. Feng, L. Liu, J. Zhang, H. Aslan, M. Dong, J. Mater. Chem. B **2017**, 5, 8631–8652.
(115) N. Kashef, Y.-Y. Huang, M. R. Hamblin, Nanophotonics **2017**, 176, 139–148.
(116) H. S. Kim, E. J. Cha, H. J. Kang, J. H. Park, J. Lee, H. D. Park, Environ. Res. **2019**, 172, 34–42.
(117) R. Khurana, A. S. Kakatkar, S. Chatterjee, N. Barooah, A. Kunwar, A. C. Bhasikuttan, J. Mohanty, Front. Chem. **2019**, 7, 452.
(118) S. Liu, S. Qiao, L. Li, G. Qi, Y. Lin, Z. Qiao, H. Wang, C. Shao, Nanotechnology **2015**, 26, 495602.
(119) Y. Gao, J. Wang, D. Hu, Y. Deng, T. Chen, Q. Jin, J. Ji, Macromol. Rapid Commun. **2019**, 40, 1800763.
(120) I. Di Bari, A. Fraix, R. Picciotto, A. R. Blanco, S. Petralia, S. Conoci, G. Granata, G. M. L. Consoli, S. Sortino, RSC Adv. **2016**, 6, 105573–105577.
(121) M. J. Hajipour, K. M. Fromm, A. Akbar Ashkarran, D. Jimenez de Aberasturi, I. R. de Larramendi, T. Rojo, V. Serpooshan, W. J. Parak, M. Mahmoudi, Trends Biotechnol. **2012**, 30, 499–511.
(122) M. A. Sherwani, S. Tufail, A. A. Khan, M. Owais, PLoS One **2015**, 10, 1–20.

(123) E. Darabpour, N. Kashef, S. M. Amini, S. Kharrazi, G. E. Djavid, J. Drug Deliv. Sci. Technol. **2017**, 37, 134–140.
(124) A. A. Tawfik, J. Alsharnoubi, M. Morsy, Photodiagnosis Photodyn. Ther. **2015**, 12, 215–220.
(125) L. Misba, S. Kulshrestha, A. U. Khan, Biofouling **2016**, 32, 313–328.
(126) R. Rahimi, F. Fayyaz, M. Rassa, Mater. Sci. Eng. C **2016**, 59, 661–668.
(127) K. A. D. F. Castro, N. M. M. Moura, A. Fernandes, M. A. F. Faustino, M. M. Q. Simões, J. A. S. Cavaleiro, S. Nakagaki, A. Almeida, Â. Cunha, A. J. D. Silvestre, et al., Dye. Pigment. **2017**, 137, 265–276.
(128) F. Manjón, M. Santana-Magaña, D. García-Fresnadillo, G. Orellana, Photochem. Photobiol. Sci. **2010**, 9, 838–845.
(129) F. Manjón, M. Santana-Magaña, D. García-Fresnadillo, G. Orellana, Photochem. Photobiol. Sci. **2014**, 13, 397–406.
(130) O. Planas, R. Bresolí-Obach, J. Nos, T. Gallavardin, R. Ruiz-González, M. Agut, S. Nonell, Molecules **2015**, 20, 6284–6298.
(131) C. P. McCoy, R. A. Craig, S. M. McGlinchey, L. Carson, D. S. Jones, S. P. Gorman, Biomaterials **2012**, 33, 7952–7958.
(132) T. Yao, J. Wang, Y. Xue, W. Yu, Q. Gao, L. Ferreira, K.-F. Ren, J. Ji, J. Mater. Chem. B **2019**, 7, 5089–5095.
(133) K. J. Moor, C. O. Osuji, J. H. Kim, ACS Appl. Mater. Interfaces **2016**, 8, 33583–33591.
(134) M. L. Frade, S. R. de Annunzio, G. M. F. Calixto, F. D. Victorelli, M. Chorilli, C. R. Fontana, Molecules **2018**, 23, 473.
(135) C.-P. Chen, C.-M. Hsieh, T. Tsai, J.-C. Yang, C.-T. Chen, Int. J. Mol. Sci. **2015**, 16, 20859–20872.
(136) E. Feese, H. Sadeghifar, H. S. Gracz, D. S. Argyropoulos, R. A. Ghiladi, Biomacromolecules **2011**, 12, 3528–3539.
(137) B. L. Carpenter, E. Feese, H. Sadeghifar, D. S. Argyropoulos, R. A. Ghiladi, Photochem. Photobiol. **2012**, 88, 527–536.
(138) T. Akbari, M. Pourhajibagher, F. Hosseini, N. Chiniforush, E. Gholibegloo, M. Khoobi, S. Shahabi, A. Bahador, Photodiagnosis Photodyn. Ther. **2017**, 20, 148–153.
(139) E. Gholibegloo, A. Karbasi, M. Pourhajibagher, N. Chiniforush, A. Ramazani, T. Akbari, A. Bahador, M. Khoobi, J. Photochem. Photobiol. B Biol. **2018**, 181, 14–22.
(140) V. T. Anju, P. Paramanantham, S. L. Sruthil, A. Sharan, A. Syed, N. A. Bahkali, M. H. Alsaedi, K. K., S. Busi, Photodiagnosis Photodyn. Ther. **2019**, 27, 305–316.

Claudia Cecilia Vera obtained a Bachelor in Science in Biotechnology degree (2014) from Tucuman National University (UNT, Argentina). During her Ph.D. in biochemistry (2019), under the supervision of Dr. Rosana Chehín from UNT and Dr. Dulce Papy-Garcia from Université Paris-Est, she studied the role of matrix-associated glycosaminoglycanes on triggering protein tau pathologic processes associated with the development of Alzheimer's disease. In 2019, she obtained a postdoctoral fellowship from CONICET to work at the Bionanotechnology Institute (INBIONATEC, CONICET) in Santiago del Estero, Argentina. Her research focuses on the formulation of supramolecular platforms carrying photosensitizers for their application in antimicrobial photodynamic therapy

Fiorella Giovanna Tulli obtained her B.Sc. in chemistry (2014), and Ph.D. in Food Science and Technology (2019) at the Santiago del Estero National University (UNSE, Argentina). Her PhD study was focused on the design, development, and characterization of electrochemical (bio)sensors using different nanomaterials to carry out the detection of antioxidant compounds in different plant extracts. In 2019, she obtained a postdoctoral fellowship from CONICET to work at the Bionanotechnology Institute (INBIONATEC, CONICET-UNSE) in Santiago del Estero. Her research focuses on the design of nanocomposites platforms with photosensitizing and photocatalytic properties for water decontamination and pollutant sensing.

Claudio Darío Borsarelli was born in Rio Cuarto, Argentina, and earned his B.Sc. (1990) and Ph.D. (1994) in chemistry from Rio Cuarto National University (UNRC). After spending 3 years as a postdoctoral fellow at the Max-Planck Institute of Chemical Radiation (Germany) with Prof. Silvia Braslavsky, he moved in 1999 to Santiago del Estero National University in Argentina, where currently is Titular Professor and Principal Researcher at the National Research Council of Argentina (CONICET). Since 2016 he is serving as director of the Institute of Bionanotechnology (CONICET-UNSE). He also has received a Georg Forster fellowship in 2009 from the Alexander von Humboldt Foundation of Germany, and he was awarded by the American Photochemical Society and Argentinean Physical Chemistry Association (AAIFQ). His research interest includes photosensitized modifications of organic molecules and macromolecules of biological and alimentary interest, photobiology, and photocatalytic processes.

Anales de la Asociación Química Argentina

División Jóvenes Profesionales

Mini-Review

DEGRADATION OF SELECTED AGRICULTURAL PESTICIDES BY PHOTOSENSITIZED AND FENTON-LIKE PROCESSES

Eduardo A. Gatica [1], José Natera [1,2] and Walter A. Massad [2*]

[1] Instituto para el Desarrollo Agroindustrial y de la Salud (IDAS). CONICET – UNRC. Facultad de Agronomía y Veterinaria - Universidad Nacional de Río Cuarto.
[2] Instituto para el Desarrollo Agroindustrial y de la Salud (IDAS). CONICET – UNRC. Depto. De Química – FCEF-QyN - Universidad Nacional de Río Cuarto.

**Autor Corresponsal: wmassad@exa.unrc.edu.ar*

Graphical abstract

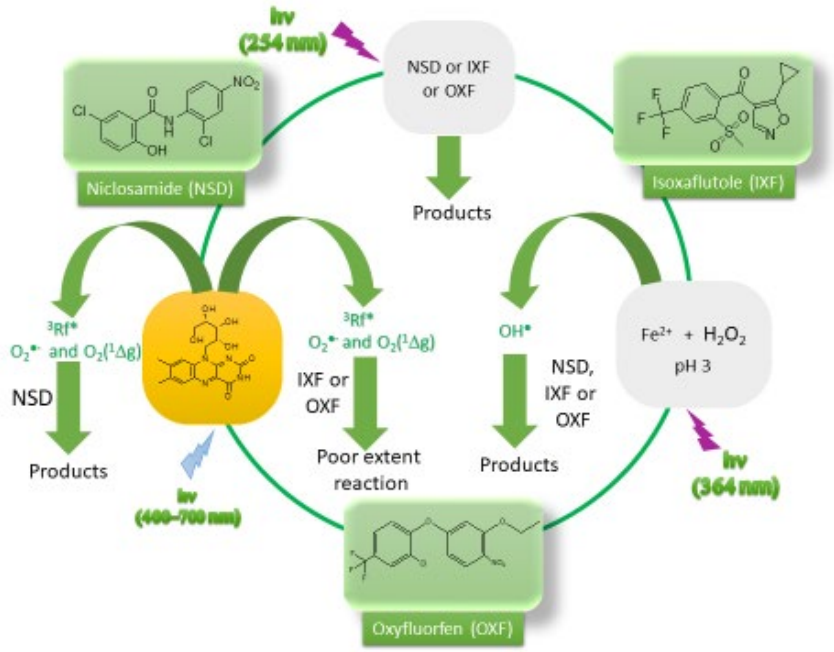

Resumen

En este trabajo se presenta el estudio de la degradación de contaminantes (Q) mediante la utilización de métodos sustentables. Los contaminantes investigados fueron distintos herbicidas y un antiparasitario perteneciente a distintas familias químicas: Isoxaflutole (IXF), Oxyfluorfen (OXF) y Niclosamida (NSD, antiparasitario). La fotodegradación se realizó empleando fotólisis directa y sensibilizada en presencia de Riboflavina (Rf). La Rf, normalmente presente en aguas naturales, es un fotosensibilizador que absorbe en la región visible del espectro y que, en presencia de radiación visible, genera especies reactivas de oxígeno tales como oxígeno singlete y anión radical superóxido. Además, se estudió la degradación de estos

compuestos por los procesos Fenton y Foto-Fenton. Estos procesos se caracterizan por generar el radical hidroxilo ($HO^{\bullet}$) en solución, el cual es una especia altamente oxidante capaz de mineralizar los compuestos orgánicos. Empleando Rf como fotosensibilizador los herbicidas no se degradan, pero NSD sí lo hace. IXF, OXF y NSD se degradaron por el $HO^{\bullet}$ generado por Foto-Fenton y los fotoproductos generados durante la fotólisis fueron detectados por HPLC-UV-Vis. En el caso de IXF, se determinaron las posibles estructuras químicas de los fotoproductos utilizando HPLC-MS/MS. Los resultados generales sugieren que la fotodegradación natural, empleando radiación visible y fotosensibilización, es una posible vía degradativa para NSD, pero no para los herbicidas. El resto de los compuestos estudiados se degradan por fotoirradiación directa, con un bajo valor de rendimiento cuántico y por Foto-Fenton con una buena velocidad de degradación.

Abstract

This paper presents the study of the degradation of pollutants (Q) through the use of sustainable methods. Different herbicides and an antiparasitic belonging to different chemical families were investigated: Isoxaflutole (IXF), Oxyfluorfen (OXF) and Niclosamide (NSD, antiparasitic). Photodegradation was performed using direct and sensitized photolysis in the presence of Riboflavin (Rf). Rf, normally present in natural waters, is a photosensitizer that absorbs in the visible region of the spectrum and that, in the presence of visible radiation, generates reactive oxygen species such as singlet oxygen and superoxide radical anion. In addition, the degradation of these compounds by Fenton and photo-Fenton processes was studied. These processes are characterized by the generation of the hydroxyl radical ($HO^{\bullet}$) in aqueous solution, which is a highly oxidizing spice capable of mineralizing organic compounds. Using Rf as a photosensitizer the herbicides do not degrade, but NSD does. IXF, OXF and NSD were degraded by the $HO^{\bullet}$ generated by photo-Fenton and the photoproducts generated during the photolysis were detected by HPLC-UV-Vis. In the case of IXF, the possible chemical structures of the photoproducts were determined using HPLC-MS / MS. The general results suggest that natural photodegradation, using visible radiation and photosensitization, is a possible degradative pathway for NSD, but not for herbicides. The rest of the compounds studied are degraded by direct photoirradiation, with a low quantum yield value and by Photo-Fenton with a good degradation rate.

Palabras Clave: *Riboflavina, foto-Fenton, pesticidas, fotodegradación sensibilizada, especies reactivas de oxígeno.*

Keywords: *Riboflavin, photo-Fenton, pesticides, sensitized photodegradation, reactive oxygen species.*

1. Introduction

The contamination of surface and underground waters is caused by the accidental incorporation or intentional emptying of different types of industrial waste, household and agricultural pesticides, to mention some of the main anthropogenic sources. Pesticide contamination is common in agricultural-livestock places and in agrochemical distribution sites due to technological advances in agricultural activities during the last 5 decades, this is attributed to the growing world population, which demands quantity and quality of foods [1]. However, this new technologies are based largely on the use of agrochemicals such as insecticides, fungicides and herbicides [2] which often become in aquatic pollutants (Q). The treatment of contaminated areas remains a global problem, the inadequate disposal of such waste can cause soil contamination [3], and water surface or underground [4].

The elimination of such Q can be carried out by chemical and/or biological treatments, but few are broad and convenient. For example, incineration is currently the only practical option, but it is expensive, requires long-distance transportation to a treatment center and is strongly resisted by populations [5]. Biological processes such as bioremediation [6–8] is an alternative but it has some drawbacks such as: slow degradation rate, low specificity, incomplete metabolism and low survival capacity of bacterial strains in natural environments [9,10]. With respect to chemical degradation procedures, some of the most relevant are photochemicals, where direct photolysis could be applied to most of the Q, but it has a very low degradation efficiency for most pesticides[11]. Sensitized photolysis may constitute an alternative for the degradation of Q, although many of these compounds are transparent to natural light, they can be degraded through the action of photosensitizing substances whose characteristics is to absorb light and produce excited states with the ability to initiate a cascade of photoprocesses in which highly reactive species are generated, such as singlet oxygen ($O_2(^1\Delta_g)$) and superoxide radical anion ($O_2^{\bullet-}$) [12–18]. One of the most interesting photosensitizers is Riboflavin (Rf, Figure 1), a substance that is found in many everyday products (such as food and drugs) that could eventually act as a native

photogenerator of ROS like $O_2(^1\Delta_g)$ and $O_2^{\bullet-}$ with quantum yields of 0.47 and 0.009, respectively [19,20]. In addition, the vitamin constitutes one of the most important endogenous visible-light-absorbing photosensitizers in mammals [21]. From the environmental point of view, Rf is present as traces in natural waters courses and water bodies and has been postulated as a possible sensitizer for the natural photooxidative degradation of contaminants [14,22,23].

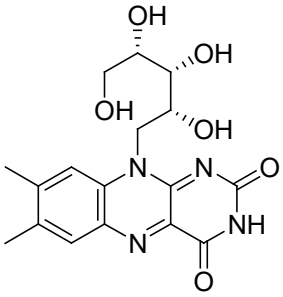

Figure 1. Chemical structure of Riboflavin (Rf).

More recently, numerous contributions have been reported using advanced processes oxidation (AOP)[24–29] for the degradation of Q. The AOPs uses H_2O_2, O_3 and O_2 to generate the main reactive species, the hydroxyl radical ($HO^{\bullet}$), thought chemical, photochemical, sonochemical or radiolysis methods.

In this review we present a summary studies of the degradation of organic compounds used in agricultural activities belonging to different chemical families by direct and sensitized photolysis, as well as AOPs, in particular Fenton and Fenton-like processes. This are the herbicides Isoxuflatole (IXF) which belong to the family of isoxazoles, Oxifluorfen (OXF) derived from compounds with diphenyl ether nucleus (herbicide) and the antiparasitic Niclosamide (NSD) which is a phenolic derivative.

Regarding the experimental methodology and materials you can consult the different publications carried out in our research group [12,14–16,30–35].

2. Herbicide Isoxaflutole (IXF)

Isoxaflutole (5-Cyclopropyl-4-[2-(methylsulfonyl)-4-(trifluoromethyl)benzoyl]isoxazole, IXF) belongs to the family of isoxazoles (Figure 2), it is a pro-herbicide (it has no herbicidal activity by itself) that spontaneously reorganizes in the presence of water hydrolyzing to diketonitrile ([2-cyclopropyl-3- (2-methyl sulfonyl-4 (trifluoromethyl) benzoyl)) -3-oxopropane-nitrile], DKN) which is a phytotoxic compound with herbicidal activity [36], which is an inhibitor of the enzyme 4-hydroxy-phenylpyruvate dioxygenase (4-HPPD) that participates in the synthesis of carotenoids [37,38].

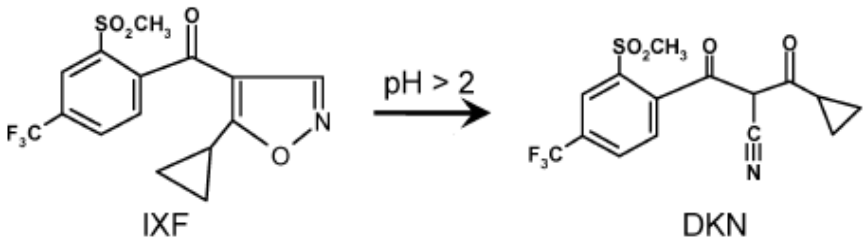

Figure 2. hydrolysis of IXF [39]

The United States Environmental Protection Agency (EPA) restricted the use of IXF because it is a probable human carcinogen, and it has a high potential for contamination of surface ground and groundwater [40] reaching concentration values of 0.4 μg/L in surface water and 0.00025 μg/L in groundwater [41]. IXF in water is hydrolyzed to DKN with an average lifetime of 433 h at pH 3 and 43 h at pH 8,42 therefore in natural waters its hydrolysis is favored and causes high contamination thereof, reaching DKN concentration values of 2.0 μg/L in surface water and 0.23 μg/L in groundwater [41].

Regarding to the presence of IXF in soil, it is hydrolyzed to DKN and its adsorption-desorption depends on the organic matter content of the soil [35], DKN is retained in soils with high content of organic matter, iron oxides and aluminum hydroxide [42], but the advantage in this system is

that DKN is biologically degraded to a derivative of benzoic acid [2-methylsulfonyl-4-trifluoromethylbenzoic acid (BA)], which is a non-toxic compound [43–45].

An alternative for the treatment of water contaminated by IXF, and its DKN hydrolysis product, is the oxidation with hypochlorite (ClO^-) which causes the oxidation of DKN to BA, with the disadvantage that toxic chlorinated intermediates are formed in this process [39]. For this reason, the degradation of IXF was studied using other methodologies, which are mentioned in the objectives, such as direct photolysis, sensitized, Fenton and photo-Fenton processes.

From the studies carried out, it was found that IXF has a quantum yield of direct photolysis relatively low ($\Phi = (4.7 \pm 0.3)\cdot 10^{-3}$) and it is not degraded by $O_2(^1\Delta_g)$, $O_2^{\bullet -}$ and by the singlet or triplet excited states of Rf.

With regard to the Fenton and Fenton-like process, Figure 3 (Inset (a)) compares the degradation of IXF by Fenton and photo-Fenton processes performed under the same experimental conditions and for different reaction times. In the Fenton experiment, no changes in [IXF] were observed during a reaction period of 5.2 hours. Meanwhile, for photo-Fenton measurements, changes of [IXF] as a function of irradiation time could be adjusted to a pseudo first order kinetics (0.015 ± 0.001 min^{-1}) reaching a 99% conversion in 310 min. The main reactive species in the photo-Fenton process is $HO^{\bullet}$; from a competitive method, a reaction rate constant value of $(1.0 \pm 0.1)\cdot 10^9$ $M^{-1}s^{-1}$ was measured for the reaction between IXF and $HO^{\bullet}$ in aqueous solution Figure 3 (main) [35].

Inset (b) of Figure 3 shows the variation of total organic carbon (TOC) of an IXF solution treated by the photo-Fenton process. After 98% degradation of IXF, 88% was completely mineralized and the reaction products were monitored by HPLC. Measures of UHPLC-MS / MS allowed to determine the possible structures of the products, based on these results a mechanism for the reaction of IXF with $HO^{\bullet}$ was proposed (Scheme 1) [35], where $HO^{\bullet}$ can attack to the carbon atom of the carbonyl group (pathway 1) or to the aromatic ring (pathway 2).

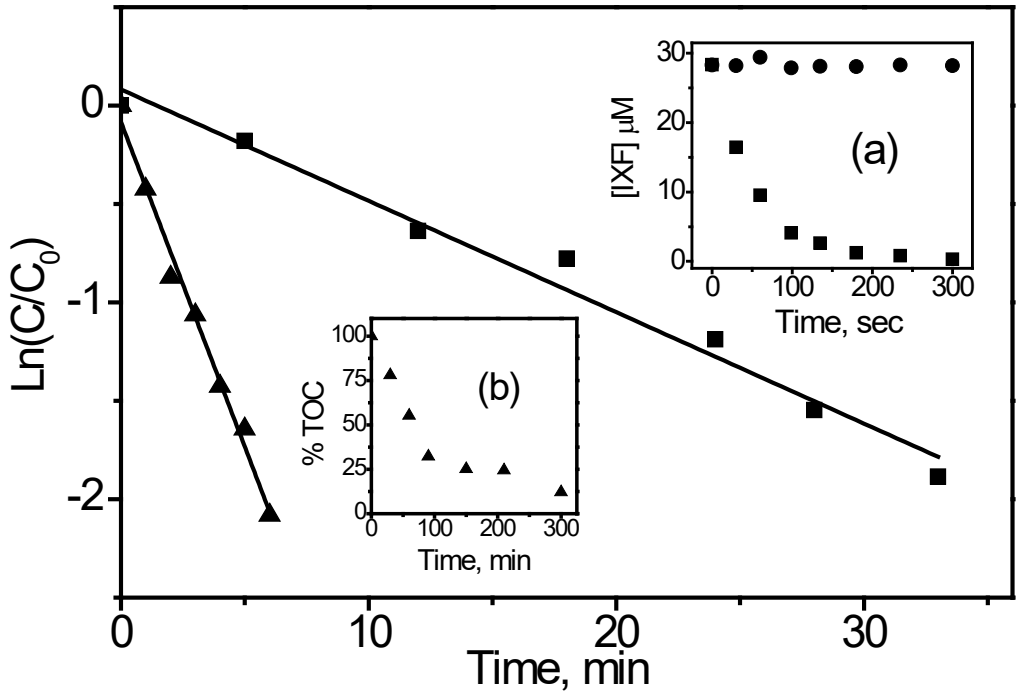

Figure 3. Rate constant determination for the reaction of IXF with HO•, first-order plots for the (■) [IXF] = 28 μM and (▲) [Phe] = 28 μM degradation in a photo-Fenton system. Inset (a): Degradation of 28 μM IXF by (●) Fenton and (■) photo-Fenton in aqueous media at different reaction times. Fenton reagent: $[H_2O_2]_0 = 1.0 \cdot 10^{-2}$ M, $[Fe^{2+}]_0 = 5.2 \cdot 10^{-5}$ M at pH = 3 adjusted by $HClO_4$ 0.1 M. Inset (b): Total organic carbon in a [IXF] = 28 μM solution upon irradiation in a photo-Fenton treatment. In all the experiments, the irradiation system was a Rayonet RPR-200 equipped with eight 6-W fluorescent black lamps with emission centered at 364 nm.

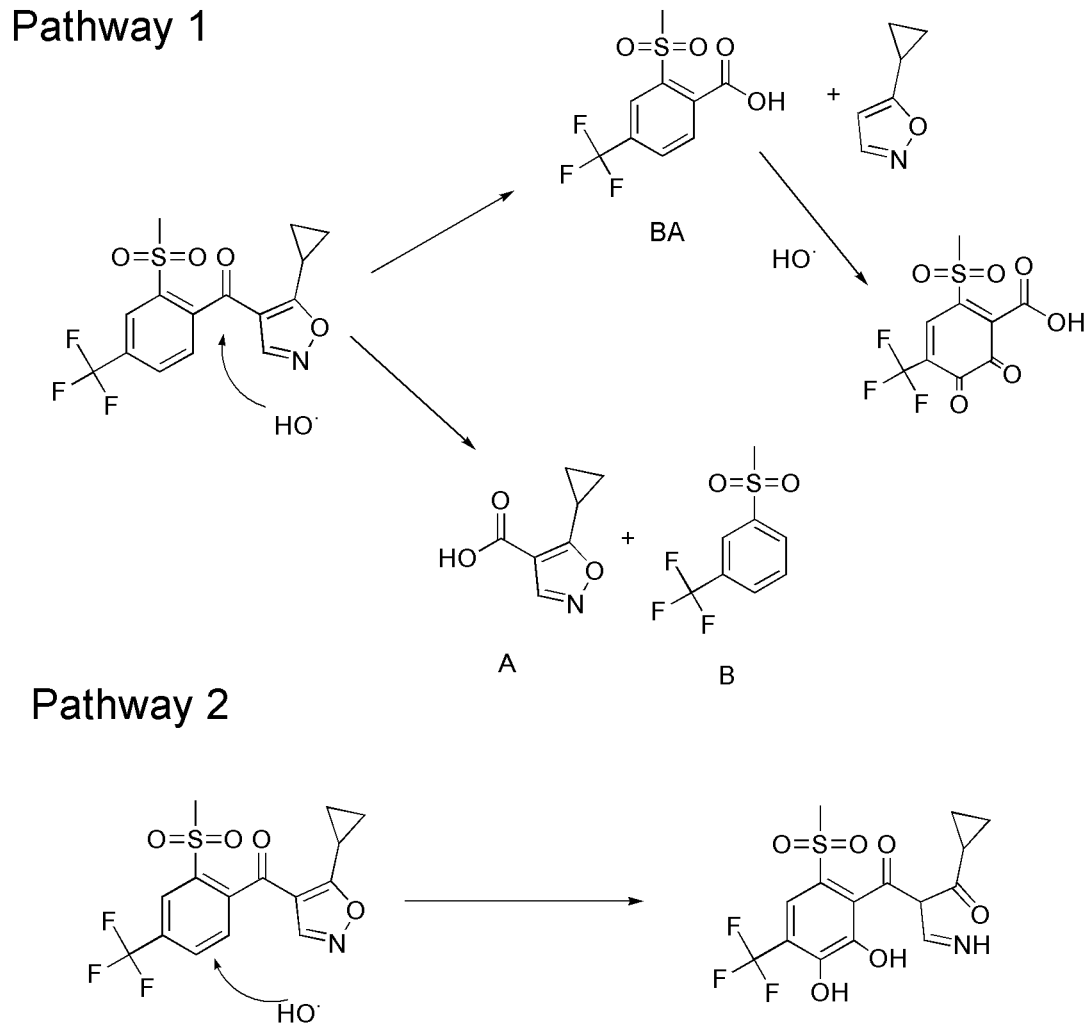

Scheme 1. Proposed pathways for the photo-Fenton degradation of IXF. Pathway 1: attack of the HO• to the C = O to produce different products. Pathway 2: hydrogen abstraction reaction in the aromatic ring, giving catechol derivatives.

3. Oxyfluorfen Herbicide (OXF)

It is a herbicide with diphenyl ether nucleus (2-chloro-1-(3-ethoxy-4-nitrophenoxy)-4-(trifluromethyl)benzene, OXF, Figure 4) and is used for the control of monocotyledons and broadleaf weeds in soy, sunflower, peanut, citrus, tobacco, etc., it requires the presence of light to exhibit phytotoxic activity [46,47]. OXF it is an inhibitor of the protoporphyrinogen oxidase enzyme, and it is not metabolized in plants and undergoes very little translocation and

phototransformation, this suggests that the abiotic pathway as the most effective path to its degradation. It is considered very toxic to aquatic organisms [48], being its solubility in water of 0.1 mg/L, which can contaminate surface water through runoff [48]. This herbicide degrades at a temperature greater than 50 ºC and its photodecomposition in water is slower than in soil with a half-life for the latter of approximately 30 to 56 days [49].

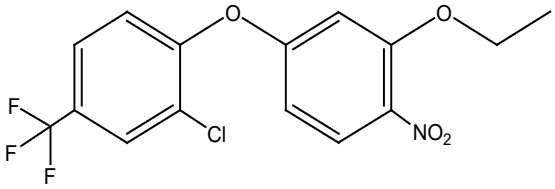

Figure 4. Oxyfluorfen (OXF)

OXF is not degraded by microbial action or hydrolysis [50], the content of soil organic matter and clay influencing its persistence and activity [50–52], and its absorption in soil is very high, so the contamination of groundwater is unlikely.

There are few studies of direct photodegradation of OXF according to the existing literature, due to the low solubility of OXF in water the direct photolysis studies have been carried out by UV radiation in pure organic solvents and in a 50% V/V MeOH/H_2O mixture achieving the gradation of OXF [53,54]. Regarding sensitized photolysis and Fenton processes, there was not bibliographic background, for this reason, studies of sensitized photolysis and Fenton processes were carried out. Given the low solubility of OXF, the studies were related in microheterogeneous medium using hydroxypropyl-beta-cyclodextrin (HP-β-CD) since in addition to increasing the solubility it has been shown that, in certain occasions, HP-β-CD produces an increase in the efficiency of Fenton processes.

Previous to photodegradation experiments, the OXF-HP-β-CD system was characterized (reaction (1), scheme 2). This was done by measuring the spectral changes of OXF at different

concentrations of HP-β-CD (Figure 5), where it is observed an increase in the maximum absorption at 330 nm increases as the concentration of HP-β-CD increases. According to the results obtained, OXF is associated with HP-β-CD. From the absorption changes at 330 nm (Figure 5, Inset), the association constant of OXF with HP-β-CD (Kas) was determined by applying the Scott model [55,56], giving a value of 210 ± 10 M^{-1}. When the data is adjusted to Scott's model, the formation of the OXF complex with HP-β-CD results in a 1:1 stoichiometry.

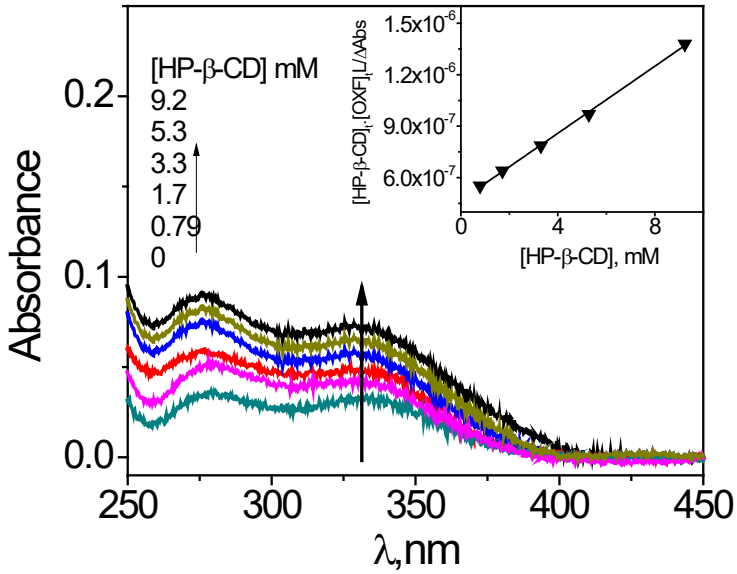

Figure 5. OXF absorption spectra at different concentrations of HP-β-CD in mM and [OXF] = 6 μM. Insert: determination of the Kas for the OXF ([OXF] = 6 μM) association with HP-β-CD using the Scott model at 330 nm [55,56].

With respect to the photodegradation studies, the ROS photogenerated by ^{3}Rf* ($O_2(^1\Delta_g)$ and/or $O_2^{\bullet-}$) or by electron transfer processes from ^{1}Rf* and/or ^{3}Rf* do not degrade OXF. Also, no changes in the [OXF] was observed after 3 hrs under Fenton reaction conditions.

However, OXF is decomposed by the photo-Fenton process Figure shows the OXF concentrations for the different reaction times obtained from HPLC measurements (Figure 5, Inset) in an aqueous medium with HP-β-CD 0.037 M.

Changes in [OXF] as a function of irradiation time were fitted to a zero order kinetics (k′ = (9.8 ± 0.5)·10^{-7} min^{-1} (reactions (8)-(11), Figure 6) reaching a conversion value of 93 % in 30 minutes. The order of kinetics could be attributed to the formation of a ternary complex (OXF-HP-β-CD-Fe^{2+}). This type of ternary complex has been previously reported in the degradation of trinitrotoluene (TNT) and phenanthrene (PHE) by photo-Fenton (TNT- HP-β-CD-Fe^{2+}) and (PHE-HP-β-CD-Fe^{2+}); as well as in the degradation of hydrophobic organic compounds by Fenton [32,57]. If this type of complex is formed in the degradation of OXF by photo-Fenton, the radical HO• is formed near of the OXF and can react with OXF without having to diffuse in solution. Furthermore, the reaction of the radical HO• with HP-β-CD have a rate constant of 2.6·10^{9} $M^{-1}s^{-1}$ [57], since the HP-β-CD concentration is 1186 times larger than the OXF, the degradation of the herbicide would be very slow or would not degrade if the ternary complex was not formed.

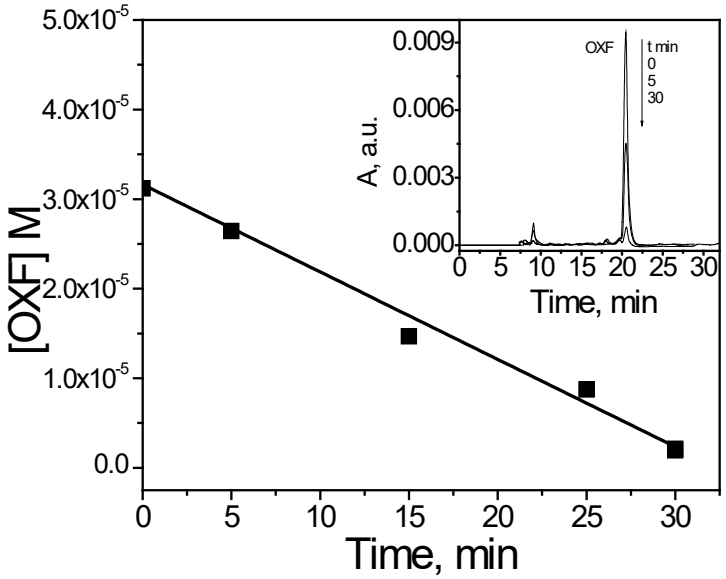

Figure 6. OXF degradation by photo-Fenton. $[OXF]_0$ = 3.1·10^{-5} M, $[H_2O_2]_0$=1.0·10^{-2} M, $[Fe^{2+}]_0$ = 5.2·10^{-5} at pH 3 given by $HClO_4$ 0.1 M. [HP-β-CD] = 0.037 M. Insert: Chromatograms at different photolysis times. Irradiation source: 12 lamps of 8 W each one, emission at 364 nm. Chromatographic conditions: FM, ACN/H_2O 75/25 V/V, FV= 0.5 mL/min and $\lambda_{detec.}$= 375 nm. Column C18 (250 mm x 4.60 mm 5 μm).

For this process, taking as reference the degradation of phenanthrene by photo-Fenton in HP-β-CD solution [57], the mechanism shown in the Scheme 2 is proposed.

$$OXF + HP\text{-}\beta\text{-}CD \rightleftarrows OXF\text{-}HP\text{-}\beta\text{-}CD \quad Kas_1 = 210\ M^{-1} \tag{1}$$

$$OXF + HP\text{-}\beta\text{-}CD + Fe^{2+} \rightleftarrows Fe^{2+}\text{- }HP\text{-}\beta\text{-}CD\text{-}OXF \tag{2}$$

$$H_2O_2 + Fe^{2+} \rightarrow Fe^{3+} + OH^- + HO^\bullet \tag{3}$$

$$HO^\bullet + Fe^{2+} \rightarrow Fe^{3+} + OH^- \tag{4}$$

$$HO^\bullet + H_2O_2 \rightarrow H_2O + HOO^\bullet \tag{5}$$

$$HOO^\bullet + Fe^{3+} \rightarrow O_2 + Fe^{2+} + H^+ \tag{6}$$

$$Fe(OH)^{2+} + h\nu \rightarrow Fe^{2+} + HO^\bullet \tag{7}$$

$$OXF + HO^\bullet \rightarrow P(8) \tag{8}$$

$$OXF\text{-}HP\text{-}\beta\text{-}CD + HO^\bullet \rightarrow P(9) \tag{9}$$

$$Fe^{2+}\text{-}HP\text{-}\beta\text{–}CD\text{-}OXF + H_2O_2 + h\nu \rightarrow Fe^{3+}\text{- }HP\text{-}\beta\text{-}CD\text{ -}OXF(HO^\bullet) \tag{10}$$

$$Fe^{3+}\text{-}HP\text{-}\beta\text{-}CD\text{-}OXF(HO^\bullet) \rightarrow P(11) \tag{11}$$

$$HP\text{-}\beta\text{-}CD + HO^\bullet \rightarrow P(12) \tag{12}$$

Scheme 2. Possible mechanism in the degradation of OXF by photo-Fenton, in micro-heterogeneous medium.

4. Antiparasitary Niclosamide (NSD)

Niclosamide (5-chloro-N-(2-chloro-4-nitrophenyl)-2-hydroxybenzamide, NSD) belongs to the family of medications called anthelmintics (Figure 7). It is used in the treatment of conditions caused by different types of worms (specifically against cestodes), its activity against these worms is due to the inhibition of glucose absorption and oxidative phosphorylation in mitochondria [58]. Its use extends to a wide variety of animal species (cattle, sheep, goats and pigs, dogs and cats) including humans [32].

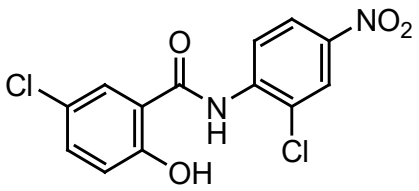

Figure 7. Niclosamide (NSD)

NSD is poorly absorbed in the intestine and is excreted in the feces almost unmodified, due to this it is of low toxicity for the organisms that are treated with it. Nevertheless, NSD is toxic to fish, zooplankton, molluscs and amphibians, and to a lesser extent in birds [59,60]. This compound is practically insoluble in water, being little soluble in the pH range of 8-10 [61]. β-cyclodextrin (β-CD) and HP-β-CD have been used to increase its the solubility, in this new media the NSD solubility was $4 \cdot 10^{-6}$ M and $3 \cdot 10^{-5}$ M respectively [58]. With respect to the fate of this compound in the environment, the average life time ranges from 8.1 to 3.9 days when it is in the sediments [62], while in buffered aqueous solution or in tank water hydrolysis is insignificant after 56 days [63]. In soil, the average life time depends on its depth and humidity, being 199 h at 0.5 mm and 1064 h at 3.0 mm deep on dry soil, with respect to soil moisture the average life time is 2 to 5 times higher in dry soil than wet soil [64].

Due to the environmental concern on the NSD, direct and sensitized photodegradation studies in homogeneous and micro-heterogeneous media were carried out. In addition, the degradation of NSD was studied by Fenton and photo-Fenton processes [33,34].

5. Photolysis of NSD at 254 nm

Direct photolysis of NSD at 254 nm (radiation source: 4 lamps of 8 W each) was performed in two different media: MeOH and 0.05 M MeOH / NaOH. To determine the NSD photodegradation quantum yield a relative method was applied and the herbicide 2-Chloro-4,6-diamino-1,3,5-Triazine (CDAT, $\Phi = 0.0069$) was used as a reference.

The degradation in alkaline medium was higher than in MeOH, with degradation rate of NSD in alkaline medium being 3 times higher than in MeOH. The Φ measured were $(9.0 \pm 0.7)\cdot10^{-5}$ and $(2.7 \pm 0.2)\cdot10^{-4}$ for MeOH and MeOH / NaOH respectively. These results indicate a low photodegradation efficiency at 254 nm for NSD, independent of the degree of ionization of the phenolic -OH group.

6. Riboflavin Sensitized Photolysis

From literature it is known that NSD forms an inclusion complexes with HP-β-CD and Rf is associated with HP-β-CD [34], as mentioned for sensitized photolysis the following reaction mechanism is proposed (Scheme 3):

$$NSD + HP\text{-}\beta\text{-}CD \rightleftarrows NSD\text{-}HP\text{-}\beta\text{-}CD \quad (Kas_1 = 20.7\ M^{-1})^{58} \tag{13}$$

$$NSD\text{-}HP\text{-}\beta\text{-}CD + HP\text{-}\beta\text{-}CD \rightleftarrows NSD\text{-}(HP\text{-}\beta\text{-}CD)_2 \quad (Kas_2 = 342\ M^{-1})^{58} \tag{14}$$

$$Rf + HP\text{-}\beta\text{-}CD \rightleftarrows Rf\text{-}HP\text{-}\beta\text{-}CD \quad (Kas = 5.75\ M^{-1})^{65} \tag{15}$$

$$Rf + h\nu \rightarrow {}^1Rf^* \rightarrow {}^3Rf^* \tag{16}$$

$$Rf\text{-}HP\text{-}\beta\text{-}CD + h\nu \rightarrow {}^1Rf\text{-}HP\text{-}\beta\text{-}CD^* \rightarrow {}^3Rf\text{-}HP\text{-}\beta\text{-}CD^* \tag{17}$$

$${}^3Rf^* + NSD \rightarrow P(18) \tag{18}$$

$${}^3Rf^* + NSD\text{-}HP\text{-}\beta\text{-}CD \rightarrow P(19) \tag{19}$$

$${}^3Rf^* + NSD\text{-}(HP\text{-}\beta\text{-}CD)_2 \rightarrow P(20) \tag{20}$$

$${}^3Rf^* \rightarrow P(21) \tag{21}$$

$${}^3Rf^* + NSD \rightarrow Rf^{\bullet-} + NSD^{\bullet+} \tag{22}$$

$${}^3Rf^* + NSD\text{-}HP\text{-}\beta\text{-}CD \rightarrow Rf^{\bullet-} + NSD\text{-}HP\text{-}\beta\text{-}CD^{\bullet+} \tag{23}$$

$${}^3Rf^* + NSD\text{-}(HP\text{-}\beta\text{-}CD)_2 \rightarrow Rf^{\bullet-} + NSD\text{-}(HP\text{-}\beta\text{-}CD)_2{}^{\bullet+} \tag{24}$$

$$Rf^{\bullet-} + H^+ \rightarrow RfH^{\bullet} \tag{25}$$

$$2\ RfH^{\bullet} \rightarrow Rf + RfH_2 \tag{26}$$

$$RfH_2 + O_2({}^3\Sigma_g^-) \rightarrow RfH_2{}^{\bullet+} + O_2{}^{\bullet-} \tag{27}$$

^{3}Rf- HP-β-CD*+ NSD → P(28) (28)

^{3}Rf- HP-β-CD*+ NSD-HP-β-CD → P(29) (29)

^{3}Rf- HP-β-CD*+ NSD-(HP-β-CD)$_2$ → P(30) (30)

^{3}Rf- HP-β-CD*→ P(31) (31)

^{3}Rf- HP-β-CD*+ NSD → Rf-HP-β-CD$^{\bullet-}$ + NSD$^{\bullet+}$ (32)

^{3}Rf- HP-β-CD*+ NSD-HP-β-CD → Rf-HP-β-CD$^{\bullet-}$ + NSD-HP-β-CD$^{\bullet+}$ (33)

^{3}Rf- HP-β-CD*+ NSD-(HP-β-CD)$_2$ → Rf-HP-β-CD$^{\bullet-}$ + NSD-(HP-β-CD)$_2^{\bullet+}$ (34)

Rf-HP-β-CD$^{\bullet-}$ + H$^+$ → RfH-HP-β-CD$^\bullet$ (35)

2 RfH-HP-β-CD$^\bullet$ → Rf-HP-β-CD + RfH$_2$-HP-β–CD (36)

RfH$_2$-HP-β-CD + O$_2$($^3\Sigma_g^-$) → RfH$_2$- HP-β-CD$^{\bullet+}$ + O$_2^{\bullet-}$ (37)

O$_2^{\bullet-}$ + NSD → P(38) (38)

O$_2^{\bullet-}$ + NSD-HP-β-CD → P(39) (39)

O$_2^{\bullet-}$ + NSD-(HP-β-CD)$_2$ → P(40) (40)

^{3}Rf* + O$_2$($^3\Sigma_g^-$) → Rf + O$_2$($^1\Delta_g$) (41)

^{3}Rf- HP-β-CD*+ O$_2$($^3\Sigma_g^-$) → Rf- HP-β-CD + O$_2$($^1\Delta_g$) (42)

O$_2$($^1\Delta_g$) → O$_2$($^3\Sigma_g^-$) + hν (43)

O$_2$($^1\Delta_g$) + NSD → O$_2$($^3\Sigma_g^-$) + NSD (44)

O$_2$($^1\Delta_g$) + NSD → P(45) (45)

O$_2$($^1\Delta_g$) + NSD-HP-β-CD → O$_2$($^3\Sigma_g^-$) + NSD-HP-β-CD (46)

O$_2$($^1\Delta_g$) + NSD-HP-β-CD → P(47) (47)

O$_2$($^1\Delta_g$) + NSD-(HP-β-CD)$_2$ → O$_2$($^3\Sigma_g^-$) + NSD-(HP-β-CD)$_2$ (48)

O$_2$($^1\Delta_g$) + NSD-(HP-β-CD)$_2$ → P(49) (49)

Scheme 3. Possible processes in the sensitized photolysis of NSD with Rf in micro-heterogeneous medium, reactions (13) to (49).

7. Comparison of photosensitized processes in the media studied

For comparison purposes, Table 1 shows the values of the quenching rate constants of ^{3}Rf* (^3k_q) and $O_2(^1\Delta_g)$ (k_t and k_r) for the NSD systems plus aqueous HP-β-CD, NSD in MeOH and NSD in alkalized MeOH.

Table 1. Quenching rate constant of ^{3}Rf* (^3k_q) and $O_2(^1\Delta_g)$ (overall (k_t) and reactive (k_r)) by NSD in methanol, methanol plus NaOH and aqueous HP-β-CD.

Solvent	^3k_q ($M^{-1}s^{-1}$)	k_t ($M^{-1}s^{-1}$)	k_r ($M^{-1}s^{-1}$)
MeOH	$(2.3 \pm 0.1)\cdot10^9$	$(6.0 \pm 0.3)\cdot10^5$	$(5.8 \pm 0.3)\cdot10^5$
MeOH + 50 mM NaOH		$(8.1 \pm 0.4)\cdot10^6$	$(1.8 \pm 0.1)\cdot10^6$
HP-β-CD	$(5.1 \pm 0.3)\cdot10^7$	$(1.7 \pm 0.1)\cdot10^8$	$(2.4 \pm 0.1)\cdot10^7$

The ^3k_q value determined in the NSD system plus HP-β-CD (reactions (18) - (24) and (28) - (34), Scheme 3) was approximately two orders of magnitude lower than that obtained using MeOH as solvent. A similar result has already been observed by Sengupta *et al.*, comparing the quenching of ^{3}Rf* by triethylamine (TEA) in aqueous solution, in the presence and absence of β-CD [66]. Returning to our case, and with the reasoning of Sengupta *et al.*, two factors could cooperate to the observed reduction in the value of ^3k_q:

(A) As mentioned, NSD forms inclusion complexes with HP-β-CD while Rf forms only H-bond with the -OH of the HP-β-CD [58]. The immediate consequence of this fact could be evident by a decrease in the collision frequency between NSD-HP-β-CD, NSD-(HP-β-CD)$_2$ and ^{3}Rf-HP-β-CD*, affecting the efficiency of the electron transfer process.

(B) If the radicals generated in reactions (22) - (24) and (32) - (34) in Scheme 3 are not adequately stabilized the back electron transfer between the ionic pair could predominates. This could occur if the solvation near HP-β-CD is reduced enough to produce a decrease in the

hydrogen abstraction of water molecules by the transient species $Rf^{\bullet -}$ y Rf-(HP-β-CD)$^{\bullet +}$ (reactions (25) y (35), Scheme 3) to form the neutral radicals. According to the above, the micro-heterogeneous systems appear to be less efficient in forming the stabilized neutral radical RfH-HP-β-CD$^{\bullet}$ than the free species of $Rf^{\bullet -}$ present in a homogeneous medium using MeOH (reaction (25), Scheme 3).

Both factors could simultaneously cooperate in a kind of synergistic effect, in the case of electron-mediated deactivation of $^3Rf^*$, ^{3}Rf-HP-βCD* by NSD-HP-β-CD and NSD-(HP-β-CD)$_2$.

With respect to the values of k_t and k_r (Table 1), which represent the quenching processes of $O_2(^1\Delta_g)$ by NSD, NSD-HP-β-CD and NSD-(HP-β-CD)$_2$, which are considerably higher when Q is encapsulated in the aqueous cyclodextrin system compared to dissolved in MeOH. This result is based on the mechanistic interpretation of the interaction of electron donor species, such as phenols, with the electrophilic species $O_2(^1\Delta_g)$. This process involves an intermediate meeting complex that has a certain degree of charge transfer character, represented by the scheme in Scheme 4 [67,68].

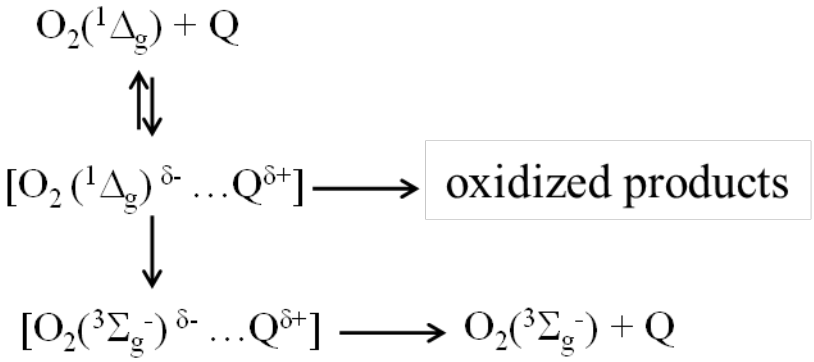

Scheme 4. Generation and evolution of the excited encounter complex, between $O_2(^1\Delta_g)$ and NSD. For simplicity Q represents: NSD-(HP-β-CD)$_2$, NSD-HP-β-CD and NSD.

8. Comparative experiments of sensitized photoxidation of NSD and phenol (FE)

Since NSD is a phenolic derivative, for comparison phenol (FE) was used to measure their relative reactivity; in addition, phenol is consider a contaminating model due to its extensive use

in industry, Figure 8 shows the relative rates of oxygen consumption (VRCO) for the sensitized photolysis by Rf and Rose Bengal (RB), in the different media used: microheterogeneous (aqueous solution of HP-β-CD) and homogeneous (MeOH). As observed, NSD has greater reactivity than FE in all the systems studied.

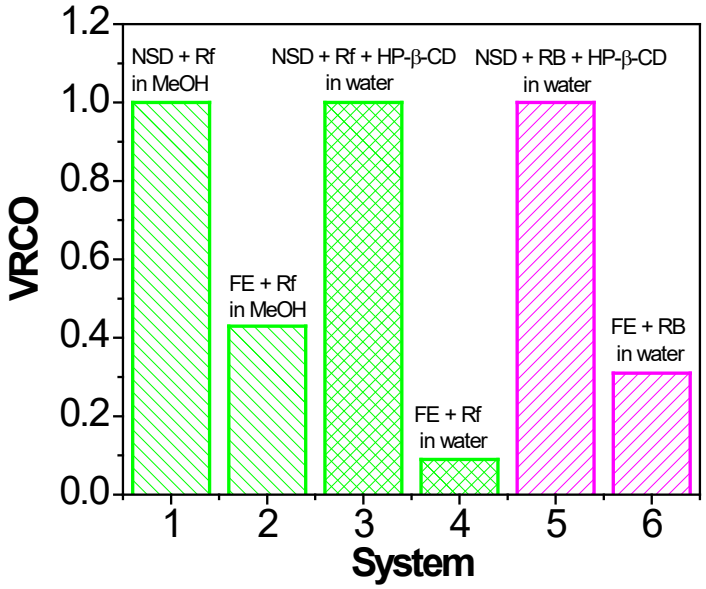

Figure 8. Diagram of relative rates of oxygen consumption for: (1) 0.5 mM NSD + Rf; (2) 0.5 mM FE + Rf; (3) Rf in MeOH solution and Rf (Abs.445 nm) = 0.4 (3) 0.1 mM NSD + Rf; (4) 0.1 mM FE + Rf; (5) 0.1 mM NSD + RB; (6) 0.1 mM FE + RB. Rf ($Abs._{445\ nm}$) = 0.43 and RB ($Abs._{555\ nm}$) = 0.44 in 0.037 M HP-β-CD in aqueous solution. Irradiation source: 150W halogen lamp.

It is clearly shown in Figure 8, that the VRCO in photosensitization using Rf and RB is much faster in HP-β-CD aqueous solution of NSD than the FE in water. In addition, the VRCO for FE in the photosensitized-RB system is three times greater than that observed for photosensitization of Rf. As demonstrated, FE exhibits limited reactivity in its molecular form towards $O_2(^1\Delta_g)$ [69]. This means that the combined action of the ROS, $O_2^{\bullet-}$ and $O_2(^1\Delta_g)$, oxidizes the NSD species (NSD, NSD-HP-β-CD y NSD-$(HP\text{-}\beta\text{-}CD)_2$), using Rf as a photosensitizer, constitute an efficient system, compared to the total oxidation observed for FE using the same photosensitizer.

The comparison of the results between the overall photooxidation efficiency for the Rf sensitized systems in MeOH and in aqueous media are also remarkable. As shown in Figure 8, the VRCO for aqueous encapsulated NSD is approximately five times faster than the corresponding one in MeOH, always relative to the VRCO of FE in the respective media. In this case, the increased polarity of the solvent and the effects of ionization constitute the driving force in increasing the photodegradation rate mediated by $O_2(^1\Delta_g)$ of NSD.

9. Fenton and photo-Fenton processes

Fenton and Photo-Fenton reactions were carried out in an aqueous medium with 0.037 M HP-β-CD, in these experiments HP-β-CD was used as additive for direct and sensitized photolysis, where NSD forms inclusion complexes. Moreover, the presence of Fe^{2+} very likely form a ternary complex (NSD-HP-β-CD-Fe^{2+}) similar to the OXF photo-Fenton degradation using the same reaction conditions, according to bibliographic background is proposed a mechanism for the degradation of NSD by photo-Fenton [57] similar to that of OXF degradation.

Figure 9 shows that [NSD] decreases over the time in a photo-Fenton system, this suggests that NSD reacts with $HO^{\bullet}$, as mentioned above, NSD is a derivative of phenol, it has been reported that phenols are reactive towards $HO^{\bullet}$, as for example, FE [70], 4-chlorophenol (4-ClFE) [71,72]. In the case of FE a complete mineralization was achieved, were catechols and hydroquinones are formed as intermediates and finally the opening of the ring conduce to the CO_2 and H_2O formation [70]. For the 4-ClFE, different photoproducts are obtained, such as resorcinol, hydroquinone, FE, 4-chlorocatechol, chlorohydroquinone, benzoquinone and 1,2,4-trihydroxybenzene [71,72].

The values of [NSD] as a function of the irradiation time for a photo-Fenton process are adjusted to zero order kinetics ($k' = (1.1 \pm 0.1)\cdot10^{-6}$ M min^{-1}) (Figure 9), reaching a 90% conversion value

in 20 minutes of reaction. The reaction order could be attributed to the hypothesis that the ternary complex is formed ($k' = (1.1 \pm 0.1)\cdot10^{-6}$ M min^{-1}).

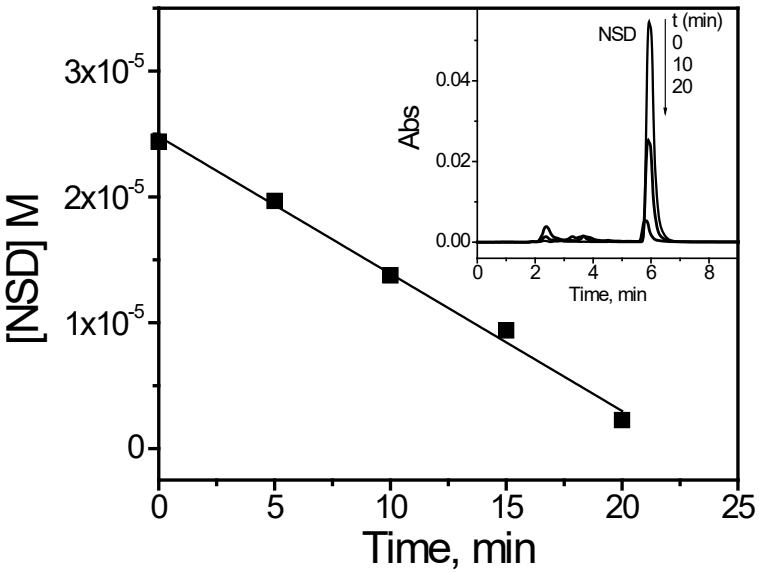

Figure 9 Changes in the [NSD] in function of the time of reaction for the photo-Fenton system. $[NSD]_0=2.3\cdot10^{-5}$ M, $[H_2O_2]_0 = 1.0\cdot10^{-2}$ M, $[Fe^{+2}]_0 = 5.2\cdot10^{-5}$ at pH 3 given by $HClO_4$ 0.1 M. Aqueous solution of HP-β-CD 0.037 M. **Insert**: Chromatograms at different photolysis times. Irradiation source: Rayonet reactor with 12 UV-lamps (364 nm) of 8 W each. Chromatographic conditions: Mobile phase: ACN/H_3PO_4 (1%) 80/20 V/V, FV=1mL/min y $\lambda_{detec.}$= 333 nm. Column C18 Phenomenex Gemini 5 U C18 110 Å (250 mm x 4.60 mm 5 µm).

Figure 9 Changes in the [NSD] in function of the time of reaction for the photo-Fenton system. $[NSD]_0 = 2.3\cdot10^{-5}$ M, $[H_2O_2]_0 =1.0\cdot10^{-2}$ M, $[Fe^{+2}]_0 = 5.2\cdot10^{-5}$ at pH 3 given by $HClO_4$ 0.1 M. Aqueous solution of HP-β-CD 0.037 M. Insert: Chromatograms at different photolysis times. Irradiation source: Rayonet reactor with 12 UV-lamps (364 nm) of 8 W each. Chromatographic conditions: Mobile phase: ACN/H_3PO_4 (1%) 80/20 V/V, FV=1mL/min y $\lambda_{detec.}$ = 333 nm. Column C18 Phenomenex Gemini 5 U C18 110 Å (250 mm x 4.60 mm 5 µm).

10. Conclusions

In general, it can be concluded that, depending on the results obtained, the herbicides studied are not degraded by photosensitized process by Rf, so probably in a natural aquatic environment such photodegradation would not occur. To achieve their degradation, processes that generate reactive species with greater oxidizing power like the hydroxyl radical must be used, this radical is generated in the advanced oxidation processes such as photo-Fenton system. Thus, when a residue containing herbicides such as those studied is available, a POA treatment should be carried out before being discarded.

With respect to NSD, a phenolic derivative, in a natural aquatic environment, it is very likely that it will be degraded by photolysis photosensitized by Rf, which could constitute a means that contributes to its decrease in aquatic environments. On the other hand, the mechanistic and kinetic information presented can help to understand the potential photodegradative processes that may be operating in that environment.

The use of aqueous solutions of CDs allowed to increase the concentration of the Q due to their low water solubility. In this way it was avoided to use mixtures of organic solvent and water as a dissolution medium. Therefore, the photodegradation process turns out to be more environmentally friendly avoiding the use of organic solvent. Another aspect to highlight for the micro-heterogeneous medium is the increase in the efficiency of the photodegradative processes of the Q (OXF and NSD) compared to homogeneous media.

Acknowledgements

Thanks are given to Consejo Nacional de Investigaciones Científicas y Técnicas (CONICET), Agencia Nacional de Promoción Científica y Tecnológica (ANPCyT), Agencia Córdoba Ciencia (ACC) and Secretaría de Ciencia y Técnica of the Universidad Nacional de Río Cuarto (SECyT UNRC), all from Argentina, for financial support.

References

(1) Guzzella, L.; Pozzoni, F.; Giuliano, G. Environ. Pollut. **2006**, 142, 344–353.
(2) Liu, Y.; Pan, X.; Li, J. J. Agric. Environ. Ethics **2015**, 28, 203–216.
(3) Dasappa, S. M.; Loehr, R. C. Water Res. **1991**, 25, 1121–1130.
(4) Habecker, M. A. Environmental contamination at Wisconsin pesticide mixing/loading facilities: Case study, investigation and remedial action evaluation, Wisconsin Department of Agriculture, Trade, and Consumer Protection, Agricultural Resource Management Division, **1989**.
(5) Steverson, E. Environ. Sci. Technol. **1991**, 25, 1808–1814.
(6) Boopathy, R. Bioresour. Technol. **2000**, 74, 63–67.
(7) Gavrilescu, M.; Demnerová, K.; Aamand, J.; Agathos, S.; Fava, F. New Biotechnol. 2015, 32, 147–156.
(8) Ortega-Calvo, J. J.; Tejeda-Agredano, M. C.; Jimenez-Sanchez, C.; Congiu, E.; Sungthong, R.; Niqui-Arroyo, J. L.; Cantos, M. J. Hazard. Mater. **2013**, 261, 733–745.
(9) Gnanasalomi, V. D. V.; Jebapriya, G. R.; Gnanadoss, J. J. Int J Comput Algorithm 2013, 2, 273–278.
(10) Prasad, M.; Garg, A.; Maheshwari, R. Int J LifeSc Bt Pharm Res **2012**, 1, 11–21.
(11) Mansour, M.; Feicht, E.; Méallier, P. Toxicol. Environ. Chem. **1989**, 20–21, 139–147.
(12) Haggi, E.; Bertolotti, S.; García, N. A. Chemosphere **2004**, 55, 1501–1507.
(13) Okamura, H.; Sugiyama, Y. Chemosphere **2004**, 57, 739–743.
(14) Barbieri, Y.; Massad, W. A.; Díaz, D. J.; Sanz, J.; Amat-Guerri, F.; García, N. A. Chemosphere **2008**, 73, 564–571.
(15) Escalada, J. P.; Gianotti, J.; Pajares, A.; Massad, W. A.; Amat-Guerri, F.; García, N. A. J. Agric. Food Chem. **2008**, 56, 7355–7359.
(16) Díaz, M.; Luiz, M.; Alegretti, P.; Furlong, J.; Amat-Guerri, F.; Massad, W.; Criado, S.; García, N. A. J. Photochem. Photobiol. Chem. **2009**, 202, 221–227.
(17) Escalada, J. P.; Pajares, A.; Gianotti, J.; Biasutti, A.; Criado, S.; Molina, P.; Massad, W.; Amat-Guerri, F.; García, N. A. J. Hazard. Mater. **2011**, 186, 466–472.
(18) Xu, F.; Song, X.-N.; Sheng, G.-P.; Luo, H.-W.; Li, W.-W.; Yao, R.-S.; Yu, H.-Q. Sep. Purif. Technol. **2015**, 142, 18–24.
(19) Krishna, C. M.; Uppuluri, S.; Riesz, P.; Jr, J. S. Z.; Balasubramanian, D. Photochem. Photobiol. **1991**, 54, 51–58,
(20) Morales, G.; Pajares, A.; Natera, J.; Escalada, J. P.; Massad, W.; García, N. A. J. Photochem. Photobiol. Chem. **2017**, 344, 49–55.
(21) Cardoso, D. R.; Libardi, S. H.; Skibsted, L. H. Food Funct. **2012**, 3, 487–502.
(22) Pajares, A.; Bregliani, M.; Massad, W.; Natera, J.; Challier, C.; Boiero, L.; Montenegro, M.; García, N. A. J. Photochem. Photobiol. B **2014**, 135, 48–54.
(23) Escalada, Juan P; Pajares, Adriana; Bregliani, Mabel; Biasutti, Alicia; Criado, Susana; Molina, Patricia; Massad, Walter; García, Norman A. Advanced Oxidation Technologies; Sustainable Energy Developments; CRC Press, **2014**; pp 59–80.
(24) Zaviska, F.; Drogui, P.; Mercier, G.; Blais, J.-F. Rev. Sci. Eau **2009**, 22, 535.
(25) Jović, M.; Manojlović, D.; Stanković, D.; Dojčinović, B.; Obradović, B.; Gašić, U.; Roglić, G. J. Hazard. Mater. **2013**, 260, 1092–1099.
(26) Babuponnusami, A.; Muthukumar, K. J. Environ. Chem. Eng. **2014**, 2, 557–572.
(27) Bokare, A. D.; Choi, W. J. Hazard. Mater. **2014**, 275, 121–135.
(28) Oturan, M. A.; Aaron, J.-J. Crit. Rev. Environ. Sci. Technol. **2014**, 44, 2577–2641.
(29) Cheng, M.; Zeng, G.; Huang, D.; Lai, C.; Xu, P.; Zhang, C.; Liu, Y. Chem. Eng. J. **2016**, 284, 582–598.
(30) Escalada, J. P. Procesos Fotoquímicos en la Degradación de Varios Agroquímicos Contaminantes Acuáticos. Un Estudio Cinético y Mecanístico, Tesis Doctoral en Ciencias Químicas. Tesis Doctoral en Ciencias Químicas, UNRC, **2011**.
(31) Escalada, J. P.; Pajares, A.; Gianotti, J.; Biasutti, A.; Criado, S.; Molina, P.; Massad, W.; Amat-Guerri, F.; García, N. A. J. Hazard. Mater. **2011**, 186, 466–472.
(32) Gatica, E. Estudio de los mecanismos de fotodegradación directa y sensibilizada de contaminantes acuáticos, Universidad Nacional de Río Cuarto (UNRC), Río Cuarto, **2017**.
(33) Natera, J.; Gatica, E.; Challier, C.; Possetto, D.; Massad, W.; Miskoski, S.; Pajares, A.; García, N. A. Redox Rep. **2015**, 20, 259–266.
(34) Gatica, E.; Natera, J.; Pajares, A.; Gambetta, C.; Sancho, M. I.; Massad, W. A.; García, N. A. J. Photochem. Photobiol. Chem. **2017**, 348, 295–304.
(35) Gatica, E.; Possetto, D.; Reynoso, A.; Natera, J.; Miskoski, S.; Gerónimo, E. D.; Bregliani, M.; Pajares, A.; Massad, W. A. Photochem. Photobiol. **2019**, 95, 901–908.
(36) Beltran, E.; Fenet, H.; Cooper, J. F.; Coste, C. M. J. Agric. Food Chem. **2000**, 48, 4399–4403.
(37) Pallett, K. E.; Little, J. P.; Sheekey, M.; Veerasekaran, P. Pestic. Biochem. Physiol. **1998**, 62, 113–124.
(38) Viviani, F.; Little, J. P.; Pallett, K. E. Pestic. Biochem. Physiol. **1998**, 62, 125–134.
(39) Lerch, R. N.; Lin, C. H.; Leigh, N. D. J. Agric. Food Chem. **2007**, 55, 1893–1899.
(40) Federal Register Document Issue for 1998-09-23

https://www.federalregister.gov/documents/1998/09/23 (accessed Nov 6, **2016**).
(41) Lin, C.-H.; Lerch, R. N.; Thurman, E. M.; Garrett, H. E.; George, M. F. J. Agric. Food Chem. **2002**, 50, 5816–5824.
(42) Wu, S. H.; Goyne, K. W.; Lerch, R. N.; Lin, C.-H. J. Environ. Qual. **2011**, 40, 528–537.
(43) Ramanarayanan, T.; Narasimhan, B.; Srinivasan, R. J. Agric. Food Chem. **2005**, 53, 8848–8858.
(44) Alletto, L.; Benoit, P.; Bergheaud, V.; Coquet, Y. Environ. Pollut. **2008**, 156, 678–688.
(45) Sims, G. K.; Taylor-Lovell, S.; Tarr, G.; Maskel, S. Pest Manag. Sci. **2009**, 65, 805–810.
(46) Fadayomi, O.; Warren, G. F. Weed Sci. **1976**, 24, 598–600.
(47) Vanstone, D. E.; Stobbe, E. H. Weed Sci. **1979**, 27, 88–91.
(48) US EPA-Oxyfluorfen (Pc Code 111601) - csr_PC-111601_5-Apr-93_122.pdf http://www.epa.gov/pesticides/chem_search/cleared_reviews/csr_PC-111601_5-Apr-93_122.pdf (accessed Aug 7, **2015**).
(49) C.R Worthing, R. Y. H. The Pesticide Manual, 9th ed., British Crop Protection Council, **1991**, p. 643.
(50) Wauchope, R. D.; Buttler, T. M.; Hornsby, A. G.; Augustijn-Beckers, P. W. M.; Burt, J. P. Reviews of Environmental Contamination and Toxicology; Reviews of Environmental Contamination and Toxicology; Springer New York, **1992**; pp 1–155.
(51) Fadayomi, R. O. Behavior of Diphenyl Ether Herbicides in Plants and Soil. Ph.D. thesis, Purdue University, West Lafayette, **1975**.
(52) Ahrens, W. H.; Edwards, M. T.; Weed Science Society of America; Weed Science Society of America; Herbicide Handbook Committee. Herbicide handbook, Weed Science Society of America, Champaign, Ill., **1994**.
(53) Scrano, L.; Bufo, S. A.; D'Auria, M.; Emmelin, C. J. Photochem. Photobiol. Chem. **1999**, 129, 65–70.
(54) Chakraborty, S. K.; Chakraborty, S.; Bhattacharyya, A.; Chowdhury, A. J. Environ. Sci. Health Part B **2013**, 48, 919–926.
(55) Scott, R. L. Recl. Trav. Chim. Pays-Bas **1956**, 75, 787–789.
(56) Brewster, M. E.; Loftsson, T. Adv. Drug Deliv. Rev. **2007**, 59, 645–666.
(57) Mousset, E.; Oturan, N.; van Hullebusch, E. D.; Guibaud, G.; Esposito, G.; Oturan, M. A. Water Res. **2014**, 48, 306–316.
(58) Devarakonda, B.; Hill, R. A.; Liebenberg, W.; Brits, M.; de Villiers, M. M. Int. J. Pharm. **2005**, 304, 193–209.
(59) Boogaard, M. A.; Bills, T. D.; Johnson, D. A. J. Gt. Lakes Res. **2003**, 29, Supplement 1, 529–541.
(60) Dai, J.; Coles, G. C.; Wang, W.; Liang, Y. Trans. R. Soc. Trop. Med. Hyg. **2010**, 104, 304–306.
(61) The Merck index: an encyclopedia of chemicals, drugs, and biologicals, 13th ed., Merck Research Laboratories, Whitehouse Station, NJ, **2001**.
(62) Muir, D. C. G.; Yarechewski, A. L. J. Agric. Food Chem. **1982**, 30, 1028–1032.
(63) Schultz, D. P.; Harman, P. D. Hydrolysis and photolysis of the lampricide 2,5-dichloro-4-nitrosalicylanilide (Bayer 73), Investigations in Fish Control, Federal Government Series 85, U.S. Fish and Wildlife Service, **1978**.
(64) Frank, M. P.; Graebing, P.; Chib, J. S. J. Agric. Food Chem. **2002**, 50, 2607–2614.
(65) Morrison, P. W. J.; Connon, C. J.; Khutoryanskiy, V. V. Mol. Pharm. **2013**, 10, 756–762.
(66) Sengupta, C.; Sarangi, M. K.; Sau, A.; Mandal, D.; Basu, S. J. Photochem. Photobiol. Chem. **2015**, 296, 25–34.
(67) Gorman, A. A.; Gould, I. R.; Hamblett, I.; Standen, M. C. J. Am. Chem. Soc. **1984**, 106, 6956–6959.
(68) Tanielian, C.; Wolff, C. Photochem. Photobiol. **1988**, 48, 277–280.
(69) García, N. A. J. Photochem. Photobiol. B **1994**, 22, 185–196.
(70) Huang, Y.-H.; Huang, Y.-J.; Tsai, H.-C.; Chen, H.-T. J. Taiwan Inst. Chem. Eng. **2010**, 41, 699–704.
(71) Gomez, M.; Murcia, M. D.; Gomez, J. L.; Gomez, E.; Maximo, M. F.; Garcia, A. Appl. Catal. B Environ. **2012**, 117–118, 194–203.
(72) Karci, A. Chemosphere **2014**, 99, 1–18.

Eduardo A. Gatica has a degree in Chemical Engineering from the Faculty of Engineering from the National University of Río Cuarto (UNRC), Río Cuarto, Argentina, and a Master's Degree in Analytical Chemistry from the National University of San Luis (UNSL), San Luis, Argentina. In 2017, he obtained his Ph.D. in Chemical Sciences from the UNRC, under the supervision of Dr. Walter Massad (UNRC). Currently, Dr. Gatica teaches at the Faculty of Agronomy and Veterinary Medicine (FAV-UNRC) and holds a professorship at the School of Engineering and Environmental Sciences at the National University of Villa Mercedes (UNViMe), San Luis, Argentina. At present, Dr. Gatica is participating as a member of research projects on Sustainable Chemical Employment in the Elimination of Aquatic Pollutants at the FAV-UNRC, Dept. of Chemistry - FCEF-QyN - UNRC at the Institute for Agroindustrial and Health Development (IDAS). CONICET – UNRC and is directing a research project on Degradation of Aquatic Pollutants at UNViMe.

José Natera was born in 1979 in Rio Cuarto (Cordoba), Argentina. He studied Chemistry at the Universidad Nacional de Río Cuarto (UNRC) where he graduated in 2003. He completed his Ph.D. degree with Professor Luis Otero, where he worked on the Research and Development of Organic Optoelectronic Systems and Devices (2006-2010) and acquired a doctoral internship at Universidad Jaime I, Castellon de la Plana, Spain and in Hahn-Meitner-Institut, Berlin, Germany. He obtained a postdoctoral fellowship under the direction of Prof. Norman Garcia to investigate the Photoinduced interactions by visible light between vitamin B2 and vitamins B1, B3 and B6 in aqueous solution (2010-2012).
He currently holds the positions of Professor and Scientific Researcher of CONICET (the National Research Council of Argentina). His research centers on the use of sustainable chemistry in the elimination of aquatic pollutants. Kinetic-mechanistic studies on photodegradation of latest generation herbicides.

Walter A. Massad was born in 1972 in Quitilipi (Chaco), Argentine. He studied Chemistry at the Universidad Nacional de Córdoba (UNC) where he graduated in 1994. He obtained his Ph.D. in 2002 from the UNC, under the supervision of Dr. Gerardo A. Argüello. He has completed two postdocs in photochemistry and photobiology, the first under the direction of Dr. Norman A. García at the Universidad Nacional de Río Cuarto (2003-2005) and the second with Dr. Santi Nonell at the Instituto Químico de Sarriá, Universidad Ramón Llull., Barcelona, Spain (October 2009 - March 2010). He currently holds the positions of Professor and Scientific Researcher of CONICET (the National Research Council of Argentina) in the Institute for Agroindustrial and Health Development (IDAS). The research work is focused on the elucidation of kinetic, mechanism and identification of the degradation products of different pollutants through photochemical processes friendly to the environment.

Anales de la Asociación Química Argentina

División Jóvenes Profesionales

Mini-Review

LIGHT-MEDIATED ACTIVATION OF ORGANIC MOLECULES. TOWARD GREENER CHEMICAL TRANSFORMATIONS

Gabriela Oksdath-Mansilla, Javier I. Bardagí* and María E. Budén

INFIQC, Departamento de Química Orgánica, Facultad de Ciencias Químicas, Universidad Nacional de Córdoba, X5000HUA Córdoba, Argentina

**Autor Corresponsal: jibardagi@unc.edu.ar*

Graphical abstract

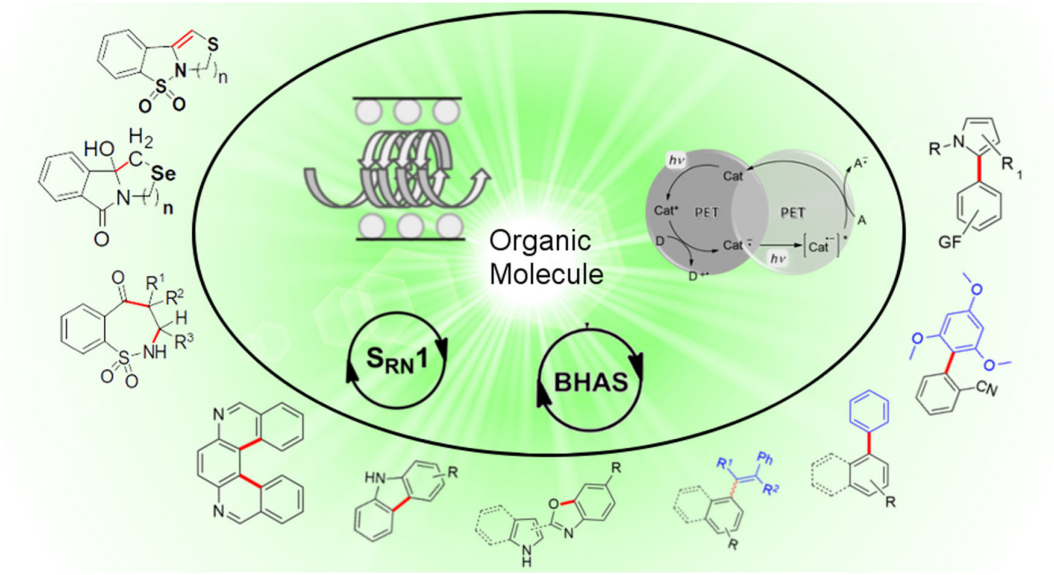

Resumen

El desarrollo de estrategias sintéticas alternativas a la química tradicional, que sean más sostenibles y saludables es de vital importancia para el futuro del planeta. Las metodologías clásicas comúnmente utilizan sustancias auxiliares o reactivos tóxicos en cantidades estequiométricas, temperaturas elevadas (baja eficiencia energética), etc. Las reacciones promovidas por luz se presentan como una excelente oportunidad para el desarrollo de nuevos métodos sintéticos en línea con este concepto, ya que la luz puede considerarse como un reactivo limpio que no deja residuos. En este contexto, la fotoquímica orgánica (con o sin fotocatalizador) es una herramienta poderosa para la obtención de moléculas con alta complejidad estructural, de una manera sencilla y en condiciones suaves. Si bien las transformaciones promovidas por luz pueden considerarse como alternativas sintéticas, la fotoquímica con un interés industrial se ha visto

limitada debido a problemas en el proceso de escalado. En los últimos años, el uso de la tecnología de flujo continuo se ha utilizado con éxito para mejorar varias aplicaciones fotoquímicas, proporcionando un mejor control sobre las condiciones de reacción, selectividad y reproducibilidad.

En este trabajo, describimos la activación de moléculas orgánicas mediante el empleo de la luz. Particularmente, se presentan ejemplos donde la luz será utilizada tanto para la preparación como la funcionalización de heterociclos mediante reacciones de Transferencia Electrónica (TE). Estas transformaciones involucran la formación de radicales iones y neutros mediante procesos catalíticos y no-catalíticos reductivos u oxidativos. Específicamente, se discute la reactividad de especies radicalarias centradas en carbono, nitrógeno, azufre y selenio, que permiten obtener nuevas uniones C-C y C-Heteroátomo, incluyendo ejemplos aplicados a la síntesis de moléculas con interés biológico y farmacológico.

Abstract

The development of new methodologies to replace the classical approach is crucial for sustainable chemical production, since many classical methodologies usually need auxiliary substance, stoichiometric toxic reagent, high temperature (poor energy efficiency), etc. Photoinduced reactions present an excellent opportunity for the development of environmentally friendly methodologies: light is a clean reactive without residual waste. In this context, synthetic organic photochemistry (with and without a photocatalyst) is a powerful tool for creating molecules with high structural complexity, in a simple way, and under mild conditions. Photo-transformation could be considered as an alternative synthetic organic tool but, the use of photochemistry with an industrial interest has been limited in regards to the scaling-up of sustainable and safer processes. Recently, the use of continuous-flow technology has been employed successfully to improve several photochemical synthetic applications, providing better control over the reaction conditions, improving their selectivity, and reproducibility.

Here, we describe the activation of organic molecules in different transformations, driven by light. Particularly, examples will be presented where the light will be used both for the preparation and the functionalization of heterocycles by means of Electron Transfer (ET) reactions. These transformations involve catalytic and non-catalytic oxidative or reductive processes, which generate radical ions and neutral radicals as intermediates. Specifically, the reactivity of species derived from carbon, nitrogen, sulfur, and selenium, and their participation in the generation of new C-C and C-heteroatom bonds are discussed. Examples are shown including photocatalytic and base promoted C-H substitutions, cycloaddition reactions, between others presenting also recent advances in the synthesis of compounds with of biological and pharmaceutical interest.

Palabras Clave: *fotoquímica, fotocatálisis, química en flujo, heterociclos*

Keywords: *photochemistry, photocatalysis, flow-chemistry, heterocycles*

1. Introduction

Light-mediated processes have served to the chemist to transform light energy into chemical energy in a similar way photosynthetic organisms have been doing for millions of years to sustain life on Earth. Not surprisingly this approach to drive chemical transformations is considered an optimal source of energy for green chemistry: light is a clean and cheap reactive without residual waste. In addition, the advance on the conversion of renewable energy sources to electricity and electricity to light became photochemical transformations excellent strategies for the utilization of clean and renewable energy sources like wind, solar radiation, and geothermal power in the synthesis of valuable materials.

In particular transformation of light energy into redox equivalence via a photoredox process allows activation of bonds by Single Electron Transfer (SET). In this process, a molecule absorbs light and transforms into its excited state and it simultaneously becomes more oxidizing and reducing. In this way, the absorption of a photon allows chemical redox reactions that are thermodynamically or kinetically impossible in the dark [1]. Radical ion intermediates ($D^{+\cdot}$ and $A^{\cdot-}$ see for instance Figure 1) are primarily formed from Photo-induced Electron Transfer (PET) reactions which evolves to the final product. Significantly, the majority of radical ions subsequently undergo a second chemical step to transform into either radicals or ions (for example see Figures 3 and 17), serving as the real key reactive species to react with other molecules. However, some radical ions still remain as key species directly participating in some chemical reactions.

An important aspect of light-mediated activation of organic molecules is its catalytic approach driven by a photocatalyst which absorb light and make this energy available for not absorbing molecules. Both energy transfer (sensitization) and SET reaction (PET) have been used in photocatalytic transformation [2–6].

Visible light-mediated photo-redox catalysis is becoming a solid field in synthetic organic chemistry [7–11]. By this strategy, visible light energy is transformed into redox energy to activate

chemical bonds and drive synthetically important chemical reactions. Metal complex of Ru and Ir are highly responsible for this development because of their good photophysical (long-lived excited states) and electrochemical properties [4]. However, the high price and potential toxicity of transition metals have driven interest in organic dye as a photocatalyst, for instance, Eosin Y and 10-methylacridinium ions have been successfully used for multiple syntheses of organic compounds [6,12,13]. Usually, organic photocatalysts are less photo-stable and their excited state lifetimes are shorter compared with metal photocatalyst. As a consequence, longer reaction times and higher catalyst loading are generally necessary. In spite of this lower quality, organic photocatalysts have shown to be a good alternative in many reactions initially development by metals complexes (for example see ref 8). Besides, most of the organic dyes are cheaper and much more available than metals catalyst and little effort have been put in the real development of an organic photocatalyst as compared to its metal counterpart.

The mechanism of photoredox catalysis is described in Figure 1 and starts with the irradiation of a photocatalyst followed by a single electron transfer (SET). The term 'oxidative quenching' and 'reductive quenching' are used to describe the two distinctive pathways. As can be seen, independently if oxidative or reductive quenching is taking place, a pair of radical ions (anion $A^{\cdot -}$ and cation $D^{+\cdot}$) are produced and the final product could be the same.

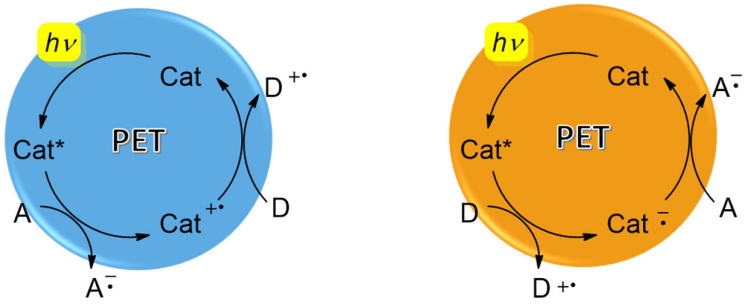

Figure 1. Typical catalytic cycles involved in visible-light photoredox catalysis A) Oxidative quenching (left) B) Reductive quenching (right)

Access to highly reactive aryl radicals could be done by visible light PET in a typical photoredox catalytic approach as depicted in Figure 1. In doing so an aromatic compound with a suitable leaving group (Ar-X) is necessary, which will leave taking the extra electron injected (X^-) [14]. However, taking this approach, only electron-deficient arenes, such as diazonium salts ($X = N^{2+}$) could be used as precursors specially if organic dyes are used. Although this problem could be solved in part changing the catalysis [15], it is related to the energy of the light used in the transformation and will reach a limit if we want to keep the catalyst stable to air and moisture. By designing an approach that resembles the Z-scheme of natural photosynthesis, it has been possible to overcome this limitation using a stable organic catalyst (Figure 2) [10,16,17]. Using a consecutive photoinduced electron transfer (conPET) processes, the energy of two photons are collected in one photoredox catalytic cycle allowing a challenged reduction process with visible light photons.

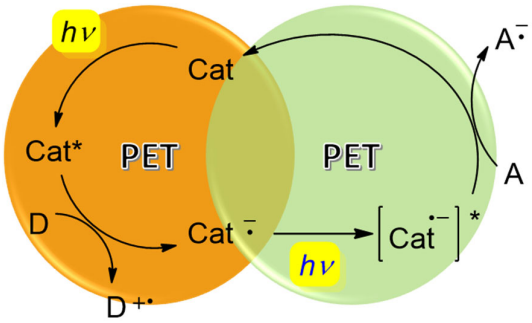

Figure 2. Consecutive Photostimulated Electron Transfer (conPET) photoredox catalysis

Here, we present examples where the light will be used both for the preparation and the functionalization of heterocycles by means of Electron Transfer (ET) reactions. These transformations involve catalytic and non-catalytic oxidative or reductive processes, which generate radical ions and neutral radical intermediates.

2. Photoinduced Reactions via a non-catalytic process

2.1 Transformation involving radical cations

As was mentioned before, a SET process is a straightforward and efficient way to access highly reactive radical ions intermediates, being of great value in organic synthesis. In competition with back-electron transfer reaction, the radical ions can participate in a fragmentation pathway. In this context, nature and kinetics of a secondary reaction of the radical ion intermediates are key in order to design a synthetic strategy.

In particular, sulfur-containing compounds can be oxidized by SET to generate radical cation intermediates. In this case, sulfide radical cation can undergo fragmentation processes involving the cleavage of the C-S bond or of a β bond to the sulfur atom [18,19]. Even though many kinetic studies of fragmentation reaction of sulfide radical cations have been reported, the application of this radical cation intermediates in a synthetic strategy has not been widely explored and continues to be a challenge for organic photochemist. In this context, our group gained experience in the use and development of synthetic methodologies involving different photochemical processes. Our research focuses on the study of oxidative or reductive processes by PET, which generates radical cations or radical anions, respectively, and involve the reactivity study of species derived from sulfur and selenium; and their participation in the generation of new C-C and C-heteroatom bonds [20–24].

One of our first evaluations of the sulfide radical cation chemistry was the study of photochemical reactions of thiiranes radical cation [25]. These sulfide compounds undergo PET reactions with Chloranil as a sensitizer, in the presence of CH_3OH (or another possible oxygen centered nucleophile), giving the ketone derivatives through cleavage of C-S bond of the thiirane radical cation (Path b, Figure 3). Additionally, the corresponding alkene was observed by a desulphurization process of the radical cation intermediate.

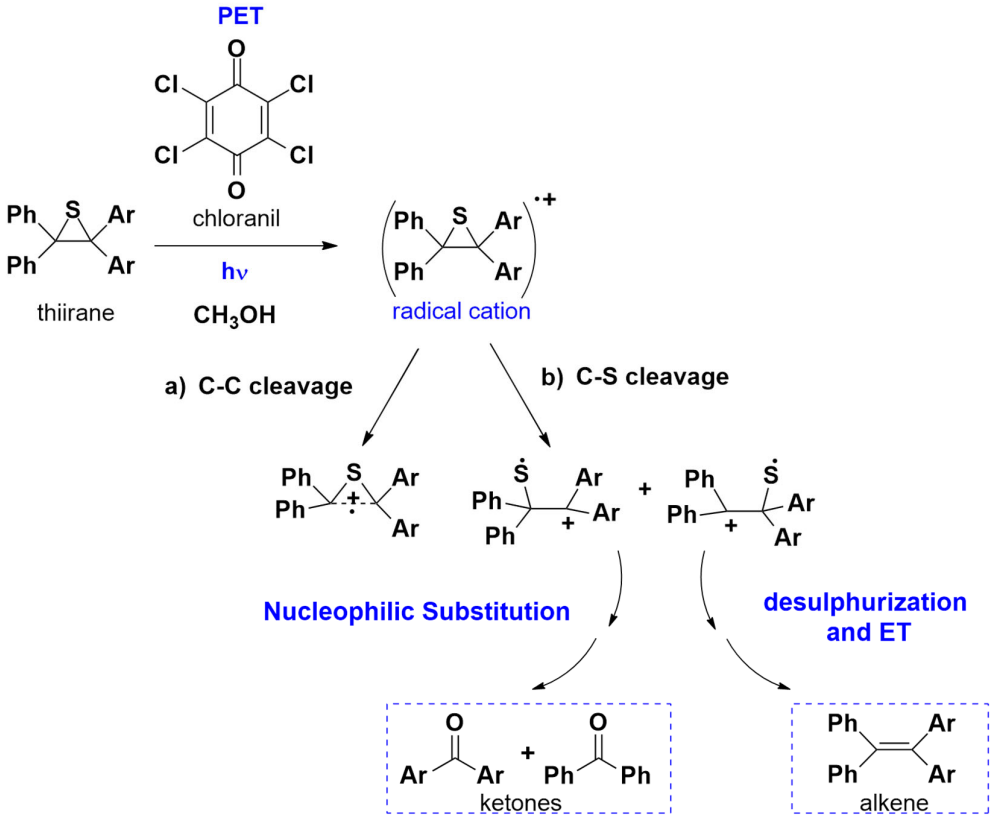

Figure 3. Photochemical ring-opening of thiirane induced by Chloranil in the presence of CH_3OH

The protection of carbonyl groups is often a necessary step in organic synthesis, especially in the total synthesis of natural products and multifunctional organic compounds. In these approach, 1,3-dithianes and 1,3-dithiolanes, are commonly used protecting groups due to their easy synthesis and high stability under both acidic and basic conditions.26 Even though many procedures are available for dithianes deprotection, those include drastic conditions or excess amounts of toxic reactants such as heavy metal salts [27,28].

For this reason, employing light-mediated activation as a greener protocol is of great interesting to the synthetic community. Taking into account the possibility of generating ketone derivatives by C-S cleavage of radical cation intermediates, we evaluated the photodeprotection of 1,3-dithianes in the presence of Thiapyrylium. Through steady-state photolysis, laser flash

photolysis, and theoretical calculations we elucidated the mechanistic details of the photodeprotection [29]. In this case, an ET process between dithiane to triplet sensitizer is extremely fast, and the decay of dithiane radical cation was not affected by the presence of water or oxygen as a consequence of a favorable unimolecular fragmentation pathway. Finally, the lack of reaction under nitrogen atmosphere, the requirement of oxygen for good conversion yields, the inhibition of the photodeprotection process by the presence of p-benzoquinone, and the absence of a labeled carbonyl final product when the reaction is performed in the presence of H218O all suggest that the superoxide anion drives the deprotection reaction (Figure 4).

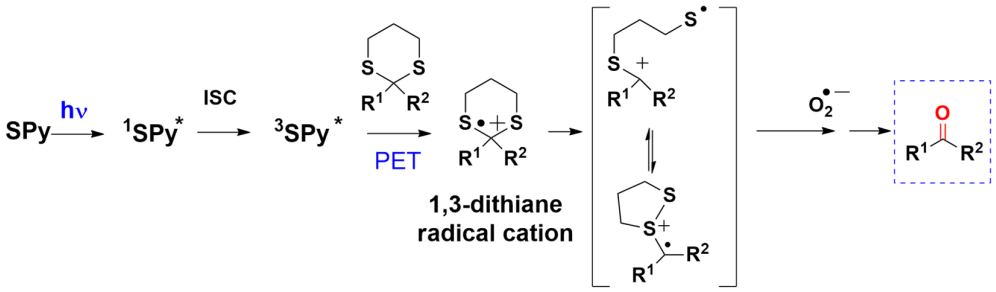

Figure 4. Photodeprotection of 1,3-dithianes by PET

In order to explore new photoinduced SET reactions with synthetic value; we investigated the photocyclization reactions of N-(thioalkyl)-saccharins. In this context, we developed an strategy to olicyclic sultams involving an intramolecular ET between the triplet excited saccharin moiety and the sulfur atom [29]. Sultams are important types of heterocyclic sulfonamide compounds due to their pharmaceutical and industrial importance [30–33]. Particularly, in the photocyclization under study, the sulfide radical cation intermediate undergoes cleavage of the C-H bond β to the sulfur atom. The radical ion pair generated evolves through a proton transfer from neighboring C-H of the thioalkyl radical cation to the ketyl radical anion of saccharin moiety. For N-thioalkyl-saccharin derivatives reactivity and chemoselectivity is highly sensitive to photochemical reaction conditions (reaction atmosphere, solvent, and irradiation wavelength). Polycyclic sultams are favored in the absence of oxygen with an efficient population of the triplet state by

solvent sensitization (path a, Figure 5). On the other hand, the presence of molecular oxygen changes the course of the reaction into an efficient photooxygenation of N-thioalkyl-saccharins at the sulfur atom level (path b, Figure 5).

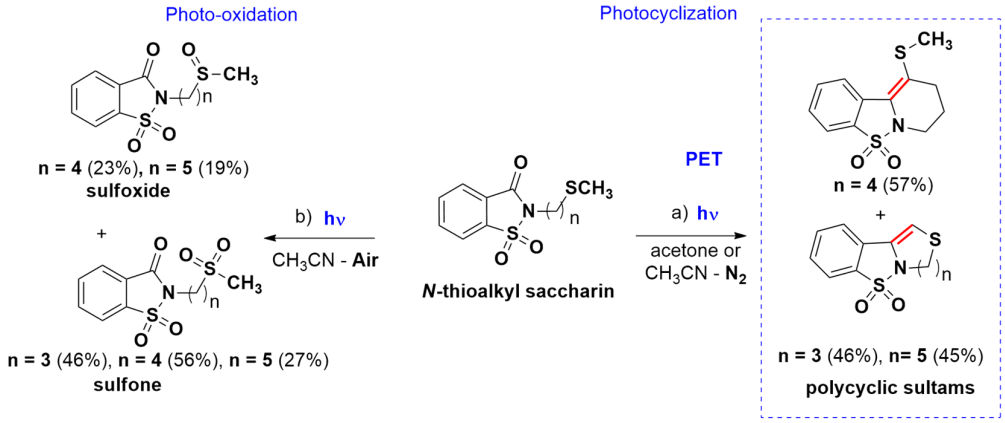

Figure 5. Photocyclization and photo-oxidation of N-thioalkyl saccharin derivates

With these results, we continue exploring the photoreactivity of saccharin oriented to synthetic applications. Benzosultam is a common functionality present in many different biologically active compounds and, thus, a relevant target for drug discovery. These heterocyclic sulfonamides are more rigid and may assume fewer conformations compared to open chain sulfonamides, which in turn make these compounds relevant pharmaceuticals with a broad spectrum of biological activities. Sulfonamides have an extensive biological profile, known to exhibit antibacterial, anti-carbonic anhydrase, diuretic, hypoglycemic, antithyroid, anti-inflammatory, anticonvulsant, antihypertensive, and anticancer properties [34].

Due to the biological importance of benzosultams, the development of different synthetic methods to prepare these compounds at large scale is of great interest for organic and medicinal chemists [35–37]. In this context, synthetic organic photochemistry arrives as a powerful tool for the preparation of natural products as well as molecules with high structural complexity, in a simple and efficient way. Particularly, the synthesis of natural products or target molecules which display biological activity is an essential part of drug discovery. The Active Pharmaceutical

Ingredients (APIs) generally have an inherent complexity associated with their molecular framework many times accessible by photochemical approach in shorter approach. Besides, the development of safer and more sustainable synthetic protocols could have a high impact on the pharma industry. In relation to this, the advantages of continuous-flow process improved photochemical syntheses and nowadays interesting applications in the synthesis of heterocycles and in drug discovery processes can be found [38]. Furthermore, there is a growing interest in applying different scale-up strategies of continuous multistep synthesis to develop active pharmaceutical ingredients (APIs) which include at least one photochemical step. One remarkable feature of the use of continuous-flow processes is the easy scaling up ability using different reactor volumes or parallel multi-reactors (numbering-up) [39,40], with a consequent increment of productivity. Additionally, due to the size of the microreactor, faster mixing is achieved, enhancing the mass- and heat-transport thus providing a high reproducibility of the conditions and improving the selectivity of the reaction [41]. Besides, photochemical transformations can similarly benefit from improved yields, decreased reaction time-scales, and reduced catalyst loadings, due to the highly efficient irradiation that results from having a short path length.

Based on the multiple steps involved in the synthesis of seven-membered sultams compounds as time demanding procedure, we designed a novel, straightforward and more convenient synthetic method in one-pot to obtain seven-membered sultams which involve the use of commercially available and inexpensive reagents under mild conditions (Figure 6) [42]. A photochemical reaction in flow proved to be better than standard batch reaction conditions, where a lower concentration of alkenes was used to prevent competitive photoreactions. This procedure involves operationally simpler reaction steps, faster reaction times, and significant improvements in the reaction scalability. A complementary computational study allowed us to rationalize some experimental findings. The obtained mechanistic picture is different from other related reactions. A nucleophilic attack of the nitrogen atom in its excited state was found to control the reactivity

and the regiochemistry of the reaction. The follow-up reactions take place in the ground state leading to the seven-member cyclic product without the mediation of the formal [2+2] cycloadduct.

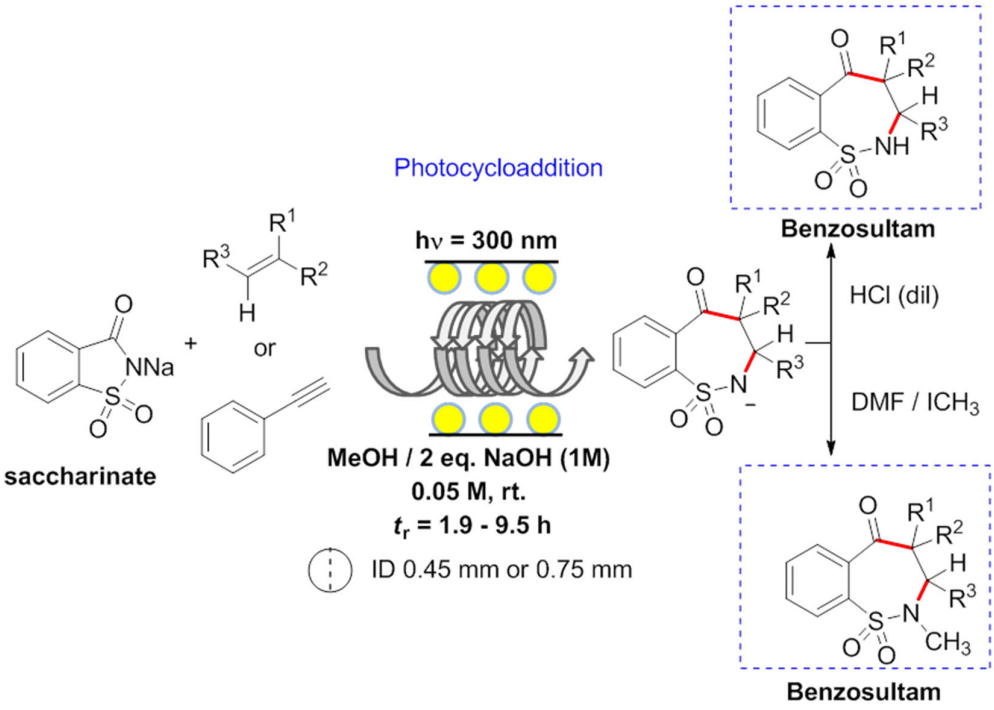

Figure 6. Photocycloaddition strategy in continuous flow to obtain benzosultam derivates.

Although selenium belongs to the same group in the periodic table as that of sulfur, they both differ in several physical, chemical, and physiological properties. For instance, replacing cysteine (Cys) for selenocysteine (Sec) in the active site of enzymes increases the catalytic activity by several hundred folds [43]. Consequently, there has been a growing interest in the synthesis of organoselenium compounds due to their use in bioorganic chemistry, enzymology, and medicine. These compounds exhibit various types of biological activities including antitumor, anti-inflammatory, antibacterial and antifungal. Many selenium-containing compounds with biological activity are heterocycles, and their syntheses represent an important challenge for chemists.44 Based in this, we explored the synthesis of N-(selenoalkyl)phthalimides and further aspects concerning the scope and limitations for the synthesis of new organoselenium tricyclic

ring systems (Figure 7) [45]. Furthermore, we studied the photochemistry of these compounds, evaluating the efficiency of the photocycloaddition reaction as a function of the distance between the electron donor and electron acceptor as well as the stability of the radical intermediates.

Photocycloaddition of these compounds is of great synthetic interest and leads to the construction of a variety of cyclic compounds including six-, seven- and even nine-member selenacycles. It is noteworthy that these scaffolds are difficult to obtain by conventional procedures. In addition, the azabicycles obtained are benzofused analogues to bioactive pyrrolizidine and indolizidine alkaloids and within this context the reported photochemical procedure is a useful alternative to the currently available multistep synthesis. In the course of this research we evaluated the ability of selenium as an electron donor group in intramolecular electron transfer reactions, being it an additional contribution to the study of the phthalimide system.

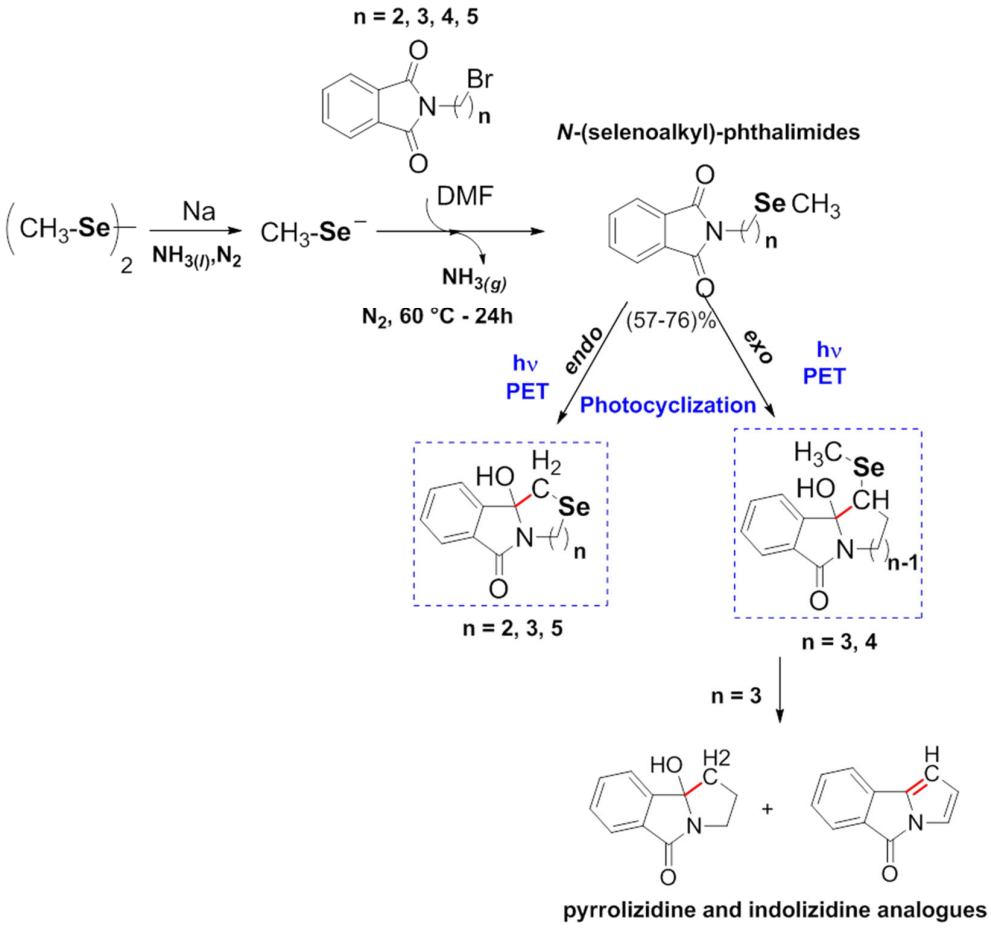

Figure 7. Synthesis and evaluation of the photo-reactivity of N-(selenoalkyl)phthalimides.

2.2 Transformations involving radicals anions

Carbon-centered radicals can be formed through the fragmentation of radical anions from aryl and alkyl halides (ArX and RX), among others. In this case, the substrate (ArX or RX) accepts an electron from a donor as opposed to the previously described reactions of sulfur and selenium compounds. Hence, the SET from a donor reagent to ArX (or RX) produces a radical anion that can undergo a fragmentation process releasing an anion X- and giving the desired carbon-centered radical. This radical can react by a chain reaction with both nucleophiles by an SRN1 process or with neutral acceptors, like benzene or alkenes, by base-promoted homolytic aromatic substitution (BHAS) reactions. In such cases, SET and fragmentation of the former radical anion usually constitute the initiation step.

In the last fifteen years, SRN1 and related mechanisms have been shown to be important tools for the synthesis of heterocycles in transition metals free reactions, thereby proving to be greener and more sustainable procedures. One of the most used strategies to obtain heterocycles in SRN1 reactions is an intramolecular approach, where the nucleophile and the leaving group are in the same molecule. Depending on the distance between the leaving group (X) and the nucleophilic center (Nu^-), the flexibility of spacer, and the nature of the nucleophile, this type of reaction may lead to the formation of new C-C or C-Heteroatom bonds (C-N, C-O, etc.) [46]. In this regard, the photostimulated reaction of 2-halo-N-phenylaniline derivatives (R=Me, t-Bu, Ph, OMe, pyrrolyl) affords the intramolecular C-C bond carbazoles in very good yields (Figure 8). Supported reported data, control experiments we proposed the mechanism picture of Figure 8. An initial reaction of diphenylamide with KOtBu gives the diphenylamide anion, which by PET forms the dianion radical. Then, C-X bond fragmentation delivers the distonic radical anion, which by a C-C bond formation gives the conjugated radical anion. By ET, the radical anion yielded the substitution product, which finally gives carbazole, the more stable tautomer (Figure 8) [47].

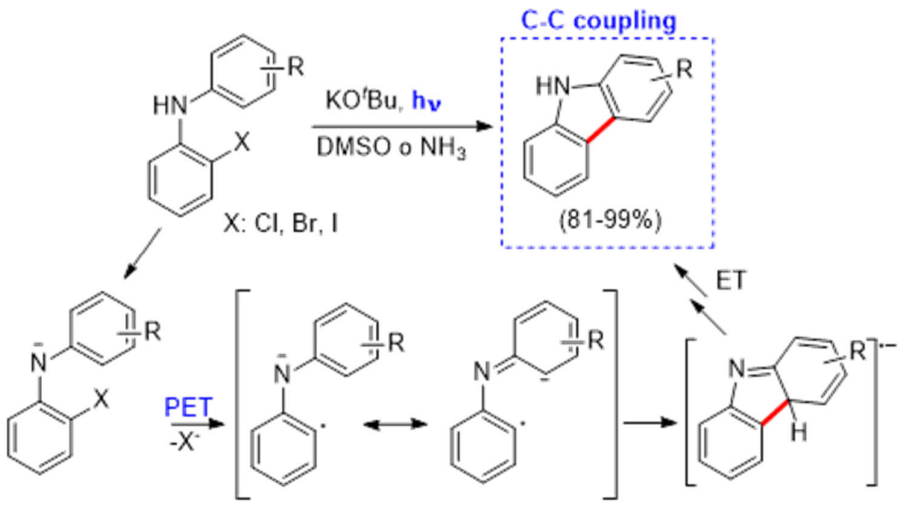

Figure 8. Synthesis of carbazoles through intramolecularSRN1 cyclization

Moreover, we carried out the synthesis of carbazoles by N-arylation reaction of 2`-halo-[1,10-biphenyl]-2-amines under irradiation in basic medium (Figure 9). In general, biphenylamines with an Electron-Donating Group (EDG) like Me or OMe behave in the same way as H giving both, cyclized and reduced products. On the other hand, biphenylamines containing Electron-Withdrawing Groups (EWG) like CN, COOEt or CF3 gave only the corresponding carbazole.48 The photochemical and photophysical experiments and computational studies suggested that carbazoles are produced via the SRN1 mechanism. However, the difference in the selectivity could be attributed to the difference in the nature of the step. Through computational and photophysical studies we determine that for anion with EDG, ET from tBuO- (or dimsyl anion) to excited anion could be involved meanwhile for anions with EWG homo-coupled redox reaction take place [49].

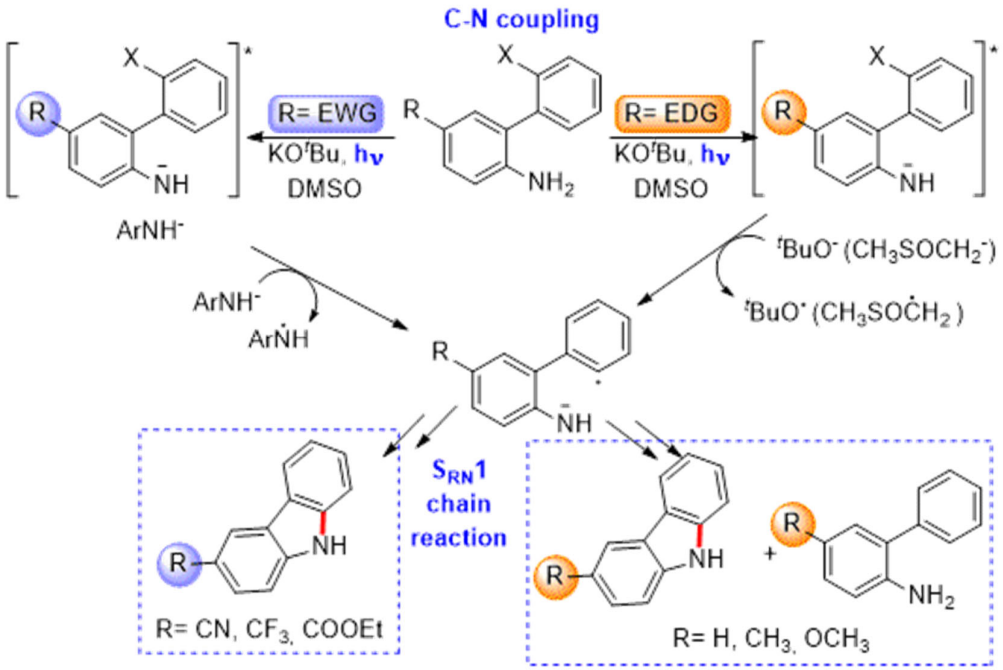

Figure 9. Synthesis of carbazoles by intramolecular C-N bond forming reaction

Similar to the anions of diarylamines (Figure 8), we used other anilines to obtain new heterocycles through the intramolecular C-C bond formation. For instance, the intramolecular arylation of iodobenzyl phenyl amide anion afforded phenanthridines in very good yields. Although dihydrophenanthridines were the ring closure products, they oxidized spontaneously in the work-up to finally give the corresponding phenanthridines (Figure 10) [50]. Using this methodology, we produced condensed benzophenanthridines, such as benzo[a]phenanthridine, benzo[c]phenanthridine, and naphtho[2,3-a]phenanthridine. Furthermore, the methodology was extended to the synthesis of Trispheridine, a natural product, in 75% yield [51].

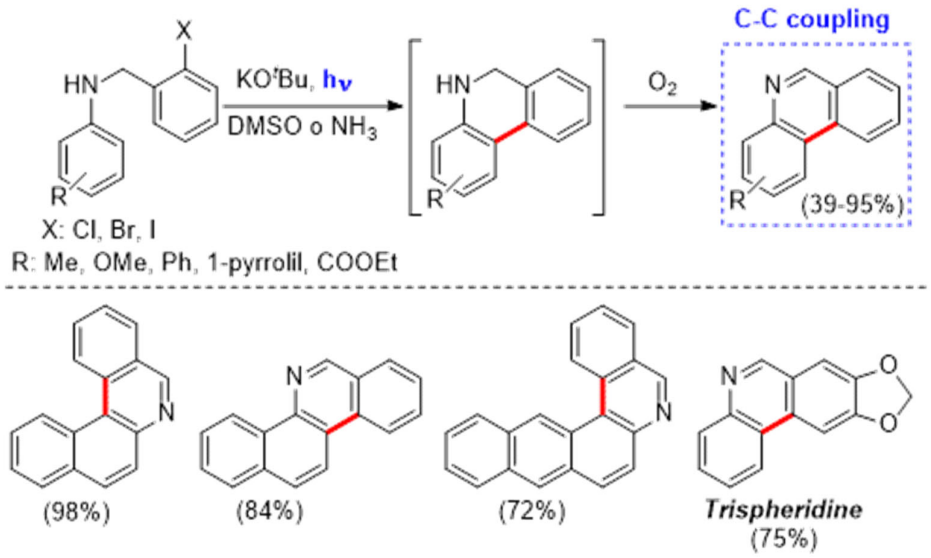

Figure 10. Synthesis of phenanthridines through intramolecular SRN1 cyclization

Taking into account the previous results, we carried out double ring closure reactions by intramolecular SRN1 where two 6-membered rings are formed in one step. In this regards, the photostimulated reaction in liquid ammonia of the bis(2-iodobenzyl)benzene-1,4-diamine gave two isomeric products: dibenzo[a,k][4,7]phenanthroline (46 %yield, s-cis product) and isoquinolino[3,4-b]phenanthridine (25% yield, s-trans product, Figure 11) [52]. Under these reaction conditions, the oxidation is not spontaneously, and oxidation with MnO_2 in $CHCl_3$ was necessary for a full aromatic product formation.

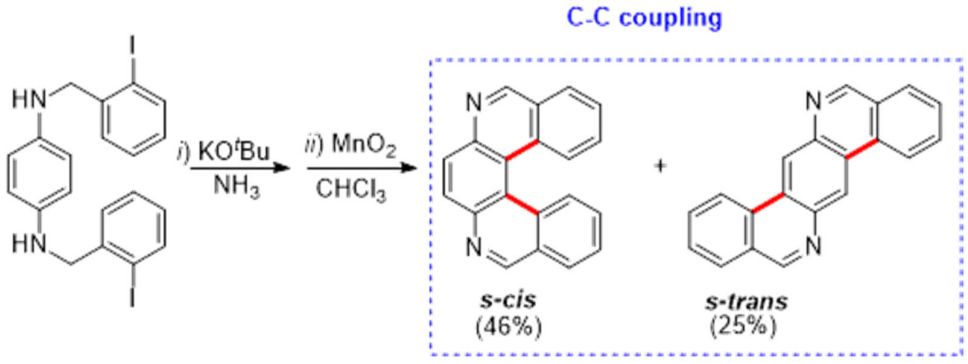

Figure 11. Iterative double cyclization reaction by intramolecular intramolecular SRN1.

Not only the amine anion is useful in intramolecular reactions, as an extension of this system, we tested the pyrrole anion. The photostimulated reaction of N-(2-halobenzyl)pyrazoles, with excess KOtBu in liquid ammonia or DMSO, afforded the 2H-pyrazolo[3,4-c]isoquinolines by a cyclization reaction with C-C bond formation in position four of the pyrazole ring, followed by spontaneous oxidation of the substitution products to yield 2H-pyrazolo[3,4-c]isoquinolines (Figure 12) [53].

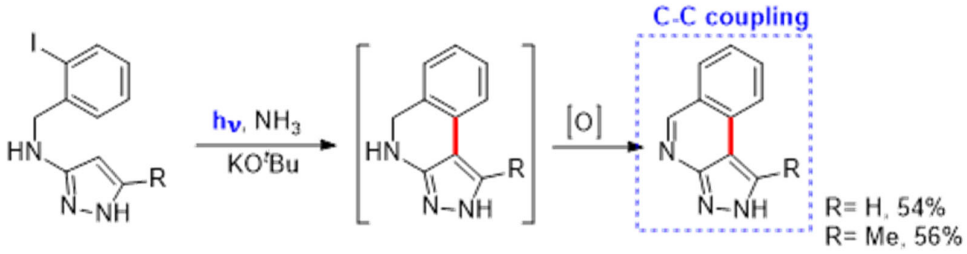

Figure 12. Synthesis of 2H-pyrazolo[3,4-c]isoquinolines by intramolecular SRN1.

Following the same methodology, the indolecarboxylate anion gave C-C bond formation in good yield (54% yield of chromeno[4,3-b]indol-6(11H)-one, Figure 13). However, using this anion but changing the bridge by amide, afford indolylbenzoxazole and pyrrolylbenzoxazoles from indololocarboxamides and pyrrolocarboxamide, respectively. Unexpectedly, we recovered these products in good to excellent yields by C-O bond formation (Figure 13) [54].

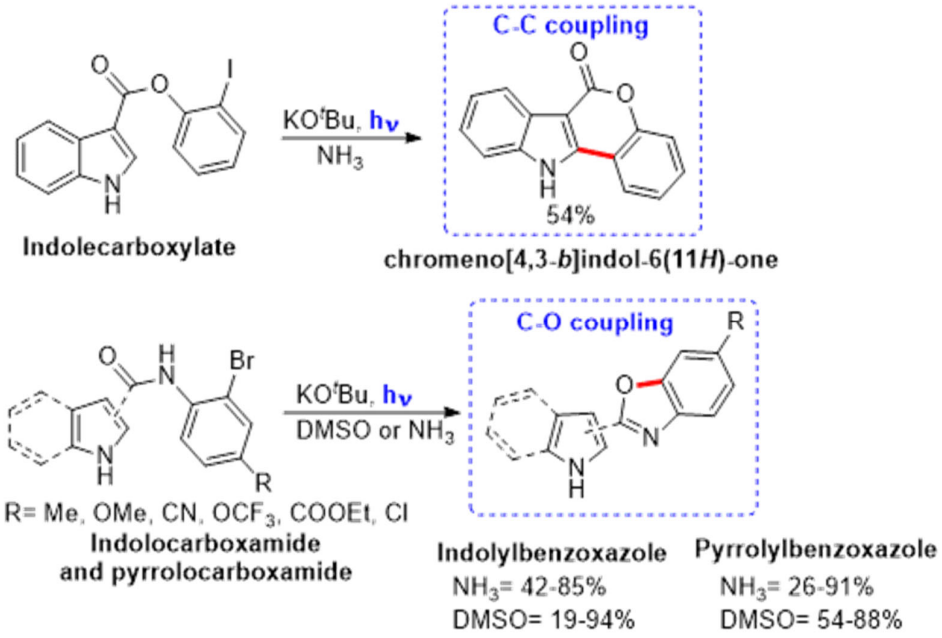

Figure 13. Synthesis of chromeno[4,3-b]indol-6(11H)-one, indolylbenzoxazole and pyrrolylbenzoxazole.

The indolocarboxamides bear two hydrogens, namely, indole N-H and amide C(O)N-H moieties, both can be ionized under basic reaction conditions; however, the pKas of these compounds are unknown in liquid ammonia or DMSO. Then we decided to perform a computational calculations and determined that the indole anion is energetically more stable than the amide anion by 2.1 kcal/mol. Moreover, the reaction only occurred under photostimulation and it was inhibited by *p*-DNB, which suggests that there are probably ET events taking place. On the base of photochemical and photophysical experiments, we proposed that indolylbenzoxazole product was obtained from indole-anion, by an intramolecular ET. Once formed, the diradical collapse to give after tautomerization the C-O product (Figure 14) [55].

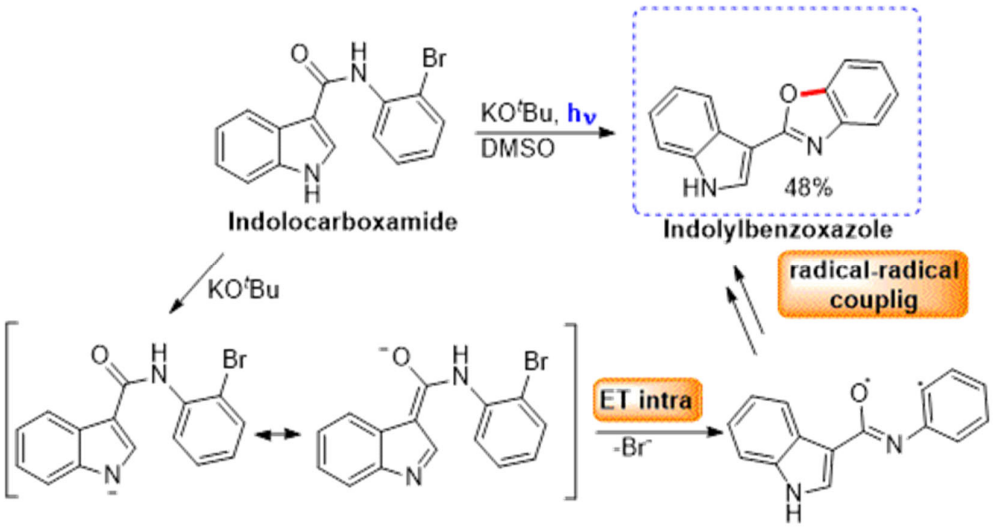

Figure 14. Mechanism proposed for indolylbenzoxazole synthesis.

Through intramolecular SRN1 reactions, other heterocycles have been prepared. Thus, alkaloids of the aporphine and homoaporphine [56], imidazoles [57], dibenzothiazines [58], the four carboline regioisomers [59], and other fused heterocycles [60], with very good yields (Figure 15).

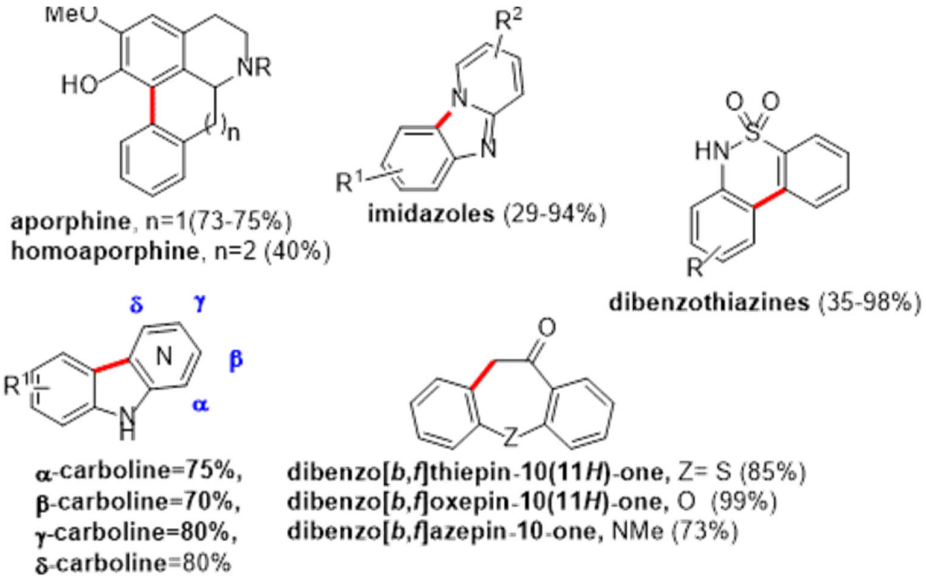

Figure 15. Fused heterocycles obtained by intramolecular SRN1 reactions.

As mentioned above, carbon radical is able to add to neutral molecules by means of a HAS type mechanism. In 2008, it was shown that KOtBu triggered the addition reaction of ArI and/or ArBr

to pyridazine and other electron-poor aromatic rings under elevated temperatures or MW irradiation [61]. Furthermore, the construction of biaryl compounds from inactivated aromatic rings by direct C-H activation using KOtBu and DMEDA [62] or 1,10-phenanthroline [63,64] as ligands was also reported. Nowadays, these methodologies have been successfully extended to different systems by intra and inter approaches [65].

Taking into account that KOtBu is able to form anion radicals from ArX by ET in photostimulated SRN1 reactions, we employed this strategy for prepared biaryls from ArX and benzene with only KOtBu and light at room temperature (Figure 16, A) [66]. Likewise, we achieved the synthesis of E-stilbenes by photoinduced Heck-type reaction by means of a C-H functionalization of alkenes at room temperature without extra solvent but with 18-crown-6 ether in only 15 min (Figure 16, B) [67].

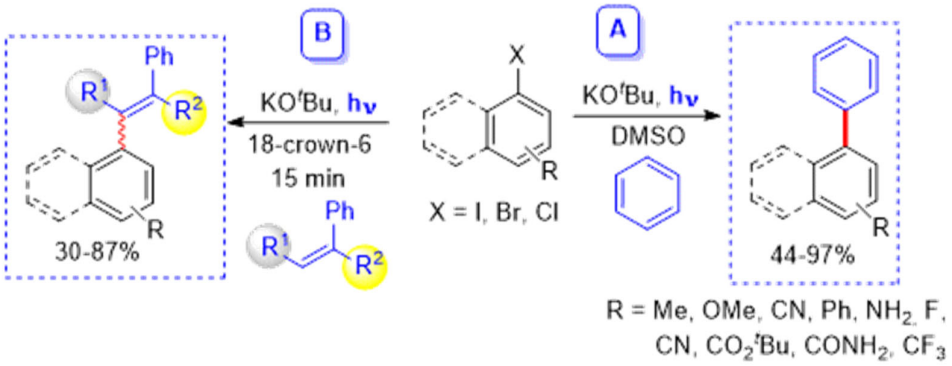

Figure 16. Synthesis of biaryls and E-stilbenes by photo-BHAS and Heck-type reactions.

All these photoinduced reactions take place in DMSO in the presence of a strong base, such as KOtBu. So, a complete mechanistic picture for C-H functionalization was performed with a comparative and detail study in the initiation step allowing as to conclude that the reaction with KOtBu or NaH with DMSO forms the dimsyl anion, which acts as electron donor after excitation. We propose two alternatives for this namely, a direct ET from an excited state or a photo-ejection of an electron from the dimsyl anion [68].

3. Consecutive Photoredox Catalysis with visible light (conPET)

The first reported example of consecutive Photo Electron Transfer catalysis (conPET) used perylene diimides (PDI) as catalyst.16 PDI form stable radical anion under nitrogen upon photoirradiation in the presence of sacrificial electron donors, such as amines. The stable colored radical anion could be then further excited under visible light irradiation and the excited radical anion is reducing enough to transfer an electron to suitable aryl halide substrates. This SET yields the corresponding radical anions ($Ar{-}X^{\bullet-}$) and later the aryl radicals as was described in the previous section (Figure 17). The generated aryl radical is useful for C–H arylation reactions in the presence of suitable (hetero)aryl radical trapping reagents. Taking this into account we performed the reaction in DMSO under nitrogen, and using pyrrole derivatives as aryl radical trapping reagent, and obtained C–H arylated products. These biologically relevant compounds could be prepared in good yields as depicted in Figure 18. Unprotected pyrroles could also be used as a trapping reagent obtaining good isolated yields of products. In these reactions, we used triethylamine as an additive to promote radical anion formation of PDI as depicted in Figure 17.

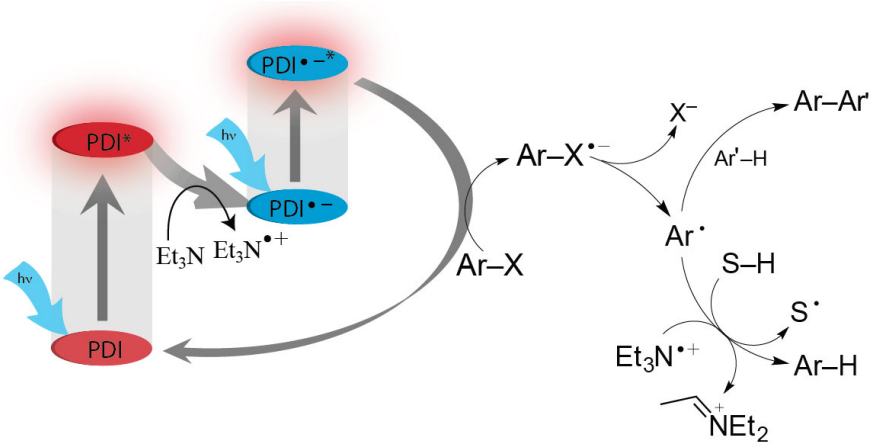

Figure 17. "Z" like proposed conPET catalytic cycle using PDI. (Reproduced with permission from Ref. [16]. Copyright 2014, AAAS.).

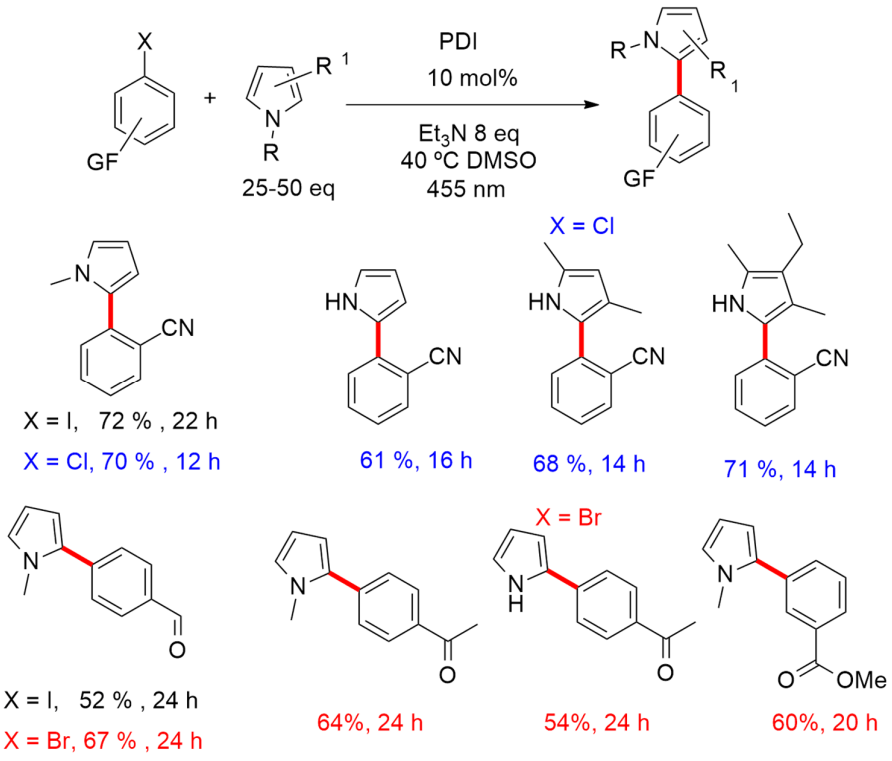

Figure 18. PDI catalyzed C–H arylation yields using aryl halides and visible light.

Later, the concept was extended to Rhodamine 6G (Rh 6G) photocatalyst. Its radical anion is relatively stable in the absence of oxygen, and upon photoexcitation with blue light is able to transfer an electron to aryl halides [17]. Using this catalyst, König's group achieve the C-H arylation of pyrroles, 1,3,5-trimetoxybenzene and 1,1-diphenylethene using aryl halide and (hetero)aryl halides with good yields [10]. Another interesting example includes the synthesis of pyrrolo[1,2-a]quinoline and ullazines starting from suitable aryl bromides and using alkynes as trapping agents. Radical addition to alkynes gave an alkenyl radical, which follows an intramolecular C-H homolytic aromatic substitution on a pyrrole ring [69].

It is also known that anthraquinones forms colored radical anions upon single-electron reduction (Figure 19). Anthraquinone radical anions have reduction potentials typically > –0.9 [vs. saturated calomel electrode (SCE)] [70], and can be obtained electrochemically, chemically, or through photoinduced single-electron transfer (SET) processes in the presence of a suitable electron donor under an inert atmosphere. As a consequence, it is not surprising they have been

used for photo-oxidative transformations under visible light, for instance in the oxidation of benzene to phenol [71].

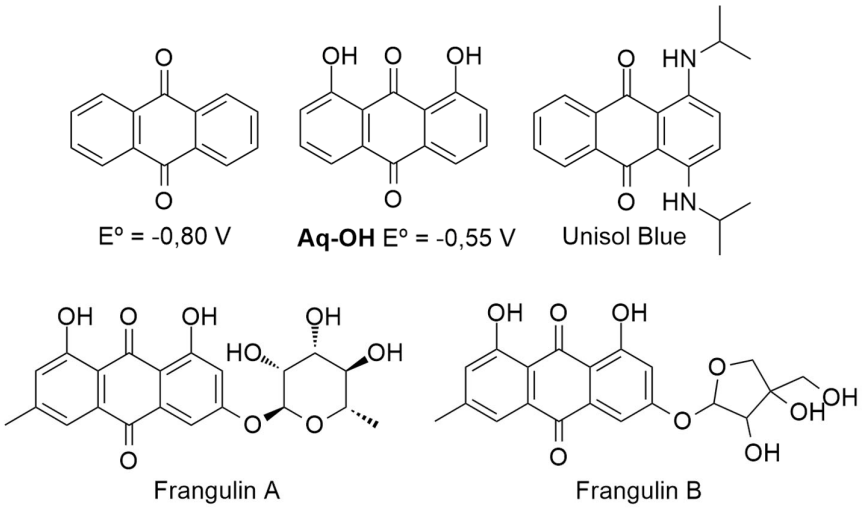

Figure 19. Structure of anthraquinone derivatives (E° vs SCE).

However, back in the 1980s, Erikssen et al showed that the excited states of the radical anions of quinone derivatives are powerful reductants and can transfer electrons to organic substrates with relative high reduction potentials ranging –1.9 V vs. SCE. Although SET to these substrates was probed to be feasible [72], it has not synthetic value until anthraquinones were used in photoredox catalytic reductive transformations [73].

Based in the previous results we anticipated that anthraquinone could promote reductive conPET transformation. Initially, we studied several derivatives of anthraquinone in photoredox catalytic reduction of aryl halide substrates for metal-free dehalogenation reactions (Figure 20) [73]. Catalysts including Anisol blue (used for microscopy) with amino substituents and others with alkyl and OH probed to be suitable for the photo dehalogenation. However, only hydroxy antharquinones [including 1,8-dihydroxy-9,10-anthraquinone (Aq-OH)] and naturally occurring Frangulin A/B gave synthetically relevant results. Then, Aq-OH was selected for further experiments because of the better chemical yield of the product and its availability. The scope of the method was explored and good-to-excellent photoreduction yields were obtained with aryl bromide with electron withdrawing groups but fail in the case of bromobenzene. Reduction of

iodobenzene and 4-iodotoluene was possible (25-27 %) and some aryl chlorides could also be reduced in the conditions reported.

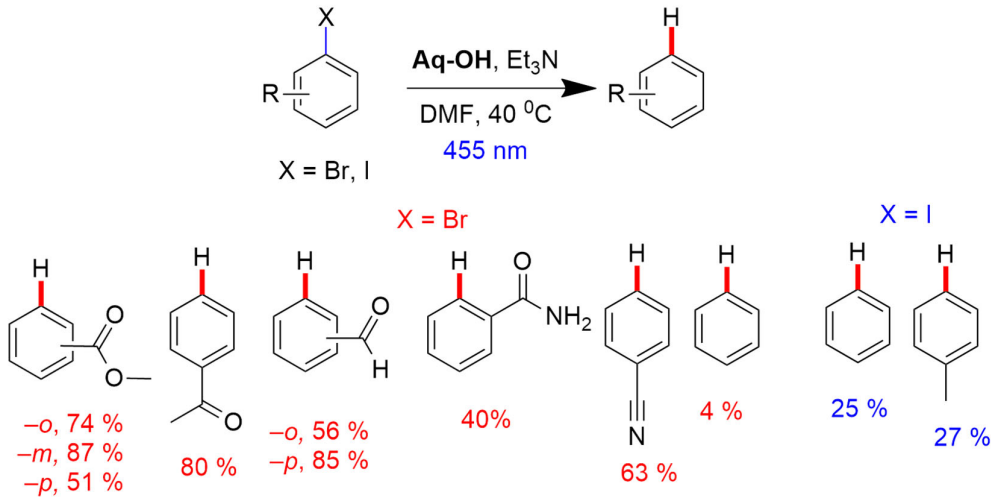

Figure 20. Metal-free photo dehalogenation reactions.

Next, we probed C–C bond-forming reactions with arenes, heteroarenes, and unsaturated double bonds through the generation of aryl radicals. In this case, hydrogen-atom abstraction became a competing reaction and the radical cation of the amine or the solvent could be the source of a hydrogen atom to form the reduction product. However, when a reaction mixture containing 2-bromobenzonitrile, Aq-OH, N,N-diisopropylethylamine (DIPEA), and benzene was irradiated with blue LEDs, the desired product was obtained in 14 % yield (Figure 21). In a similar way, when thiophene and furan were introduced as the radical trapping reagents, products from C-H substitutions at 2 position were obtained in low isolated yields of ca. 20 %. When 1,3,5- trimethoxybenzene was used as a trapping reagent for the 2-cyanophenyl radical, the expected product was obtained in 60 % isolated yield.

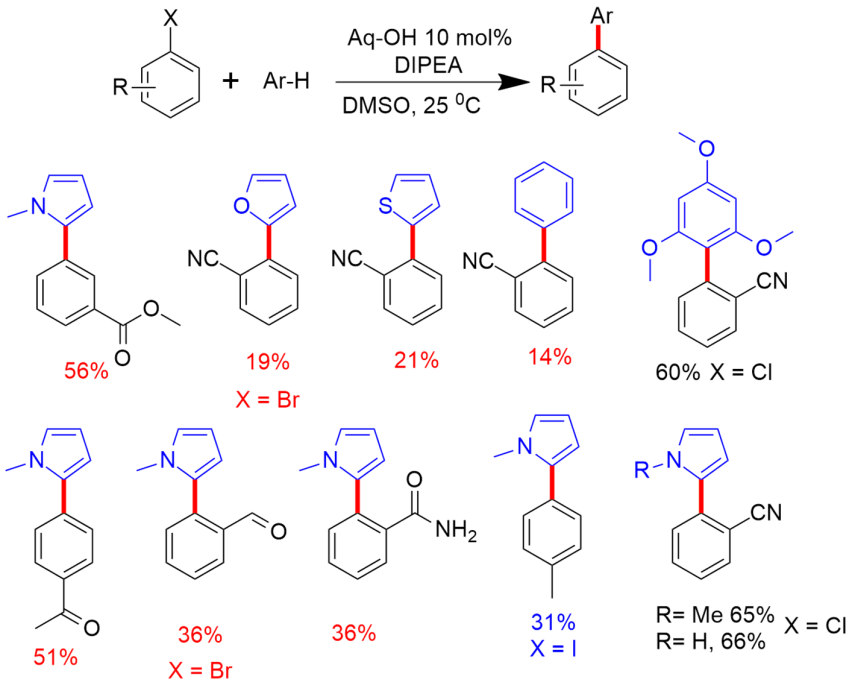

Figure 21. C-H arylation reactions using aryl halides

Using different aryl bromides the C–H arylated products were isolated in moderate-to-good yields using pyrrole derivatives as trapping reagents including unprotected pyrrole (Figure 21). Besides, the C–H functionalization reaction of 1,1-diphenylethylene with 2-bromobenzonitrile gave 2-(2-cianophenyl)-1,1-diphenylethylene in 42 % yield. On the other hand, 4′-Bromoacetophenone gave a mixture of the C-H substitution product 4-(2,2-diphenylvinyl)acetophenone and addition product 4-(2,2-diphenyl-1-ethyl)acetophenone in a combined 58 % isolated yield. The C–H arylation reactions were also effective for aryl chlorides and aryl iodides as precursors of aryl radicals (Figure 21).

Although a complete mechanistic picture of this complex reaction was not elucidated, on the basis of previous reports and spectroscopic investigations we delineated a plausible mechanism (Figure 22). Upon visible-light photoexcitation, the excited state of Aq-OH is quenched by Et3N to generate the radical anion Aq-$OH^{\cdot-}$ (and $Et_3N^{\cdot+}$), which forms the semiquinone anion, Aq-OH-H^{-}, through protonation and successive reduction. The Aq-OH-H^{-} luminescence was significantly quenched by reactive aryl bromides but was not affected by unreactive ones, such

as 4-Bromoanisole supporting a SET from the excited state of this anion. In this way, the generated $Ar–X^{\cdot-}$ subsequently fragments to yield aryl radicals that either abstract a hydrogen atom or react with (hetero)aryls or unsaturated double bonds to yield the corresponding C–C coupling products after oxidation and release of a proton as depicted in Figure 17 for PDI photocatalysts.

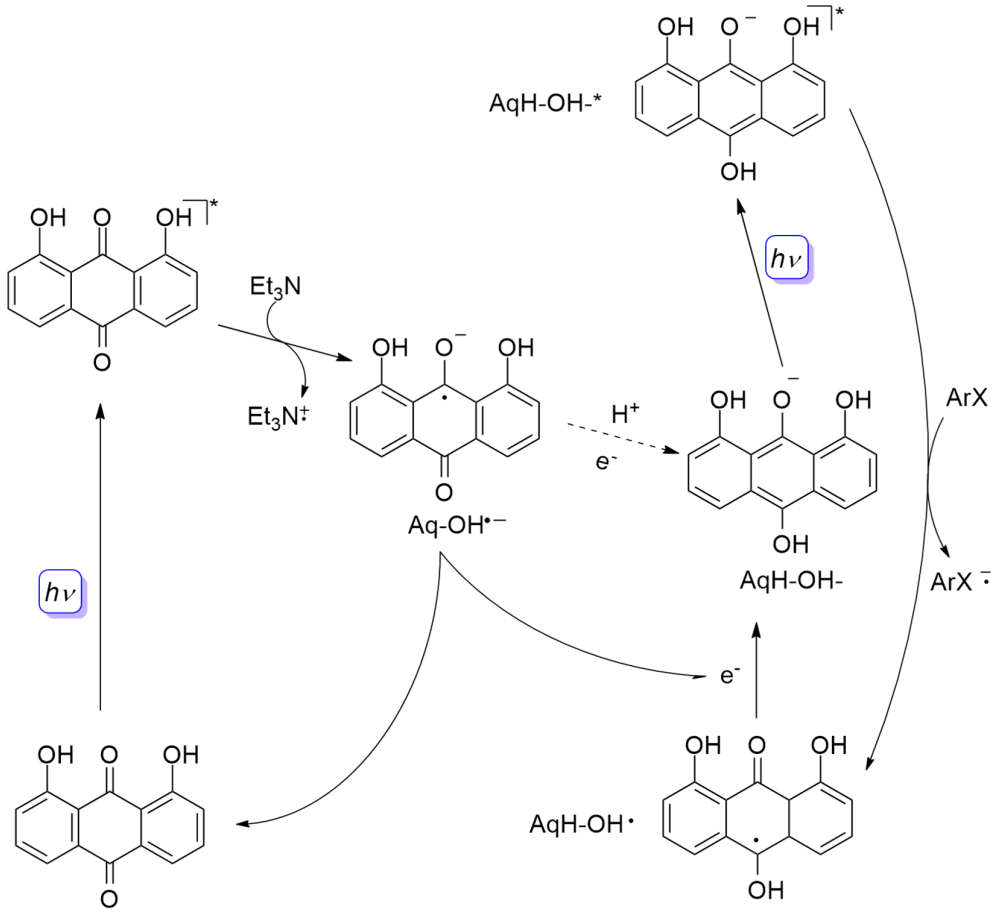

Figure 22. Partial mechanistic picture for aryl halide activation with catalytic Aq-OH.

4. Outlook

Complementary strategies have been reported for the syntheses and functionalization of substituted heteroarene derivatives and heterocycles based on radical addition to arenes, radical-nucleophilic intramolecular substitution (SRN1), intramolecular PET, via [2+2] cycloaddition and photoredox catalysis. In this context, photoredox catalysis offers a valuable alternative to

more conventional experimental conditions, which involved single-electron transfer promoted by photoactivable catalysts under visible light. As photocatalysts, organic dyes can be used as alternative as transition-metal-based complexes due to they are less expensive and ecologically friendly. The photo(redox)-catalyzed reactions have increased during the last decade to encompass quite a broad scope of possible transformations. It is expected this efficient chemical tool will be further developed to provide versatile pathways for late-stage functionalization of complex molecules, as already initiated by some research groups. However, challenges still need scientific attention relate to photo-catalyzed transformations, for instance, the activation of less reactive precursors that could be obtained from natural resources but keeping the practical procedures simple and accessible (air stable catalyst, non-dry conditions, etc). This will demand not only the extension of the actual procedures but also the development of new mechanistic approaches and combinations.

Nowadays, scientists and engineers are increasingly thinking in a sustainable way when they design their research programs. It is clear that green chemistry and engineering principles go beyond concerns over hazards from chemical toxicity and include considerations of energy conservation, waste reduction, and lifecycle such as the use of more sustainable or renewable feedstocks, and are accordingly being designed for the entire life cycle of the product. Over the last decade, the use of continuous-flow chemistry has emerged as a powerful technique employed successfully to the improvement of several synthetic applications.

In addition, with the technological advances, can be performed a specific photochemical reaction in multistep processes. Currently, organic chemists just have to evaluate the best route to drive total synthesis. For this reason, future challenges will be related to the combination, in individual flow-modules, of multicatalysis methodologies such as photocatalysis, enzymatic catalysis, organocatalysis, and metal catalysis, to access chiral compounds with biological interest..

Acknowledgements

This work was supported in part by Agencia Córdoba Ciencia, Consejo Nacional de Investigaciones Científicas y Técnicas (CONICET), Secretaría de Ciencia y Tecnología, Universidad Nacional de Córdoba (SECyT) and Agencia Nacional de Promoción Científica y Técnica (ANPCyT).

References

(1) Albini, A.; Fagnoni, M. Photochemically-Generated Intermediates In Synthesis; Albini, A., Fagnoni, M., Eds.; John Wiley & Sons, Inc.: Hoboken, New Jersey, **2013**.
(2) Ravelli, D.; Dondi, D.; Fagnoni, M.; Albini, A. Chem. Soc. Rev. 2009, 38, **1999**.
(3) Yoon, T. P. ACS Catal. **2013**, 3, 895–902.
(4) Prier, C. K.; Rankic, D. a; MacMillan, D. W. C. Chem. Rev. **2013**, 113, 5322–5363.
(5) Pause, L.; Robert, M.; Savéant, J.-M. J. Am. Chem. Soc. **1999**, 121, 7158–7159.
(6) Romero, N. A.; Nicewicz, D. A. Chem. Rev. **2016**, 116, 10075–10166.
(7) Marzo, L.; Pagire, S. K.; Reiser, O.; König, B. Angew. Chemie - Int. Ed. **2018**, 57, 10034–10072.
(8) Rossi, R.; Bardagi, J.; Buden, M. Curr. Org. Synth. **2017**, 14, 398–429.
(9) Javier I. Bardagi, Sofía Caby, S. M. S.-C. and G. O.-M. In Photoisomerization: Causes, Behavior and Effects; Sampedro, D., Ed.; Nova Science Publishers, Inc., **2019**; p 235.
(10) Bardagi, J. I.; Ghosh, I. In Visible Light-Active Photocatalysis; Ghosh, S., Ed.; Wiley-VCH Verlag GmbH & Co. KGaA: Weinheim, Germany, **2018**; pp 75–114.
(11) McAtee, R. C.; McClain, E. J.; Stephenson, C. R. J. Trends Chem. **2019**, 1, 111–125.
(12) Hari, D. P.; König, B. Chem. Commun. (Camb). **2014**, 50, 6688–6699.
(13) Fukuzumi, S.; Ohkubo, K. Chem. Sci. **2013**, 4, 561–574.
(14) Ghosh, I.; Marzo, L.; Das, A.; Shaikh, R.; König, B. Acc. Chem. Res. **2016**, 49, 1566–1577.
(15) Nguyen, J. D.; D'Amato, E. M.; Narayanam, J. M. R.; Stephenson, C. R. J. Nat. Chem. **2012**, 4, 854–859.
(16) Ghosh, I.; Ghosh, T.; Bardagi, J. I.; Konig, B. Science (80-.). **2014**, 346, 725–728.
(17) Ghosh, I.; König, B. Angew. Chemie Int. Ed. **2016**, 55, 7676–7679.
(18) Lanzalunga, O. Phosphorus. Sulfur. Silicon Relat. Elem. **2013**, 188, 322–330.
(19) Baciocchi, E.; Bietti, M.; Lanzalunga, O. J. Phys. Org. Chem. **2006**, 19, 467–478.
(20) Oksdath-Mansilla, G.; Argüello, J. E.; Peñéñory, A. B. Tetrahedron Lett. **2013**, 54, 1515–1518.
(21) Oksdath-Mansilla, G.; Peñéñory, A. B. Tetrahedron Lett. **2007**, 48, 6150–6154.
(22) Heredia, A. A.; Peñéñory, A. B. RSC Adv. **2015**, 5, 105699–105706.
(23) Soria-Castro, S. M.; Peñéñory, A. B. Beilstein J. Org. Chem. **2013**, 9, 467–475.
(24) Oksdath-Mansilla, G.; Peñéñory, A. B. J. Phys. Org. Chem. **2011**, 24, 1136–1143.
(25) Puiatti, M.; Argüello, J. E.; Peñéñory, A. B. European J. Org. Chem. **2006**, 2006, 4528–4536.
(26) Greene, T. W.; Wuts, P. G. M. Protective Groups in Organic Synthesis, 3rd ed.; John Wiley & Sons, Inc: New York, 779.
(27) Burghardt, T. E. J. Sulfur Chem. **2005**, 26, 411–427.
(28) Banerjee, A. K.; Laya, M. S. Russ. Chem. Rev. **2000**, 69, 947–955.
(29) Oksdath-Mansilla, G.; Hajj, V.; Andrada, D. M.; Argüello, J. E.; Bonin, J.; Robert, M.; Peñéñory, A. B. J. Org. Chem. **201**5, 80, 2733–2739.
(30) Majumdar, K. C.; Mondal, S. Chem. Rev. **2011**, 111, 7749–7773.
(31) Tang, X.; Li, Z.; Li, Y.; Liu, W.; Yu, P.; Li, L.; Guo, Y.; Yang, C. Chem. Res. Chinese Univ. **2015**, 31, 71–77.
(32) Majumdar, S.; Juntunen, J.; Sivendran, S.; Bharti, N.; Sloan, K. B. Tetrahedron Lett. **2006**, 47, 8981–8982.
(33) Csakai, A.; Smith, C.; Davis, E.; Martinko, A.; Coulup, S.; Yin, H. J. Med. Chem. **2014**, 57, 5348–5355.
(34) Ilardi, E. A.; Vitaku, E.; Njardarson, J. T. J. Med. Chem. **2014**, 57, 2832–2842.
(35) Laha, J. K.; Bhimpuria, R. A.; Kumar, A. M. Org. Chem. Front. **2017**, 4, 2170–2174.
(36) Fawad Zahoor, A.; Akhtar, R.; Ahmad, S.; Ali Raza Naqvi, S.; Gul Khan, S.; Suleman, M. Heterocycles **2017**, 94, 1389.
(37) Debnath, S.; Mondal, S. European J. Org. Chem. **2018**, 2018, 933–956.
(38) Politano, F.; Oksdath-Mansilla, G. Org. Process Res. Dev. **2018**, acs.oprd.8b00213.
(39) Kuijpers, K. P. L.; van Dijk, M. A. H.; Rumeur, Q. G.; Hessel, V.; Su, Y.; Noël, T. React. Chem. Eng. **2017**, 2, 109–115.
(40) Morse, P. D.; Beingessner, R. L.; Jamison, T. F. Isr. J. Chem. **2017**, 57, 218–227.

(41) Loubière, K.; Oelgemöller, M.; Aillet, T.; Dechy-Cabaret, O.; Prat, L. Chem. Eng. Process. Process Intensif. **2016**, 104, 120–132.
(42) Figueroa, F. N.; Heredia, A. A.; Peñéñory, A. B.; Sampedro, D.; Argüello, J. E.; Oksdath-Mansilla, G. J. Org. Chem**. 2019**, 84, 3871–3880.
(43) Hazebrouck, S.; Camoin, L.; Faltin, Z.; Strosberg, A. D.; Eshdat, Y. J. Biol. Chem. **2000**, 275, 28715–28721.
(44) Nicolaou, K. C.; Petasis, N. A. Selenium in Natural Products Synthesis; CIS Ins.: Philadelphia, **1984**.
(45) Oksdath-Mansilla, G.; Heredia, A. A.; Argüello, J. E.; Peñéñory, A. B. Photochem. Photobiol. Sci. **2015**, 14, 726–736.
(46) Bardagi, J. I.; Budén, M. E.; Rossi, R. A. Targets Heterocycl. Syst. Chem. Prop. Vol. 20 **2016**, 36.
(47) Budén, M. E.; Vaillard, V. A.; Martin, S. E.; Rossi, R. A.; Budén, M. E.; Vaillard, V. A.; Martin, S. E.; Rossi, R. A. J. Org. Chem. **2009**, 74, 4490–4498.
(48) Guerra, W. D.; Rossi, R. A.; Pierini, A. B.; Barolo, S. M. J. Org. Chem**. 2015**, 80, 928–941.
(49) Guerra, W. D.; Budén, M. E.; Barolo, S. M.; Rossi, R. A.; Pierini, A. B. Tetrahedron **2016**, 72, 7796–7804.
(50) Budén, M. E.; Rossi, R. A. Tetrahedron Lett. **2007**, 48, 8739–8742.
(51) Budén, M. E.; Dorn, V. B.; Gamba, M.; Pierini, A. B.; Rossi, R. a. J. Org. Chem**. 2010**, 75, 2206–2218.
(52) Peisino, L. E.; Camargo Solorzano, G. P.; Budén, M. E.; Pierini, A. B. RSC Adv. **2015**, 5, 36374–36384.
(53) Vaillard, V. A.; Budén, M. E.; Martín, S. E.; Rossi, R. A. Tetrahedron Lett. **2009**, 50, 3829–3832.
(54) Vaillard, V. A.; Guastavino, J. F.; Budén, M. E.; Bardagí, J. I.; Barolo, S. M.; Rossi, R. A. J. Org. Chem. **2012**, 77, 1507–1519.
(55) Vaillard, V. A.; Rossi, R. A.; Argüello, J. E. Org. Biomol. Chem. **2012**, 10, 9255–9261.
(56) Barolo, S. M.; Teng, X.; Cuny, G. D.; Rossi, R. A. J. Org. Chem. **2006**, 71, 8493–8499.
(57) Barolo, S. M.; Wang, Y.; Rossi, R. A.; Cuny, G. D. Tetrahedron **2013**, 69, 5487–5494.
(58) Guerra, W. D.; Rossi, R. A.; Pierini, A. B.; Barolo, S. M. J. Org. Chem. **2016**, 81, 4965–4973.
(59) Laha, J. K.; Barolo, S. M.; Rossi, R. A.; Cuny, G. D. J. Org. Chem. **2011**, 76, 6421–6425.
(60) Guastavino, J. F.; Rossi, R. A. J. Org. Chem. **2012**, 77, 460–472.
(61) Yanagisawa, S.; Ueda, K.; Taniguchi, T.; Itami, K. Org. Lett. **2008**, 10, 4673–4676.
(62) Liu, W.; Cao, H.; Zhang, H. H.; Zhang, H. H.; Chung, K. H.; He, C.; Wang, H.; Kwong, F. Y.; Lei, A. J. Am. Chem. Soc. **2010**, 132, 16737–16740.
(63) Shirakawa, E.; Itoh, K.; Higashino, T.; Hayashi, T. J. Am. Chem. Soc. **2010**, 132, 15537–15539.
(64) Sun, C.-L.; Li, H.; Yu, D.-G.; Yu, M.; Zhou, X.; Lu, X.-Y.; Huang, K.; Zheng, S.-F.; Li, B.-J.; Shi, Z.-J. Nat. Chem. **2010**, 2, 1044–1049.
(65) Sun, C.; Shi, Z. Chem. Rev. **2014**, 114, 9219–9280.
(66) Budén, M. E.; Guastavino, J. F.; Rossi, R. A. Org. Lett. **2013**, 15, 1174–1177.
(67) Guastavino, J. F.; Budén, M. E.; Rossi, R. A. J. Org. Chem. **2014**, 79, 9104–9111.
(68) Budén, M. E.; Bardagí, J. I.; Puiatti, M.; Rossi, R. A. J. Org. Chem. **2017**, 82, 8325–8333.
(69) Das, A.; Ghosh, I.; König, B. Chem. Commun. **2016**, 52, 8695–8698.
(70) Kushkhov, K. B.; Musaev, Y. I.; Kharaev, A. M. **2004**, 40, 203–207.
(71) Lü, J.-M.; Rosokha, S. V; Neretin, I. S.; Kochi, J. K. J. Am. Chem. Soc. **2006**, 128, 16708–16719.
(72) Robertson, P. K. J.; Eggins, B. R. J. Chem. Soc. Perkin Trans. 2 **1994**, No. 8, 1829.
(73) Bardagi, J. I.; Ghosh, I.; Schmalzbauer, M.; Ghosh, T.; König, B. European J. Org. Chem. **2018**, 2018, 34–40.

Gabriela Oksdath-Mansilla obtained her degree in Chemistry (2006) at Universidad Nacional de Córdoba (Argentina). Then, she joined Prof Alicia Peñeñory's group as a Ph.D. CONICET-fellow, dealing with Photoinduced Electron Transfer processes (2010). In 2008 she has been a Visiting Scholar to the Prof. Ian Barnes lab in the Bergische Universität, Physikalische Chemie from Wuppertal (Germany), exploring the photochemical atmospheric reactivity of sulfur-containing compounds. In 2017 she has been a Visiting Researcher to the Prof. Burkhard König Group, in the Faculty of Chemistry and Pharmacy, Regensburg University (Germany), studying organic synthesis using visible light photoredox catalysis. In 2019 she spent eight months in the Institute for Nanoscale Science and Technology, College of Science and Engineering; Flinder University (Australia), working in chemical transformations in continuous-flow using Vortex

Fluidic Device, under the supervision of: Prof. Colin Raston and co-supervision of Prof. Justin Chalker. Since 2013 she is a researcher (INFIQC-CONICET), at the Departamento de Química Orgánica, Facultad de Ciencias Químicas, Universidad Nacional de Córdoba (Argentina), where she is currently developing new synthetic strategies using continuous-flow technology. Her research interest is the development of greener, scalable and innovative approach for preparing organo-sulfur and organo-selenium-containing compounds.

Javier Ivan Bardagi obtained his PhD in Chemistry from Universidad Nacional de Córdoba (UNC), Argentina, in 2009 and working under the supervision of Dr. Roberto A. Rossi. Between February 2010 and April 2012, he stayed as a postdoctoral Fellow at the Department of Organic Chemistry. Soon after he was an AvH postdoctoral Fellow at the group of Burkhard König at the Regensburg University, Germany until March 2014. From 2009 he is an Assistant Professor at the Departamento de Química Orgánica, Facultad de Ciencias Químicas - Universidad Nacional de Córdoba and from 2015 he is also appointed Researcher (INFIQC-CONICET) at the same University. Where he has started his research program on (electro)photocatalysis for organic synthesis.

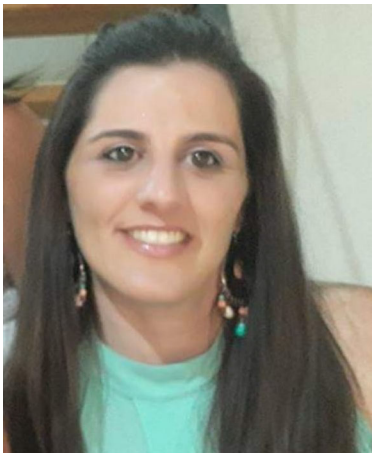

María Eugenia Budén has got a degree in chemistry in Chemistry (2004) at Universidad Nacional de Córdoba (Argentina). Then, she joined Prof Roberto Rossi's group as a Ph.D. CONICET-fellow, dealing with Photoinduced Electron Transfer processes (2010), where she worked on the synthesis of heterocycles by SRN1 reaction. In 2011 she spent ten months in the Barcelona University (Spain), working in the synthesis of polycyclic derivatives by cross metathesis reaction. In 2017 she has been a Visiting Researcher to the Prof. Maurice Medebielle Group, in the Claude Bernard Lyon 1 University (Lyon, France), studying organic synthesis of tetracyclic indole by Electron Transfer. Since 2013 she is a researcher (INFIQC-CONICET), at the Departamento de Química Orgánica, Facultad de Ciencias Químicas - Universidad Nacional de Córdoba (Argentina), where she is currently developing new synthetic strategies to obtain novel heterocycles compounds using visible light photoredox catalysis.

Anales de la Asociación Química Argentina

División Jóvenes Profesionales

Mini-Review

OXIDATION OF BIOMOLECULES PHOTOSENSITIZED BY PTERIN DERIVATIVES

M. Laura Dántola, Mariana Vignoni, Mariana P. Serrano, Carolina Lorente, Andrés H. Thomas*

Instituto de Investigaciones Fisicoquímicas Teóricas y Aplicadas (INIFTA), Departamento de Química, Facultad de Ciencias Exactas, Universidad Nacional de La Plata, CCT La Plata-CONICET. Casilla de Correo 16, Sucursal 4, (1900) La Plata, Argentina.

**Autor Corresponsal: athomas@inifta.unlp.edu.ar*

Graphical abstract

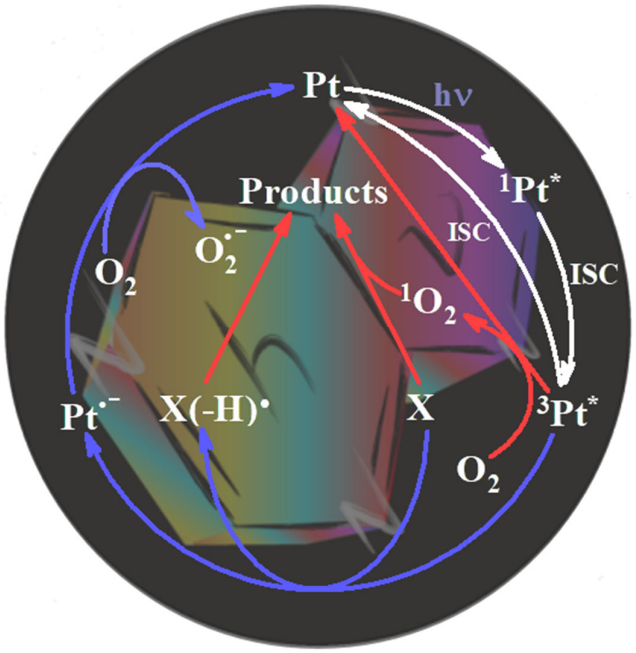

Depending on the target molecule (X), pterin-photosensitized oxidations may be purely *type I* (electron transfer) or *type II* (singlet oxygen, $^1O_2$), or a combination of both.

Resumen

La importancia biológica y médica de las reacciones fotosensibilizadas se relaciona principalmente con su participación en los procesos involucrados en el desarrollo de cáncer de piel y de terapias fotodinámicas para el tratamiento del cáncer e infecciones. Las pterinas, son una familia de compuestos heterocíclicos derivados de la 2-amino-4-pterinidinona, que se encuentran ampliamente distribuidas en los sistemas vivos

participando de importantes funciones biológicas. En condiciones patológicas, como es el caso del vitiligo, pterinas oxidadas se acumulan en las manchas blancas de la piel de los pacientes que sufren este desorden de la pigmentación. Estas moléculas son fotoquímicamente activas, bajo radiación UV-A (320 – 400 nm), fluorescen, producen radicales orgánicos y especies reactivas de oxígeno, y también sufren reacciones de fotooxidación. Nuestro grupo de investigación, ha estudiado desde hace más de 20 años, la degradación fotosensibilizada por pterinas de biomoléculas tales como ADN, proteínas, lípidos y sus componentes. Los resultados experimentales incluyen análisis cinético, evaluación de la interacción entre los estados excitados de las pterinas con diferentes sustratos, detección de especies radicalarias, y la identificación de productos bajo diferentes condiciones experimentales. Dependiendo de la molécula blanco, las pterinas pueden fotosensibilizar la oxidación de las mismas por mecanismo *tipo I* (transferencia de electrones) o *tipo II* (oxígeno singlete, $^1O_2$), o una combinación de ambos. En este artículo, presentamos un resumen de los cambios químicos fotosensibilizados por pterinas bajo irradiación UV-A en diferentes biomoléculas y los mecanismos involucrados.

Abstract

The biological and medical importance of photosensitized reactions is mainly related to their participation in processes involved in the development of skin cancer and in photodynamic treatments against cancer and infections. Pterins, a family of heterocyclic compounds derived from 2-aminopteridin-4(1H)-one, are widespread in living systems and participate in important biological functions. In pathological conditions, such as vitiligo, oxidized pterins accumulate in the white skin patches of patients suffering this depigmentation disorder. These molecules are photochemically active and, under UV-A excitation (320–400 nm), they can fluoresce, produce organic radicals and reactive oxygen species and undergo photooxidation. Our research group has investigated for more than 20 years the degradation of biomolecules such as DNA, proteins, lipids, and their components, photosensitized by pterins under UV-A irradiation. The experimental results include kinetics analysis, evaluation of interaction between pterins excited states with different substrates, detection of radical species, and identification of products, under different experimental conditions. Depending on the target molecule, pterin-photosensitized oxidations may be purely *type I* (electron transfer) or *type II* (singlet oxygen, $^1O_2$), or a combination of both. In this article, we present a summary of the chemical changes photoinduced by pterins upon UV-A irradiation in different biomolecules and the mechanisms involved.

Palabras Clave: *pterinas, fotosensibilización, ADN, proteínas, lípidos*

Keywords: *pterins, photosensitization, DNA, proteins, lipids*

1. Introduction

Pterins and their derivatives belong to a family of heterocyclic compounds which were uncovered over a century ago, with the isolation of its first members from the pigment of the wings of a butterfly (Pteridae) [1, 2]. Nowadays, it is known that these compounds are present in different biological systems and play various roles. Besides acting as pigments, pterins participate in other relevant biological functions which includes being the light- harvesting antenna of DNA photolyases, enzymes involved in DNA repair processes after UV irradiation [3-5], as well as behaving as coenzymes [6, 7] and enzymes inhibitors [8].

These compounds, structurally related to 2-aminopteridin-4(1*H*)-one or pterin (Ptr), can exist in living systems in different redox states and may be classified into three classes according to this property: fully oxidized (or aromatic) pterins, and dihydro and tetrahydro derivatives (Figure 1). Finally, they behave as weak acids in aqueous solution. The dominant equilibrium at pH > 5 involves the lactam group (pyrimidine ring) (Figure 1). The pK_a of this equilibrium is *ca.* 8 for the aromatic pterins and *ca.* 10 for dihydropterin derivatives. Other functional groups of the pterin moiety (*e.g.*, the 2-amino group or ring N-atoms) have pK_a values < 2 [9].

The most common pterin derivatives are 6-substituted compounds (Table 1). According to the molecular weight and the functional groups of these substituents, pterins can be divided into two groups: (i) unconjugated pterins, containing substituents with one carbon atom or a short hydrocarbon chain, and (ii) conjugated pterins, with larger substituents containing a *p*-aminobenzoic acid (PABA) moiety. In Table 1 the molecular structures of the most common substituents are shown together with the names of the corresponding oxidized pterin derivatives. Analogous derivatives can be found for dihydro and tetrahydro pterins.

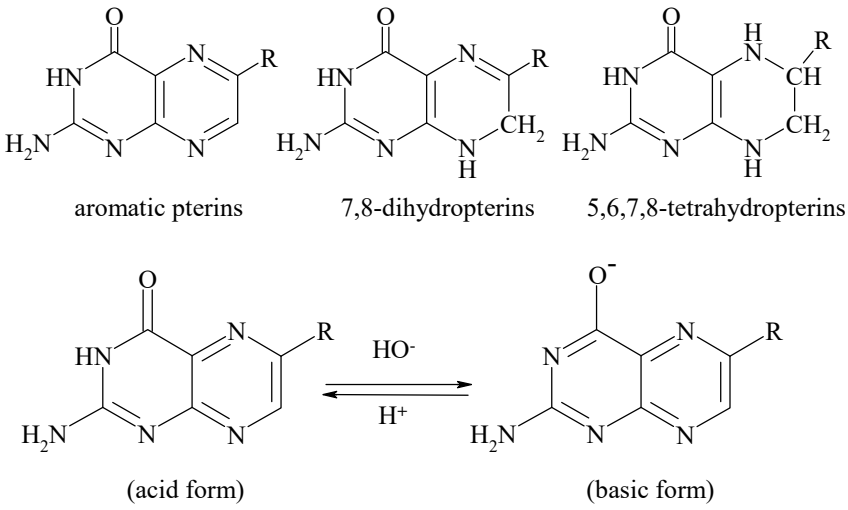

Figure 1. Molecular structures of pterins and the acid–base equilibrium in aqueous solution.

Table 1. Molecular structures of the substituents of the most common aromatic pterin derivatives.

R	Compound
Unconjugated pterins	
-H	pterin (Ptr)
-CH_3	6-methylpterin (Mep)
-CH_3	6,7-dimethylpterin (Dmp)
-CHO	6-formylpterin (Fop)
-COOH	6-carboxypterin (Cap)
-$(CHOH)_2$-CH_3	biopterin (Bip)
-$(CHOH)_2$-CH_2OH	neopterin (Nep)
Conjugated pterins	
-CH_2-PABA	pteroic acid (Pte)
-CH_2-PABAGlu	folic acid (PteGlu)

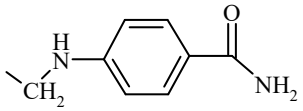
-CH_2-PABA

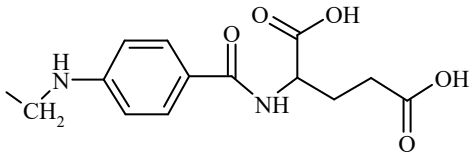
-CH_2-PABA-Glu

Pterins are present in human epidermis given that 5,6,7,8-tetrahydrobiopterin (H_4Bip) is an essential cofactor for aromatic amino acid hydroxylases [10] and participates in the regulation of melanin biosynthesis [11]. In vitiligo, a skin disorder characterized by a defective protection against UV radiation due to the acquired loss of constitutional pigmentation [12], H_4Bip metabolism is altered [13, 14]. Dihydro and oxidized pterin derivatives, such as biopterin (Bip) and 6-carboxypterin

(Cap), accumulate in the affected tissues at concentrations significantly higher than those reported for healthy cells [15].

The photochemistry and photophysics of pterins is relevant to understand the harmful effects of radiation on skin, particularly in pigmentation disorders, where these compounds are present in higher concentrations. Pterins are photochemically reactive in aqueous solutions and, under UV-A excitation (320 – 400 nm), they can fluoresce, undergo photooxidation to produce different products, and generate reactive oxygen species (ROS) such as singlet oxygen ($^1O_2$) and superoxide anion ($O_2^{\bullet-}$) [13, 16, 17]. Different studies have demonstrated or suggested that pterins are involved in photochemical processes that take place in biological systems. Just to mention some relevant examples: (i) excited states of oxidized pterins are photogenerated in the skin of patients suffering from vitiligo [6,11], (ii) the photodegradation *in vivo* of folic acid has been demonstrated[18], (iii) folic acid derivative 5,10-methenyltetrahydrofolate is the light-harvesting antenna in DNA photolyases [3], enzymes involved in DNA repair after UV irradiation.

Most of the solar UV energy incidence on Earth's surface corresponds to UV-A radiation, which can induce damage mostly through photosensitized reactions [19]. A photosensitized reaction is defined as a photochemical alteration occurring in one molecular entity as a result of the initial absorption of radiation by another molecular entity called photosensitizer [20]. These processes may be mediated by endogenous or exogenous photosensitizers and can take place through different mechanisms: the generation of radicals, *e.g.*, *via* electron transfer or hydrogen abstraction (*type I* mechanism), and the production of $^1O_2$ (*type II* mechanism) [21].

In 1997 Ito and Kawanishi demonstrated for the first time that upon excitation with UV-A radiation pterins are able to photoinduce DNA damage [22]. More recently, the mechanism involved in the photosensitization of biomolecules by pterins were investigated in a series of studies carried out with free nucleotides [23, 24] and amino acids [25, 26]. It was shown that pterins can act as photosensitizers through both *type I* and *type II* mechanisms and that the predominant one depends on a combination of many factors, such as quantum yields of $^1O_2$ production by the

photosensitizer, reactivity of the substrate towards $^1O_2$, target molecule redox potential and presence of selective scavengers in the media.

Considering the studies mentioned in the previous paragraph, after UV-A excitation of a given pterin derivatives (Pt) and formation of its triplet excited state ($^3Pt^*$, Reaction 1), two competitive mechanisms can be summarized to explain the photooxidation of different biological substrates (S) (Reactions 1-7). *Type I* mechanism is initiated by an electron transfer from S to $^3Pt^*$, yielding the corresponding pair of radical ions (pterin radical anion ($Pt^{\bullet-}$) and radical cation of the biological substrate ($S^{\bullet+}$), Reaction 2). $Pt^{\bullet-}$ reacts by ground state oxygen (O_2) to produce $O_2^{\bullet-}$ and regenerate Pt (Reaction 3). The spontaneous disproportionation of $O_2^{\bullet-}$ in aqueous solution leads to the formation of hydrogen peroxide (H_2O_2) (Reaction 4). The radical $S^{\bullet+}$ (or its deprotonated form, $S(-H)^{\bullet}$) may react with O_2, H_2O or $O_2^{\bullet-}$ to yield oxidized products (Reaction 5) or with other organic radicals ($R^{\bullet}$) (Reaction 6). On the other hand, in the *type II* mechanism the process starts with an energy transfer from $^3Pt^*$ to O_2 leading to the production of singlet molecular oxygen ($O_2(^1\Delta_g)$, denoted as $^1O_2$) (Reaction 7), one of the main activated species responsible for the damaging effects of light on biological systems (photodynamic effects) [27]. In this case the oxidation of S occurs by reaction with $^1O_2$ (reaction 8).

$$Pt \longrightarrow {}^1Pt^* \longrightarrow {}^3Pt^* \qquad (1)$$

Type I mechanism

$$^3Pt^* + S \longrightarrow Pt^{\bullet-} + S^{\bullet+} \qquad (2)$$

$$Pt^{\bullet-} + O_2 \longrightarrow Pt + O_2^{\bullet-} \qquad (3)$$

$$2\ H^+ + 2\ O_2^{\bullet-} \longrightarrow H_2O_2 + O_2 \qquad (4)$$

$$S^{\bullet+}/S(-H)^{\bullet} \xrightarrow{O_2/H_2O/O_2^{\bullet-}} S(ox) \qquad (5)$$

$$S^{\bullet+}/S(-H)^{\bullet} + R^{\bullet} \longrightarrow S\text{-}R \qquad (6)$$

Type II mechanism

$$^3Pt^* + {}^3O_2 \longrightarrow Pt + {}^1O_2 \qquad (7)$$

$$S + {}^1O_2 \longrightarrow \longrightarrow S(ox) \qquad (8)$$

In the context of our investigations on the photochemistry and photosensitizing properties of pterins, we present in this article an overview of pterin-photosensitized damage in peptides and proteins, DNA and nucleotides, and lipids. We have focused our attention on the mechanisms involved and on the chemical modifications undergone by the different biomolecules used as substrates. The most relevant results, from a biological point of view, are summarized and discussed in this review.

2. Nucleotides, oligonucleotides and DNA

Photosensitization processes introduces mutagenic lesions on DNA molecules, which leads to carcinogenic processes at cellular level [28, 29]. Pteridines induce the oxidation of DNA and its component after absorption of UV-A radiation, and the mechanisms involved depends on the type of the nucleobase, purine or pyrimidine.

Photosensitized oxidation of purines by Ptr takes place only in aerated aqueous solution. Purines nucleotides, 2′-deoxyadenosine 5′-monophosphate (dAMP) and 2'-deoxyguanosine 5'-monophosphate (dGMP), are both oxidize during UV-A radiation in the presence of Ptr. Since dAMP is not oxidizable by $^1O_2$, its oxidation reveals a pure *type I* mechanism (Reactions 2-5). Indeed, after UV-A absorption by Ptr, dAMP undergoes a one-electron oxidation, yielding the corresponding radical ion ($dAMP^{\bullet+}$), which reacts with O_2 and H_2O, to form the products 8-oxo-7,8-dihydro-2'-deoxyadenosine 5'-monophosphate (8-oxo-dAMP) and a tetracyclic compound (8-P-dAMP) with a –OP(=O)(OH)O– bridge formed between the deoxyribose phosphate substituent and the C-8 of the adenine moiety (Figure 2) [30, 31].

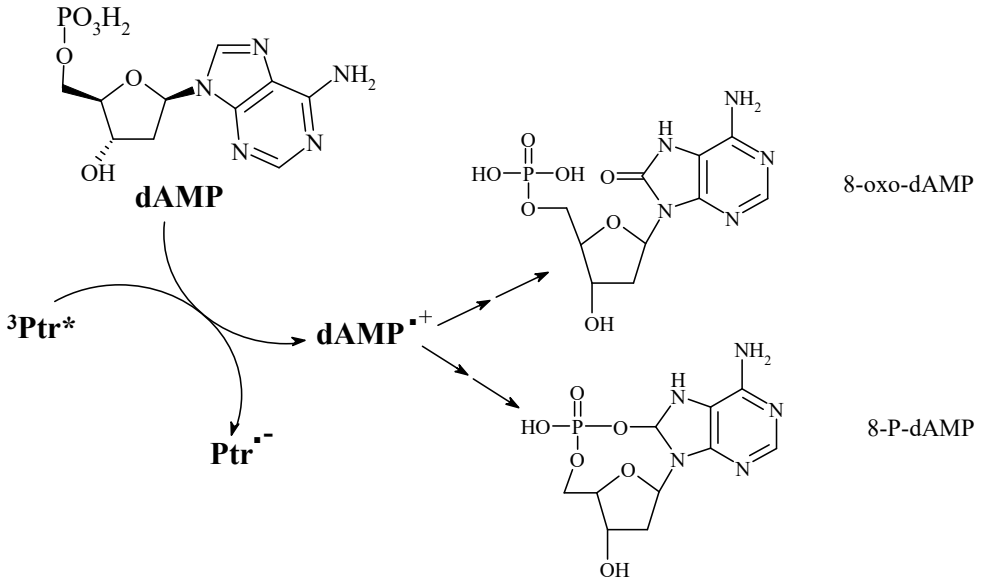

Figure 2. Products of Ptr photosensitized oxidation of dAMP (from Reference 31).

In contrast, the oxidation of dGMP photosensitized by Ptr occurs through two competing mechanisms: (1) electron transfer between dGMP and ^{3}Ptr* (*type I*) (Reactions 2-5) and (2) reaction of dGMP with $^1O_2$ produced by Ptr (*type II*) (Reactions 7-8) [23, 24]. The electron transfer reaction between ^{3}Ptr* and dGMP, yields the corresponding radical pair, and dGMP$^{\bullet+}$ immediately deprotonates to give dGMP(-H$^+$)$^\bullet$. This radical is oxidized by $O_2^{\bullet-}$ and/or O_2 and/or hydration to yield different products that have been identified: the deoxyribonucleoside 5'-monophosphate derivatives of dehydroguanidinohydantoin (dDGhMP), guanidinohydantoin (dGhMP), imidazolone (dIzMP), oxazolone (dZMP) and an adduct consisting of dGMP and dDGhMP (Figure 3) [32]. Several products, have also been described for the reaction between guanine and $^1O_2$ [33]. In the case of the photosensitization of dGMP with Ptr, the deoxyribonucleoside 5'-monophosphate derivative of spiroimidantoine (SpMP) was identified as a product of the oxidation by this ROS.

Thymidine 5'-monophosphate (dTMP), a pyrimidine nucleotide, is also oxidized by UV-A photosensitization with Ptr. In this case only mechanisms initiated by electron transfer are

involved, in contrast to that observed for purine nucleotides. Upon irradiation, consumption of the substrate is observed in the presence and in the absence of O_2 [24, 34]. These processes are relevant from a biological point of view because they demonstrate that thymine, which is frequently assumed as a non-reactive nucleobase, can be damaged under UV-A radiation. Moreover, the photosensitized damages can take place at low O_2 concentration and even under anaerobic conditions, which is important since the intracellular concentration of O_2 in tissues is much lower than that corresponding to air-equilibrated aqueous solutions. Under aerobic conditions, as in the case of purine nucleotides, electron transfer from the substrate to $^3Ptr^*$ leads to the formation of a radical cation ($dTMP^{\bullet+}$), which undergoes two main competitive reactions: deprotonation and hydration (Figure 4). The resulting radicals evolve to at least 4 stable oxidized products: thymidine glycol 5'-monophophate (dTMPGly), 5-hydroxy-5-methylhydantoin 5'-monophosphate (5-OH-5MHMP), 5-formyl-2'-deoxyuridine 5'-monophosphate (5-FordUMP) and 5-(hydroxymethyl)-2'-uridine 5'-monophosphate (5-HmdUMP) (Figure 4). On the other hand, upon irradiation under anaerobic conditions, the formation of an adduct between the pterinic moiety and the nucleotide was observed, due to coupling of the radical $PtrH^{\bullet}$ (C-centered radical on the C-6 or C-7 position of the pterin moiety) and $dTMP(-H)^{\bullet}$ (neutral methylene radical), which yields the product Ptr-dTMP(-2H) when is exposed to air (Figure 4). Similar results were obtained with dCMP, but with lower efficiency.

The formation of the photoadduct Ptr-dTMP(-2H) was also investigated on a short thymine oligomer, 5-mer oligonucleotide (dT_5) [35]. When oxygen-free aqueous solutions containing dT_5 and Ptr were exposed to UV-A radiation, several products, with absorbance in the UV-A region and fluorescence around 450 nm were observed, indicating that, after the electron transfer step, the radicals ions combine to yield an adduct where the pterinic moiety is covalently attached to the oligonucleotide.

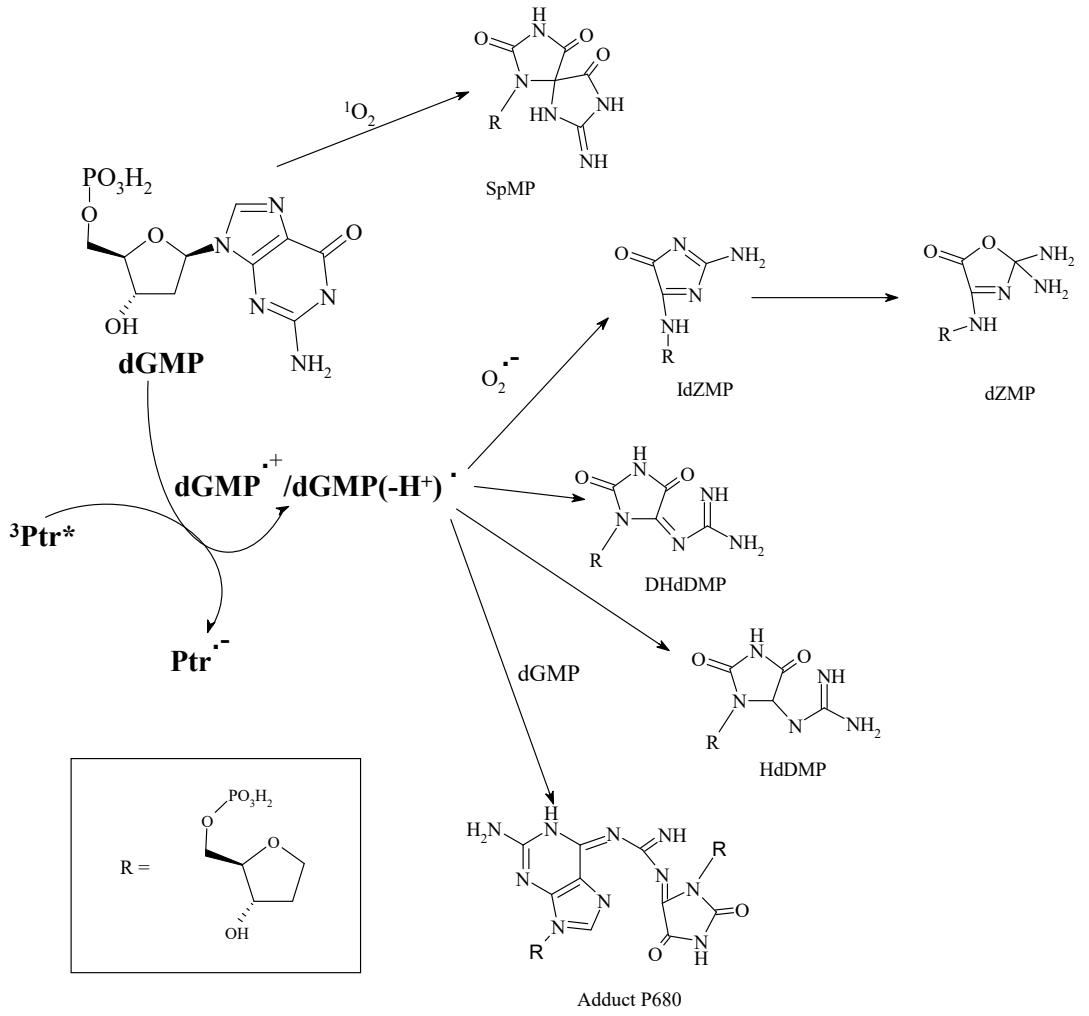

Figure 3. Products of Ptr-photosensitized oxidation of dGMP.

Additionally, at least two isomeric oligonucleotides bearing two molecules of Ptr were also detected, indicating that the covalent binding of the first Ptr moiety does not prevent the addition of a second one due to steric hindrance. On the other hand, UV-A irradiation of air-equilibrated aqueous solutions containing dT_5 and Ptr leads to degradation of the oligonucleotide, but the products do not show absorption in the UV-A region neither fluorescence upon excitation at 350 nm, indicating that in the presence of oxygen binding of the pterin moiety to the oligonucleotide does not take place, in agreement with the behavior observed using dTMP as a substrate.

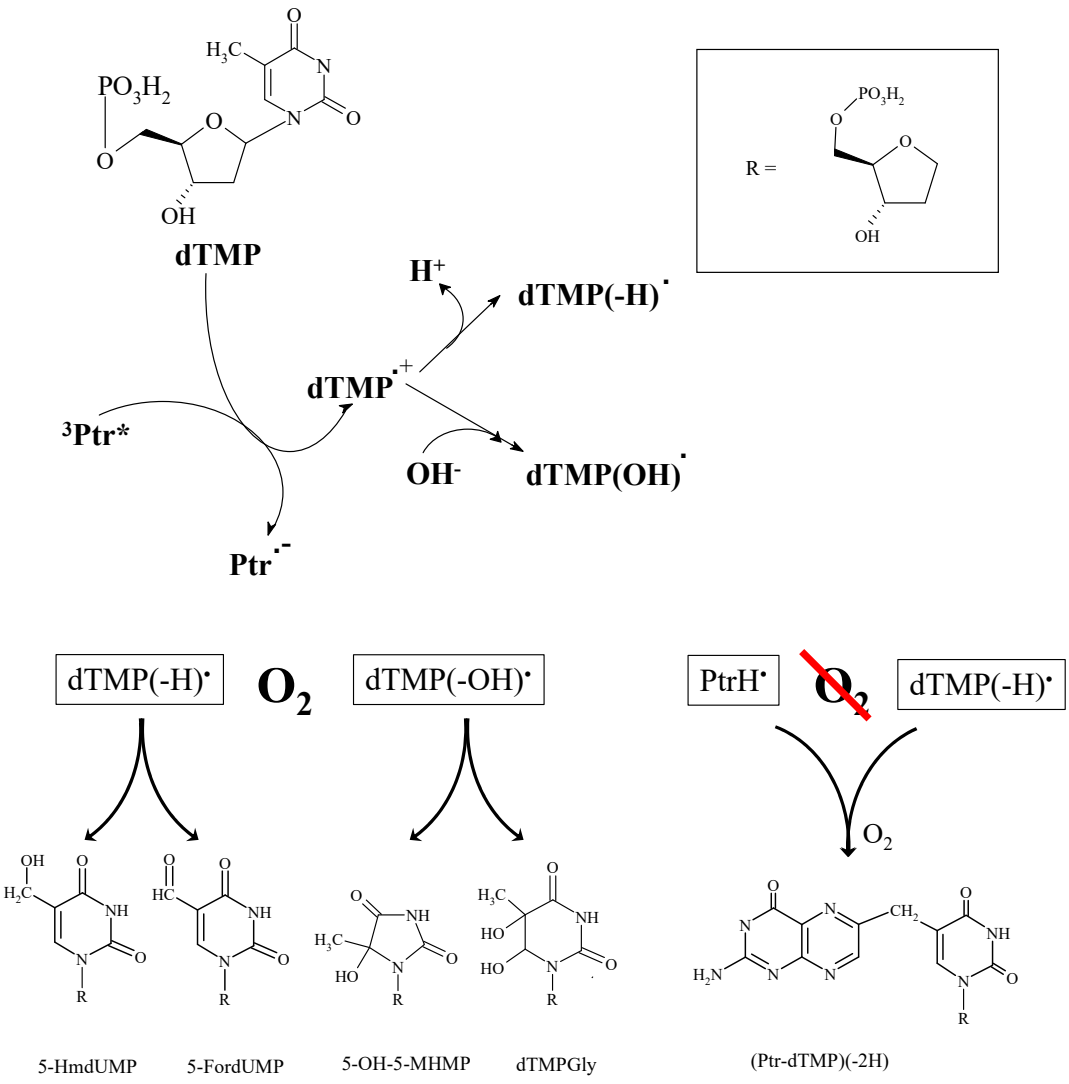

Figure 4. Products and mechanism of the degradation of dTMP photosensitized by Ptr.

The first evidence of Ptr-photosensitized degradation of DNA was in double-stranded chains in 1997 [22], and later on pUC18 plasmid [36]. In both articles it was reported that, upon excitation with UV-A radiation, pterins are able to photoinduce DNA damage. Taking into account indirect evidence, the mechanism involved in this process was proposed to be an electron transfer with the subsequent formation of the guanine radical cation and a pterin radical anion. On the contrary, an article reporting Ptr-photosensitized damage on PBR 322 plasmid [37], indicates that the main mechanism responsible for the photoinduced cleavage of plasmid DNA was a *type II* photosensitized oxidation.

Recently, we have reported damage on double stranded calf thymus DNA in UV-A irradiated aqueous solutions containing Ptr. After control experiments discarding any interaction between Ptr and DNA, the incorporation of Ptr to DNA molecules was evaluated [35]. Upon irradiation in anaerobic conditions, the treated DNA molecules show absorbance at 340 nm and fluorescence with a maximum at ~ 450 nm, suggesting the incorporation of Ptr to DNA molecules, in a relation of one molecule of Ptr every 9 base pairs. In aerobic conditions, irradiation in the presence of Ptr causes random cleavage in the DNA molecules, yielding fragments of different molecular weights. These results are in agreement with previously data reported for plasmidic DNA [36].

3. Amino acids, peptides and proteins

Proteins, due to their relatively high abundance, their ability to bind chromophores, and the reactivity of particular amino acid residues, are one of the preferential targets of the photosensitized damaging effects of UV radiation on biological systems [38]. Currently, it is accepted that the photosensitization of proteins occurs mainly through the reactions of $^1O_2$ with tryptophan (Trp), tyrosine (Tyr), histidine (His), methionine and cysteine side-chains [39]. However, in the last decade we have demonstrated that pterins are able to photoinduce damage in free amino acids, peptides and proteins through both *type I* and *type II* mechanism, being the *type I* mechanism the main contribution in the photosensitization process [25, 26, 40]. We have focused our attention on the chemical modifications of Tyr and Trp residues because these amino acids are particularly susceptible to a variety of oxidizing agents [41].

The oxidation of Trp photosensitized by Ptr takes place through both *type I* and *type II* mechanisms, the first being the predominant one. Product analysis revealed that two main products are formed in the process. One of them is hydroxytryptophan (HO-Trp) (Figure 5), which has been detected in the skin of patients affected by vitiligo [42]. The other one is N-formylkynurenine (NFK) (Figure 5). Other minor product is kynurenic acid (KA) (Figure 5), formed by several reactions steps from NFK.

Tyr is an important target in the study of the photodynamic effects of UV-A radiation in living systems, not only due to its reactivity towards $^1O_2$ [43, 44], but also because this amino acid plays a key role in polymerization and cross-linking of proteins [45, 46] *via* reactions initiated by Tyr radicals [47, 48]. Mechanistic analysis indicates that the Ptr-sensitized oxygenation/oxidation of Tyr does not involve $^1O_2$, and proceeds through an electron transfer-initiated process. In this mechanism, the one-electron oxidation of Tyr leads to the formation of the corresponding radical, $Tyr^{\bullet+}$/$Tyr(-H)^{\bullet}$, which can react with O_2 (and with $O_2^{\bullet-}$ and H_2O) (Reaction 5), to yield a series of oxidation products, such as DOPA and *o,o´*-dityrosine (Tyr_2) (Figure 6). The formation of Tyr_2 is important from a biological point of view because it implies that pterins might photoinduce the oligomerization and crosslinking of proteins in vivo.

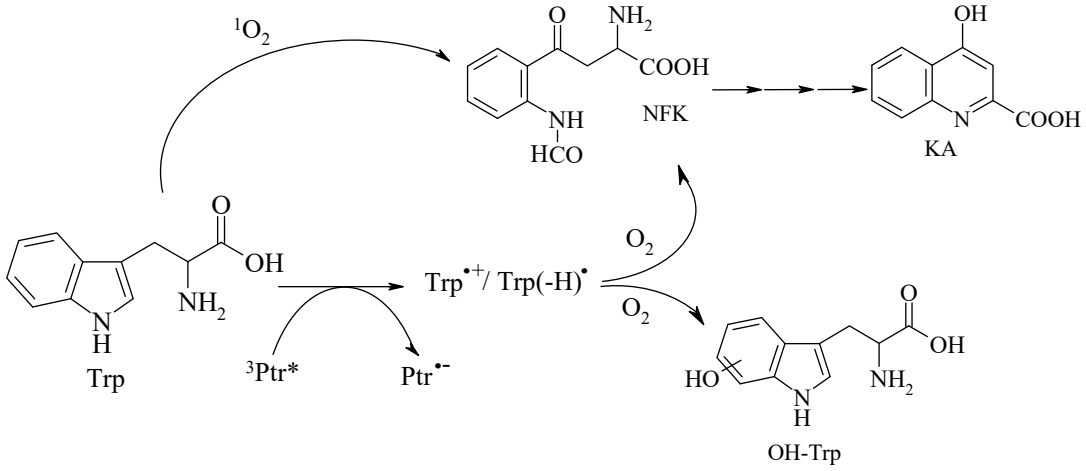

Figure 5. Products of Ptr photosensitized oxidation of Trp.

In the context of our investigations on the photosensitizing properties of pterins, we have also explored reactions that affect biomolecules involved in the pigmentation of the skin. In this way, we performed studies with α-melanocyte-stimulating hormone (α-MSH) and related peptides, tyrosinase (TYR) and albumins (bovine serum albumin (BSA) and human serum albumin (HSA)) as substrates.

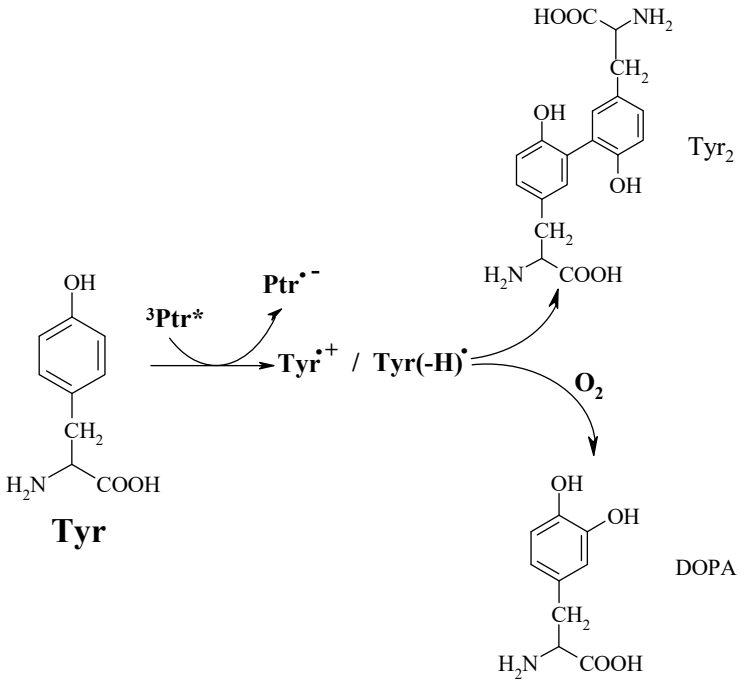

Figure 6. Products of Ptr photosensitized oxidation of Tyr

α-MSH is a short peptide, with Trp and Tyr residues in its sequence, that stimulates the production and release of melanin by melanocytes in the skin and hair. When aerated aqueous solutions containing α-MSH and Ptr were exposed to UV-A radiation, the peptide consumption and H_2O_2 generation were observed, but without significant change in the photosensitizer concentration. In this process Trp and Tyr residues are damaged and new fluorescent compounds were formed. One of these compounds exhibits an emission band with a peak maximum coinciding with that expected for Tyr_2 and the cross-linking between two peptide molecules was observed [49].

To avoid interferences in the characterization of the photoproducts, two peptides in which the amino acid sequence of α-MSH was mutated were used. In the peptide named $\alpha\text{-MSH}_{W9G}$, the Trp residue in position 9 was mutated to a glycine (Gly), whereas in the peptide named $\alpha\text{-MSH}_{Y2G}$, the Tyr residue in position 2 was mutated, also to a Gly residue. During the photosensitization of $\alpha\text{–MSH}_{Y2G}$, the Trp residue was consumed, and at least three major

products were detected. The spectroscopic characterization of these products suggested that the Trp residue was oxidized to NFK and HO-Trp. No dimeric products were observed with this peptide. However, during the photosensitization of α-MSH$_{W9G}$, two simultaneous processes occur: dimerization and incorporation of oxygen. These results confirm that the dimerization observed in α-MSH is due to the crosslinking of Tyr residues [50].

Albumin is the most abundant plasma proteins, and their main biological function is the transport of a wide variety of molecules. Besides, it is present in human skin [51], where there is an autocrine synthesis and regulation [52]. It has been reported that in patients affected by vitiligo, epidermal albumin oxidation takes place, but the mechanism of this process has not been elucidated [53]. We have studied the capability of Ptr to photoinduce chemical and structural changes in BSA and HSA. The results obtained for both proteins were very similar, as is expected due to the high structural homology between the two proteins. When air-equilibrated aqueous solutions of albumin and Ptr were exposed to UV-A radiation, the oligomerization of the protein was observed [48, 54]. For HSA, it was found that oligomers with more than 10 HSA molecules were formed. The emission spectra of the oligomer fraction revealed the presence of Tyr$_2$, suggesting that this product is, at least in part, responsible for the bonds between albumin molecules. Moreover, upon irradiation, the intensity of the Trp emission of the albumin decreased as a function of irradiation time, indicating the modification of this amino acid residue. NFK was identified as one of the photooxidation products of albumin.

To find out if the observed photoinduced chemical modifications on proteins can affect the activity of enzymes, experiments using tyrosinase (TYR, L-tyrosine, L-dopa: oxygen oxidoreductase, EC 1.14.18.1)) as a substrate were performed [55]. This biomolecule was chosen because it is an essential enzyme in the biosynthesis of melanin. A fast inactivation of the enzyme was recorded when TYR was exposed to UV-A radiation in the presence of Ptr. The mechanistic analysis suggested that the photoinactivation of TYR is initiated by an electron transfer reaction and takes place *via* a *type I* mechanism.

We extended our studies on the photoinactivation of TYR to folic acid (PteGlu) and its oxidation products (6-formylpterin (Fop) and carboxypterin (Cap)) because the photodegradation of PteGlu, an important vitamin, has been proposed as one of the reasons for the development of skin tanning in evolution. The activity of TYR decreased significantly when the enzyme was exposed to radiation in the presence of PteGlu [56]. The results suggest that PteGlu itself is unable to inactivate the enzyme, but its photoproducts, Fop and Cap, photoinduce its inactivation, being Fop the most efficient photosensitizer. These results provide evidence that processes photosensitized by pterins might affect the synthesis of melanin and, in consequence, play a key role in pigmentation disorders.

4. Phospholipids

In a study performed using cervical cancer cells (HeLa), we ascertained that pterins are readily incorporated into the cells, that cell death takes place upon UV-A irradiation of pterins, and that the integrity of the cell membrane is affected, among other alterations undergone by the cells [57]. Taking into account these results and to go further with the investigation of the photosensitizing properties of pterins, we decided to start investigating the photoinduced damage of biomembranes by pterins.

Lipid peroxidation is involved in many physiological and pathological events, and is usually due to oxidative stress [58-60]. This process can proceed by different mechanisms [61]. The most important one involves free radicals, where the initiation phase includes hydrogen atom abstraction, and the most abundant compounds of lipid membranes, phospholipids containing polyunsaturated fatty acids (PUFAs), are the main targets. Light accelerates lipid peroxidation quite substantially [62-64], and endogenous or exogenous photosensitizers can act through both *type I* and *II* mechanisms.

Therefore, we have investigated the oxidation of large unilamellar vesicles (LUVs) of soybean phosphatidylcholine (SoyPC) photoinduced by Ptr [65]. SoyPC LUVs were exposed to UV-A irradiation prepared in the presence and absence of Ptr. Conjugated dienes and trienes were detected in the treated samples, revealing that Ptr is able to photoinduced lipid peroxidation. Mechanistic studies suggested that the process would be initiated by an electron transfer step, whereas $^1O_2$ would not be involved as the main pathway. Additionally, several hydroperoxides corresponding to the oxidation of different PC derivatives were found as photoproducts, such as PC(16:0/18:2)-OOH, PC(18:1/18:2)-OOH and PC(18:2/18:2)-OOH. Moreover, when the irradiation time increases, hydroperoxides suffered cleavages in the carbon chain generating short-chain secondary oxidation products (aldehyde, ketones and carboxy products). Additionally, it was revealed that Ptr is not encapsulated in the inner fraction of vesicles, but is able to freely cross the phospholipid bilayer.

Lipophilic photosensitizers able to bind to biomembranes usually are more efficient in phototriggering lipid peroxidation than hydrophilic photosensitizers [66-69]. Therefore, new lipophilic pterin derivatives were synthesized. Four compounds were obtained with the decyl carbon chain attached to position N3 or O of Ptr (Figure 7). Conjugation of a decyl-chain to the pterin moiety dramatically increases its solubility in common organic solvents and also enables its facile intercalation in LUVs membranes [70, 71]. Constant binding were determined obtaining values comparable with other lipophilic molecules [72, 73]. In addition, decyl-pterins present more efficient intersystem crossing to the triplet excited states compared to Ptr, showing higher $^1O_2$ quantum yields, and lower fluorescence emission.

To investigate whether lipophilic pterins are better lipid peroxidation photosensitizers, the efficiency of *O*-decyl-Ptr (Figure 7) was evaluated and compared to its hydrophilic parent compound, Ptr. Investigation in SoyPC LUVs showed that the formation of conjugated dienes and trienes and lipid hydroperoxides is much faster using *O*-decyl-Ptr than Ptr.

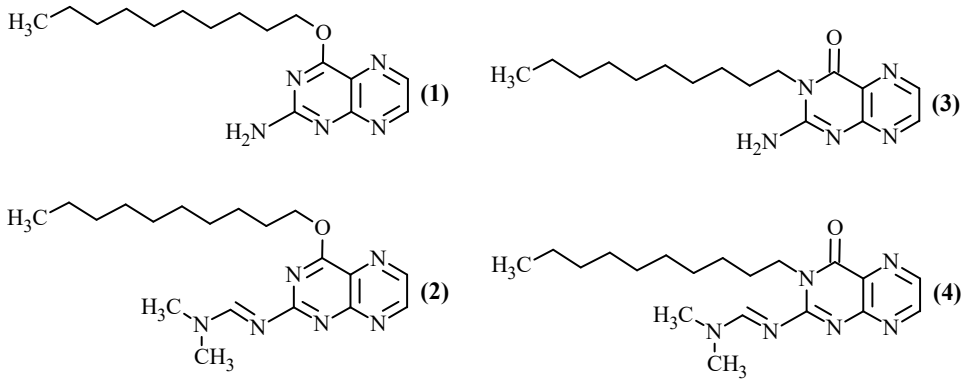

Figure 7. Synthetized lipophilic pterins (1) 4-(Decyloxy)pteridin-2-amine, (2) N′-(4-(Decyloxy) pteridin-2-yl)-N,N-dimethylformimidamide, (3) 2-Amino-3-decylpteridin-4(3H)-one and (4) N′-(3-Decyl-4-oxo-3,4-dihydropteridin-2-yl)-N,N-dimethylformimidamide.

In order to better investigate the chemical changes photoinduced by *O*-decyl-Ptr in PUFAs, products formed in the photosensitization of LUVs of DLPC (PC 18:2/18:2) were analyzed. In particular, products with the incorporation of one oxygen atom (hydroxyl derivative), two oxygen atoms (one hydroperoxide or two hydroxyl groups) [74], (Figure 8) and the incorporation of oxygen atoms with the loss of two H (keto derivatives) were characterized. In addition, short chain secondary products were identified, *e.g.*, 2-(9-carboxy-nonanoyl)−LPC and 2-(9-oxononanoyl)−LPC (Figure 8). Taking into account previous studies on lipid peroxidation[75,76], these phospholipid oxidation products are formed after rearrangement and cleavages of hydroxylderivatives or LO$^{\bullet}$ radicals, produced by reduction of hydroperoxides. A kinetic qualitative assessment of the formation of the different products, suggested that no accumulation of hydroperoxides took place before the production of hydroxy derivatives and short chain secondary products, which might indicate a fast photosensitized conversion of the former into the latter.

The alteration of the permeability of vesicles upon UV-A irradiation in the presence of pterins was also evaluated. In these studies SoyPC LUVs and DLPC giant unilamellar vesicles (GUVs) were used as substrates and Ptr and *O*-decyl-Ptr were employed as photosensitizers. Results demonstrated pterin mediated photosensitization leads to an increase in the permeability of the

membrane, revealing that the photochemical process causes damage of the structure of the membrane. It is also worth mentioning that the interaction of *O*-decyl-Ptr with the biomembranes due to the presence of the alkyl side chain, dramatically favors the photoinduced increase of permeability when compared with experiments performed with Ptr. This is in agreement with the fact that the formation of oxidized products is much faster using *O*-decyl-Ptr than Ptr.

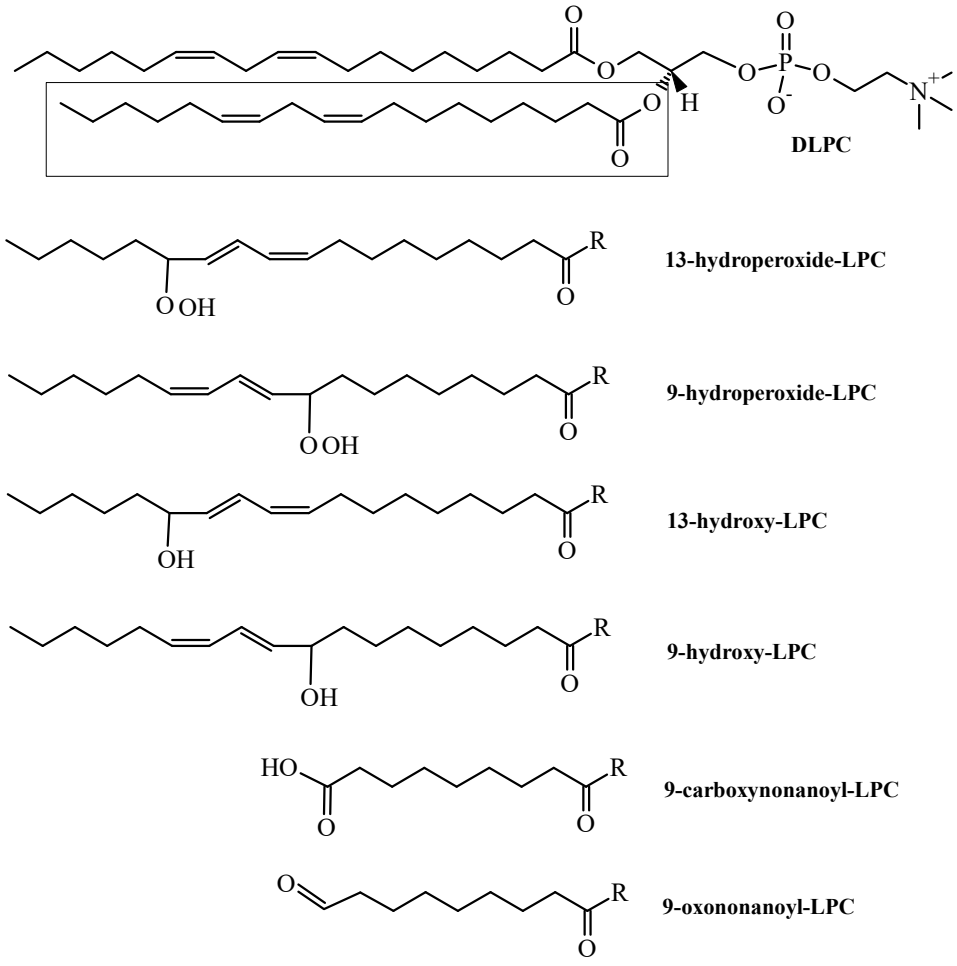

Figure 8. Several products found after photosensitized lipid peroxidation of DLPC LUVs by *O*-decyl-Ptr.

It is well known that oxidation of the double bond(s) on the acyl tails(s) of the unsaturated phospholipids promotes lipid hydroperoxidation [61]. When hydroperoxide species accumulate in the membrane, large membrane fluctuation ending in surface area increase were reported, with

no increase in membrane permeability [68, 69, 77]. In contrast, pore formation is observed when oxidized lipids with shortened chains are present in the biomembranes [78, 79]. Therefore, the significant increase in membrane permeability in LUVs and GUVs experiments are consistent with the detection of shortened oxidized lipids. However, in phase contrast optical microscopy experiments, neither membrane fluctuations nor area increase preceded membrane contrast fading, suggesting there is no hydroperoxide accumulation in agreement with our product analysis. In this way, our results furnish valuable information regarding the photodynamic mechanism of action of *O*-decyl-Ptr in biomembranes which, in turn, may perturb cell homeostasis and trigger cell death.

Acknowledgements

The present work was mainly supported by the following Argentinean institutions: Consejo Nacional de Investigaciones Científicas y Técnicas (CONICET), Agencia de Promoción Científica y Tecnológica (ANPCyT), and Universidad Nacional de La Plata (UNLP). The authors also acknowledge the following foreign institutions that supported their collaborations abroad: Centre National de la Recherche Scientifique (CNRS, France), Sao Paulo Research Foundation (FAPESP, Brazil), National Science Foundation (NSF, USA) and Consejo Superior de Investigaciones Científicas (CSIC, Spain). The authors thank Esther Oliveros, André M. Braun, Patricia Vicendo, Alexander Greer, Gabriela Petroselli, Sandra Estébanez, Lara O. Reid, Carolina Castaño, M. Noel Urrutia, Ernesto A. Roman, Miguel A. Miranda, M. Luisa Marín, Virginie Lhiaubet-Vallet, Claudio D. Borsarelli, Mauricio S. Baptista and Rosangela Itri for their crucial contributions to this work.

References

(1) W. Pfleiderer, in Chemistry and Biology of Pteridines and Folates, eds. J. E. Ayling, M. Gopal Nair and C. M. Baugh, Plenum Press, New York, **1993**, vol. 338, pp. 1-16.
(2) B. Wijnen, H. L. Leertouwer and D. G. Stavenga, J. Insect Physiol., **2007**, 53, 1206-1217.
(3) J. E. Hearst, Science, **1995**, 268, 1858.
(4) J. L. Johnson, S. Hamm-Alvarez, G. Payne, G. B. Sancar, K. V. Rajagopalan and A. Sancar, Proc. Natl. Acad. Sci. U. S. A., **1988**, 85, 2046-2050.
(5) P. F. Heelis, S.-T. Kim, T. Okamura and A. Sancar, J. Photochem, Photobiol. B: Biol, **1993**, 17, 219-228.
(6) C. A. Nichol, G. K. Smith and D. S. Duch, Annu. Rev. Biochem., **1985**, 54, 729-764.
(7) J. M. Hevel and M. A. Marietta, Biochemistry, **1992**, 31, 7160-7165.
(8) A. W. Schüttelkopf, L. W. Hardy, S. M. Beverley and W. N. Hunter, J. Mol. Biol., **2005**, 352, 105-116.
(9) A. Albert, Biochem. J., **1953**, 54, 646-640.
(10) I. Ziegler, Med. Res. Rev., **1990**, 10, 95-114.

(11) K. U. Schallreuter, J. M. Wood, M. R. Pittelkow, M. Gütlich, K. R. Lemke, W. Rödl, N. N. Swanson, K. Hitzemann and I. Ziegler, Science, **1994**, 263, 1444-1446.
(12) S. J. Glassman, Clinical Science, **2011**, 120, 99-120.
(13) K. U. Schallreuter, J. Moore, J. M. Wood, W. D. Beazley, E. M. Peters, L. K. Marles, S. C. Behrens-Williams, R. Dummer, N. Blau and B. Thöny, J. Invest. Dermatol., **2001**, 116, 167–174.
(14) K. U. Schallreuter, J. Moore, J. M. Wood, W. D. Beazley, E. M. Peters, L. K. Marles, S. C. Behrens-Williams, R. Dummer, N. Blau and B. Thöny, J. Invest. Dermatol, **2001**, 116, 167–174.
(15) H. Rokos, W. D. Beazley and K. U. Schallreuter, Biochem. Biophys. Res. Commun., **2002**, 292, 805–811.
(16) K. V. Neverov, E. A. Mironov, T. A. Lyudnikova, A. A. Krasnovskij and M. S. Kritskij, Biokhimiya, **1996**, 61, 1627-1636.
(17) C. Lorente and A. H. Thomas, Acc. Chem. Res., **2006**, 39, 395-402.
(18) R. F. Branda and J. W. Eaton, Science, **1978**, 201, 625-626.
(19) J. Cadet and T. Douki, J. Invest. Dermatol, **2011**, 131, 1005-1007.
(20) S. E. Braslavsky, Pure Appl. Chem., **2007**, 79, 293-465.
(21) M. S. Baptista, J. Cadet, P. Di Mascio, A. A. Ghogare, A. Greer, M. R. Hamblin, C. Lorente, S. C. Nunez, M. S. Ribeiro, A. H. Thomas, M. Vignoni and T. M. Yoshimura, Photochem. Photobiol., **2017**, 93, 912-919.
(22) K. Ito and S. Kawanishi, Biochemistry, **1997**, 36, 1774-1781.
(23) G. Petroselli, M. L. Dántola, F. M. Cabrerizo, A. L. Capparelli, C. Lorente, E. Oliveros and A. H. Thomas, J. Am. Chem. Soc., **2008**, 130, 3001-3011.
(24) M. P. Serrano, M. Vignoni, C. Lorente, P. Vicendo, E. Oliveros and A. H. Thomas, Free Radical Biol. Med., **2016**, 96, 418-431.
(25) A. H. Thomas, M. P. Serrano, V. Rahal, P. Vicendo, C. Claparols, E. Oliveros and C. Lorente, Free Radical Biol. Med., **2013**, 63, 467-475.
(26) C. Castaño, M. L. Dántola, E. Oliveros, A. H. Thomas and C. Lorente, Photochem. Photobiol., **2013**, 89, 1448-1455.
(27) P. Di Mascio, G. R. Martinez, S. Miyamoto, G. E. Ronsein, M. H. G. Medeiros and J. Cadet, Chem. Rev., **2019**.
(28) F. El Ghissassi, R. Baan, K. Straif, Y. Grosse, B. Secretan, V. Bouvard, L. Benbrahim-Tallaa, N. Guha, C. Freeman, L. Galichet and V. Cogliano, The Lancet Oncology, **2009**, 10, 751-752.
(29) W. Ting, K. Schultz, N. N. Cac, M. Peterson and H. W. Walling, Int. J. Dermatol, **2007**, 46, 1253-1257.
(30) G. Petroselli, R. Erra-Balsells, F. M. Cabrerizo, C. Lorente, A. L. Capparelli, A. M. Braun, E. Oliveros and A. H. Thomas, Org. Biomol. Chem., **2007**, 5, 2792-2799.
(31) C. Lorente, G. Petroselli, M. L. Dántola, E. Oliveros and A. H. Thomas, Pteridines, **2011**, 22, 111-119.
(32) M. P. Serrano, S. Estebanez, M. Vignoni, C. Lorente, P. Vicendo, E. Oliveros and A. H. Thomas, New J. Chem., **2017**, 41, 7273-7282.
(33) J.-L. Ravanat, G. R. Martinez, M. H. G. Medeiros, P. Di Mascio and J. Cadet, Arch. Biochem. Biophys., **2004**, 423, 23-30.
(34) S. Estébanez, A. H. Thomas and C. Lorente, ChemPhysChem, **2018**, 19, 300-306.
(35) S. Estébanez, C. Lorente, M. G. Tosato, M. A. Miranda, M. L. Marín, V. Lhiaubet-Vallet and A. H. Thomas, Dyes Pigm., **2019**, 160, 624-632.
(36) C. Lorente, A. H. Thomas, L. S. Villata, D. Hozbor, A. Lagares and A. L. Capparelli, Pteridines, **2000**, 11, 100-105.
(37) T. Offer, B. N. Ames, S. W. Bailey, E. A. Sabens, M. Nozawa and J. E. Ayling, The FASEB Journal, **2007**, 21, 2101-2107.
(38) M. J. Davies, Biochem. Biophys. Res. Commun., **2003**, 305, 761-770.
(39) D. I. Pattison, A. S. Rahmanto and M. J. Davies, Photochem. Photobiol. Sci., **2012**, 11, 38-53.
(40) M. L. Dantola, L. O. Reid, C. Castaño, C. Lorente, E. Oliveros and A. H. Thomas, Pteridines, **2017**, 28, 105-114.
(41) M. J. Davies, The Biochemical journal, **2016**, 473, 805-825.
(42) K. U. Schallreuter, M. A. E. L. Salem, N. C. J. Gibbons, A. Martinez, R. Slominski, J. Lüdemann and H. Rokos, FASEB Journal, **2012**, 26, 2457-2470.
(43) S. Criado, A. T. Soltermann, J. M. Marioli and N. A. Garcia, Photochem. Photobiol., **1998**, 68, 453-458.
(44) A. Wright, W. A. Bubb, C. L. Hawkins and M. J. Davies, Photochem. Photobiol., **2002**, 76, 35-46.
(45) N. Rabgaouli, A. Slaoui-Hasnaoui and J. Torreilles, Free Rad. Biol. Med, **1993**, 14, 519-529.
(46) D. A. Malencik and S. R. Anderson, Biochemistry, **1996**, 35, 4375-4386.
(47) R. Amadò, R. Aeschbach and H. Neukom, in Methods Enzymol., Academic Press, **1984**, vol. 107, pp. 377-388.
(48) L. O. Reid, E. A. Roman, A. H. Thomas and M. L. Dántola, Biochemistry, **2016**, 55, 4777-4786.
(49) C. Castaño, C. Lorente, N. Martins-Froment, E. Oliveros and A. H. Thomas, Org. Biomol. Chem., **2014**, 12, 3877-3886.

(50) C. Castaño, M. Vignoni, P. Vicendo, E. Oliveros and A. H. Thomas, J. Photochem. Photobiol. B: Biol., **2016**, 164, 226-235.
(51) J. Katz, G. Bonorris and A. L. Sellers, Clinical Science, **1970**, 39, 725-729.
(52) S. Hasse, S. Kothari, H. Rokos, S. Kauser, N. Y. Schürer and K. U. Schallreuter, Experimental Dermatology, **2005**, 14, 182-187.
(53) H. Rokos, J. Moore, S. Hasse, J. M. Gillbro, J. M. Wood and K. U. Schallreuter, J. Raman Spectrosc., 2004, 35, 125-130.
(54) A. H. Thomas, B. N. Zurbano, C. Lorente, J. Santos, E. A. Roman and M. Laura Dántola, J. Photochem. Photobiol. B: Biol., **2014**, 141, 262-268.
(55) M. L. Dántola, A. D. Gojanovich and A. H. Thomas, Biochem. Biophys. Res. Commun., **2012**, 424, 568-572.
(56) 56. M. L. Dántola, B. N. Zurbano and A. H. Thomas, J. Photochem. Photobiol. B: Biol., **2015**, 149, 172-179.
(57) M. P. Denofrio, C. Lorente, T. Breitenbach, S. Hatz, F. M. Cabrerizo, A. H. Thomas and P. R. Ogilby, Photochem. Photobiol., **2011**, 87, 862-866.
(58) A. Catalá, Chem. Phys. Lipids, **2009**, 157, 1-11.
(59) M. Repetto, J. Semprine and A. Boveris, Lipid Peroxidation: Chemical Mechanism, Biological Implications and Analytical Determination, **2012**.
(60) A. Catala, Frontiers in Physiology, **2015**, 5.
(61) E. Niki, Free Radical Biol. Med., **2009**, 47, 469-484.
(62) R. Bonnett, Chemical aspects of photodynamic therapy, Gordon and Breach Science Publishers, Amsterdam, The Netherlands, **2000**.
(63) T. J. Dougherty, C. J. Gomer, B. W. Henderson, G. Jori, D. Kessel, M. Korbelik, J. Moan and Q. Peng, J. Natl. Cancer Inst., **1998**, 90, 889-905.
(64) M. R. Hamblin and P. Mroz, Advances In Photodynamic Therapy: Basic, Translational And Clinical Artech House, Inc, Norwood, MA, **2008**.
(65) A. H. Thomas, Á. Catalá and M. Vignoni, Biochim. Biophys. Acta, Biomembr., **2016**, 1858, 139-145.
(66) I. R. Calori and A. C. Tedesco, J. Photochem Photobiol B: Biol, **2016**, 160, 240-247.
(67) S. Ytzhak, S. Bernstein, L. M. Loew and B. Ehrenberg, Progress in Biomedical Optics and Imaging - Proceedings of SPIE, **2009**.
(68) K. A. Riske, T. P. Sudbrack, N. L. Archilha, A. F. Uchoa, A. P. Schroder, C. M. Marques, M. S. Baptista and R. Itri, Biophys. J., **2009**, 97, 1362-1370.
(69) G. Weber, T. Charitat, M. S. Baptista, A. F. Uchoa, C. Pavani, H. C. Junqueira, Y. Guo, V. A. Baulin, R. Itri, C. M. Marques and A. P. Schroder, Soft Matter, **2014**, 10, 4241-4247.
(70) M. Vignoni, N. Walalawela, S. M. Bonesi, A. Greer and A. H. Thomas, Mol. Pharm., **2018**, 15, 798-807.
(71) N. Walalawela, M. Vignoni, M. N. Urrutia, S. J. Belh, E. M. Greer, A. H. Thomas and A. Greer, Photochem. Photobiol., **2018**, 94, 834-844.
(72) N. G. Angeli, M. G. Lagorio, E. A. S. Román and L. E. Dicelio, Photochem. Photobiol., **2000**, 72, 49-56.
(73) I. R. Calori, D. S. Pellosi, D. Vanzin, G. B. Cesar, P. C. S. Pereira, M. J. Politi, N. Hioka and W. Caetano, J. Braz. Chem. Soc., **2016**, 27, 1938-1948.
(74) M. Vignoni, M. N. Urrutia, H. C. Junqueira, A. Greer, A. Reis, M. S. Baptista, R. Itri and A. H. Thomas, Langmuir, **2018**, 34, 15578-15586.
(75) A. Reis and C. M. Spickett, Biochim. Biophys. Acta, Biomembr., **2012**, 1818, 2374-2387.
(76) S. Khoury, C. Pouyet, B. Lyan and E. Pujos-Guillot, Anal. Bioanal. Chem., **2018**, 410, 633-647.
(77) J. Wong-ekkabut, Z. Xu, W. Triampo, I. M. Tang, D. Peter Tieleman and L. Monticelli, Biophys. J., **2007**, 93, 4225-4236.
(78) W. Caetano, P. S. Haddad, R. Itri, D. Severino, V. C. Vieira, M. S. Baptista, A. P. Schröder and C. M. Marques, Langmuir, **2007**, 23, 1307-1314.
(79) K. A. Runas and N. Malmstadt, Soft Matter, 2015, 11, 499-505.

María Laura Dántola was born in Berisso, Argentina, in 1979. She obtained her degree in Biochemistry at the Universidad Nacional de La Plata (UNLP), Argentina, in 2005. She was awarded a PhD in Science at the UNLP in 2008. She started as an Assistant Researcher in Prof. Thomas's group at Research Institute of Theoretical and Applied Physical Chemistry (INIFTA, UNLP) in 2010. Currently, she works at INIFTA as Independent Researcher of CONICET. Her main research interest deals with the photosensitization of proteins and its components using different pterin derivatives as photosensitizer, focusing its attention on the mechanisms involved in these processes.

Mariana Vignoni obtained her degree in Biochemistry at the Universidad Nacional de La Plata (UNLP), Argentina, in 2007. She did her PhD in the group of Dr. Andres Thomas at INIFTA (Research Institute of Theoretical and Applied Physical Chemistry) from the UNLP. She did a post-doctoral fellowship at the University of Ottawa in Prof. Scaiano's group. She started as an Assistant Researcher in Prof. Thomas's group at INIFTA in 2013. She is currently an Adjunct Researcher and her main research activities deal with photosensitization of lipid membranes and synthesis of new lipophilic photosensitizers.

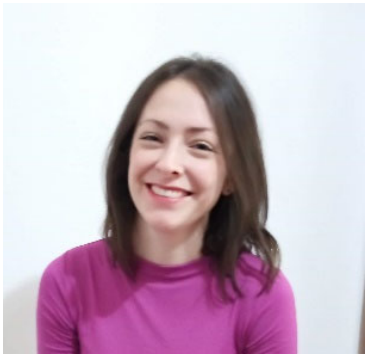

Mariana Serrano has been carrying research activities in the field of photochemistry and photosensitization processes with biological targets, specifically nucleotides, with special interest of processes related to skin diseases, such as vitiligo. The PhD thesis of Dr. Mariana Serrano (2010-2014), is an example of the approach between photochemistry and biomedical processes. Studying photosensitization process in nucleotides initiated by pterins, a group of molecules presents in the skin of patients suffering from vitiligo. Her background is related to mechanisms and chemical kinetics of reactions involving biomolecules with a broad range of analytical techniques, such as liquid chromatography, mass spectrometry and fluorescence spectroscopy. Currently, Dr. Serrano research covers aspects of photochemistry of reactions occurring in heterogenous systems.

Carolina Lorente was born in La Plata, Argentina, in 1968. She obtained a degree in Biochemistry and a Ph.D. in Science at the Universidad Nacional de La Plata (UNLP). She held a postdoctoral position at the Universidad de Buenos Aires (UBA). She currently works at the Theoretical and Applied Physical Chemistry (INIFTA, UNLP) as Independent Researcher of CONICET. Her research interest is the study of the mechanisms involved in photosensitized reactions, their biological implications and the search for antioxidants that can prevent these mechanisms.

Andrés H. Thomas was born in La Plata, Argentina, in 1968. He studied at the Universidad Nacional de La Plata (UNLP) and was awarded a PhD degree in 2001. After a postdoctoral fellowship at the University of Buenos Aires, he joined the Argentinean National Research Council (CONICET) as Assistant Researcher. Currently, he is Professor of the Faculty of Science of UNLP, and he works at the Institute of Theoretical and Applied Research on Physical Chemistry (INIFTA) as Principal Researcher of CONICET. His research interests include photophysics and photochemistry of biomolecules and photosensitized processes of biological and medical interest.

Anales de la Asociación Química Argentina

División Jóvenes Profesionales

Mini-Review

CURRENT LANDSCAPE OF THE SPECTROSCOPIC AND PHOTOCHEMICAL PROPERTIES OF β-CARBOLINE ALKALOIDS IN AQUEOUS MEDIA TOWARDS UNDERSTANDING THEIR BIOLOGICAL ROLE. REVIEW

Juan G. Yañuk[1], Fernando D. Villarruel[1, 2], M. Lis Alomar[1], Federico A. O. Rasse-Suriani[2], M. Micaela Gonzalez[1], Eduardo Gonik[1,2], Lorean Madriz[2], Ronald Vargas[1], Rosa Erra-Balsells[3, 4], M. Paula Denofrio[1], and Franco M. Cabrerizo[1, *]

1 Instituto Tecnológico de Chascomús (INTECH), Universidad Nacional de San Martín (UNSAM) - Consejo Nacional de Investigaciones Científicas y Técnicas (CONICET), Av. Intendente Marino Km 8.2, CC 164, (B7130IWA) Chascomús, Argentina. E-mail: fcabrerizo@intech.gov.ar
2 INIFTA - CONICET, Universidad Nacional de La Plata, Diag. 113 y 64 (1900), La Plata, Argentina.
3 Universidad de Buenos Aires. Facultad de Ciencias Exactas y Naturales. Departamento de Química Orgánica. Pabellón II, 3er P., Ciudad Universitaria, (1428) Buenos Aires, Argentina.
4 CONICET, Universidad de Buenos Aires. Centro de Investigación en Hidratos de Carbono (CIHIDECAR). Facultad de Ciencias Exactas y Naturales. Pabellón II, 3er P., Ciudad Universitaria, (1428) Buenos Aires, Argentina.

**Autor Corresponsal: fcabrerizo@intech.gov.ar*

Graphical abstract

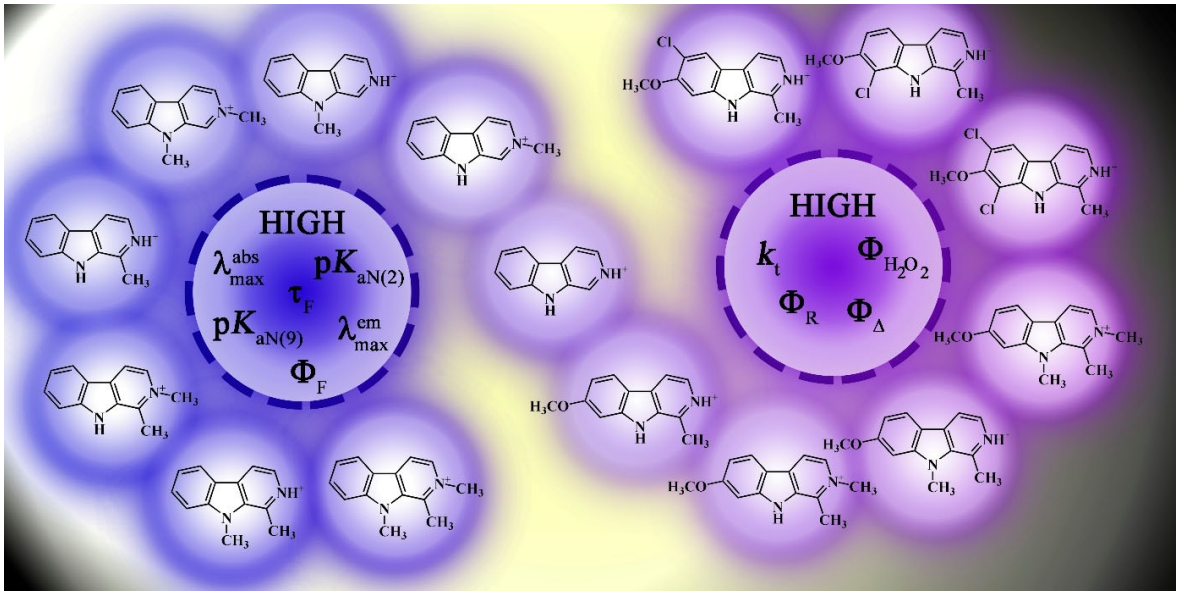

Resumen

Las β-carbolinas (βCs) constituyen una familia de alcaloides estructuralmente relacionados con el 9H-pyrido[3,4-b]indol o norharmano. Estos alcaloides están presentes en una amplia gama de organismos vivos, filogenéticamente muy distantes entre sí, incluidos diversos organismos fototróficos. A pesar de su gran abundancia en la naturaleza y su demostrada participación en diversos procesos biológicos, aún quedan múltiples aspectos por explorar y comprender relacionados con las propiedades fotoquímicas y fotobiológicas de estos alcaloides. Mas aún, en la mayoría de los casos, aún no se conocen las bases moleculares de los procesos en los que participan. En este trabajo de revisión, presentamos las propiedades espectroscópicas, químicas y fotoquímicas más relevantes de un grupo representativo de βCs aromáticas y parcialmente hidrogenadas, observadas en entorno acuoso. Todos los aspectos fundamentales aquí discutidos representan un aporte clave para comprender y conjeturar acerca del posible rol biológico de estos alcaloides.

Abstract

β-carbolines (βCs) comprise a large variety of naturally occurring alkaloids structurally related to 9H-pyrido[3,4-b]indole or norharmane, widely spread in a vast range of phylogenetically distant species, including phototrophic organisms. Despite their abundance in nature and the well-established relevance of these alkaloids, their photochemical and photobiological properties as well as their main biological role remain unclear. Moreover, in most of the cases, the fundamental aspects and molecular basis of the mechanisms involved still remain poorly understood. In this review, we summarize the most relevant spectroscopic, chemical and photochemical properties observed in aqueous environment for a representative set of full-aromatic, dihydro- and tetrahydro-βCs. All the fundamental aspects herein discussed provide key insights to theorize and/or surmise about the biological role that these compounds might have.

***Palabras Clave**: Fotoquímica, Espectroscopía, Fluorescencia, Especies Reactivas, Electroquímica.*

***Keywords:** Photochemistry, Spectroscopy, Fluorescence, Reactive Species, Electrochemistry.*

1. Introduction

1.1. Biological distribution

β-carbolines (βCs, **Schemes 1a-c**) comprise a large variety of naturally occurring alkaloids structurally related to 9H-pyrido[3,4-b]indole (**1a**). βCs have been found in a vast range of phylogenetically distant species including *Rhizaria, Alveolata* and *Amoebozoa* (protists organisms), *Stramenopiles* (unicellular diatoms and blue-green algae organisms) [1], *Opisthokonta*

(a monophyletic clade including both the animal and fungus kingdoms, together with the eukaryotic microorganisms grouped in the paraphyletic phylum *Choanozoa*) [2-9], *Archaeplastida* (land plants, green and red algae) [10-15], *Urochordata* (ascidians) [16-18] and *Arthropoda* (insects and arachnids) [19-23]. Relative concentration of these alkaloids showed great variances between biological species [24].

N-methyl derivatives, including normelinonine F (**1b**) and melinonine F (**2b**) were found in the root bark of *Strychnos usambarensis* plant (from Rwanda) [12]. **1b** was also found in aqueous crude extract as well as in coelemic fluid of the solitary ascidian *Cnemidocarpa irene* (collected in Hokkaido, Japan) [18]. More than forty halogenated-βCs have been found in sea invertebrates, algae, cyanobacteria and other organisms [21-23] *e.g.*, Eudistomin N (**1j**) and Eudistomin O (7-bromo-9H-pyrido[3,4-b]indole, 7-bromo-norharmane or **1k**) [25-27], were detected in ascidia *Eudistoma olivaceum* (from the Caribbean Sea), whereas 7-bromo-2-methyl-9H-pyrido[3,4-b]indole (**1n**) and 7-bromo-1,2-dimethyl-9H-pyrido[3,4-b]indole (**2f**) were isolated from the solitary ascidian *Cnemidocarpa irene*, and woodinine (**11**) in ascidia *Eudistoma fragum* (from coastal zone of New Caledonia) [28, 29]. Hydroid *Aglaophenia pluma* produces **1l**, **1m**, **2e**, among others [30]. Chloro-nostocarboline (**1e**) was found in several phototrophic organisms including *Nostocales* cyanobacteria (spread in Europe, Southwest Asia, Australia and New Zealand) [21]. Bauerine alkaloids (**1g**, **1h** and **1i**) were isolated from a terrestrial blue-green alga called *Dichotrix baueriana* [1]. Partially hydrogenated and full aromatic βCs have been simultaneously found in a wide range of living species [31] *e.g.*, **5** and **3a** were isolated from *Peganum harmala* (native in Africa, the Mediterranean, Middle East and South Asia). The Amazonian plant *Banisteriopsis caapi* contains high levels of dihydro-βCs [32], whereas **5**, **6** and **8** and the related full aromatic βCs were found in the cuticle of two different fluorescent scorpion species *Centruroides vittatus* and *Pandinus imperator* [33]. The biosynthesis of βCs give rise to the accumulation of these alkaloids within different human body tissues and fluids such as human brain, cerebrospinal fluid, plasma, urine and pineal glands. βCs are also normal constituents of

some photosensitive tissues/organs including skin, retina and crystalline of the eye [2-7, 34-36]. Environmental conditions or dietary habits (alcohol intake or smoking) increases the basal levels of **1a**, **2a**, **13** and **14** [2, 7, 8, 34, 37].

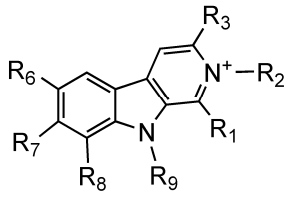

Short name	R_1	R_2	R_3	R_6	R_7	R_8	R_9
9H-pyrido[3,4-b]indole or norharmane (**1a**)	-H	-	-H	-H	-H	-H	-H
2-methyl-9H-pyrido[3,4-b]indole or normelinonine F (**1b**)	-H	$-CH_3$	-H	-H	-H	-H	-H
9-methyl-9H-pyrido[3,4-b]indole (**1c**)	-H	-	-H	-H	-H	-H	$-CH_3$
2,9-dimethyl-9H-pyrido[3,4-b]indole (**1d**)	-H	$-CH_3$	-H	-H	-H	-H	$-CH_3$
6-Chloro-2-methyl-9H-pyrido[3,4-b]indole or chloro-nostocarboline (**1e**)	-H	$-CH_3$	-H	-Cl	-H	-H	-H
6,8-dichloro-2-methyl-9H-pyrido[3,4-b]indole (**1f**)	-H	$-CH_3$	-H	-Cl	-H	-Cl	-H
7-chloro-9-methyl-2H-pyrido[3,4-b]índole or bauerine A (**1g**)	-H	-	-H	-H	-Cl	-H	$-CH_3$
7,8-dichloro-9-methyl-2H-pyrido[3,4-b]indole or bauerine B (**1h**)	-H	-	-H	-H	-Cl	-Cl	$-CH_3$
7,8-dichloro-1-hydroxy-9-methyl-2H-pyrido[3,4-b]indole or bauerine C (**1i**)	-OH	-	-H	-H	-Cl	-Cl	$-CH_3$
6-bromo-9H-pyrido[3,4-b]indole or eudistomine N (**1j**)	-H	-	-H	-Br	-H	-H	-H
7-bromo-9H-pyrido[3,4-b]indole or eudistomine O (**1k**)	-H	-	-H	-H	-Br	-H	-H
6-bromo-1-ethyl-9H-pyrido[3,4-b]indole (**1l**)	$-CH_2CH_3$	-	-H	-Br	-H	-H	-H
6,8-dibromo-1-ethyl-9H-pyrido[3,4-b]indole (**1m**)	$-CH_2CH_3$	-	-H	-Br	-H	-Br	-H
7-bromo-2-methyl-9H-pyrido[3,4-b]indole (**1n**)	-H	$-CH_3$	-H	-H	-Br	-H	-H
3-carboxylic-9H-pyrido[3,4-b]indole acid (**1o**)	-H	-	-COOH	-H	-H	-H	-H
3-carboxylic-9H-pyrido[3,4-b]indole acid N-methylamide or βCMAM (**1p**)	-H	-	$-CONHCH_3$	-H	-H	-H	-H
1-methyl-9H-pyrido[3,4-b]indole or harmane (**2a**)	$-CH_3$	-	-H	-H	-H	-H	-H
1,2-dimethyl-9H-pyrido[3,4-b]indole or melinonine F (**2b**)	$-CH_3$	$-CH_3$	-H	-H	-H	-H	-H
1,9-dimethyl-9H-pyrido[3,4-b]indole (**2c**)	$-CH_3$	-	-H	-H	-H	-H	$-CH_3$
1,2,9-trimethyl-9H-pyrido[3,4-b]indole (**2d**)	$-CH_3$	$-CH_3$	-H	-H	-H	-H	$-CH_3$
6-bromo-1-methyl-9H-pyrido[3,4-b]indole (**2e**)	$-CH_3$	-	-H	-Br	-H	-H	-H
7-bromo-1,2-dimethyl-9H-pyrido[3,4-b]indole (**2f**)	$-CH_3$	$-CH_3$	-H	-H	-Br	-H	-H
6-methoxy-1-methyl-9H-pyrido[3,4-b]indole (**2g**)	$-CH_3$	-	-H	$-OCH_3$	-H	-H	-H
7-methoxy-1-methyl-9H-pyrido[3,4-b]indole or harmine (**3a**)	$-CH_3$	-	-H	-H	$-OCH_3$	-H	-H
7-methoxy-1,2-dimethyl-9H-pyrido[3,4-b]indole (**3b**)	$-CH_3$	$-CH_3$	-H	-H	$-OCH_3$	-H	-H
7-methoxy-1,9-dimethyl-9H-pyrido[3,4-b]indole (**3c**)	$-CH_3$	-	-H	-H	$-OCH_3$	-H	$-CH_3$
7-methoxy-1,2,9-trimethyl-9H-pyrido[3,4-b]indole (**3d**)	$-CH_3$	$-CH_3$	-H	-H	$-OCH_3$	-H	$-CH_3$
6-Chloro-7-methoxy-1-methyl-9H-pyrido[3,4-b]indole (**3e**)	$-CH_3$	-	-H	-Cl	$-OCH_3$	-H	-H
8-Chloro-7-methoxy-1-methyl-9H-pyrido[3,4-b]indole (**3f**)	$-CH_3$	-	-H	-H	$-OCH_3$	-Cl	-H
6,8-diChloro-7-methoxy-1-methyl-9H-pyrido[3,4-b]indole (**3g**)	$-CH_3$	-	-H	-Cl	$-OCH_3$	-Cl	-H
7-hydroxy-1-methyl-9H-pyrido[3,4-b]indole or harmol (**4**)	$-CH_3$	-	-H	-H	-OH	-H	-H

Scheme 1a. Chemical structures of full-aromatic β-carboline species mentioned in the present work.

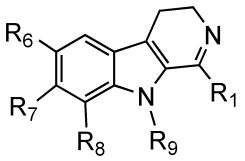

Short name	R_1	R_6	R_7	R_8	R_9
7-methoxy-1-methyl-3,4-dihydro-9H-pyrido[3,4-b]indole or harmaline (**5**)	$-CH_3$	-H	$-OCH_3$	-H	-H
7-hydroxy-1-methyl-3,4-dihydro-9H-pyrido[3,4-b]indole or harmalol (**6**)	$-CH_3$	-H	-OH	-H	-H
6-methoxy-1-methyl-3,4-dihydro-9H-pyrido[3,4-b]indole or harmalane (**7**)	$-CH_3$	$-OCH_3$	-H	-H	-H

Scheme 1b. Chemical structures of dihydro-β-carboline species mentioned in the present work.

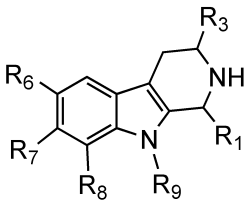

Short name	R_1	R_3	R_3	R_6	R_7	R_8	R_9
7-methoxy-1-methyl-1,2,3,4-tetrahydro-9H-pyrido[3,4-b]indole or tetrahydro-harmaline **(8)**	$-CH_3$	-H	-H	-H	$-OCH_3$	-H	-H
6-chloro-1-methyl-1,2,3,4-tetrahydro-9H-pyrido[3,4-b]indole (**9**)	$-CH_3$	-H	-H	-Cl	-H	-H	-H
6-bromo-1-methyl-1,2,3,4-tetrahydro-9H-pyrido[3,4-b]indole (**10**)	$-CH_3$	-H	-H	-Br	-H	-H	-H
(1*R*)-6-Bromo-2-methyl-1-[(2*S*)-1-methyl-2-pyrrolidinyl]-2,3,4,9-tetrahydro-1H-β-carboline or woodinine (**11**)	$-C_5H_{10}N$	$-CH_3$	-H	-Br	-H	-H	-H
1,2,3,4-tetrahydro-9H-pyrido[3,4-b]indole or tetrahydro-βC (**12**)	-H	-H	-H	-H	-H	-H	-H
1-methyl-1,2,3,4-tetrahydro-9H-pyrido[3,4-b]indole-3-carboxilic acid (**13**)	$-CH_3$	-H	-COOH	-H	-H	-H	-H
6-hydroxy-1,2,3,4-tetrahydro-9H-pyrido[3,4-b]indole (**14**)	-H	-H	-H	-HO	-H	-H	-H
6-hydroxy-1-methyl-1,2,3,4-tetrahydro-9H-pyrido[3,4-b]indole (**15**)	$-CH_3$	-H	-H	-HO	-H	-H	-H
(1-carboxyethyl)-1,2,3,4-tetrahydro-9H-pyrido[3,4-b]indole-1,3-dicarboxylic acid or kitasetalic acid (**16**)	-COOH $-CH_2CH_2COOH$	-H	-COOH	-H	-H	-H	-H

Scheme 1c. Chemical structures of tetrahydro-β-carboline species mentioned in the present work.

1.2. Biosynthesis

To date, information regarding βCs' biosynthesis is still incomplete and the chemical processes involved needs to be deeply understood. The formation of tetrahydro-βCs would involve a catalyzed Pictet-Spengler (PS) condensation from tryptophan and aldehydes. Genome sequencing and analysis of plants and microorganisms reveal that several genes would encode enzymes with Pictet-Spenglerase (PSase) function [38]. However, to date, only a few of them were expressed and characterized. The type and number of enzymes involved in this process differ from one organism to another. In plants, strictosidine synthase (STR) catalyzes the condensation reaction between tryptamine and secologanin to give rise the formation of the corresponding tetrahydro-βC [39-42]. On the contrary, different multi-functional enzyme families would be responsible for the biosynthesis of these alkaloids in several microbial agents [43, 44]. Recent findings were made in microbial enzymes involved in this process. In particular, dimers of Microbial Homodimeric enzyme (McbB) [45], isolated from marine actinomycete *Marinactinospora thermotolerans* (found in marine sediment of south China sea) catalyze the PS reaction between *L*-tryptophan and oxaloacetaldehyde [43]. The NscbB PSase, isolated from *Nocardiopsis synnemataformans* DSM 44143 (a bacterial strain derived from patient kidney transplant) showed βCs production using *L*-

tryptophan and methylglyoxal as substrate [38]. In a recent work, a unique enzymatic system for the βCs biosynthesis was identified in *Kitasatospora setae*. In this microorganism, KslB putatively uses *L*-tryptophan and α-ketoglutaric acid as substrates for the formation of the tetrahydro-βC kitasetalic acid and the subsequent production of full aromatic βC derivatives by KslA [46]. In *Chaetomium globosum* fungi, FPSase catalyzes the synthesis of several compounds with a βC skeleton, using flavipin (a fungal aldehyde) and *L*-tryptophan derivatives. *Saccharomyces cerevisiae* lab cultures showed formation of 1-methyl-1,2,3,4-tetrahydro-β-carboline-3-carboxylic acid (**13**). The authors also demonstrated that the expression of FPSase is up-regulated by 1-methyl-*L*-tryptophan [47].

Tetrahydro-βC skeleton (**Scheme 1c**) can be further modified giving rise to the formation of a vast set of derivatives, such as dihydro-, epoxy-, keto, isomeric hydroxy, and/or full aromatic βCs widely distributed in all living organisms. The formation of these compounds may be enzymatically catalyzed. For instance, in microbial agents, McbB complex would also contribute to the formation of decarboxylated and fully aromatized βC, respectively [43]. Other enzymatic (*i. e.*, cytochrome *P*-450cam) and/or non-enzymatic processes can also play an important role [48,49]. However, in most cases, such as **13** [50], oxidation and/or full-aromatization processes still remain unclear. Moreover, taking into account the presence of these alkaloids in aerial organs exposed to sun light (leaves, stems and others) possible photochemical pathways where suggested very recently (see below) [51].

1.3. Biological activity and/or pharmacological effect

A broad spectrum of biological and pharmacological activity has been reported for different βC alkaloids, in a structure-dependent manner [31, 52-66]. This include a strong interaction with biomacromolecules such as DNA and proteins inducing, among others, inhibitory effects on enzymatic activities, on tumor and microbial growth as well as phototherapeutic properties:

1.3.1 Interaction with macromolecules of biological relevance. Different biological effects, including cell-growth inhibition, in which βCs would play a role have been attributed to their intrinsic ability to interact with double-stranded DNA molecules. To date, several attempts have been made in order to elucidate the mode of interaction between these alkaloids and genetic material. Several studies reveal that the interaction between βC alkaloids and cell-free DNA is mainly ruled by hydrophobic and coulombic attractive forces, and the strength as well as the mode of interaction depend on the chemical structure of the βC derivative and the pH media [59-63, 67]. Due to their planar structure, the mode of interaction suggested for full aromatic βCs (including **1a-d**, **1p**, **2a-d**, **3a-f**) involves a partial intercalation of the βC-indolic ring into the stacked base-pairs, placing the βC-pyridinic ring towards the protic environment. This phenomenon is more evident in the cases of protonated species (present at pH < 7) and quaternary derivatives where coulombic attraction between the N-methylpyridinium cationic nitrogen and the negatively charge DNA backbone interaction would play a key role [68]. The higher the number of non-polar small substituents placed at the βC-ring enhances the intercalative capability of the alkaloids. This is quite evident in the cases of **3a**, **3c** and other (short) alkyl-substituted βCs showing the highest DNA-binging constants. The presence of deoxylated amino sugar in βCs–carbohydrate hybrid increases the intercalating capability of these alkaloids [69]. On the contrary, increasing the number and/or the size of the substituents on the main βC-ring causes more steric hindrance that yield a decrease in the extent of the interaction [70, 71]. In addition, a decrease in the planarity of the βC-ring due to partial hydrogenation of the pyridinic ring (*e.g.*, **5**) greatly decreases the intercalation possibility [72]. For this compound, the interaction with DNA grooves has also been demonstrated by linear and circular dichroism studies [73]. Other partially hydrogenated βCs, such as **6**, bind strongly with specific DNA sequences (GC polymer) [74].

Numerous enzymatic systems alter their functionality after interaction with βCs. In this regard, **2a** proved to be an inhibitor of endonuclease activity of phage T4-induced UV endonuclease. Also, while **2a**, **3a** and **5** were found to inhibit human Topoisomerase (Topo) I activity, amino acid

functionalized derivatives significantly inhibited Topo II-mediated DNA relaxation and Topo II-mediated cleavable complex formation. Compounds **2a**, **3a**, **3b** and **3d** showed to be reversible competitive inhibitors of Monoamine Oxidase A (MAO-A); however, **1a** inhibited preferentially MAO-B. In addition, some cyclin dependent kinases (CDKs) were inhibited by **3a** and Leishmania protein kinase C was inhibited by **5** [52]. Finally, variety of βCs' pharmacological effects are related to their capability of interact with receptor systems. Thus, *(i)* binding at benzodiazepine ones can be either anxiolytic, anxiogenic sedative, tremorgenic, proconvulsant or convulsant [75]; *(ii)* the interaction of **3a** and **5** with 5-hydroxytryptamine receptor produce hypothermia in rats [76] and *(iii)* **2a** binding at imidazoline receptors causes hypotension in rats [77].

1.3.2 Antitumoral activities. These alkaloids are able to suppress the growth of several lines of cancer cells *in vitro* and *in vivo*, hinting their potential use in cancer therapy [78]. Mechanisms of action involve the interaction with DNA and proteins. Structure-Activity studies reveal that βC skeleton is an important basis for the design and synthesis of new antitumor drugs. Moreover, the type and position of the substituents drastically modulate the antitumor efficiency, *e.g.*, N-2 and N-9 alkyl-substitution, and/or 6-bromo, 7-alkoxy, amino, amida or tiourea groups at C-3, as well as the presence of amino groups at C-1 or benzyl substituent at C-2 improve the antitumor activity of the βC-ring.

1.3.3 Antimicrobial activities. Microbial resistance is a global health emergency. Despite the many efforts that have been made to address this challenge, new drugs that might help to improve efficacy and pharmacokinetics of actual therapies are a real need. In the last decades, βCs have attracted great interest in the scientific community and their antimicrobial effect against multiple microorganisms have been tested:

i) Antiparasitic effects. Several compounds of this family (**1a**, **2a**, **3a**, **4**, **5**, **6**, **12** and **13**) were evaluated for *in vitro* activity against *Trypanosoma cruzi* epimastigotes. It was found that a fully unsaturated pyrido-indole ring system seems to be a necessary condition for optimal trypanosomicidal activity. A possible mechanism of action could be the respiratory chain

inhibition [79]. In addition, **3a** showed to be active against *Leishmania donovani* promastigotes both *in vitro* and *in vivo*. Apparently, the mechanism of action involves necrosis by a non-specific membrane damage [80]. Moreover, **2a** and **3a** displayed weak antileishmanial activity toward both the promastigote and the amastigote forms of *Leishmania infantum*, leading to an accumulation of parasites in the S–G2M phases of the cell-cycle because of the interaction with DNA molecule. However, **5** exerted a strong antileishmanial activity toward the intracellular amastigote form. This action could partly result from the capacity of the alkaloid to prevent parasite internalization within macrophages by inhibiting *Leishmania* protein kinase C activity [81].

In vitro assays showed that βC derivatives are promising antiplasmodial agents against the K1 strain of *Plasmodium falciparum* resistant to chloroquine and pyrimethamine. In particular, quaternary β-carbolinium cations such as **1b** showed the highest antiplasmodial activity with a very low cytotoxicity against L6 cells [82]. However, this compound was not active in the *Plasmodium berghei* mouse model. Also, compounds **3a**, **9** and **10** demonstrated to be effective against different *P. falciparum* strains in *in vitro* studies, with a mechanism that underlies the inhibition of the heat shock protein 90 (Hsp90) by the occupation of the ATP binding site. Besides, these compounds potentiated the effects of existing antimalarial agents in combined treatments in *in vivo* experiments [83, 84].

Alomar *et al.* showed that treatment of extracellular tachyzoites of *Toxoplasma gondii* with **1a**, **2a** and **3a** produced a decrease in the invasion and replication rates and caused either delayed or no monolayer lysis compared with the untreated parasites [55].

ii) Antiviral effects. Ishida *et al.* evaluated the capability of various βCs to inhibit Human Immunodeficiency Virus (HIV) replication in H9 lymphocytic cells. They found that substitution of the parent compound **2a** with a methoxy group at position 7, yielding **3a**, or an alkyl group at the indole nitrogen led to increased anti-HIV activity [85].

Compound **5** has demonstrated to exert a potent *in vitro* activity against Herpes Simplex Virus Type 1 (HSV-1), through the retarding of immediately early (IE) events by blocking the binding of IE complex on the Infected Cell Protein 0 (ICP0) promoter, leading to reduced expression of ICP4 and ICP27, which are necessary to regulate DNA synthesis and completion of the viral life cycle. Moreover, this alkaloid also reduced virus yields in cutaneous infected Balb/C mice [86]. On the other hand, **3a** showed to significantly reduce HSV-2 RNA transcription, protein synthesis, and virus titers in a dose dependent manner, by a mechanism that involves the suppression of MAPK or NF-κB host signaling pathways HSV-activated [87].

Some 1,3-disubstituted βC derivatives bearing a substituted carbohydrazide group at C-3 were evaluated for their antiviral activity against vaccinal poliovirus (VP) and HSV-1. A compound with a phenyl group at C-1 and a 4-methoxybenzylidene-carbohydrazide group at C-3, was the most active. By analyzing viral plaque pattern, authors concluded that this alkaloid inhibits virus dissemination to neighboring cells [88].

Very recently, the antiviral activity of **1c**, **2c** and **2g** against HSV type 1 and 2 was demonstrated by Gonzalez *et al*. [66]. These compounds did not affect virus attachment and were not virucidal. Apparently, they exert their action through multiple mechanisms, mainly mediated by down-regulating expression of early (E) and late (L) proteins at early phases after penetration, by arresting DNA replication and by altering ICP0 late location at the cytoplasm, where it participates in immune evasion**.**

Compounds **4** and **3c** were inhibitory of four different serotypes of Dengue Virus (DENV), being serotype DENV-2 the most susceptible one. Moreover, **3c** affected the spreading of the infection, by impairing the maturation and release of virus particles from infected cells to the extracellular medium [89].

*1.3.4 Effect against other microorganisms. Nor*melinonine F (**1b**) as well as two chloro derivatives **1e** and **1f** display potent cyanobactericidal and algicidal activity against photosynthetic aquatic organisms (*i.e.*, *Microcystis aeruginosa*, *Synechococcus* and *Kirchneriella contorta*) [90].

Also, some βCs have proved to be active against phytopathogenic fungi such as *Penicillium digitatum* and *Botrytis cinerea*, both causal agents of common postharvest diseases on fruit and vegetables. In this case, the full aromatic βCs **1a**, **2a**, **3a** and **4** exhibited inhibitory effect on conidia germination, whereas the partially reduced βCs **5** and **6** only produced germination delay. Among all compounds, **4** showed the highest inhibitory effect, with the inhibition of mycelial growth, preventing sporulation [53]. Moreover, antifungal activity of this alkaloid strongly depends on pH, being protonated form active against both phytopathogens, while the neutral, zwitterionic and/or anionic species lack inhibitory ability [54].

1.4. Neurotoxic and neuroprotective effects

N-2 unsubstituted βCs (*e. g.*, **1a**) cross the blood-brain barrier penetrating into the brain [91, 92], where they are enzymatically converted into the corresponding cationic N-2 methyl-derivatives (*e. g.*, **1b** and **1d**) [93]. Cationic species can, then, accumulate into the brain tissue. It has been demonstrated that βC alkaloids and their derivatives might exert different neurological effects in a structure-dependent manner. *E.g.*, quaternary N(2)-methyl derivatives were described as potential pathogenetic factors in Parkinson's disease [94-96]. The main mechanism through which these alkaloids would exert their effect seems to be the mitochondrial respiratory inhibition [97]. In the particular case of **1d**, a neurotoxic effect was observed due to the activation of the apoptotic cascade [98, 99]. On the contrary, **1c** could exert neuroprotective and neuron-differentiating effects[100]. In addition, normelinonine F (**1b**) and some bromo-derivatives such as **1n** and **2f** were found to be inhibitors of acetylcholinesterase (AchE), with activities similar to those of galantamine (an AChE inhibitor clinically used for the treatment of mild to moderate Alzheimer's disease (AD) and various other memory impairments, in particular those of vascular origin) [18]. Recently, some synthetic bivalent βCs showed to be good in butyrylcholinesterase (BuChE) inhibition, β-amyloid deposits disaggregation and neuroprotection, becoming promising candidates to treat AD [101].

1.5. Photo-triggered process and phenomena were βCs would play a role

On the contrary to the numerous reports concerning biochemical and/or pharmaceutical properties of βCs, only few studies describe the βCs role when subject to photoexcitation [57-61, 64, 65, 102]. Briefly, full aromatic βCs including, among others, **1a, 1c, 2a, 2c**, **3a** and **3c**, induce photosensitized damage to cell-free DNA [57, 59-61, 70, 71]. The process depends on the strength of the interaction and the spectroelectrochemical properties of the photosensitizer (βCs). The main mechanism involves a direct electron/proton transfer reaction (*Type I*) from the protonated photoexcited βCs and the DNA nucleobases giving rise to oxidative damage accounted for by the formation of oxidized purine nucleobases (8-oxo-7,8-dihydroguanine and formamidopyrimidines), sites of base loss (AP sites) and the concomitant DNA photocleavage (single-strand breaks, SSBs), in a dose-dependent manner. In general, reactive oxygen species, such as singlet oxygen, superoxide anion and hydrogen peroxide, do not have a key role in the overall oxidative DNA damage photosensitized by βCs.

Some particular βCs, such as **3a** and its derivatives, show a broader damage profile that not only include oxidized purines and AP-sites, but also oxidized pyrimidines as well as cyclobutane pyrimidine dimers (CPDs). The formation of the latter photoproduct mainly occurs through triplet–triplet energy transfer (TTET) from the triplet electronic excited state of the photosensitizer to the triplet electronic state of the pyrimidine (mostly, thymine). This process is thermodynamically favored for those photosensitizers having energy triplet values (E_T) larger than 267 kJ mol^{-1}.

Specific damage induced by photoexcited βC derivatives has been reported. In some cases, such as βCs–carbohydrate hybrids that selectively induces cleave at the guanine sites, this behavior is a direct consequence of the interaction mode (see above) [69]. On the contrary, the specific behavior shown by other derivatives are closely related to their intrinsic photophysical properties. This is the case of **3e** that shows quite a unique behavior, leading to the formation of single-strand breaks (SSBs) and AP-sites via a concerted and stereospecific hydrolytic attack as a consequence of a strong change in the local H^+ and OH^- concentrations in the surroundings of the DNA helix [62].

Photoexcited βCs also induce damage on several cell lines and unicellular organisms including mammalian cells [58,66,101,102], bacteria [103], fungi [54], viruses, among others [104, 105]. In particular, it was demonstrated that βC and its derivatives can be fast up-taken by different cell lines [56, 64, 106, 107], accumulating into the lysosomes. Upon UV-visible photoexcitation, necrotic cell death is photoinduced [71, 106, 107]. Although other intracellular components could be targeted by photoexcited βCs, it has been demonstrated that **1a**, **2a**, **3a**, **3c** as well as other βC derivatives induce damage on intracellular DNA [64, 71, 108-110]. In this regards, damage on V79 cells' DNA induced by **3a** and **3c** was reported giving rise to the formation of oxidative modified purines.

In plants, it has been suggested an active role of some βCs in the (photo-triggered) defense response mechanism against insects, webworms, etc. [14]. Despite these facts, the main photobiological role of these alkaloids and the mechanisms involved in those processes are, up to now still poorly understood.

2. Photophysics of βCs in aqueous solution

βCs' spectroscopic, chemical and photochemical properties strongly depend on their molecular structure as well as on the nature of the environment (solvent, pH, oxygen partial pressure, etc.)[59,60,111-122]. In the following section, the most relevant photophysical properties of a selected group of βCs are summarized (**Scheme 2**). Selected spectroscopic and photophysical parameters are listed in **Table 1**. The influence of several experimental parameters such as pH and oxygen partial pressure is also discussed.

2.1. Acid-base equilibria in aqueous solution

In aqueous media, pH and the chemical nature of the substituents as well as their relative position on the βC scaffold delimit the net charge of βCs. Over the entire pH-range, most of the *N*-

unsubstituted full-aromatic βCs show two distinctive acid-base equilibria involving the protonation/deprotonation of the pyridinic (N-2) and indolic (N-9) nitrogen, respectively (**Scheme 3a**). Dihydro-βCs show the same ionizable groups, N-2 and N-9 (**Scheme 4**). However, it is noticeable that N-2 acquires characteristics of aliphatic amines (see below). Naturally, the latter equilibria are not observed for those βCs showing non-protic substituents attached to either N-2 and/or N-9. In particular, cationic di-*N*-substituted-βCs do not show any acid-base equilibrium; whereas mono-*N*-substituted-βCs (either N-2 or N-9) only show one reversible protonation/deprotonation equilibrium involving N-9 and N-2, respectively (**Schemes 3b** and **3c**). It is noteworthy that zwitterionic species produced upon N-9 deprotonation of quaternary methyl-βCs (βCZ) might be involved in a tautomeric equilibrium with the corresponding anhydrous base or quinonic species (βCQ) (**Scheme 3c**) [119]. However, in water and other polar solvents, the latter equilibrium is displaced towards the βCZ species [124]. When the βC-ring bear additional ionizable substituents other equilibria can be observed. *E. g.*, due to the presence of a hydroxyl group at C-7, **4** and **6** show (in the entire pH range 2 – 14) up to five different species: cationic, neutral, zwitterionic, mono- and di-anionic species (**Scheme 5**).

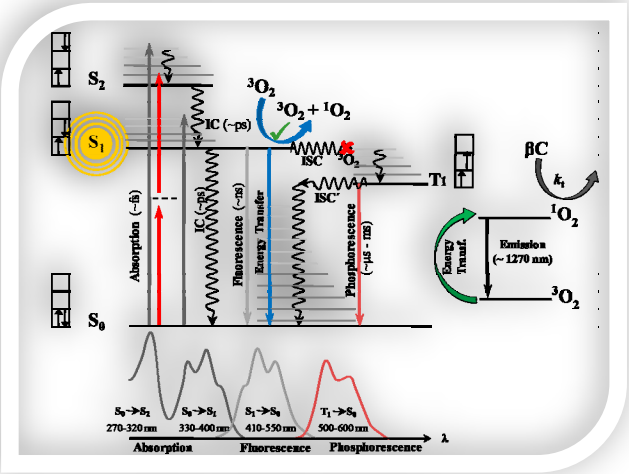

Scheme 2. A modified Jablonsky's diagram illustrating the most relevant photophysical processes of βCs. IC and ISC denote internal conversion and intersystem crossing, respectively [123]. For some βCs, $S_1 \rightarrow S_0$ internal conversion can effectively compete with $S_1 \rightarrow T_1$ intersystem crossing in the overall O_2-induced deactivation of the first electronic excited state (S_1).

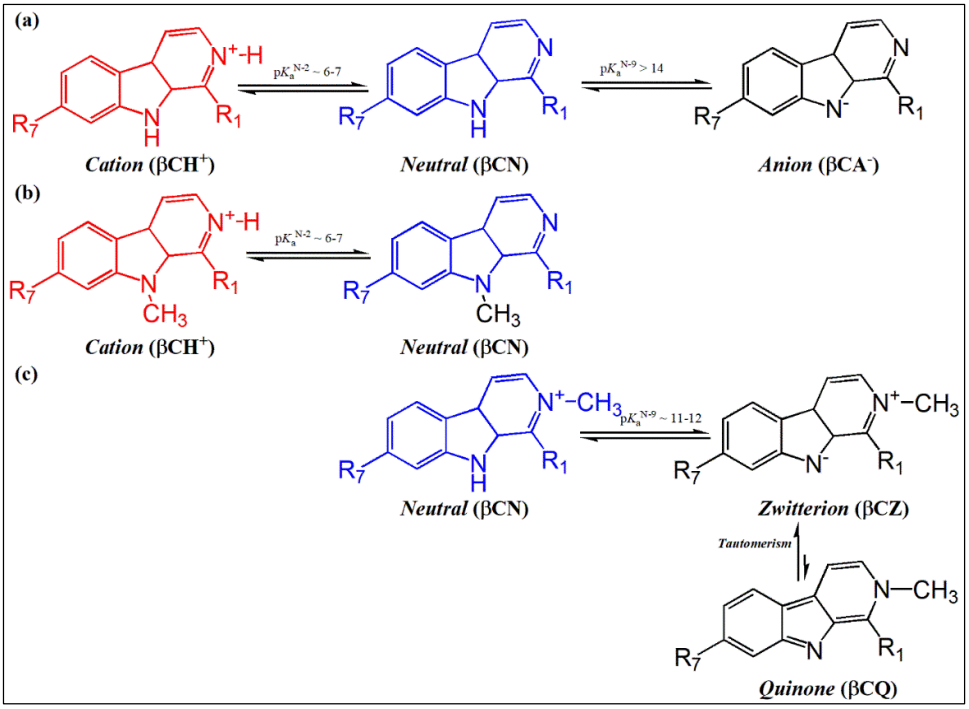

Scheme 3. Acid-base equilibria observed for full-aromatic **(a)** *N*-unsubstituted βCs, **(b)** 9-methyl-βCs and **(c)** 2-methyl-βCs in aqueous solutions.

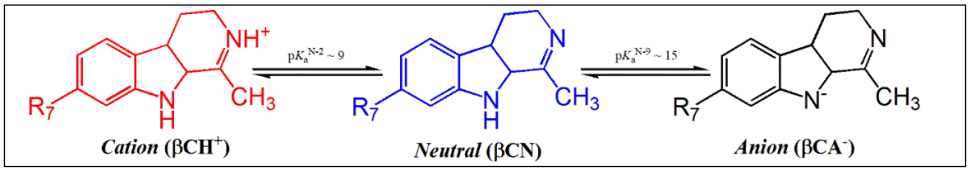

Scheme 4. Acid-base equilibria observed for dihydro-derivatives, such as **5** and **7**, in aqueous solution.

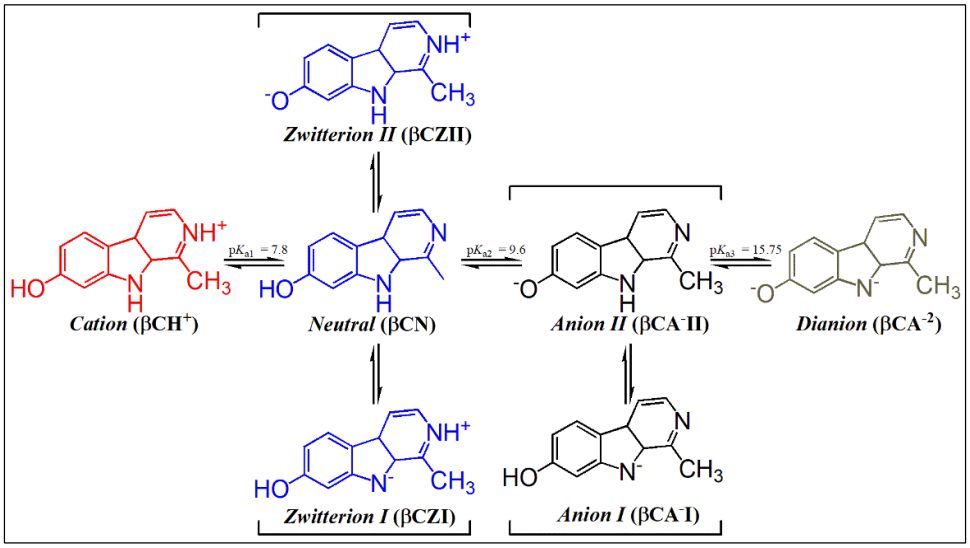

Scheme 5. Acid-base equilibria observed for **4** in aqueous solutions. From Ref. (159).

A quantitative analysis of these acid-base equilibria shows that the dissociation equilibrium constant (K_a) values depend on the relative position of the substituents as well as on the aromatization of the main βC ring. Briefly, data listed in **Table 1** suggest that: ***(i)*** *N*-unsubstituted full-aromatic βCs show $pK_a^{(N\text{-}2)}$ and $pK_a^{(N\text{-}9)}$ values of ~ 7 [113, 120, 121, 125-129] and > 14 [120, 121, 125-129], respectively. ***(ii)*** In partially hydrogenated βCs such as **5**, **6** and **7** (**Scheme 4**), the basicity of N-2 nitrogen atom is increased ($pK_a^{(N\text{-}2)} \sim 9$) [51,115,126,127], with respect to the corresponding full-aromatic species (**Table 1**), as a consequence of the acquired aliphatic characteristic [120, 130, 131]. ***(iii)*** 2-methyl-β-carbolinium iodide salts (**1b**, **2b** and **3b**) show $pK_a^{(N\text{-}9)}$ values ~ 11 [119-121]. Therefore, the presence of the methyl group at N-2 enhances the acidity of the proton placed at indolic nitrogen (N-9) with respect to the corresponding *N*-unsubstituted βCs ($\Delta pK_a^{(N\text{-}9)} \sim 3$ pH units). ***(iv)*** The larger the number of electron donor substituents placed at the βC scaffold (-H, $-CH_3$ and $-OCH_3$, in **1a**, **2a** and **3a** moieties, respectively), the lower the acidity of the -NH indolic group. On the contrary, the larger the number of electron withdrawing groups (such as chlorine atoms), increases the acidity of both ionizable N-2 and N-9 groups [112, 113, 116, 122, 132]. The latter effect is accounted for by the fact that chlorine-atom would decrease the proton affinity (PA) [132].

According to the above description, both protonated and neutral species of full-aromatic βCs are present in the solution under physiologically relevant pH-conditions. In this regard, quaternary (**1b**, **1d**, **2b**, **2d**, **3b** and **3d**) and partially hydrogenated βCs (**5**, **6** and **7**) would represent exceptions in which cationic species are the only physiologically relevant species in the electronic ground state.

2.2. Electrochemistry of βCs

Voltammetric profiles of various tetrahydro-βC derivatives on platinum electrode were explored, for the first time, by Allen *et al.* more than 60 years ago [133]. Under acidic conditions (0.1 N HCl

in 50% aq. MeOH), βCs bearing a methoxy group at position C-6 showed specific anodic oxidation ($0.71 < E_{1/2} < 0.85$ V *vs*. SCE, where $E_{1/2}$ is the half-wave potential) involving a one electron transfer followed by a probable hydroxylation of the βC-indolic ring. On the contrary, under neutral pH conditions (0.2 M LiCl in MeOH), almost all the βC derivatives investigated showed an anodic peak ($0.45 < E_{1/2} < 0.87$ V *vs*. SCE) and after a two electrons transfer process the formation of N-oxide intermediates was suggested in the cases of N-9 unsubstituted derivatives.

The presence of different substituents contributes to additional electrochemically assisted oxidative pathways. *E. g.*, the voltammetric profile of 6-hydroxy-1,2,3,4-tetrahydro-βC (**14**), recorded in aqueous solution at physiological pH (7.4) on a pyrolytic graphite electrode, showed a two consecutive oxidation peaks (E_p = 0.26 and 0.34 V *vs*. SCE, measured at scan rate of 5 mV s^{-1}) ascribed to the formation of a radical intermediate and C-5 centered carbocation, respectively[134]. Upon reorganization, *i. e.* upon a radical-radical or ion-substrate reactions, both intermediates dimerize to produce 5,5'-bi-(6-hydroxy-1,2,3,4-tetrahydro-βC). In addition, the carbocation intermediate can also react with water to produce 5,6-dihydroxy-1,2,3,4-tetrahydro-βC that is rapidly oxidized to 1,2,3,4-tetrahydro-βC-5,6-dione (**Scheme 6a**). In basic medium, reactions take place at lower potentials due to Nernstian behavior (E_p^I = 0.766 - 0.068 pH and E_p^{II} = 0.89 – 0.074 pH, both in V *vs*. SCE with scan rate of 5 mV s^{-1} and pH between 3.0 to 9.2 for 0.20 mM of **13**). On the other hand, a set of 1,2,3,4-tetrahydro-βCs-1- and -3-carboxylic acids showed a distinctive behavior [135]. On platinum electrodes, the investigated compounds follow electrochemical oxidation in a structure-dependent manner. Briefly, tetrahydro-derivatives are oxidized giving rise to the formation of the corresponding 3,4-dihydro- and full aromatic-βCs. The overall process involves a net loss of two electrons and two protons and the concomitant decarboxylation (**Scheme 6b**). Also in basic medium reactions take place at lower potentials. The oxidation appears to take place through the N-9 indolic nitrogen.

Upon anodic condition, dihydro-βCs **5** and **6** follow a two consecutive one-electron / one-proton transfer steps with peak potentials values E_p^I (**5**:**6**) ~0.81:0.46 and E_p^{II} (**5**:**6**) ~1.00:0.70 V *vs*. Ag-

AgCl (**Table 2**) leading to the formation of the corresponding full-aromatic derivatives[136,137]. Further two-electron oxidation of full aromatic βCs, including **1a**, **2a** and **3a**, occurs at higher oxidation potential (**Table 2**) in a structure-dependent manner. The shape and the position of the peaks observed in cyclic voltammograms strongly depend on the nature of the electrode. Briefly, at carbon nanotubes-modified glassy carbon (CNTGC) voltammetric responses were enhanced with respect to bare glassy carbon (GC). Oxidation peaks at 0.97 V (**2a**), 1.06 V (**3a**), 0.81 and 1.00 V (**5**) and 0.46 and 0.70 V (**6**) *vs*. Ag/AgCl (pH 7 and scan rate of 50 mV s^{-1}), were obtained at the CNTGC. The corresponding peak currents were much larger, between 6 and 10 fold higher, than those obtained at a bare GC (**Table 2**) [136]. Since overpotentials showed no changes with respect to the unmodified electrode, the enhanced voltammetric responses was attributed to the surface area. Under these conditions, authors reported good stability of the modified electrode without evidence of passivation. On the contrary, when gold electrodes were used a consecutive electron / proton transfer steps, with peak potentials values at 0.60 and 1.27 V (**2a**), 0.50, 0.94, 1.05 and 1.22 V (**3a**), and 0.31, 0.58, 0.96 and 1.20 V (**5**) *vs*. Ag/AgCl, were observed (**Table 2**)[137]. The pH as well as the type and position of the substituents bared by the βC-ring also affect the relative oxidation potential values observed as well as the final fate of the oxidative process. Briefly, a more complex pattern of reaction has been envisaged for full aromatic βCs (**Scheme 6c**). N-2 unsubstituted βCs follow a two consecutive one-electron/one-proton transfer steps, whereas the cationic βC derivatives show these oxidative steps at very high oxidation peak potentials (at 0.93 and 1.15 V (**2b**); 0.92 and 1.24 V (**2d**); 0.95 and 1.18 V (**3b**), and 0.91 and 1.20 V (**3d**) *vs*. Ag/AgCl) with a concomitant thermal reorganization giving rise to the formation of the corresponding full aromatic N-2 unsubstituted βCs. The indolic nitrogen N-9 plays a key role in the thermal reorganization of the radical intermediate produced from N-2 unsubstituted βCs subject to high anodic potentials.

It is noteworthy that, although pioneers in the study of the electrochemistry of this family of alkaloids, a direct comparison between the oxidation potentials reported in all the studies

mentioned above is clearly compromised because these values come from potentiodynamic measurements. Moreover, experimental conditions such as βCs´ concentration, pH and electrode surface are different among all the studies as well as the adsorbed states were not characterized. Therefore, it does not represent the true thermodynamic information because it also depends on the specific conditions (scan rate, kinetic constant, diffusion coefficients and electrode nature) of the experiment. For quantitative comparisons of the potential values, it is recommended to consider the same research work. In addition, it is worth mentioning that in all the cases only the oxidation processes were documented. To date, reduction processes still remain unexplored. Correlating the structure-reactivity relationship with the reversible and / or formal potentials and *in situ* spectroelectrochemical measurements is an open research challenge, which can help the fundamental understanding of the observed trends. Thus, the study of the redox behavior of βCs remains a fertile research field that needs to be further explored.

2.3. Thermal stability of βCs under highly alkaline pH-conditions

Chemical stability of non-irradiated βCs is sensitive to the βC chemical structure as well as to the pH experimental condition. Under dark conditions, acidic ($3 < pH < 5$) βC air-equilibrated aqueous solutions showed a great stability (up to, at least, 60 days), independently of the chemical structure of the alkaloid investigated (*i. e.*, full-aromatic unsubstituted, N-methyl or chloro-derivative, as well as for dihydro-derivatives) [62, 112, 113, 116, 122]. In air-equilibrated neutral or highly alkaline aqueous solutions, both the chemical structure of the βC and solvent play a determining role in the overall stability. The latter fact is more evident in the case of chloroharmine derivatives (**3e**, **3f** and **3g**). In particular, **3f** and **3g** are less stable than **3e** when subject to slightly alkaline aqueous solution [116]. The latter fact was ascribed to the presence of the chlorine atom at the position C-8 in the βC scaffold. The short distance between the chlorine atom and the indolic-NH group in both 8-chloro-substituted βCs would account for the formation of an intramolecular hydrogen-bridge-

like interaction yielding a higher rate of reaction (probably a nucleophilic substitution of the chlorine atom by a hydroxyl group and/or a βC dimerization-like reaction) [116].

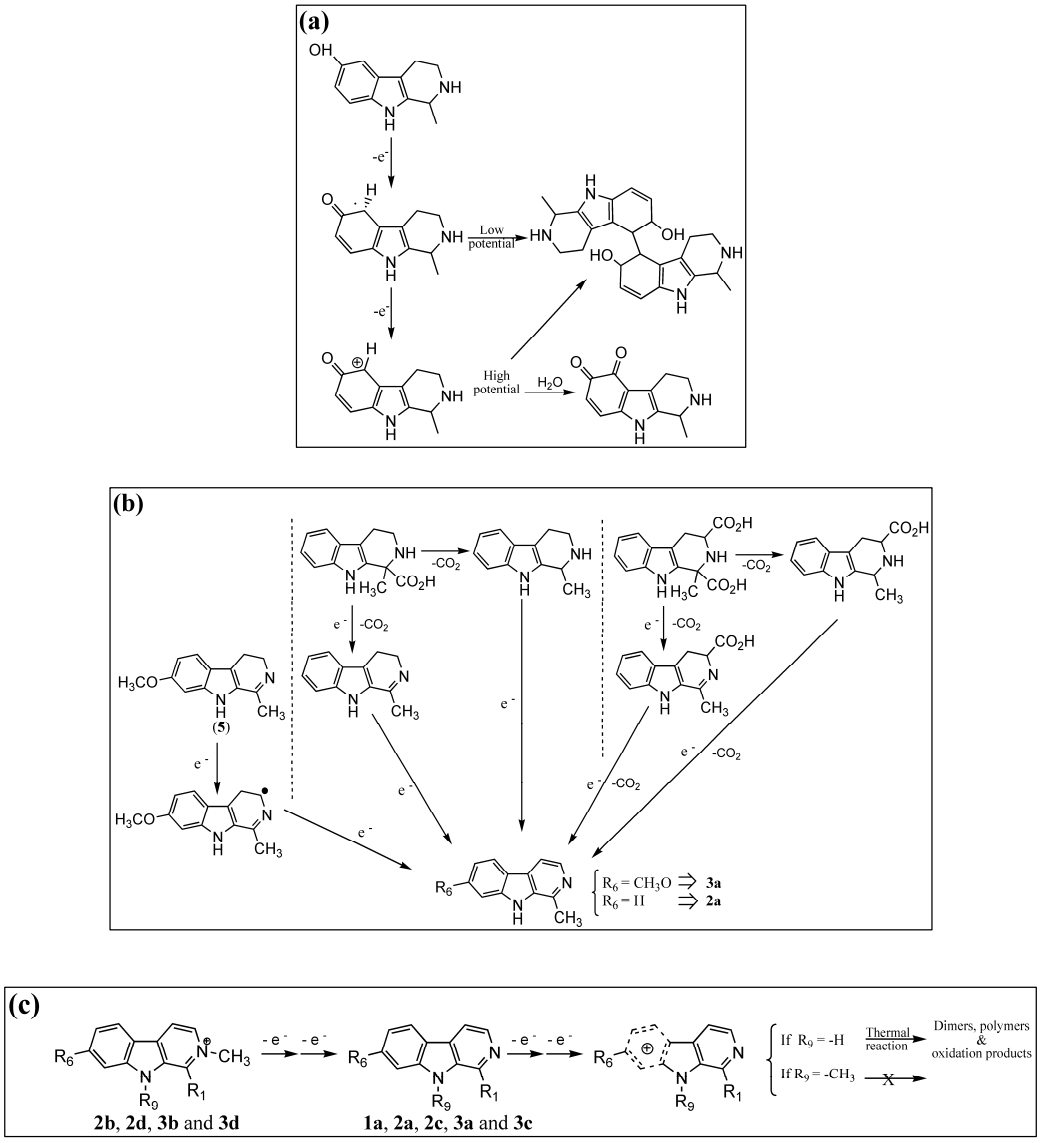

Scheme 6. Mechanism proposed for the electrochemical oxidation of representative examples of βC derivatives.

However, the stability of the neutral species of chloroharmines increases when subject either to organic (ethanol or acetonitrile) [115, 117] or buffer air-equilibrated aqueous solutions (pH 7.4) [62]. Under highly alkaline pH conditions, the three compounds are unstable. On the contrary, *N*-methyl derivatives (**1b-d**, **2b-d** and **3b-d**) show a quite high stability in the entire pH-range $2 < pH < 11$[122].

2.4. UV-visible absorption spectroscopy

Full-aromatic βCs show quite typical UV-visible absorption spectra characterized by three broad absorption bands placed at 200- 260 nm, 260 – 320 nm and 320 – 400 nm, corresponding the electronic transitions $S_0 \rightarrow S_3$, $S_0 \rightarrow S_2$ and $S_0 \rightarrow S_1$, respectively. **Figure 1a** shows, as representative example, spectra of each acid-base species of **3a**, whereas **Figure 2** shows those of **3a-g**. The relative position and intensity of the latter bands vary within each prototropic and/or ionic species. Typically, the protonated species of N-2 unsubstituted-βCs as well as quaternary (both called cationic species, **C**) show a similar spectral-pattern (see red lines in **Figures 1a and 2**). This observation is ascribed to the fact that the nonbonding (*n*) electron pair of the pyridine nitrogen (N-2) is taking part of the *σ*-bond formed either with the methyl group or with the proton[138]. Thus, the enhancement of the overlapping between molecular orbitals leads to an extended π–system [139], evidenced by the bathochromic shift in their absorption spectra with respect to **N** (**Figure 1**, red and blue lines, respectively). In the case of the anionic species (**A**), present when N-9 unsubstituted alkaloids are subject to highly alkaline conditions, a bathochromic shift is observed with respect to both **N** and **C**. The latter effect is ascribed to a higher electron density and extension of the π-system due to the negative charge at N-9. Pure spectra of **A** for **3a** obtained by hybrid (hard-soft) modeling analysis is depicted in **Figure 1a**.

Dihydro-derivatives also show three broad absorption bands together with the same pH-dependence (*i. e.*, protonated species show a bathochromic shift with respect to the corresponding neutral one). However, it is noteworthy that protonated species of dihydro-βCs show a quite intense electronic transition ($\varepsilon \sim 20.000\ M^{-1}\ cm^{-1}$) in the visible region and the lowest-energy absorption band is shifted towards higher wavelength than the corresponding full-aromatic derivative. The latter fact is of a great relevance from the photobiological point of view.

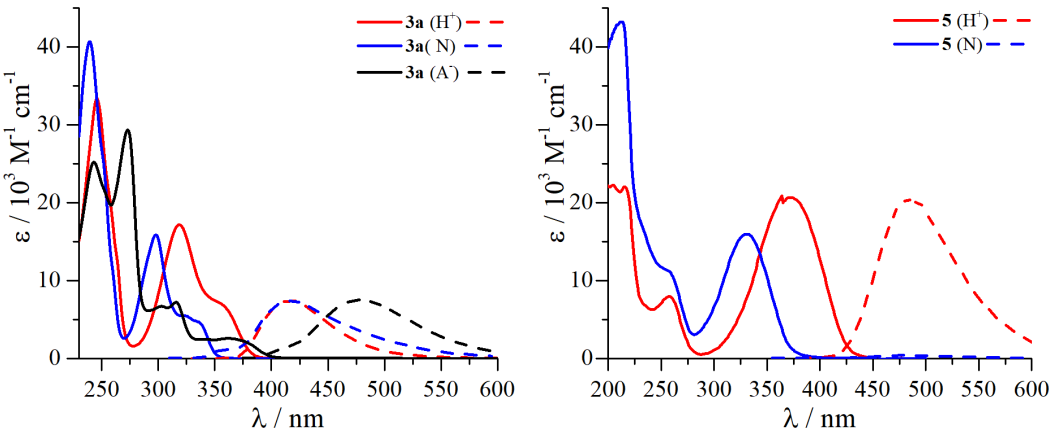

Figure 1. UV-visible absorption (solid lines) and normalized fluorescence emission (dashed lines) spectra of: **(a) 3a** and **(b) 5**. Spectra were recorded in aqueous solutions under three different pH conditions: 4.4 - 5.0 (**red lines**), 9.0 - 9.5 (**blue lines**) and 13.0 - 14.5 (**black lines**). Optimized molar absorptivity of deconvoluted spectra of the anionic species of **3a** was obtained applying the hybrid (hard-soft) modelling methodology described elsewhere [122].

The presence of different substituents induces changes on the electronic distribution of the βC-scaffold, having an impact on the relative position and intensity of the absorption bands. The overall effect strongly depends on the chemical nature of the substituent as well as on the total number of substituents and relative position. For example, the presence of electronic donor substituents such as methyl groups was investigated for full-aromatic βCs and a clear bathochromic shift was observed in all the absorption bands (**Figure 2a**). The latter effect is more evident when the substitution takes place at N-9 position that induces a red-shift of ~ 15 - 20 nm with respect to the N-unsubstituted βC. This effect seems to be additive: the larger the number of N-methyl groups attached to the βC scaffold, the larger the bathochromic shift. Thus, *N*-methyl-derivatives reach relatively higher absorbances in the visible region of the electromagnetic spectra. Taking into account that enzymatically induced methylations occurs *in vivo* rather frequently, then special attention on this particular βC derivatives as endogenous photoactive chromophores should be paid.

On the other hand, the presence of chlorine atoms in the full-aromatic βC, **3a**, give rise to a

different behavior. Briefly, chloroharmines show the typical bathochromic shift and hyperchromicity in all the absorption bands when comparing **C** species with respect to the corresponding **N** (**Table 1)**. However, **C** show a clear bathochromic shift of the lowest absorption band ($S_0 \rightarrow S_1$) and an hypsochromic shift of the $S_0 \rightarrow S_2$ transition band (with the exception of **3f**) when comparing with **3a** (**Figure 2b**). On the contrary, the chlorine atom on the neutral species (**N**) induces a clear effect only on the lowest energy absorption band: the $S_0 \rightarrow S_1$ transition either of **3e**, **3f** and **3g** are red-shifted with respect to **3a**; whereas the maximum of absorption of the other electronic transitions show no significant differences [140]. In addition, in aqueous solution, the presence of a chlorine atom at position C-6 of the protonated βC scaffold prompts a better resolution of the absorption bands (*i.e.*, transitions $S_0 \rightarrow S_1$ and $S_0 \rightarrow S_2$, in **3e** and **3g**). Spectral profile recorded in organic solvents shows some similarities and other quite remarkable differences with respect to the spectra recorded in aqueous solution, that are well discussed therein [115-117, 132]. TD-DFT analysis of the two lowest energy bands of both protonated and neutral chloroharmines shows that the main molecular orbitals (MOs) involved in the $S_0 \rightarrow S_1$ and $S_0 \rightarrow S_2$ electronic transitions are the highest occupied MO (HOMO, H), the lowest unoccupied MO (LUMO, L) and the second highest occupied MO (H–1). The second lowest unoccupied MO (L+1) makes only minor contributions to those electronic transitions [115, 116]. For all the compounds, with the exception of **3f**, the first excited state, which corresponds to a $S_0 \rightarrow S_1$ electronic transition, is predominantly a H→L transition [141]. The second excited state, $S_0 \rightarrow S_2$, corresponds to a H–1→L transition. **3f** would represent an exception, since the $S_0 \rightarrow S_1$ electronic transition corresponds to a H–1→L transition and $S_0 \rightarrow S_2$ electronic transition is of H→L nature.

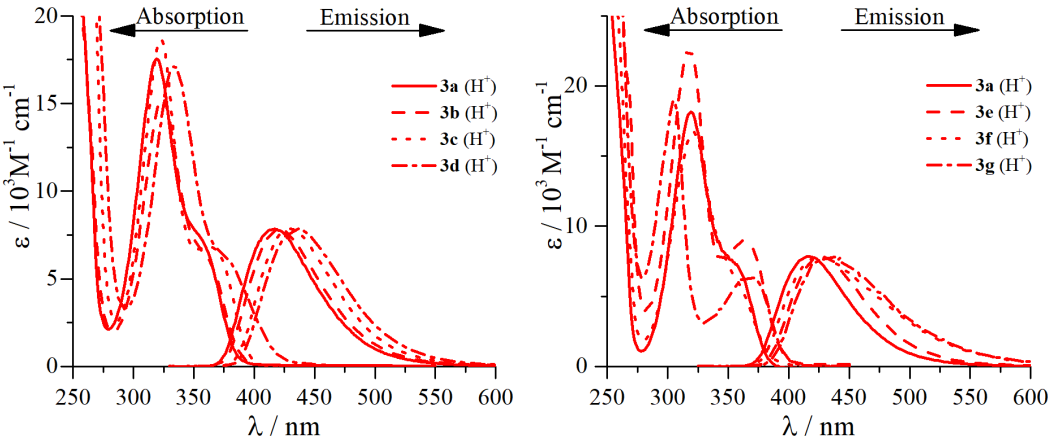

Figure 2. UV-visible absorption and emission normalized spectra of acidic (pH 4.8) aqueous solution of **(a)** Compounds **3a**, **3b**, **3c** and **3d** and **(b)** Compounds **3a**, **3e**, **3f** and **3g**.

2.5. Fluorescence emission of βCs: effect of pH- and oxygen partial pressure.

Steady-state and time-resolved fluorescence spectroscopy of βCs have been very well documented and discussed in the literature [61, 112-122, 124-128]. As representative examples, we present and comment herein on the fluorescence properties of a set of βCs recorded in aqueous media under the pH-range 3.0 - 14.0. For comparative purposes, normalized emission and excitation spectra are depicted in **Figures 1** and **2** and the most relevant parameters (maximum emission wavelength (λ_{em}^{max}), number and type of emitting species, fluorescence quantum yields (Φ_F) and fluorescence lifetime (τ_F)) are listed in **Table 1**.

Briefly, βCs are quite efficient fluorophores ($0.20 < \Phi_F < 0.99$), showing a broad emission band placed at the visible region of the electromagnetic spectra (400 nm – 650 nm). Typically, in aqueous solution, up to four emitting species can be identified from photoexcited *N*-unsubstituted-βCs, with τ_F values in the nanosecond domain: ***(i)*** photoexcited protonated (^{1}[**C**]*, λ_{em}^{max} ~ 420 - 450 nm, $\Phi_F > 0.7$, τ_F ~ 20 ns, with exception of **3a**), ***(ii)*** neutral (^{1}[**N**]*, λ_{em}^{max} ~ 360-380 nm, Φ_F ~ 0.2, $\tau_F < 0.5$ ns), ***(iii)*** anionic (^{1}[**A**]*, λ_{em}^{max} ~ 480 – 490 nm, τ_F ~ 10 ns) and ***(iv)*** zwitterionic (^{1}[**Z**]*, λ_{em}^{max} ~ 520 – 540 nm, τ_F ~ 5 ns, with the exception of **1b**) species (**Scheme 7a**). Certainly, each emitting species shows distinctive Φ_F and τ_F values. Briefly, photophysic of **N** is very

sensitive to the environment (solvent) and it shows the shortest values (Φ_F < 0.2 and τ_F < 0.5 - 2 ns). This fact is a consequence of the presence of other competing deactivation pathways (*i. e.*, proton-transfer reactions in the electronic excited states, see below). On the contrary, **C**, **Z** and **A** can show quite unusual higher Φ_F and τ_F values. The pH strongly modulates the relative contribution of each acid-base species to the overall emission spectra.

The presence of different substituents as well as changes in the experimental conditions (solvent, pH and oxygen partial pressure) have a distinctive impact on the type and number of emitting species as well as λ_{em}^{max}, Φ_F and τ_F [62, 113, 116, 122]. For example, methylation at N-2 and/or N-9 induces an increase in both Φ_F and τ_F values, in addition to a bathochromic shift (up to 20 nm) in the emission spectra. The shift correlates with the one observed in the absorption spectra. This effect is more evident for (N-9)-methyl-βCs that show an enhancement of the radiative deactivation pathways of ~5 – 10%, whereas such effect is negligible or null when the substitution takes place at N-2.

As it was mentioned above, methyl groups block either one or both pyridinic (N-2) and/or indolic (N-9) acid-base equilibria, giving rise to the disappearance of some emitting species. In particular, ^{1}[**N**]* and ^{1}[**A**]* cannot be observed in the cases of (N-2)-methyl-βCs (**Scheme 7b**). In the cases of (N-9)-methyl-βCs, neither ^{1}[**Z**]* nor ^{1}[**A**]* species will be formed (**Scheme 7c**); whereas for dimethyl-βCs, ^{1}[**C**]* is the only dominant species present in the solution (**Scheme 7d**).

The presence of the substituents at the carbon atoms of the βC scaffold do not affect the number and type of acid-base equilibria observed. However, they have an influence on the relative position of the emission band as well as on the acid-base equilibria of both the electronic ground (S_0, see above) and excited states (S_1). This is better represented by methoxy- (**3a**) and chloro-substituted βCs (**3e**, **3f** and **3g**) listed in **Table 1**. In the particular case of chloroharmines, **C** and **N** species show a noticeable bathochromic shift (~ 15 nm) of the maximum of emission relative to **3a**, that is consistent with the bathochromic shift observed on the UV-vis absorption spectra (see above). Moreover, the presence of the chlorine atoms induces a decrease in the overall Φ_F with respect to

3a. For this particular set of chloro-derivatives, internal conversion ($S_1 \rightarrow S_0$) seems to be the operative deactivation pathway [142].

Two additional and quite distinctive behavior of *N*-unsubstituted-βCs in the aqueous solutions that deserve to be highlighted: ***(i)*** On the one hand, it is a fact that even under neutral and highly alkaline conditions ($7.0 < pH < 12$), the presence of both ^{1}[**C**]* and ^{1}[**Z**]* can be detected. This fact is a consequence of the already demonstrated enhancement (up to 4 - 7 pH units) on the relative acidity and basicity of N-9 and N-2 groups that takes place upon photoexcitation [113]. Thus, when the electronic excited state (S_1) becomes populated, a fraction of ^{1}[**N**]* is protonated and/or deprotonated, during the lifetime of its S_1, giving rise to the formation of ^{1}[**C**]* and ^{1}[**Z**]*, which then emits. The extent of this proton transfer reaction is more evident in the cases of **1c** and **2c** (~ 90%) [113] and **3e**-**3f** (~ 50%) [116]. ***(ii)*** On the other hand, oxygen partial pressure quenches the excited states of some βCs, in particular with those showing the longest fluorescence lifetimes (**1a**, **1c**, **2a** and **2c**). However, on the contrary to the general rule that quenching of an organic molecule's fluorescent state by oxygen proceeds via induced intersystem crossing and population of the lowest excited triplet state (T_1) (*i. e.*, as in the case of the chlorine effect, a heavy atom effect), oxygen might also induce internal energy conversion ($S_1 \rightarrow S_0$) as deactivation pathway (see below) [113, 114].

2.6. Singlet oxygen production upon photo-excitation

It has been documented that βCs are able to photosensitize singlet oxygen ($^1O_2$) formation, even upon two-photon excitation [113]. Quantum yields of singlet oxygen production (Φ_Δ) have been determined for a large number of derivatives (**Table 1**). In general, in aqueous solutions, βCs show quite low Φ_Δ values ($0.08 < \Phi_\Delta < 0.22$). The chemical structure of each alkaloid has a direct impact on the overall efficiency observed [56, 61, 112-114, 116]. Both full-aromatic (**3a**) as well as dihydro-βC derivatives (**5**) having a methoxy group as substituent at the position C-7 show the highest Φ_Δ values ($\Phi_\Delta \sim 0.2$). Quaternary βCs show intermediate Φ_Δ values ($0.10 < \Phi_\Delta < 0.16$) and (N-2)-

unsubstituted-βCs show the lowest values ($0.08 < \Phi_\Delta < 0.10$). The pH also modulates Φ_Δ values. Briefly, protonated species show efficiencies slightly higher than the corresponding neutral species. Oxygen deserves a special mention. Some βCs show a quite distinctive behavior when subject to high oxygen partial pressure.

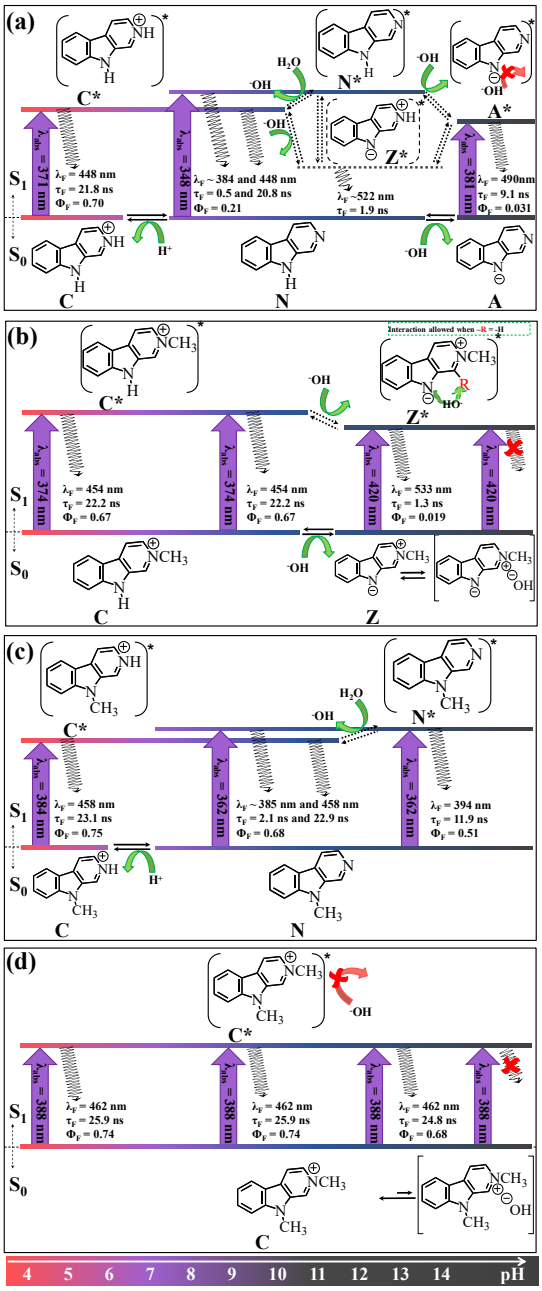

Scheme 7. (a), **(b)**, **(c)** and **(d)** species of **1a** and its *N*-methyl-derivatives (**1b**, **1c** and **1d**, respectively), present in the pH-range 2 - >14. Drawings represent the dominant acid-base species present as a function of the pH according to the scale at the bottom. Green and red arrows represent the relevant and negligible processes, respectively. Black solid and dashed arrows indicate processes or equilibria taking place in the ground (S_0) and first electronic excited (S_1) states, respectively. From Ref. (122)

As it was mentioned above, oxygen-induced deactivation of the fluorescent states (S_1) of some derivatives proceed efficiently via $S_1 \rightarrow S_0$ internal conversion (IC). Such an oxygen-induced $S_1 \rightarrow S_0$ IC results, to a small extent, in the production of singlet molecular oxygen, $O_2(^{a1}\Delta_g)$; a formally spin-forbidden process (**Scheme 2**).

2.7. Quenching of singlet oxygen by βCs

The rate of total deactivation of $^1O_2$ (k_t) by a given compound is closely related with its intrinsic efficiency and/or capability as antioxidant agents (**Scheme 2**). In aqueous solution, βCs show relatively high k_t values ranging from ~10^6 - ~10^8 M^{-1} s^{-1} (**Table 1**) [116, 143]. In general, neutral species show higher values than the corresponding protonated ones. The latter trend was predicted by Quantitative Structure Property Relationship analysis and demonstrated experimentally [143]. When comparing the latter values with those reported for other species widely accepted as antioxidant agents (*e. g.*, β-carotene showing, in solutions, k_t values ~10^{10} $M^{-1}s^{-1}$) [144], βCs seems to be less efficient. However, values observed under intracellular conditions may be quite distant from the values observed in bulk solutions. This was very recently demonstrated that the addition of β-carotene (the "golden standard" in the field) do not modified the lifetime of intracellular $^1O_2$ and, therefore, it cannot exert antioxidant protection via a direct reaction with this particular ROS [145].

Table 1. Summary of spectroscopic and photophysical data of the acid-base species of different βCs.

Compound	pK_a in S_0 [a]	pH	Species in S_0 [b]	λ_{abs} / nm [c]	$\varepsilon(\lambda)$ / 10^3 M^{-1} cm^{-1} [d]	Species in S_1 [b]	λ_F / nm [e]	Φ_F [f]	τ_F / ns [g]	Φ_Δ [h] (k_T / M^{-1} s^{-1})
[ae] **1a**	p$K_a^{(N-2)}$: 6.5 [i], 6.85 (± 0.03) [j], 7.2 [m], 7.9 [n] p$K_a^{(N-9)}$: 14.07 [o], 14.49 (± 0.07) [u], 14.5 [i, m, n], 14.53 (± 0.04) [j, k], 18 (± 2) [j, l]	4	βCH$^+$	371 [v], 370 [m]	4.30 [v]	^{1}[βCH$^+$]*	448 [v], 445 [m], 450 [n], 454 [xx]	0.70 [v], 0.58 [xx]	21.8, 22.0 [n], 21.2 [xx]	0.10 [v] (3.1 x 10^6)
		10	βCN	337 [v] and 348 [v], 348 [m]	4.01 and 3.89 [v]	^{1}[βCN]* and ^{1}[βCH$^+$]*	384 [v], 380 [n], 385 [m] 448 [v]	0.21 [v]	< 0.5 20.8	0.08 [v] (2.8 x 10^7)
		14	βCN and βCA$^-$	337 and 348 381 [o], 390 [m], 380 [u]	3.48 [o]	^{1}[βCA$^-$]* and ^{1}[βCZ]*	490 [o],490 [l], 450 [j, u], ~460 [t] 522 [o], 510 [m, n], 511 [j] ~520 [i]	0.03, 0.057 [u]	9.1 1.9, 1.6 [n]	---
[ae] **1b**	--- p$K_a^{(N-9)}$: 10.9 (± 0.02), 10.9 [n]	4	βC-CH$_3^+$	374, 375 [n]	4.10	^{1}[βC-CH$_3^+$]*	454, 455 [n]	0.67	22.2, 22.9 [n]	0.11
		9	βC-CH$_3^+$	374	4.10	^{1}[βC-CH$_3^+$]*	454	0.67	22.2	0.11
		13 - 14	βC-CH$_3$Z	420, ~420 [n]	3.06	^{1}[βC-CH$_3$Z]*	533, 510 [n]	0.02	1.3, 1.32 [n]	---
[ae] **1c**	p$K_a^{(N-2)}$: 6.3 (± 0.3), 6.91 ± 0.05 [t] ---	4	βCH$^+$	384 [v], ~390 [t]	4.84 [v]	^{1}[βCH$^+$]*	458 [v], ~455 [t]	0.75 [v]	23.1 [v], 23.1 [t]	0.10 [v]
		10	βCN	349 and 362 [v, t]	5.06 and 5.25 [v]	^{1}[βCN]* and ^{1}[βCH$^+$]*	~385 [v]~390 [t] 458 [v]	0.68 [v]	2.1 [v] 22.9 [v]	0.08 [v]
		14	βCN	349 and 362	5.15 and 5.25	^{1}[βCN]*	394	0.51	11.9	---
[ae] **1d**	---	4	βC-CH$_3^+$	388	3.8	^{1}[βC-CH$_3^+$]*	462	0.74	25.9	0.16
		9	βC-CH$_3^+$	388	3.8	^{1}[βC-CH$_3^+$]*	462	0.74	25.9	0.16
		14	βC-CH$_3^+$	388	3.8	^{1}[βC-CH$_3^+$]*	462	0.68	24.8	---
[ae] **2a**	p$K_a^{(N-2)}$: 7.34 (± 0.03) [j], 7.37 (± 0.04) [p, q], 7.7 [m] p$K_a^{(N-9)}$: 14.37 [o], 14.47 (± 0.07) [j, k], 14.50 (± 0.07) [u], 14.6 (± 0.1) [p, q], 20 (± 1) [j, l]	4	βCH$^+$	365 [v], 364 [m], 364.4 [p, r]	4.45 [v]	^{1}[βCH$^+$]*	431, 430 [m, z], 433.5 [p, r], 440 [xx]	0.85 [v], 0.83 [xx]	20.5 [v], 21.2 [l], 20.0 [xx]	0.09 [v] (2.2 x 10^6)
		10	βCN	335 [v] and 348 [v], 346 [m], 346.8 [p]	4.80 and 4.50 [v]	^{1}[βCN]* and ^{1}[βCH$^+$]*	374, 378 [m], 384 [p] 431, 433.5 [p]	0.47 [v]	0.6 [z] 20.1 [z]	0.10 [v] (5.0 x 10^7)
		13 - 14	βCN and βCA$^-$	336 and 347; 336 [p] and 349 [p] 375 [o], 375 [m], 374 [p, s], 383 [j], 375 [u]	3.39 [o], 3.83 [j]	^{1}[βCA$^-$]* and ^{1}[βCZ]*	482 [o],440 [j, u], 445 [p] 496 [o], 483 [m], 490.5 [p, s], 491 [j]	0.23, 0.056 [u]	9.1	---
[ae] **2b**	--- p$K_a^{(N-9)}$: 11.5 (± 0.1), 11.2 [j]	4	βC-CH$_3^+$	368, 366 [j]	3.5	^{1}[βC-CH$_3^+$]*	436, 437 [j]	0.95	21.0	0.10
		9	βC-CH$_3^+$	368	3.5	^{1}[βC-CH$_3^+$]*	436	0.95	20.1	0.10
		13 - 14	βC-CH$_3$Z	407	3.4	^{1}[βC-CH$_3$Z]*	503, 511 [j]	0.11	6.9	---
[ae] **2c**	p$K_a^{(N-2)}$: 6.6 (± 0.1) ---	4	βCH$^+$	378 [v]	5.03 [v]	^{1}[βCH$^+$]*	444 [v]	0.93 [v]	24.5 [v]	0.09 [v]
		10	βCN	346 and 360 [v]	4.36 and 4.25 [v]	^{1}[βCN]* and ^{1}[βCH$^+$]*	~374 [v] 444 [v]	0.68 [v]	2.5 [v] 23.8 [v]	0.10 [v]
		14	βCN	346 and 360	4.36 and 4.25	^{1}[βCN]*	374	0.43	7.1	---
[ae] **2d**	---	4	βC-CH$_3^+$	382	4.1	^{1}[βC-CH$_3^+$]*	451	0.94	25.4	0.15
		9	βC-CH$_3^+$	382	4.1	^{1}[βC-CH$_3^+$]*	451	0.94	25.4	0.15
		13 – 14	βC-CH$_3^+$	382	4.1	^{1}[βC-CH$_3^+$]*	451	0.83	24.6	---
[ae] **3a**	p$K_a^{(N-2)}$: 7.5 [v], 7.73 (± 0.03) [j], 7.7 [x], 8.0 [m] p$K_a^{(N-9)}$: 14.22 [o], 14.5 [m], > 14 [x], 14.43 (± 0.03) [j, k, u], 21 (± 1) [j, l]	4	βCH$^+$	350 [v], 355 [m]	7.86 [v], 7.59 [x]	^{1}[βCH$^+$]*	417, 418 [m], 419 [x], 425 [xx]	0.49 [v, w], 0.45 [xx]	7.0, 7.1 [w], 6.6 [xx]	0.22 [v] (3.6 x 10^6)
		10	βCN	325 [v] and 336 [v], 336 [m], 326 [x] and 338 (sh) [x]	5.35 [v] and 4.68 [v] 5.62 [x] and 4.90 [x]	^{1}[βCN]* ^{1}[βCH$^+$]* and ^{1}[βCZ]*	368 [o], 373 [m], 370 [x] 417, 424 [x] ~480	0.38 [v], 0.46 [w] 0.34 [w]	0.44, 0.41 [w] 7.0, 7.1 [w]	0.13 [v] (3.5 x 10^7)
		13 – 14	βCN and βCA$^-$	325 and 336 363 [o], 370 [m], 375 (sh) [x], 300 [u]	4.55 [o]	^{1}[βCA$^-$]* and ^{1}[βCZ]*	468 [o],435 [j, u], 430 [x] 480 [o], 476 [m], 482 [j], 480 [x]	0.45, 0.034 [u]	14.7 14.3 [w]	---
[ae] **3b**	--- p$K_a^{(N-9)}$: 11.7 (± 0.1), 11.2 (± 0.1) [x], 11.5 [m]	4	βC-CH$_3^+$	360, 360 [m], 362 [x]	6.3	^{1}[βC-CH$_3^+$]*	422, 422 [m], 420 [x], 433 [xx]	0.47, 0.45 [xx]	7.0, 6.5 [xx]	0.08
		9	βC-CH$_3^+$	360, 362 [x]	6.3	^{1}[βC-CH$_3^+$]*	422, 420 [x]	0.47	7.0	0.08
		13 -14	βC-CH$_3$Z	392, 392 [m], 398 [x]	5.3	^{1}[βC-CH$_3$Z]*	505, 482 [m], 485 [x]	0.24	11.9	---

[ae] **3c**	$pK_a^{(N-2)}$: 7.1 (± 0.1) ---	4	βCH$^+$	363 [y]	6.83 [y]	^{1}[βCH$^+$]*	430 [y]	0.43 [y]	9.1 [y]	0.16 [y]
		10	βCN	336 and 347 [y]	5.24 and 4.92 [y]	^{1}[βCN]* and ^{1}[βCH$^+$]*	~365 [y] 430 [y]	0.35 [y]	0.4 [y] 9.1 [y]	0.15 [y]
		14	βCN	336 and 347	5.24 and 4.92	^{1}[βCN]*	368	0.33	5.1	---
[ae] **3d**	---	4	βC-CH$_3^+$	368	6.8	^{1}[βC-CH$_3^+$]*	434	0.45	8.7	0.16
		9	βC-CH$_3^+$	368	6.8	^{1}[βC-CH$_3^+$]*	434	0.45	8.7	0.16
		13	βC-CH$_3^+$	368	6.8	^{1}[βC-CH$_3^+$]*	434	0.36	9.0	---
[af] **3e**	$pK_a^{(N-2)}$: 6.3 (± 0.2) $pK_a^{(N-9)}$: 10.5 (± 0.3)	4	βCH$^+$	362	9.02	^{1}[βCH$^+$]*	428	0.16	2.2	0.19 (1.4 x 10^7)
		9	βCN	342	5.66	^{1}[βCN]* ^{1}[βCH$^+$]* and ^{1}[βCZ]*	375 426 510	0.12	0.4 2.1 8.5 - 12	nd (~10^8-10^9)
[af] **3f**	$pK_a^{(N-2)}$: 6.4 (± 0.2) $pK_a^{(N-9)}$: nd	4	βCH$^+$	361[sh]	5.88	^{1}[βCH$^+$]*	423	0.11		0.22 (4.3 x 10^7)
		9	βCN	340	4.14	^{1}[βCN]* ^{1}[βCH$^+$]* and ^{1}[βCZ]*	356 423 460	0.12	0.6 2.3 8.6	nd (~10^8-10^9)
[af] **3g**	$pK_a^{(N-2)}$: 5.4 (± 0.4) $pK_a^{(N-9)}$: nd	4	βCH$^+$	369	6.33	^{1}[βCH$^+$]*	429	0.20	2.8	0.05 (1.6 x 10^7)
		9	βCN	357	5.58	^{1}[βCN]* ^{1}[βCH$^+$]* and ^{1}[βCZ]*	361 429 475	0.02	0.2 2.2 7.5	nd (~10^8-10^9)
[ag] **4**	$pK_a^{(N-2)}$: 7.8, 7.8[ab] $pK_a^{(-OH)}$: >9.6, 9.6[ab] $pK_a^{(N-9)}$: 15.83(± 0.06)[j, k], 15.75[ac, k]	4	βCH$^+$	320, 320[ab], 357[sh, ab]	19.0	^{1}[βCH$^+$]*	418[ab]	---	---	not reported
		8.4[ad]	βCN βCZ	340, 338[ab] 365, 367[ab]	9.0 8.0	^{1}[βCN]* ^{1}[βCH$^+$]* ^{1}[βCZ]*	360[ab] 420[sh, ab] 440[ab]	---	---	not reported
		13.5	βCA$^-$	331, 332[ab]	23.7	^{1}[βCA$^-$]*	450[ab]	---	---	not reported
[ah] **5**	$pK_a^{(N-2)}$: 9.7, 9.54 (± 0.03)[j], 10.0[aa] $pK_a^{(N-9)}$: 15.63(± 0.18)[j, l], 15.40 (± 0.18)[j, k]	4	βCH$^+$	372, 373[j], 372[aa]	20.65	^{1}[βCH$^+$]*	484, 480[j],480[aa]	0.40, 0.46[j], 0.32[xx]	5.9	0.02
		13	βCN	330, 330[j], 330[aa]	15.9	^{1}[βCN]* ^{1}[βCH$^+$]*	375[j], 377[aa] 484	0.01	---	0.003
[ai] **6**	$pK_a^{(N-2)}$: 8.5, 8.6[aa] $pK_a^{(-OH)}$: 11.2, 11.5[aa] $pK_a^{(N-9)}$: 16.03(± 0.28)[j, k], 16.01[ac, k]	4	βCH$^+$	371, 370[aa]	15.9	^{1}[βCH$^+$]*	475[aa]	---	---	not reported
		9.6[ad]	βCN βCZ	340, 340[aa] 430, 431[aa]	7.5 16.8	^{1}[βCN]* ^{1}[βCH$^+$]* ^{1}[βCZ]*	377[aa] 475[aa] 530[aa]	---	---	not reported
		13.1	βCA$^-$	363, 363[aa]	13.9	^{1}[βCA$^-$]* ^{1}[βCZ]*	450[aa] 530[aa]	---	---	not reported

[a] $pK_a^{(N-2)}$, $pK_a^{(N-9)}$ and $pK_a^{(OH)}$ represent the negative base 10 log of the acid dissociation constants (K_a) of pyridinic (N-2), indolic (N-9) nitrogen atoms and hydroxyl substituent placed at C-7, respectively. [b]Main acid-base species present in the solution in the ground (S_0) or first electronic excited state (S_1) of βCs, under the pH condition indicated in the second column. [c] Maximum of the lowest energy absorption band (λ_{abs}; ± 2 nm). [d] Absorption coefficient (ε) at the maximum of the lowest-energy absorption band (error ≤ 5 %). [e] Maximum of the emission band (λ_F) in aqueous solutions (± 2 nm). [f] Fluorescence quantum yields (Φ_F) and [g] fluorescence lifetimes (τ_F) measured in air-equilibrated aqueous solutions (error ≤ 7 %). [h] Quantum yield of singlet oxygen production (Φ_Δ) measured in air-equilibrated D_2O aqueous solutions (pD 7.7, error ± 10-15 %). [i] From Ref. (125), measured from **1a** (10^{-5} M) phosphate buffer solutions with 1% methanol. [j] From Ref. (120). [k] Data analyzed by the excess acidity (EA) methods. [l] Data analyzed by the Hammett acidity function (HAF). [m] From Ref. (146), measured from βC buffer solutions (0.1 M mixtures of acetic acid and sodium acetate for pH 3-4; l/15 M mixtures of Na_2HPO_4 and KH_2PO_4 for pH 5-8; 0.1 M mixtures of glycine and NaOH for pH 9-13. [n] From Ref. (126), measured from βC aqueous solutions. Note that pK_a^{N-9} of **1a** is an estimated value. [o] Data obtained from MCR-ALS and/or PARAFAC (hybrid hard-soft modeling methodology) analysis. [p] From Ref. (128). [q] Measured in phosphate buffer at ionic strength < 0.05. [r] Measured in acidic water (1 N, H_2SO_4). [s] Measured in water pH 14 (1 N, NaOH). [t] From Ref. (147) measured in aqueous solution; τ_F was measured from acidic (0.1 M, HCl) solutions. [u] From Ref. (129) measured in highly alkaline aqueous conditions (6.8 M KOH, at 25 °C). [v] From Ref. (113), measured in aqueous solutions. [w] From Ref. (148), Φ_F of HaN was measured in benzene. [x] From Ref. (127), measured in aqueous solution. pK_a values measured in water containing 10% of methanol at ionic strength < 0.04; 2-methyl-harminium tetrafluoroborate derivative was used. [y] From Ref. (61). [z] From Ref. (149). [xx] From Ref. (150), measured in water (0.1 N, H_2SO_4). [aa] From Ref. (130) [ad] βCH$^+$ and βCA$^-$ species might be present. [ae] From Ref. (122). [af] From Ref. (116). [ag] From Ref. (54). [ah] From Ref. (54). [ai] From Ref. (118).

Table 2. List of peak oxidation potential values (*vs*. Ag-AgCl) reported for a set of βC derivatives measured under different experimental conditions.

Compound	E_1 (V)	E_2(V)	E_3(V)	E_4(V)	Electrode	pH
1a	0.90	1.33			Gold	3.0
	*0.91	*1.30			Gold	3.0
2a	0.9	-			Carbon nanotube/glassy carbon	7.0
	**0.73	-			Platinum	Acid
	0.93	1.21			Gold	3.0
	*0.60	*1.27			Gold	3.0
2b	1.20				Gold	3.0
	*0.93	*1.15			Gold	3.0
2c	0.93	1.25			Gold	3.0
	*0.93	*1.25			Gold	3.0
2d	1.16				Gold	3.0
	*0.92	*1.24			Gold	3.0
3a	0.97	-			Carbon nanotube/glassy carbon	7.0
	0.94	1.22			Gold	3.0
	*0.50	*0.94	*1.05	*1.22	Gold	3.0
	0.93	1.12			Gold	5.0
3b	1.22				Gold	3.0
	*0.95	*1.18			Gold	3.0
	[a]1.03	[a]1.17			Gold	6.8
3c	0.93	1.18			Gold	3.0
	*0.93	*1.18			Gold	3.0
3d	1.16				Gold	3.0
	*0.91	*1.20			Gold	3.0
3e	[a]0.93	[a]1.17			Gold	2.0
	0.98	1.27			Gold	3.0
	[a]0.95	1.21			Gold	5.0
	[a]0.92	[a]1.28			Gold	6.8
3g	0.95	1.27			Gold	3.0
	[a]0.96	[a]1.24			Gold	6.8
5	0.62	0.98			Carbon nanotube/glassy carbon	7.0
	0.31	0.58	0.96	1.20	Gold	3.0
	0.17	0.66	1.00	1.25	Gold	5.0
6	0.39	0.73			Carbon nanotube/glassy carbon	7.0
Norharmane dimer	0.92	1.29			Gold	3.0

* Peak-values observed in the voltammograms recorded after 500 repeated cycles between 1.0 and 1.2 V. ** Potential value *vs*. standard calomel electrode (SCE). [a] Values obtained from deconvoluted signals. Ref. (133): in $NaClO_4$ (0.1 M) acidic aqueous solution, at v = 0.05 V s^{-1} and room temperature. Ref. (132): in 0.1 M phosphate buffer (pH 7.0) at v = 0.05 V s^{-1}. Ref. (131): in 0.1 M $LiClO_4$, CH_3CN:H_2O (9:1).

3. Photochemistry of βCs in aqueous media

In general, βCs are quite photostable compounds (**Table 3**). In particular, for most of the full-aromatic-βCs investigated to date (*i. e.*, **1a**, **1c**, **2a**, **2c**, **3a** and **3e-g**) it has been demonstrated that under anaerobic conditions any photochemical reaction take place. On the contrary, when subject to photoexcitation in the presence of oxygen (*i. e.*, in air-equilibrated aqueous solutions) these alkaloids follow an extremely slow photochemical degradation (*i. e.*, quantum yields of photodegradation, Φ_R, of ~ 10^{-3} – 10^{-4}) giving rise to the formation of βC-like polymers (dimers, trimers, etc.) and their correspondent hydroxylated derivatives (**Scheme 8a**). The latter reaction is pH-dependent and, particularly, protonated species (present under acidic conditions) are more reactive than the corresponding neutral forms. In addition, the overall reaction leads place to the formation of hydrogen peroxide (H_2O_2) in a similar extent (quantum yields of H_2O_2 production, Φ_{H2O2} ~ 10^{-3} – 10^{-4}). It has been proposed that the latter ROS is formed by electron transfer from S_1 to O_2 yielding the superoxide anion ($O_2^{\bullet-}$) and, as a result of its spontaneous disproportionation, H_2O_2 is produced. In the case of compounds **3e-g**, an extra photochemical oxygen-independent pathway also takes places involving the break of the C-Cl bound. This behavior was accounted by the fact that, in the first photoexcited states, the three chloroharmine derivatives investigated show a clear decrease in the electronic density over the chlorine atom.[116] Under anaerobic conditions, these chloro-βCs also give rise to the formation of H_2O_2 through a different photochemical pathway that still needs to be elucidated. Dihydro-βCs also show a distinctive oxygen-dependent photochemical behavior. To date, compound **5** has only been studied. Results show that, under anaerobic conditions, full aromatization of **5** takes places giving rise to the formation of **3a**. On the contrary, in the presence of oxygen, the hydroxylation of the βC-scaffold takes place (**Scheme 8b**).

Table 3. Summary of quantum yield of βC photodegradation (Φ_R) and hydrogen peroxide production (Φ_{H2O2}) at pH 4.

Compound	Φ_R (Ar or N_2)	Φ_R (air) (± 0.05 10^{-3})	Φ_{H2O2} (Ar or N_2) (± 0.05 10^{-3})	Φ_{H2O2} (air) (± 0.05 10^{-3})
1a	0	1.82 x 10^{-3}	0	0.46 x 10^{-3}
1c	0	0.66 x 10^{-3}	0	0.38 x 10^{-3}
2a	0	1.82 x 10^{-3}	0	0.37 x 10^{-3}
2c	0	0.68 x 10^{-3}	0	0.30 x 10^{-3}
3a	0	3.7 x 10^{-3}	0	0.84 x 10^{-3}
3e	7.9 x 10^{-3}	7.8 x 10^{-3}	1.0 x 10^{-3}	1.79 x 10^{-3}
3f	---	5.7 x 10^{-3}	---	0.77 x 10^{-3}
3g	---	4.8 x 10^{-3}	---	1.9 x 10^{-3}
5	3.16 x 10^{-3}	1.12 x 10^{-3}	nd	nd

nd: not detected

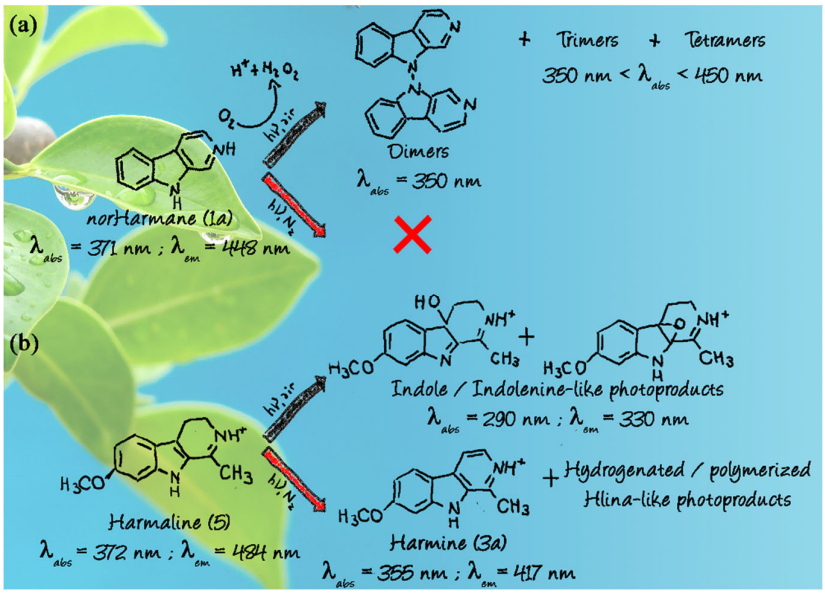

Scheme 8. Main photochemical pathways followed by photoexcited **(a)** full-aromatic-βCs. and **(b)** dihydro-derivative **5.**

4. Conclusions and Final Considerations

Data summarized herein allows us to come up with generalizations regarding the main physicochemical and photochemical properties of this family of endogenous alkaloids so-called

βCs. Data reported may also contribute to further understand and/or forecast the biological role of βCs, in particular, when they are subject to photoexcitation:

- ✓ βC alkaloids show quite strong structure- and solvent-dependent chemical properties. Their physicochemical and photochemical properties can be fine tune by changing the type and relative position of the substituent in the βC´s moiety as well as environmental parameters (*e. g.*, solvent, pH and oxygen partial pressure). **Scheme 9** summarizes the main effect of different types of βCs' substituents on several spectroscopic, chemical, photophysic and photochemical properties.

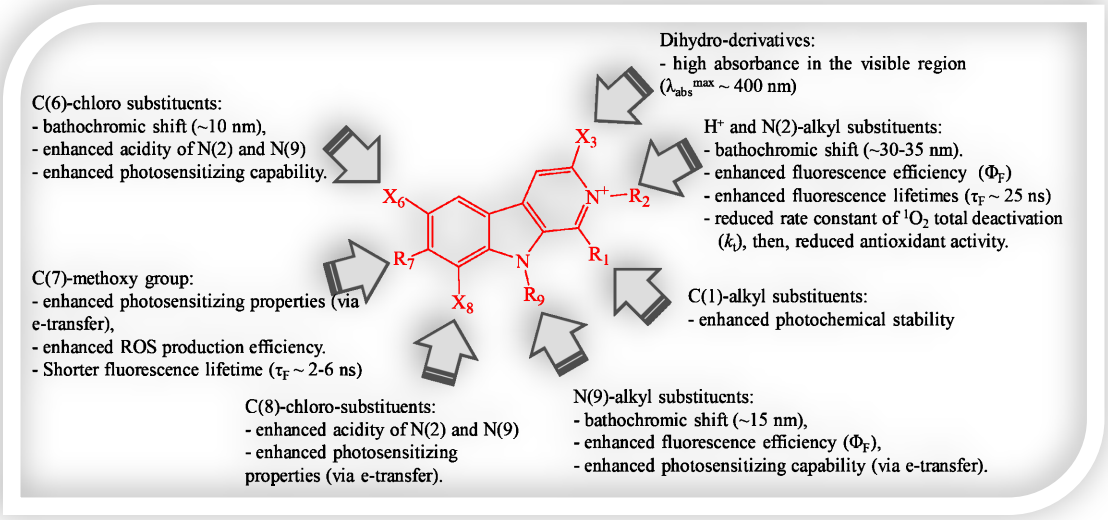

Scheme 9. Qualitative structure-photochemical properties relationship of N-unsubstituted-βCs and their methyl-, methoxy- and chloro-derivatives. These alkaloids have fine-tunable (photo)chemical properties.

- ✓ Under physiological pH conditions, protonated (and quaternary) derivatives of both full-aromatic and dihydro-βCs are present in the solution showing quite high absorbance in the UV-visible region. The latter fact in connection with the quite high intrinsic photostability ($\Phi_R \sim 10^{-3}$) shown by all these endogenous biological compounds make them potential candidates to be considered when analyzing multiple photo-triggered biological processes.

- ✓ Some βCs are found in different tropical plants, naturally subject to high doses of sunlight. Taking into consideration the fact that these alkaloids show quite high absorption coefficient in the UVB and UVA (ε up to 25.000 M^{-1} cm^{-1}) regions of the solar spectrum, they could then act as UV absorbing endogenous chromophores (*e. g.*, UV protective agents).
- ✓ Oxygen partial pressure may fine tune the relative steady state distribution of βC's photoexcited states (S_0, S_1 and T_1). Therefore, O_2 can regulate different photochemical processes that might occur in vivo.
- ✓ Their extremely high efficiency of visible light emission ($\Phi_F \sim 0.50 - 0.90$) makes these alkaloids good candidates as accessory pigments for light-harvesting in photosynthesis, as well as fluorescent-induced pollinators attraction. In addition, as naturally occurring secondary metabolites, βCs might represent an interesting alternative as fluorescent tracers [151] able for sensing changes on the pH and oxygen partial pressure in intracellular spatial domains.
- ✓ The most commonly accepted biological role of βCs is related to defense response mediated by ROS. However, their quite low efficiency of ROS production (Φ_{H2O2}, $\Phi_{OH\bullet} \sim 10^{-3}$ and $\Phi_\Delta \sim 0.08 - 0.20$) would suggest that defense response would not be a quite relevant process. ROS, and in particular singlet oxygen, can play a wide range of biological roles [152]. At low doses, ROS would play a key role in ROS-mediated intracellular signaling [152-154]. In this context, the role of βCs in photo-triggered intracellular signaling processes (pH- and ROS-mediated) should then be considered.
- ✓ Neutral and halogenated βCs are excellent candidates to act as antioxidant in living systems, under photoinduced oxidative stress. This is accounted for by the fact that these derivatives show k_T values ranged $\sim 10^7 - 10^8$ M^{-1} s^{-1}.
- ✓ Full-aromatic monomers and dimers, as well as partially hydrogenated βC derivatives represent a group of alkaloids widely distributed in a great variety of living systems. In

plants and bacteria, tetrahydro-βCs are the primary product of the Pictet-Spengler enzymatically catalyzed condensation. Tetrahydro-βC moieties are further chemically oxidized giving rise to the formation of a vast set of derivatives including dihydro- and full-aromatic βCs. Despite this, in most of the cases, both *in vivo* aromatization and dimerization still remain unclear. In this regard, light triggers both types of reactions and the oxygen partial pressure plays a key role as modulator. Therefore, photoinduced reactions have to be taken into account in the overall βC biosynthetic pathways.

- ✓ Electrochemical analysis (potentiodynamic response) shows that oxidative pathways of βCs follows different routes in a structure-dependent manner (Scheme 6). Understanding the redox mechanisms of biological compounds and processes might contribute to understand the role of these alkaloids in nature. Electron transfer reactions in living systems are important and involve complex physicochemical behavior. In general, these processes are based on electrons/protons transfer in a non-stationary condition far from equilibrium. The high sensitivity of electrochemical methods allows to reach very low detection limits, making them powerful tools to better understand the biochemical reactions involving secondary metabolites that usually occur at very low concentrations[155,156]. This could be the case of 6-hydroxy-1,2,3,4-tetrahydro-βC (14) that was reported to be accumulated in the brain upon chronic alcohol intake and its oxidative transformation might play a role in this disorder, and/or the in vivo full aromatization of the dihydro- and tetrahydro-βC derivatives enzymatically synthesized, etc.
- ✓ On the other hand, electrochemical methods can be used to properly design an electro-synthetic pathway to produce new alkaloids and/or to introduce further oxidative/reductive modifications [155], and/or to further develop cheap sensors for βC detection in complex matrices [157, 158].
- ✓ In the field of solar energy conversion, the intrinsic photoelectrochemical properties of βCs make them quite promising additives for dye sensitized solar cells (DSSC) [137]. The

use of βCs as additives in DSSC based on R-phycoerythrin pigment extracted from red algae have several implications (acting as secondary pigments harvesting UVA light, stabilizing the conformational structure of the protein and/or changing the redox potential of the main pigment) that improve the performance of DSSC devices.

Acknowledgements

This work was partially supported by UBA (0055BA) and PICT-2015-0374, 2016-0370, 2016-0130 and 2018-3193. FDV, LM, RV and JGY thank ANPCyT and CONICET for their doctoral and postdoctoral research fellowships. MMG, MLA, MPD, REB and FMC are research members of CONICET. LM, RV and FMC would also like to thanks The World Academy of Science (TWAS) and TWAS-Young Affiliate Network (TYAN) for TWAS Research Fellowship and TCGA Grants. Authors thank to Carlos G. Alberici for his technical support.

References

(1) L. K. Larsen, R. E. Moore, G. M. L. Patterson, *J. Nat. Prod*. **1994**, 57, 419-421.
(2) J. Torreilles, M. C. Guerin, A. Previero, *Biochiime.* **1985**, 67, 929-647.
(3) J. Adachi, Y. Mizoi, T. Naito, Y. Ogawa, Y. UEtani, I. Nimomiya, *J. Nutr.* **1991**, 121, 646-652.
(4) S. Manabe, J. Yuan, T. Takahashi, R. C. Urban Jr, *Exp. Eye Res.* **1996**, 63, 179-186.
(5) K. Pari, C. S. Sundari, S. Chandani, D. Balasubramanian, *J. Biol. Chem.* **2000**, 275, 2455-2462.
(6) R. Spijkerman, R. van den Eijnden, D van de Mheen, I. Bongers D. Fekkes, *Eur. Neuropsychopharm.* **2002**, 12, 61-71.
(7) U. Breyer-Pfaff, G. Wiatr, I. Stevens, H. Jörg Gaertner, G. Mundle, K. Mann, *Life Sci.* **1996**, 58, 1425-1432.
(8) D. Fekkes, A. Tuiten, I. Bom, L. Pepplinkhuizen, *Neurosci. Lett.* **2001**, 303, 145-148.
(9) W. Pfau, K. Skog, *J. Chromatogr. B Biomed. Appl.* **2004**, 802, 115-126.
(10) B. Hemmateenejad, A. Abbaspour, H. Maghami, R. Miri and M. R. Panjehshahin, *Anal. Chim. Acta*. **2006**, 575, 290-299.
(11) T.-S. Kam, K.-M. Sim, T. Koyano, K. Komiyama, *Phytochemistry*. **1999**, 50, 75-79.
(12) M. Caprasse, C. Coune, L. Angenot, *J. Pharm. Bel*.. **1983**, 38, 135-139.
(13) T.-S. Kam, K.-M. Sim, *Phytochemistry*. **1998**, 47, 145-147.
(14) K. R. Downum, *New Phytol*. **1992**, 122, 401-420.
(15) T. Herraiz, J. Galisteo, *J. Agric. Food Chem.* **2003**, 51, 7156-7161.
(16) M. A. Rashid, K. R. Gustafson, M. R. Boyd, *J. Nat. Prod*. **2001**, 64, 1454-1456.
(17) P. S. Kearns, J. C. Coll, J. A. Rideout, *J. Nat. Prod*. **1995**, 58, 1075-1076.
(18) Y. Tadokoro, T. Nishikawa, T. Ichimori, S. Matsunaga, M. J. Fujita, R. Sakai, *ACS Omega*. **2017**, 2, 1074-1080.
(19) S. J. Stachel, S. A. Stockwell, D. L. Van Vranken, *Chem. Biol*. **1999**, 6, 531-539.
(20) M. S. Siderhurst, D. M. James, C. D. Rithner, D. L. Dick, L. B. Bjostad, *J. Econ Entomol*. **2005**, 98, 1669-1678.
(21) S. Ramesh, R. Rajan, R. Santhanam, *Freshwater Phytopharmaceutical Compounds*, 1st ed., CRC Press, **2013**.
(22) B. S. Davidson, *Chem. Rev.* **1993**, 93, 1771-1791.
(23) V. M. Dembitsky, G. A. Tolostikov, *Chemistry for Sustainable Development* **2003**, 11, 451-466.
(24) T. Herraiz, D. Gonzalez, C. Ancin-Azpilicueta, V. J. Arán, H. Guillen, *Food. Chem. Toxicol*. 2010, 48, 839-845.
(25) E. Fattorusso, O. Taglialatela-Scafati, *Modern Alkaloids: Structure, Isolation, Synthesis, and Biology*, Wiley, 2008.
(26) K. L. Rinehart, J. Kobayashi, G. C. Harbour, J. Gilmore, M. Mascal, T. G. Holt, L. S. Shield, F. Lafargue, J. Am. Chem. Soc. **1987**, 109, 3378-3387.

(27) J. Kobayashi, G. C. Harbour, J. Gilmore and K. L. Rinehart, *J. Am. Chem. Soc*. **1984**, 106, 1526-1528.
(28) C. Debitus, D. Laurent and M. Païs, *J. Nat. Prod.* **1988**, 51, 799-801.
(29) J. W. Blunt, R. J. Lake, M. H. G. Munro, T. Toyokuni, *Tetrahedron Lett.* 1987, 28, 1825-1826.
(30) A. Aiello, E. Fattorusso, S. Magno, L. Mayol, *Tetrahedron*. **1987**, 43, 5929-5932.
(31) K. G. Ramawat and J.-M. Mérillon, *Natural Products: Phytochemistry, Botany and Metabolism of Alkaloids, Phenolics and Terpenes*, 1st ed., Springer Berlin Heidelberg, Berlin, Heidelberg, 2013.
(32) D. M. Wood, P. I. Dargan, *Novel Psychoactive Substances*, 1st ed., Academic Press, Boston, 2013.
(33) S. J. Stachell, S. A. Stockwell, D. L. Van Vranken, *Chem. Biol.* **1999**, 6, 531-539.
(34) G. Freund, *Annu. Rev. Pharmacol*. **1973**, 13, 217-227.
(35) M. Leino, *Exp. Eye Res.* **1984**, 38, 325-330.
(36) J. Dillon, A. Spector, K. Nakanishi, *Nature.* **1976**, 259, 422-423.
(37) E. D. Cox, J. M. Cook, *Chem. Rev*. **1995**, 95, 1797-1842.
(38) Q. Chen, S. Zhang, Y. Xie, *J. Biotechnol.* **2018**, 281, 137-143.
(39) T. M. Kutchan, *Phytochemistry.* **1993**, 32, 493-506.
(40) J. Stöckigt, L. Barleben, S. Panjikar, E. A. Loris, *Plant Physiol. Bioch*. **2008**, 46, 340-355.
(41) J. Stöckigt, A. P. Antonchick, F. Wu, H. Waldmann, *Angew. Chem. Int. Ed.* **2011**, 50, 8538-8564.
(42) X. Ma, S. Panjikar, J. Koepke, E. Loris, J. Stöckigt, *Plant Cell*. **2006**, 18, 907-920.
(43) Q. Chen, C. Ji, Y. Song, H. Huang, J. Ma, X. Tian, J. Ju, *Angew. Chem. Int. Ed.* **2013**, 52, 9980-9984.
(44) A. Aroonsri, S. Kitani, J. Hashimoto, I. Kosone, M. Izumikawa, M. Komatsu, N. Fujita, Y. Takahashi, K. Shin-ya, H. Ikeda, T. Nihira, *Appl. Environ. Microbiol*. **2012**, 78, 8015-8024.
(45) T. Mori, S. Hoshino, S. Sahashi, T. Wakimoto, T. Matsui, H. Morita, I. Abe, *Chem. Biol.* **2015**, 22, 898-906.
(46) S. Ueda, H. Ikeda, T. Namba, Y. Ikejiri, Y. Nishimoto, M. Arai, T. Nihira and S. Kitani, *J. Ind. Microbiol. Biot.* **2019**, 46, 739-750.
(47) W. Yan, H. M. Ge, G. Wang, N. Jiang, Y. N. Mei, R. Jiang, S. J. Li, C. J. Chen, R. H. Jiao, Q. Xu, S. W. Ng, R. X. Tan, *Proc. Natl. Acad. Sci. U. S. A.* **2014**, 111, 18138-18143.
(48) J. Sopková-de Oliveira Santos, J. C. Smith, M. Delaforge, H. Virelizier, C. K. Jankowski, *Eur. J. Biochem*., **1998**, 251, 398-404.
(49) I. Nemet, L. Varga-Defterdarovic, *J. Amino Acids*. **2007**, 32, 291-293.
(50) K. Backhaus, L. Ludwig-Radtke, X. Xie, S.-M. Li, *ACS Synth. Biol.* **2017**, 6, 1056-1064.
(51) F. Villarruel, M. P. Denofrio, F. A. O. Rasse-Suriani, F. S. García Einschlag, T. Schmidt De León, R. Erra-Balsells, F. M. Cabrerizo, *J. Photoch. Photobio. B.* **2019,** 199, 111600.
(52) R. Cao, W. Peng, Z. Wang, A. Xu, *Curr. Med. Chem.* **2007**, 14, 479-500.
(53) G. M. Olmedo, L. Cerioni, M. M. González, F. M. Cabrerizo, V. A. Rapisarda, S. I. Volentini, Food Microbiol. **2017**, 62, 9-14.
(54) G. M. Olmedo, L. Cerioni, M. M. González, F. M. Cabrerizo, S. I. Volentini, V. A. Rapisarda, *Front. Microbiol.* **2017**, 8.
(55) M. L. Alomar, F. A. Rasse-Suriani, A. Ganuza, V. M. Coceres, F. M. Cabrerizo, S. O. Angel, *BMC Res. Notes.* **2013**, 6, 193.
(56) K. Butzbach, F. A. O. Rasse-Suriani, M. M. Gonzalez, F. M. Cabrerizo, B. Epe, *Photochem. Photobiol*. **2016**, 92, 611-619.
(57) M. M. Gonzalez, M. P. Denofrio, F. S. Garcia Einschlag, C. A. Franca, R. Pis Diez, R. Erra-Balsells, F. M. Cabrerizo, *Phys. Chem. Chem. Phys*. **2014**, 16, 16547-16562.
(58) M. M. Gonzalez, F. A. O. Rasse-Suriani, C. A. Franca, R. Pis Diez, Y. Gholipour, H. Nonami, R. Erra-Balsells, F. M. Cabrerizo, *Org. Biomol. Chem.* **2012**, 10, 9359-9372.
(59) M. M. Gonzalez, M. Pellon-Maison, M. A. Ales-Gandolfo, M. R. Gonzalez-Baró, R. Erra-Balsells, F. M. Cabrerizo, *Org. Biomol. Chem.* **2010**, 8, 2543-2552.
(60) M. M. Gonzalez, M. Vignoni, M. Pellon-Maison, M. A. Ales-Gandolfo, M. R. Gonzalez-Baro, R. Erra-Balsells, B. Epe, F. M. Cabrerizo, *Org. Biomol. Chem.* **2012**, 10, 1807-1819.
(61) M. Vignoni, F. A. O. Rasse-Suriani, K. Butzbach, R. Erra-Balsells, B. Epe F. M. Cabrerizo, *Org. Biomol. Chem.* **2013**, 11, 5300-5309.
(62) J. G. Yañuk, M. P. Denofrio, F. A. O. Rasse-Suriani, F. D. Villarruel, F. Fassetta, F. S. García Einschlag, R. Erra-Balsells, B. Epe, F. M. Cabrerizo, *Org. Biomol. Chem.* **2018**, 16, 2170-2184.
(63) F. M. Cabrerizo, M. M. Gonzalez, M. Vignoni, M. P. Denofrio, R. Erra-Balsells, *Anales de la Academia Nacional de Ciencias Exactas, Físicas y Naturales*. **2015**, 41-62.
(64) M. Vignoni, R. Erra-Balsells, B. Epe, F. M. Cabrerizo, *J. Photochem. Photobiol. B.* **2014**, 132, 66-71.
(65) J. G. Yañuk, M. L. Alomar, M. M. Gonzalez, F. Simon, R. Erra-Balsells, M. Rafti, F. M. Cabrerizo, *Phys. Chem. Chem. Phys.* **2015**, 17, 12462-12465.
(66) M. M. Gonzalez, F. M. Cabrerizo, A. Baiker, R. Erra-Balsells, A. Osterman, H. Nitschko, M. G. Vizoso-Pinto, *Int. J. Antimicrob. Agents.* **2018**, 52, 459-468.
(67) I. X. García-Zubiri, H. D. Burrows, J. Sérgio Seixas De Melo, J. Pina, M. Monteserín, M. J. Tapia, *Photochem. Photobiol*. **2007**, 83, 1455-1464.
(68) M. Caprasse, C. Coune and L. m. *Angenot, Journal de Pharmacie de Belgique*, 1983, 38, 135-139.

(69) K. Toshima, Y. Okuno, Y. Nakajima, S. Matsumura, *Bioorg. Med. Chem. Lett.* **2002**, 12, 671-673.
(70) R. Cao, W. Peng, H. Chen, Y. Ma, X. Liu, X. Hou, H. Guan and A. Xu, *Biochem. Bioph. Res. Co.* **2005**, 338, 1557-1563.
(71) H. Guan, X. Liu, W. Peng, R. Cao, Y. Ma, H. Chen, A. Xu, *Biochem. Bioph. Res. Co.* **2006**, 342, 894-901.
(72) G. Duportail, H. Lami, *Biochim. Biophys. Acta.* **1975**, 402, 20-30.
(73) G. Duportail, *Int. J. Biol. Macromol.* **1981**, 3, 188-192.
(74) S. Sarkar, P. Pandya, K. Bhadra, *PLOS ONE*. **2014**, 9, e108022.
(75) W. Hevers, H. Lüddens, *Mol. Neurobiol.* **1998**, 18, 35-86.
(76) A.-F. M. Abdel-Fattah, K. Matsumoto, H. A.-K. Gammaz, H. Watanabe, *Pharmacol. Biochem. Behav.* **1995**, 52, 421-426.
(77) I. F. Musgrave, E. Badoer, *Br. J. Pharmacol.* **2000**, 129, 1057-1059.
(78) S. Kumar, A. Singh, K. Kumar, V. Kumar, *Eur. J. Med. Chem.* **2017**, 142, 48-73.
(79) P. Rivas, B. K. Cassels, A. Morello Y. Repetto, *Comp. Biochem. Physiol. Part C: Toxicol. Pharmacol.* **1999**, 122, 27-31.
(80) S. Lala, S. Pramanick, S. Mukhopadhyay, S. Bandyopadhyay, M. K. Basu, *J. Drug Target.* **2004**, 12, 165-175.
(81) C. Di Giorgio, F. Delmas, E. Ollivier, R. Elias, G. Balansard, P. Timon-David, *Exp. Parasitol.* **2004**, 106, 67-74.
(82) G. Van Baelen, S. Hostyn, L. Dhooghe, P. Tapolcsányi, P. Mátyus, G. Lemière, R. Dommisse, M. Kaiser, R. Brun, P. Cos, L. Maes, G. Hajós, Z. Riedl, I. Nagy, B. U. W. Maes, L. Pieters, *Bioorg. Med. Chem.* **2009**, 17, 7209-7217.
(83) A. G. Bayih, A. Folefoc, A. N. Mohon, S. Eagon, M. Anderson, D. R. Pillai, *Malaria J.* **2016**, 15, 579.
(84) D. Shahinas, G. MacMullin, C. Benedict, I. Crandall, D. R. Pillai, *Antimicrob. Agents Chemother.* **2012**, 56, 4207-4213.
(85) J. Ishida, H. K. Wang, M. Oyama, M. L. Cosentino, C. Q. Hu, K. H. Lee, *J. Nat. Prod.* **2001**, 64, 958-960.
(86) P. Bag, D. Ojha, H. Mukherjee, U. C. Halder, S. Mondal, A. Biswas, A. Sharon, L. Van Kaer, S. Chakrabarty, G. Das, D. Mitra, D. Chattopadhyay, *Antivir. Res.* **2014**, 105, 126-134.
(87) D. Chen, A. Su, Y. Fu, X. Wang, X. Lv, W. Xu, S. Xu, H. Wang, Z. Wu, *Antivir. Res.* **2015**, 123, 27-38.
(88) A. S. N. Formagio, L. T. D. Tonin, M. A. Foglio, C. Madjarof, J. E. de Carvalho, W. F. da Costa, F. P. Cardoso, M. H. Sarragiotto, *Bioorg. Med. Chem.* **2008**, 16, 9660-9667.
(89) V. M. Quintana, L. E. Piccini, J. D. Panozzo Zénere, E. B. Damonte, M. A. Ponce, V. Castilla, *Antivir. Res.* **2016**, 134, 26-33.
(90) J. F. Blom, T. Brütsch, D. Barbaras, Y. Bethuel, H. H. Locher, C. Hubschwerlen, K. Gademann, *Org. Lett.* **2006**, 8, 737-740.
(91) B. Greiner, C. Fahndrich, S. Strauss, H. Rommelspacher, *N-S Arch. Pharmacol.* **1983**, 322, 140-146.
(92) D. Fekkes, W. T. Bode, *Life Sci.* **1993**, 52, 2045-2054.
(93) M.G. Thomas, D. Sartini, M. Emanuelli, M.J. van Haren, N.I. Martin, D. M. Mountford, D. J. Barlow, F. Klamt, D. B. Ramsden, M. Reza, R. B. Parsons, *Biochem. J.* **2016**, 473, 3253-3267.
(94) M.A. Collins and E.J. Neafsey, in *Neurotoxic Factors in Parkinson's Disease and Related Disorders*, A. Storch, Collins, M.A. (Eds), Kluwer Academic/Plenum Publishers, New York, 2000, pp. 115–129.
(95) D. A. Gearhart, M. A. Collins, J. M. Lee, E. J. Neafsey, *Neurobiol. Dis.* **2000**, 7, 201-211.
(96) D. A. Gearhart, E. J. Neafsey, M. A. Collins, *Neurochem. Int.* **2002**, 40, 611-620.
(97) R. Albores, E. J. Neafsey, G. Drucker, J. Z. Fields, M. A. Collins, *PNAS U. S. A.* **1990**, 87, 9368-9372.
(98) S. Pavlovic, G. Schulze, C. Wernicke, R. Bonnet, G. Gille, L. Badiali, A. Kaminska, E. Lorenc-Koci, K. Ossowska, H. Rommelspacher, *Neuroscience.* **2006**, 139, 1525-1537.
(99) J. Hamann, H. Rommelspacher, A. Storch, H. Reichmann, G. Gille, *J. Neurochem.* **2006**, 98, 1185-1199.
(100) J. Hamann, C. Wernicke, J. Lehmann, H. Reichmann, H. Rommelspacher, G. Gille, *Neurochem. Int.* **2008**, 52, 688-700.
(101) Y. Zhao, F. Ye, J. Xu, Q. Liao, L. Chen, W. Zhang, H. Sun, W. Liu, F. Feng, W. Qu, *Bioorg. Med. Chem.* **2018**, 26, 3812-3824.
(102) I. Maisuls, E. Wolcan, O. E. Piro, G. A. Etcheverria, G. Petroselli, R. Erra-Ballsels, F. M. Cabrerizo, G. T. Ruiz, *Dalton T.* **2015**, 44, 17064-17074.
(103) K. Shimoi, H. Kawabata, I. Tomita, *Mutat. Res-Fund*. Mol. M. **1992**, 268, 287-295.
(104) J. B. Hudson, E. A. Graham, R. Fong, L. L. Hudson, G. H. N. Towers, *Photochem. Photobiol*. **1986**, 44, 483-487.
(105) J. B. Hudson, E. A. Graham, G. H. N. Towers, *Photochem. Photobiol*. **1986**, 43, 21-26.
(106) M. J. Hazen, A. I. Pérez-Gorroño, N. Ortiz-Movilla, M. L. Molero, *Boll. Chim. Farm.* **2002**, 141, 154-157.
(107) J. M. Pérez Martín, V. Labrador, P. Fernández Freire, M. L. Molero, M. J. Hazen, *J. Appl. Toxicol.* **2004**, 24, 197-201.

(108) T. Mori, A. Nakagawa, N. Kobayashi, M. W. Hashimoto, K. Wakabayashi, K. Shimoi, N. Kinae, *Radiat. Res.* **1998**, 39, 21-33.
(109) K. Shimoi, R. Miyamura, T. Mori, T. Todo, E. Ohtsuka, K. Wakabayashi, N. Kinae, *Carcinogenesis,* **1996**, 17, 1279-1283.
(110) C.-c. Chang, M. Casteliazzi, T. W. Glover, J. E. Trosko, *Cancer Res.* **1978**, 38, 4527-4533.
(111) M. Caprasse, C. Houssier, *Biochimie*. **1983**, 65, 157-167.
(112) M. M. Gonzalez, M. L. Salum, Y. Gholipour, F. M. Cabrerizo, R. Erra-Balsells, *Photochem. Photobiol. Sci.* **2009**, 8, 1139-1149.
(113) M. M. Gonzalez, J. Arnbjerg, M. Paula Denofrio, R. Erra-Balsells, P. R. Ogilby, F. M. Cabrerizo, *J. Phys. Chem. A.* **2009**, 113, 6648-6656.
(114) F. M. Cabrerizo, J. Arnbjerg, M. P. Denofrio, R. Erra-Balsells, P. R. Ogilby, *ChemPhysChem*, **2010**, 11, 796-798.
(115) D. Hrsak, L. Holmegaard, A. S. Poulsen, N. H. List, J. Kongsted, M. P. Denofrio, R. Erra-Balsells, F. M. Cabrerizo, O. Christiansen, P. R. Ogilby, *Phys. Chem. Chem. Phys.* **2015**, 17, 12090-12099.
(116) F. A. O. Rasse-Suriani, M. Paula Denofrio, J. G. Yañuk, M. Micaela Gonzalez, E. Wolcan, M. Seifermann, R. Erra-Balsells, F. M. Cabrerizo, *Phys. Chem. Chem. Phys*. **2016**, 18, 886-900.
(117) O. I. Tarzi, M. A. Ponce, F. M. Cabrerizo, S. M. Bonesi, R. Erra-Balsells, *Arkivoc.* **2005**, vii, 295-310.
(118) M. L. Alomar, M. M. Gonzalez, R. Erra-Balsells, F. M. Cabrerizo, *J. Photochem. Photobiol. B.* **2014**, 136, 26-28.
(119) I. D. Spenser, *J. Chem. Soc.* **1956**, 3659-3663.
(120) M. Balón, J. Hidalgo, P. Guardado, M. A. Muñoz and C. Carmona, *J. Chem. Soc., Perkin Trans. 2*. **1993**, 99-104.
(121) F. Tomas Vert, I. Zabala Sanchez, A. Olba Torrent, *J. Photochem.* **1983**, 23, 355-368.
(122) F. A. O. Rasse-Suriani, F. S. García-Einschlag, M. Rafti, T. Schmidt De León, P. M. David Gara, R. Erra-Balsells, F. M. Cabrerizo, *Photochem. Photobiol.* 2018, 94, 36-51.
(123) Depending on the sensitizer and its symmetry, the simultaneous absorption of two photons may or may not populate the same state as that created upon the absorption of a single higher-energy photon.
(124) A. S. Coronilla, C. Carmona, M. A. Muñoz, M. Balón, *Chem. Phys.* **2006**, 327, 70-76.
(125) S. Draxler M. E. Lippitsch, *J. Phys. Chem.* **1993**, 97, 11493-11496.
(126) R. Sakurovs K. P. Ghiggino, *J. Photochem.* **1982**, 18, 1-8.
(127) O. S. Wolfbeis, E. Fuerlinger, *Z. Phys. Chem. (Wiesbaden).* **1982**, 129, 171-183.
(128) O. S. Wolfbeis, E. Fürlinger, R. Wintersteiger, *Monatsh. Chem.* **1982**, 113, 509-517.
(129) M. Balon, M. A. Muñoz, J. Hidalgo, M. C. Carmona, M.. Sánchez, *J. Photochem.* **1987**, 36, 193-204.
(130) F. Tomas Vert, I. Zabala Sanchez, A. Olba Torrent, *J. Photochem.* **1984**, 26, 285-294.
(131) G. Petroselli, R. Erra-Balsells, P. David Gara, G. M. Bilmes, *Photochem. Photobiol. Sci*. **2012**, 11, 1062-1068.
(132) O. I. Tarzi, R. Erra-Balsells, *J. Photochem. Photobiol. B.* **2006**, 82, 79-93.
(133) M. J. Allen, V. J. Powell, *J. Electrochem. Soc*. **1958**, 105, 541-544.
(134) F. Zhang and G. Dryhurst*, J. Electroanal. Chem*. **1993**, 350, 217-233.
(135) J. M. Bobbitt, J. P. Willis, *J. Org. Chem.* **1980**, 45, 1978-1984.
(136) L. Agüí, C. Peña-Farfal, P. Yáñez-Sedeño, J. M. Pingarrón, *Electroanalysis.* **2007**, 19, 237-243.
(137) J. G. Yañuk, F. M. Cabrerizo, F. G. Dellatorre, M. F. Cerdá, *Energy Rep.* **2019**, 6, 25-36.
(138) A. Sánchez-Coronilla, M. Balón, M. A. Muñoz, C. Carmona, *Chem. Phys.* **2008**, 344, 72-78.
(139) A. Dias, A. P. Varela, M. D. Miguel, A. L. Macanita, R. S. Becker, *J. Phys. Chem.* **1992**, 96, 10290-10296.
(140) The small or null effect induced by the chlorine atom placed at C-8 was suggested to be a consequence of the short distance between the chlorine atom and the pyrrolic NH group, leading place to the formation of a hydrogen-bridge-like-interaction. Thus, two opposite effects would operate simultaneously: a weak electron-donor effect (mesomeric effect) induced by the chlorine atom together with its spatial interaction with the hydrogen of the NH group by a hydrogen-bond-like interaction.
(141) Note that TD-DFT calculations do not produce "pure" H→L or H-1→L excitations as there is a mixing of around 80-90 % of the main excitation with 20-10% of the minor contribution.
(142) Typically, the spin-orbital coupling mechanism of the heavy atom enhances the rate of intersystem crossing to the triplet state (S1→T1). However, our singlet oxygen data independently obtained as well as the data on chloroharmines photodegradation (vide infra) suggest that internal conversion (S1→S0) seems to be the operative deactivation pathway.
(143) A. G. Mercader, P. R. Duchowicz, F. M. Fernández, E. A. Castro, F. M. Cabrerizo, A. H. Thomas, *J. Mol. Graph. Model.* **2009**, 28, 12-19.
(144) F. Wilkinson, W. P. Helman, A. B. Ross, *J. Phys. Chem. Ref. Data.* **1995**, 24, 663-677.
(145) G. N. Bosio, T. Breitenbach, J. Parisi, M. Reigosa, F. H. Blaikie, B. W. Pedersen, E. F. F. Silva, D. O. Mártire, P. R. Ogilby, *J. Am. Chem. Soc.* **2013**, 135, 272-279.
(146) F. T. Vert, I. Z. Sanchez, A. O. Torrent, *J. Photochem.* **1983**, 23, 355-368.
(147) A. Sánchez Coronilla, C. Carmona, M. A. Muñoz, M. Balón, *J. Fluoresc.* **2010**, 20, 163-170.

(148) A. Dias, A. P. Varela, M. da Graça Miguel, R. S. Becker, H. D. Burrows, A. L. Maçanita, *J. Phys. Chem.* **1996**, 100, 17970-17977.
(149) D. Reyman, M. H. Viñas, G. Tardajos, E. Mazario, *J. Phys. Chem. A.* **2012**, 116, 207-214.
(150) A. Pardo, D. Reyman, J. M. L. Poyato, F. Medina, *J. Lumin.* **1992**, 51, 269-274.
(151) R. Duval, C. Duplais, *Nat. Prod. Rep.* **2017**, 34, 161-193.
(152) P. R. Ogilby, *Chem. Soc. Rev.* **2010**, 39, 3181-3209.
(153) R. W. Redmond, I. E. Kochevar, *Photochem. Photobiol.* **2006**, 82, 1178-1186.
(154) T. Finkel, *J. Cell Biol.* **2011**, 194, 7-15.
(155) M. Zatloukalová, J. Vacek, V. Simánek, *Heterocycles.* **2014**, 88, 879-897.
(156) A. M. Oliveira-Brett, V. C. Diculescu, T. A. Enache, I. P. G. Fernandes, A.-M. Chiorcea-Paquim, S. C. B. Oliveira, *Curr. Opin. Electrochem*. **2019**, 14, 173-179.
(157) L. u. Švorc, K. Cinková, A. Samphao, D. M. Stanković, E. Mehmeti and K. Kalcher, *J. Electroanal. Chem.* **2015**, 744, 37-44.
(158) M.-C. Radulescu, M.-P. Bucur, B. Bucur, G. L. Radu, *Talanta*, **2015**, 137, 94-99.
(159) F. D. Villarruel, M. P. Denofrio, R. Erra-Balsells, E. Wolcan, F. M. Cabrerizo. Phys. Chem. Chem. Phys., **2020**, 22, 20901-20913

Dr. Juan Gabriel Yañuk. Bachelor in Genetic (2012), Universidad Nacional de Misiones (UNAM), Doctor in Biochemistry and Molecular Biology (2018) and Graduated Assistant for Chemistry (2012-2014) and Mathematic (since 2014) of Universidad Nacional de San Martín (UNSAM). CONICET Postdoc (2018-2020). Research in Molecular Biology, Photochemistry and Photobiology. He published 5 papers, participated in 10 conferences.

Ing. Fernando Diego Villarruel. Agrobiotechnology Engineer (2017, UNSAM). Coursing his Chemistry Doctoral studies (since 2017) at the Faculty of Exacts Sciences, National University of La Plata (FCE, UNLP) under the counseling of Dr. García Einschlag and Dr. Cabrerizo. His research interest is focused on multivariate analysis applied to photochemical processes. Teaching assistant (since 2020) at UNSAM. He published 3 papers and participated in 5 conferences.

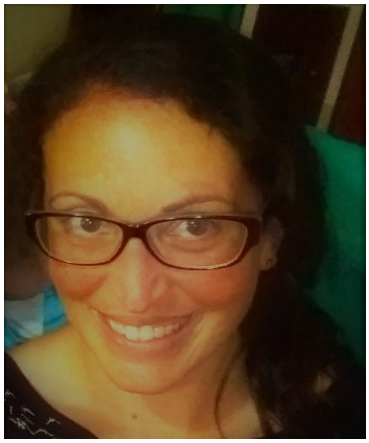

María Lis Alomar. Bachelor in Molecular Biology (2007) at Universidad Nacional de San Luis and Ph D in Sciences, Molecular Biology and Biotechnology (2015) at University of General San Martin (UNSAM, Argentina). Since 2016 she is a CONICET Assistant Researcher at the Molecular photochemistry and photobiology lab (INTECH) and Head of Practical Work in Mathematics (UNSAM). Research in Development and optimization of chemical and photodynamic methods for selective attenuation of *Toxoplasma gondii*. She published 6 papers, one book Chapter and participated in 10 conferences. She was part of the research team that received the INNOVAR award for their contribution in the development of an alternative therapy for bovine trichomoniasis treatment (2014).

Federico A. O. Rasse Suriani. Undergraduate studies in Biochemistry (2011) and Ph.D in Chemical Sciences (2016) at the National University of La Plata (UNLP). He was a Postdoctoral CONICET Research Fellow at the the Research Institute of Theoretical and Applied Physical Chemistry (INIFTA, UNLP, Argentina, 2016-2019). Since 2019 he is researcher at the Chemistry Department of the Faculty of Exacts Sciences (UNLP). His current work focuses in the application of multivariate methods in the spectroscopic data analysis and development of numerical tools for photo-induced processes kinetics modelling. He published 8 papers.

Dr. María Micaela González. Undergraduate studies in Biochemistry (2008) at the National University of La Plata (UNLP) and PhD in Biological Chemistry (2012) at the University of Buenos Aires (UBA). She was a Postdoctoral CONICET Research Fellow at the Center for Research in Carbohydrates (CIHIDECAR, UBA, 2012 – 2014). At present, Dr. González is a research member of CONICET and professor at National University of San Martín (UNSAM). She has authored 16 scientific publications and her research activities are framed within different fields of knowledge such as organic chemistry, photochemistry, photobiology and microbiology. Particularly, her current research is focused on the attenuation of pathogenic microorganisms (parasites) by photosensitization, with the main goal of creating vaccines, using this technique as a biotechnological tool.

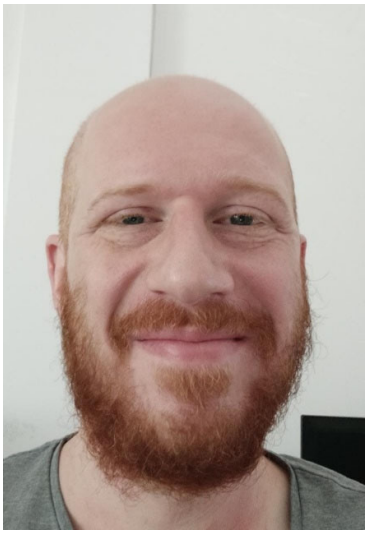

Eduardo Gonik has an undergraduate degree in Biotechnology and Molecular Biology from Universidad Nacional de La Plata (UNLP). Currently pursuing a PhD in Chemistry, focusing in photoluminescent materials and for photodynamic therapy. He is also a teaching assistant at UNLP.

Dra. Lorean Mercedes Madriz Ruiz. Chemist (2006), Doctor in Chemistry (2012) and Chemistry Professor (2012-2019) of the Universidad Simón Bolívar (USB, Venezuela). CONICET Postdoc (2019-2021) at INIFTA and Head of Practical Works (since 2019) of the UNSAM (Argentina). Research in electrochemistry, photocatalysis and environmental chemistry. She published 16 papers, participated in 60 conferences and trained 17 human resources in science and engineering. She has received financial support from TWAS, ICTP, CONICET, ACS, NSF, UNITEC, SVE and USB. To date, she is an active member of the Venezuelan Electrochemical Society. In addition, she has been a member of its board of directors (2014-2016).

Dr. Ronald Eduardo Vargas Balda. Chemical Engineer (2007), Doctor in Chemistry (2012) and Chemistry Professor (2012-2019) of the USB (Venezuela). CONICET Postdoc (2019-2020), CONICET Researcher (since 2020) at INTECH and Physics Professor (since 2020) of the UNSAM (Argentina). Research in electrochemistry, physical chemistry and photocatalysis. He published 36 papers, participated in 80 conferences and trained 42 human resources in science and engineering. In 2017 he received the Arnoldo Gabaldón award for his contribution in Chemical Sciences (ACFIMAN and UCV, Venezuela). To date, he is an active member of the Venezuelan Electrochemical Society and the TWAS Young Affiliate Network (TYAN).

Rosa Erra Balsells. Investigator Superior (CONICET) and Full Professor (Buenos Aires Univ., UBA), Argentina; Visiting Professor (Ehime Univ.), Japan. Her photochemistry and mass spectrometry related research has been recognized with the Dr. L.C. Guglialmelli Award, AQA (1982); V Centenary Award, ICI & Ministry of Education of Spain (1992); Konex Diploma (2003); Latinoamerican Academy of Sciences fellow (2019-); Third World Academy of Sciences fellow (2020-); Japan Society for Promotion of Sciences International fellow (1995-). She served Anales de la Asociación Química Argentina (Argentine Chemical Society, AQA), editorial secretary and director (1983-2001); Sociedad Argentina de Investigación en Química Orgánica, president (2007-2009); Sociedad Argentina de Espectrometría de Masa, president (2014-2019); International Mass Spectrometry Foundation, executive committee member (2019-). She is interested in photochemistry of βCs and its application both crystalline compounds and basic component of ionic liquids, as matrix (photosensitizer) in matrix assisted laser desorption/ionization (MALDI) mass spectrometry.

Dr. María Paula Denofrio. Biochemist (2006, National University of La Plata, UNLP). Ph.D. in Chemical Sciences (2011, Physical Chemistry and Photochemistry division at The Research Institute of Theoretical and Applied Physical Chemistry, INIFTA, UNLP, Argentina). She was a Postdoctoral Research Fellow at the Chascomús Institute of Technology (2011 – 2012, INTECH). In 2013 she was appointed as research member of The National Scientific and Technical Research Council (CONICET, Argentina) and professor at the National University of San Martín (UNSAM, Argentina). Her research activities focus on understanding the molecular bases of the macromolecules photodamage induced by naturally occurring alkaloids.

Franco M. Cabrerizo. BSc in Chemistry (2002, National University of La Plata, UNLP). Ph.D. in Chemical Science (2005, INIFTA, UNLP, Argentina). He was a Postdoctoral Research Fellow at the Center for Research in Carbohydrates (CIHIDECAR, National University of Buenos Aires, UBA, 2005 – 2006). Since 2010 he leads the Photochemistry and Molecular Photobiology Research Group, at Chascomús Institute of Technology (INTECH). He served as an assistant professor both at UNLP and UNSAM (2011 – 2013). In 2013 he was appointed associate professor at UNSAM. Currently, he is a research member of The National Scientific and Technical Research Council (CONICET, Argentina) and Associate Professor at National University of San Martín (UNSAM, Argentina). His current research focuses on understanding the molecular aspects of mechanisms underlying the processes triggered by UVA and/or visible light. This knowledge provides valuable information for the development of different biotechnological applications that might contribute to attend unresolved and/or neglected socially relevant local and global problems related to some infectious and chronic diseases as well as to changes in the current energy matrix towards more sustainable and renewable sources of energy. His photochemistry and photobiology related research has been recognized with the: “G. Cilento Award” (The Inter-American Photochemical Society, 2006); “Ranwel Caputto Award” (The National Academy of Science of Argentina, 2009), “Dr. Eduardo Gros prize” (The National Academy of Exact, Physics and Natural Sciences, ANCEFN, Argentina, 2015), “Dr. Eduardo Gros Award” (The Argentine Society of Research in Organic Chemistry, 2015).